

**RECOVERY OF PHYTOCHEMICALS (HAVING
ANTIMICROBIAL AND ANTIOXIDANT
CHARACTERISTICS) FROM LOCAL PLANTS**

**A Thesis Submitted to
the Graduate School of Engineering and Sciences of
İzmir Institute of Technology
in Partial Fulfillment of the Requirements for the Degree of**

DOCTOR OF PHILOSOPHY

in Chemical Engineering

**by
Evren ALTIOK**

**July 2010
İZMİR**

We approve the thesis of **Evren ALTIOK**

Prof. Dr. Semra ÜLKÜ
Supervisor

Assoc. Prof. Dr. Oğuz BAYRAKTAR
Co-Supervisor

Prof. Dr. Mustafa DEMİRCİOĞLU
Committee Member

Prof. Dr. Sacide ALSOY ALTINKAYA
Committee Member

Assoc. Prof. Dr. Durmuş ÖZDEMİR
Committee Member

Assoc. Prof. Dr. Fehime ÖZKAN
Committee Member

28.June.2010

Prof. Dr. Mehmet POLAT
Head of the Department of
Chemical Engineering

Assoc. Prof. Dr. Talat YALÇIN
Dean of the Graduate School of
Engineering and Sciences

ACKNOWLEDGMENTS

I would like to express the deepest gratitude to my supervisor, Prof. Semra ÜLKÜ and to my co-supervisor, Assoc. Prof. Oğuz BAYRAKTAR, for their guidance, advices, criticism and encouragement through all the stages of this thesis. I am grateful to my thesis committee members; Prof. Sacide ALSOY ALTINKAYA, Assoc. Prof. Durmuş ÖZDEMİR, Prof. Mustafa DEMİRCİOĞLU and Prof. Fehime ÖZKAN for their valuable contributions.

I would like to thank my friends in the İzmir Institute of Technology, especially to Beyhan Cansever ERDOĞAN for her discussions and contributions.

I would also express my special thanks to my wife, Duygu ALTIOK, for her endless support, encouragement and understanding. She gave me the moral support I required and took a great effort for growing our lovely twins, Duru ALTIOK and Damla ALTIOK.

Finally, I would like to express my indebtedness and offer my special thanks to my family for their endless supports and patients.

ABSTRACT

RECOVERY OF PHYTOCHEMICALS (HAVING ANTIMICROBIAL AND ANTIOXIDANT CHARACTERISTICS) FROM LOCAL PLANTS

The objective of the present work was to assess the selective isolation of polyphenols from olive leaf and grape skin, which are supplied from the main local plants. The effects of extraction conditions on the types and amounts of polyphenolic compounds and selective separation of them by adsorption were investigated. The batch adsorption and dynamic column studies were performed by silk fibroin and clinoptilolite. Kinetic models were used to determine the mechanism of adsorption. Dynamic column models were applied to optimize the operating parameters. The biological activities of isolated fractions from the crude extracts were determined by analyzing their antioxidant, antimicrobial and cytotoxic activities.

Recovered *trans*-resveratrol significantly inhibited all pathogenic microorganisms. However, higher concentration of grape skin crude extract is required to achieve same inhibition. Although grape skin extract did not have any effect on prostate and breast cancer cells, *trans*-resveratrol has very significant inhibition effect.

ÖZET

ANTIÖKSİDAN VE ANTİMİKROBİYAL ÖZELLİKLERE SAHİP FİTOKİMYASALLARIN YÖRESEL BİTKİLERDEN ELDESİ

Bu çalışmanın amacı yöresel bitkilerden elde edilen zeytin yaprağı ve üzüm kabuğundan ekstrakte edilen polifenollerin seçici olarak ayırımını gerçekleştirmektir. Ekstraksiyon koşullarının polifenollerin cinsi ve miktarı üzerine etkileri ve bu polifenollerin adsorpsiyon ile seçici ayırımı araştırılmıştır. Kesikli adsorpsiyon ve dinamik kolon çalışmaları ipek fibroini ve klinoptilolit ile gerçekleştirilmiştir. Adsorpsiyon mekanizması için kinetik modeller kullanılmıştır. Dinamik kolon modelleri ise çalışma parametrelerini belirlemek üzere kullanılmıştır. Ham özütten elde edilen fraksiyonların biyolojik aktiviteleri antioksidan, antimikrobiyel ve sitotoksik etkileri analizlenerek tespit edilmiştir.

Kazanılan *trans*-resveratrol tüm patojenik mikroorganizmaları etkili bir şekilde inhibe etmiştir. Fakat, aynı inhibisyonu gözlemleyebilmek için daha yüksek konsantrasyonlarda üzüm kabuğu özütüne ihtiyaç duyulmuştur. Üzüm kabuğu özütü prostat ve göğüs kanseri hücrelerine herhangi bir etki göstermezken, *trans*-resveratrol önemli bir inhibisyon etkisi göstermiştir.

TABLE OF CONTENTS

LIST OF FIGURES	x
LIST OF TABLES	xvii
CHAPTER 1. INTRODUCTION	1
CHAPTER 2. PHYTOCHEMICALS	4
2.1. Classification of Phytochemicals	4
2.2. Flavonoids	6
2.3. Antioxidant Properties and Health Effects of Phytochemicals	8
2.4. Potential Sources of Phytochemicals	9
2.4.1. Grape Pomace	9
2.4.2. Olive Leaves	11
CHAPTER 3. EXTRACTION AND DETECTION OF BIOACTIVE COMPOUNDS FROM PLANTS	15
3.1. Solid-Liquid Extraction (SLE)	15
3.2. Mass Transfer: Equations and Kinetics	18
3.3. Extraction Methods	20
3.4. Extraction of Olive Leaf Antioxidants	20
3.5. Extraction of Grape skin Polyphenols	21
3.6. Characterization of Crude Extract	25
CHAPTER 4. SEPARATION OF BIOACTIVE COMPOUNDS: ADSORPTION	27
4.1. Isolation or Selective Separation of Bioactive Compounds from Raw Plant Material	27
4.2. Adsorption	28
4.3. Silk Fibroin	32
4.4. Clinoptilolite	33

4.5. Adsorption Theory	36
4.5.1. Adsorption Kinetic	37
4.5.1.1. External Film Diffusion.....	41
4.5.1.2. Macropore Diffusion	43
4.5.1.3. Micropore Diffusion.....	46
4.5.1.4. Adsorption Reaction Models.....	52
4.5.2. Adsorption Equilibrium	53
4.5.3. Column Studies	54
CHAPTER 5. BIOLOGICAL ACTIVITIES OF PHYTOCHEMICALS	60
5.1. Antioxidant Activity	60
5.2. Antimicrobial Activity	62
5.3. Cytotoxic Activity.....	65
CHAPTER 6. MATERIALS AND METHODS	67
6.1. Materials	67
6.2. Methods.....	68
6.2.1. Pretreatments of Olive Leaf and Grape Pomace.....	70
6.2.2. Extraction	70
6.2.2.1. Extraction Studies with Grape Skin	70
6.2.2.2. Extraction Studies with Olive Leaves	70
6.2.3. Identification of Bioactive compounds	71
6.2.4. Bioactivity Tests	72
6.2.5. Adsorption Studies.....	73
6.2.5.1. Adsorbents.....	73
6.2.5.2. Adsorption of Olive Leaf Polyphenols.....	74
6.2.5.3. Adsorption of Grape Skin Polyphenols.....	76
6.2.6. Dynamic Column Studies of Grape Skin Polyphenols	79
CHAPTER 7. RESULTS AND DISCUSSIONS	82
7.1. Extraction studies.....	82

7.1.1. Extraction of Bioactive Compounds from Grape Pomace	82
7.1.2. Extraction of Bioactive Compounds from Olive Leaves	86
7.2. Identification of Bioactive Compounds	90
7.2.1. HPLC Analysis of Grape Skin Polyphenols	90
7.2.2. HPLC Analysis of Olive Leaf Polyphenols	91
7.3. Selective Isolation of Bioactive Compounds from Crude Extract: Adsorption	93
7.3.1. Adsorbents	93
7.3.2. Adsorption of Grape Skin Polyphenols on Silk Fibroin	103
7.3.3. Adsorption of Grape Skin Polyphenols on Clinoptilolite	113
7.3.4. Adsorption and Selective Separation of Olive Leaf Crude Extract (OLCE) Polyphenols on Silk Fibroin	155
7.3.5. Adsorption of Olive Leaf Polyphenols on Clinoptilolite (Clinoptilolite Rich CL5)	159
7.4. Biological Activities	168
7.4.1. Antioxidant Capacity of Crude Extracts and Fractions	168
7.4.2. Antimicrobial Activities of Crude Extracts and Fractions: MIC Values	169
7.4.3. Cytotoxic Activity	170
 CHAPTER 8. CONCLUSIONS	 172
 REFERENCES	 174
 APPENDICES	
APPENDIX A. METHODS AND BIOLOGICAL ACTIVITY TESTS	186
APPENDIX B. HPLC CHROMATOGRAMS FOR EXTRACTION EFFICIENCY	204
APPENDIX C. HPLC CALIBRATION CURVES	211

APPENDIX D. THEORITICAL EVALUATIONS OF ADSORPTION DATA.....	216
APPENDIX E. ANTIOXIDANT CAPACITY CURVES.....	232
APPENDIX F. ANTIMICROBIAL ACTIVITIES OF THE EXTRACTS AND ISOLATED FRACTIONS.....	239

LIST OF FIGURES

Figure	Page
Figure 2.1. Common simple phenol and flavonoids in plants	5
Figure 2.2. The basic unit of flavonoids	7
Figure 2.3. Chemical structures of some representative flavonoids	8
Figure 2.4. Number of publications in web of science related with the <i>trans</i> -resveratrol.....	10
Figure 3.1. Effect of different solvents on extraction yields of <i>trans</i> - resveratrol from grape canes.....	23
Figure 4.1. Diagram of active compound isolation procedures from raw plant material	28
Figure 4.2. Chemical structures of silk fibroin.....	32
Figure 4.2. (SiO ₄) ⁴⁻ or (AlO ₄) ⁵⁻ tetrahedron	34
Figure 4.3. Biomedical effects of zeolite	36
Figure 4.4. Adsorption kinetic steps.....	38
Figure 4.5. Diffusion in macropores	44
Figure 5.1. Cell wall of gram negative bacteria.....	63
Figure 5.2. Differences of the cell wall structure of gram negative and gram positive bacteria.....	64
Figure 6.1. Experimental procedure of the study	69
Figure 6.2. Sample preparation for hplc analysis of grape skin crude extract by fractional dissolution of polyphenolic compounds	72
Figure 6.3. Flow scheme of the apparatus for column study	80
Figure 7.1. Effect of extraction solvent on total phenol content of olive leaf extract A) ethanol- water solution; B) acetone-water solution	87
Figure 7.2. Effect of extraction kinetics in 70% ethanol solution.....	88
Figure 7.3. Effect of solvent type on % inhibition of ABTS radical cation.....	88
Figure 7.4. Correlation between total phenol content and % inhibition of ABTS	89
Figure 7.5. Effect of solvent on extracted amount of oleuropein and rutin per gram of olive leaf.....	90

Figure 7.6. HPLC C18 column separation of the grape skin extract's main polyphenolic compounds	91
Figure 7.7. HPLC profile of olive leaf crude extracts at two initial concentrations as A: 1.5 g CE/50 mL including 228 mg oleuropein and 28.67 mg rutin B: 1g Ce/50 mL including 162 mg oleuropein ($\approx 30\%$) and 21.2 mg rutin ($\approx 5\%$).	92
Figure 7.8. SEM photomicrographs of silk fibroin before (A1 and A2) and after adsorption (B1 and B2)	94
Figure 7.9. SEM photomicrographs of <i>trans</i> -resveratrol	95
Figure 7.10. Digital images of silk fibroin before and after adsorption of <i>trans</i> -resveratrol (Olympus SZ-61, at 45x).....	95
Figure 7.11. SEM photomicrographs of clinoptilolite after wet sieving into 5 different sizes	97
Figure 7.12. X-Ray diffractogram of wet- sieved clinoptilolite samples.....	99
Figure 7.13. XRD diffractogram of the separated fractions; A: 1000 rpm centrifuge pellet, B: 3000 rpm	101
Figure 7.14. Adsorption kinetics of <i>trans</i> -resveratrol on silk fibroin, at initial concentration of 0.091 mg <i>trans</i> -resveratrol /mL 20% aqueous ethanol. Experimental conditions: S/L: 1/40; shaking speed: 180 rpm; 30 °C.....	105
Figure 7.15. Mono-component adsorption kinetics curve for gallic acid, (+)-catechin and (-)-epicatechin on silk fibroin from 20% ethanol solution. Experimental conditions: S/L: 1/40; shaking speed: 180 rpm; 30 °C.....	105
Figure 7.16. Effect of ethanol concentration on adsorption of <i>trans</i> -resveratrol on silk fibroin. Experiment conditions: T= 30 °C, contact time: 3 h, solid-liquid ratio: 1/40, shaking speed: 180 rpm.....	106
Figure 7.17. Adsorbed amount of <i>trans</i> -resveratrol at different solid-liquid ratios.....	108
Figure 7.18. The solubility of <i>trans</i> -resveratrol in 20% ethanol solution at 30 °C.....	109
Figure 7.19. Kinetics of adsorption of <i>trans</i> -resveratrol on silk fibroin from 20% ethanol solution at 30 °C (solid-liquid ratio: 1/40).....	109

Figure 7.20. Adsorption isotherms of resveratrol on silk fibroin.....	110
Figure 7.21. Adsorption of phenolic compounds mixtures on silk fibroin in a batch study by adjusting the s/l ratio as 1/40 for 3h at 30 °C.....	111
Figure 7.22. Adsorption behaviour of silk fibroin on the three phenolic compounds; gallic acid, (+)-catechin and (-)-epicatechin in 20% of ethanol solution (T: 30 °C, solid-liquid ratio: 1/40).....	112
Figure 7.23. Effect of temperature on adsorption isotherm of <i>trans</i> - resveratrol on silk fibroin. Experimental conditions: S/L: 1/40, shaking speed: 180 rpm.	113
Figure 7.24. Adsorption kinetics of polyganum cuspaditum's <i>trans</i> - resveratrol (51.5% pure) on different amount of CL3 clinoptilolite sample (purity: 64%).....	114
Figure 7.25. Adsorption kinetics of polyganum cuspaditum's pure <i>trans</i> - resveratrol (51.5 % pure) on clinoptilolite rich CL5 sample (purity: 91%). S/L: 1/40, T: 40 °C, 150 rpm.....	114
Figure 7.26. Adsorption kinetics of high purity <i>trans</i> -resveratrol on clinoptilolite rich CL5 sample. S/L: 1/40, T: 40 °C, 150 rpm.....	115
Figure 7.27. Adsorbed amount of <i>trans</i> -resveratrol on clinoptilolite at different solid-liquid ratios	115
Figure 7.28. Change in concentrations of GA, (+)-catechin and (-)-epicatechin in liquid during the adsorption studies performed with clinoptilolite (solid-liquid ratio: 1/20, 40 °C).....	116
Figure 7.29. Effect of ethanol concentration on adsorption of <i>trans</i> - resveratrol on clinoptilolite (experiment conditions; T: 30 °C, adsorption time: 3 h, solid-liquid ratio: 0.025).....	117
Figure 7.30. Solubility of <i>trans</i> -resveratrol in 10 % of ethanol within the range of selected concentrations.	118
Figure 7.31. Adsorption isotherm of <i>trans</i> -resveratrol on CL3 clinoptilolite.....	118
Figure 7.32. Adsorption isotherm of 51.5 % pure <i>trans</i> -resveratrol on clinoptilolite rich CL5 sample.	119
Figure 7.33. Adsorption isotherm of pure <i>trans</i> -resveratrol standard on clinoptilolite rich CL5 sample	120
Figure 7.34. Effect of temperature on adsorbed amount of <i>trans</i> -resveratrol (experiment conditions; solid-liquid ratio: 0.025, <i>trans</i> -	

resveratrol concentrations: 0.254 and 0.142 mg/mL, contact time: 24 hours)	121
Figure 7.35. Effects of initial 51.5% pure <i>trans</i> -resveratrol concentrations on the adsorption kinetics; A: 15 °C; B: 25 °C and C: 40 °C. Experimental conditions: S/L: 1/40; shaking speed: 150 rpm, clinoptilolite rich CL5 sample	122
Figure 7.36. Effect of temperature on adsorption isotherm. experimental conditions: S/L: 1/40; shaking speed: 150 rpm, clinoptilolite rich CL5 sample, 51.5% <i>trans</i> -resveratrol.....	123
Figure 7.37. Effects of initial pure standard <i>trans</i> -resveratrol concentrations on the adsorption kinetics at two temperatures as 25 °C and 40 °C. Experimental conditions: S/L: 1/120; shaking speed: 150 rpm, clinoptilolite rich CL5 sample.....	124
Figure 7.38. Effect of temperature on adsorption isotherm. Experimental conditions: S/L: 1/120; shaking speed: 150 rpm, clinoptilolite rich CL5 sample, pure <i>trans</i> -resveratrol.....	125
Figure 7.39. The effect of <i>trans</i> -resveratrol solution's pH on the adsorption of <i>trans</i> -resveratrol by clinoptilolite. Experimental conditions: S/L: 1/120; 30 °C; C _i : 0.038 mg/mL; shaking speed: 150 rpm, clinoptilolite rich CL5 sample	126
Figure 7.40. pH change during the adsorption of <i>trans</i> -resveratrol.....	127
Figure 7.41. Effect of agitation speeds on <i>trans</i> -resveratrol adsorption onto clinoptilolite rich CL5 sample. Experimental conditions: C _i : 0.034 mg/mL; S/L: 1/120; 30 °C	129
Figure 7.42. Effect of particle size on pure <i>trans</i> -resveratrol adsorption onto clinoptilolite. Experimental conditions: S/L: 1/120; C _i : 0.038 mg/mL; 150 rpm; 30 °C.....	130
Figure 7.43. Adsorption of <i>trans</i> -resveratrol by acid treated clinoptilolite samples; adsorption studies were performed with solid-liquid ratio 1/40, at 35 °C during 24 Hours.....	136
Figure 7.44. Concentration changes at column outlets relative to inlet concentrations of each compounds; A: for all polyphenols, B: for gallic acid	137

Figure 7.45. Concentration changes at column outlets relative to initial concentrations of each compounds; C: (+)- catechin D: (-)-epicatechin	137
Figure 7.46. <i>Trans</i> -resveratrol concentration changes relative to initial concentration at column outlets	138
Figure 7.47. Second loading of column with polyphenols' standards mixtures	141
Figure 7.48. Effect of flow rates on breakthrough curve	143
Figure 7.49. Effect of influent concentration on breakthrough curve	144
Figure 7.50. Normalized breakthrough data obtained by changing the flow rates	145
Figure 7.51. Normalized breakthrough data obtained by changing the inlet concentrations of the sorbate	146
Figure 7.52. Effect of bed height on breakthrough curves. flow rate: 1 mL/min and C_i : 0.035 mg/mL	147
Figure 7.53. Percentage distribution of <i>trans</i> -resveratrol at eluted fractions.....	148
Figure 7.54. Elution of <i>trans</i> -resveratrol with different ethanol solutions	148
Figure 7.55. Elution of <i>trans</i> -resveratrol by 40% ethanol from column filled with silk fibroin and elution performance	149
Figure 7.56. Effect of regeneration on column performance	150
Figure 7.57. Application of Adams-Bohart model to investigate the effect of flow rate on breakthrough curve.....	151
Figure 7.58. Application of Adams-Bohart model to investigate the effect of inlet concentration on breakthrough curve	151
Figure 7.59. Application of Thomas Model to investigate the effect of flow rates on breakthrough curve.....	153
Figure 7.60. Application of Thomas Model to investigate the effect of inlet concentration on breakthrough curve	154
Figure 7.61. HPLC chromatogram of A: initial solution; B: 1 st effluent; C: 8 th effluent; D: 12 th effluent of the silk loaded column.....	156
Figure 7.62. HPLC chromatogram of eluted fraction with deionized water.....	157
Figure 7.63. HPLC chromatogram of eluted fraction with 40% ethanol	158

Figure 7.64. HPLC chromatogram of OLCE dissolved in water (10 mg/mL of deionized water). oleuropein and rutin content of OLCE was found as 244.5 mg and 45.75 mg, respectively	159
Figure 7.65. HPLC chromatograms of solution A: before adsorption, B: sample taken after 1h during the adsorption study and C: sample taken after 5 h during the adsorption study	160
Figure 7.66. Overlaid HPLC chromatograms of OLCE solutions before and after adsorption study (blue: before adsorption, green and red: after adsorption).....	161
Figure 7.67. HPLC chromatograms of oleuropein and rutin free solutions: before (blue) and after (red) adsorption study performed with pure clinoptilolite. (T: 25 °C, solid-liquid ratio: 1/40 and at 180 rpm).....	162
Figure 7.68. Adsorption kinetics of OLCE on purified clinoptilolite rich CL5 sample (<25 mm). Ci: 0.205 mg GA Eq/mL	162
Figure 7.69. Adsorption kinetics of OLCE on purified clinoptilolite rich CL5 sample (<25 mm) within 10 minutes. Ci: 0.188 mg GA Eq/mL.....	163
Figure 7.70. Effect of temperature on adsorption of OLCE on purified CL5 clinoptilolite (<25 mm). Ci: 0.079 mg GA Eq/mL	163
Figure 7.71. Solution concentration within 320 minutes	164
Figure 7.72. HPLC chromatograms of oleuropein and rutin free OLCE fraction; C _{0i} : chromatogram of selected initial C ₀ concentration, the others are HPLC chromatograms for different initial concentration of solution (C ₀ To C ₄) after reaching equilibrium.....	164
Figure 7.73. Adsorption behaviour of OLCE at different initial concentration.....	165
Figure 7.74. Effect of particle size on adsorption capacity of OLCE	166
Figure 7.75. Effect of particle size on adsorption of oleuropein and rutin free OLCE fraction	167
Figure 7.76. Effect of agitation on adsorption of oleuropein and rutin free OLCE fraction (T: 25 °C, C _i : 0.224 mg GA Eq/ mL of deionized water, solid-liquid ratio: 0.025).....	167

Figure 7.77. Sample graph for determination of IC50 values of purified
trans-resveratrol against MCF7 cell line 170

LIST OF TABLES

<u>Table</u>	<u>Page</u>
Table 2.1. The major classes of phenolic compounds in plants.....	5
Table 2.2. Common flavonoids and common foods that contain them	6
Table 2.3. Olive producing countries.....	12
Table 3.1. Solvent characteristics for natural product extraction	17
Table 3.2. Extraction methods and optimum extraction parameters studied in literature for <i>trans</i> -resveratrol.....	22
Table 4.1. Researches for purification and concentration of phytochemicals by selective adsorption	29
Table 5.1. Difference between gram positive and gram negative bacteria	63
Table 6.1. Experimental conditions for the adsorption of OLCE onto clinoptilolite at constant solid/liquid ratio (1/40)	76
Table 6.2. Experimental conditions for the adsorption of the grape skin polyphenols onto the silk fibroin; particle size of the silk fibroin was <20 µm.....	78
Table 6.3. Experimental conditions for the adsorption of the grape skin polyphenols onto the clinoptilolite	79
Table 7.1. <i>Trans</i> -resveratrol content of different part of grape pomace obtained from Muğla. Solid liquid extraction was performed with a 1:10 (solute: solvent) ratio in thermostated water bath.....	82
Table 7.2. <i>Trans</i> -resveratrol content of different part of grape pomace obtained from Urla. Solid liquid extraction was performed with a 1:10 (solute: solvent) ratio in thermostated water bath	83
Table 7.3. Polyphenol composition (mg/g dw) of grape skin extract extracted with different extraction methods and conditions.....	84
Table 7.4. Polyphenol composition of the extract obtained with the ultrasonic extraction method at 30 °C for 30 minutes by 80% methanol.....	85
Table 7.5. Peak number and abundance (% peak area) of the main phenolic compounds present in olive leaf crude extract.....	92

Table 7.6.	The purity of clinoptilolite at samples according to the method of Nakamura et al. (1992).....	100
Table 7.7.	The purity of clinoptilolite at samples according to the method of Nakamura et al. (1992).....	101
Table 7.8.	Elemental composition of clinoptilolite rich CL5 sample.....	102
Table 7.9.	Elemental composition of solution before and after OLCE adsorption studies	103
Table 7.10.	Qualitative polyphenolic components detected at fractions obtained from gradient dissolutions of crude extracts	104
Table 7.11.	Isotherm model constants	120
Table 7.12.	Macropore diffusivities for the adsorption of <i>trans</i> -resveratrol onto the clinoptilolite rich CL5 sample	132
Table 7.13.	Macropore diffusivities for the adsorption of <i>trans</i> -resveratrol onto the clinoptilolite rich CL5 sample, effect of particle size.....	133
Table 7.14.	Macropore diffusivities for the adsorption of <i>trans</i> -resveratrol onto the clinoptilolite rich CL5 sample, effect of agitation speed	134
Table 7.15.	Elemental analysis of the acid treated clinoptilolite sample performed by EDX.....	135
Table 7.16.	Adsorbed and desorbed amounts of polyphenols from the silk fibroin filled column and effect of eluting solvent on the polyphenolic compositions	139
Table 7.17.	Purity of eluted fractions.....	140
Table 7.18.	Adsorbed and desorbed amounts of polyphenols from the silk fibroin filled column and effect of eluting solvent on the polyphenolic compositions (belongs to secondly used column)	142
Table 7.19.	Purity of eluted fractions from second loading column.....	142
Table 7.20.	Parameters predicted from the Adams-Bohart model.....	152
Table 7.21.	Thomas model parameters and correlations between the theoretical and experimental values.....	155
Table 7.22.	Amount of adsorbed oleuropein and rutin (q) at different concentrations of loading.....	156
Table 7.23.	HPLC profile of phenolics eluted from column with water and 40% EtOH solution.....	158

Table 7.24. Peak number and abundance (% peak area) of the main phenolic compounds present in olive leaf crude extract.....	159
Table 7.25. Antioxidant capacities of polyphenolic compounds of standards and isolated fractions from crude extract.....	168
Table 7.26. MIC results for extract and isolated fractions.....	169
Table 7.27. IC50 values of crude extracts and isolated fractions	171

CHAPTER 1

INTRODUCTION

Many studies have been performed to investigate the active components of plant extracts, which have been used to treat many important diseases for centuries. The components are known as plant secondary metabolites and possess higher antioxidative, antimicrobial and antiviral properties.

Application of adsorption processes in pharmaceutical industry for purification purpose has become more prevalent during recent years. Adsorption is an important step in purification process in order to produce high value added products. For selectively separating the active compound from the crude extract, first of all, it is required to investigate the behaviour of the adsorbent against those polyphenolic compounds. For this purpose, the behaviour of the two adsorbents; silk fibroin and clinoptilolite, on the crude extract of the grape skin and olive leaf has been tried to be determined.

Olive leaves are rich in polyphenols, especially in oleuropein, rutin, verbacoside, apigenin-7-glucoside and luteolin-7-glucoside (Altiok et al., 2008; Baycin et al., 2007; Savournin et al., 2001; Garcia et al., 2000). The concentration of polyphenolic compounds in olive leaf changes depending on the quality, origin and variety (Campeol et al., 2003) of the plant material. Recent experimental and theoretical studies indicated that OLCE (olive leaf crude extract) has anti-HIV activity, antidiabetic effect (Eidi et al., 2009), antihypertensive property (Perrinjaquet-Moccetti et al., 2008), anti-atherosclerotic effect (Wang et al., 2008) and plasma lipid peroxidation product decreasing effect (Andreadou et al., 2006). Oleuropein is the most abundant polyphenol in olive leaves, which has been used in a number of medical treatments (Garcia et al., 2000).

Grape skin is a good source for *trans*-resveratrol, but it contains many other polyphenols including gallic acid, (+)-catechin, (-)-epicatechin, rutin, kaempferol and quercetin (Yu et al., 2005; Pinelo et al., 2006). Since gallic acid, (+)-catechin and (-)-epicatechin are polar polyphenols, they are soluble in water. On the contrary, rutin, *trans*-resveratrol, kaempferol and quercetin are not soluble in water, but they are soluble in 40% ethanol (Yu et al., 2005). Thus, due to the significant differences between the

polarities of polyphenols, separation of these compounds from each other may be accomplished based on that property.

Silk fibroin possesses a novel adsorbent property for polyphenols. Silk fibroin is an insoluble protein and has a well-defined composition, for this reason; it is preferred in some adsorption studies. So far, silk fibroin has not been used as an adsorbent for phytochemicals as it is known from the literature. Two studies by us indicate potential use of it as a novel adsorbent. Baycin et al. (2006) investigated the use of silk fibroin to adsorb oleuropein from olive leaf extract. In another study, Altıok et al. (2008) used silk fibroin to recover the proanthocyanidin from grape seed extract. Extraction of polyphenols from olive leaves by using different solvents and their aqueous forms, fractionation of polyphenols, especially oleuropein, were performed with silk fibroin filled column and this study was recently published (Altıok et al., 2008).

Clinoptilolite is very abundant in Turkey and has many applications because of its favourable properties, such as good adsorption property, ion-exchange property and molecular sieve property. Additional to that, recently, extensive researches have been performed on the application of clinoptilolite for medical purposes, in that clinoptilolite can be used for its antibacterial property, anticarcinogenic property and for the essential element supplementation and relevantly toxic compounds removing property. As we know from the literature, it is the first time that Gördes region natural clinoptilolite was used as a novel adsorbent to adsorb flavonoids from olive leaf and grape skin. Together with the beneficial health effects of clinoptilolite, this novelty may result in new innovative products for pharmaceutical industry.

The aim of this study was to selectively isolate the plant source biologically active compounds from both grape residues and olive leaves. After achieving the highest yields in extraction, adsorption studies were performed using two novel adsorbents; silk fibroin and clinoptilolite. Main phenolic compounds in these extracts were determined by HPLC analysis and quantitative analyses were performed by external calibration curve of each compound. The mixture of standard solutions of these standard compounds was prepared and batch adsorption studies were performed in order to determine the selectivity of the each adsorbent. The adsorption behaviours of these two adsorbents against *trans*-resveratrol were extensively studied and effects of many parameters were investigated. Selective separation of *trans*-resveratrol was achieved and model equations were used to explain the adsorption mechanisms. Column studies were performed with an experimental setup developed, including solid phase extractor

(SPE), HPLC and fraction collector, to optimize the parameters, such as adsorbent amount, flow rate, initial concentration. On an industrial scale, the optimization of these parameters and other operating conditions is very important for the economy of the process and can be accomplished with the help of reliable mathematical models. So, numerous mathematical models were used to determine the optimum operating conditions. Finally, the biological activity tests such as antioxidant activities, antimicrobial activities and cytotoxic effects of characterised flavonoid compounds and isolated fractions were performed in order to exhibit the importance of selective isolation.

CHAPTER 2

PHYTOCHEMICALS

Phytochemicals, which are non-nutritive plant chemicals, constitute a heterogeneous group of substances. In general, the plant chemicals that protect plant cells from environmental hazards such as pollution, stress, drought, UV exposure and pathogenic attack are called as phytochemicals. Recently, it is clearly known that they have roles in the protection of human health, when their dietary intake is significant. These compounds are known as secondary plant metabolites and have biological properties such as antioxidant activity, antimicrobial effect, modulation of detoxification enzymes, stimulation of the immune system, decrease of platelet aggregation and modulation of hormone metabolism and anticancer property. There are more than thousand known and many unknown phytochemicals. It is well-known that plants produce these chemicals to protect themselves, but recent researches demonstrate that many phytochemicals can also protect human against diseases. Because of this property, many researches have been performed to reveal the beneficial health effects of phytochemicals. Phytochemicals are not essential nutrients and are not required by the human body for sustaining life, but have important properties to prevent or to fight some common diseases.

2.1. Classification of Phytochemicals

The exact classification of phytochemicals could have not been performed so far, because of the wide variety of them. Flavonoids, flavones, glucosides and secondary plant metabolites are some of the phytochemicals can be widely seen in plants. The classification of phytochemicals can be done considering their ring structure and the number of carbon atoms substituting the ring and linking them together (Table 2.1).

Phenolic phytochemicals are the largest category of phytochemicals and the most widely distributed in the plant kingdom. The three most important groups of dietary phenolics are flavonoids, phenolic acids, and polyphenols (Figure 2.1).

Flavonoids are the largest group of plant phenols and the most studied (Balasundram et al., 2006). Phenolic acids form a diverse group that includes the widely distributed hydroxybenzoic and hydroxycinnamic acids. Phenolic polymers, commonly known as tannins, are compounds of high molecular weight that are divided into two classes: hydrolyzable and condensed tannins.

Table 2.1. The major classes of phenolic compounds in plants

Number of Carbon atoms	Basic skeleton	Class
6	C ₆	Simple phenols Benzoquinones
7	C ₆ -C ₁	Phenolic acids
8	C ₆ -C ₂	Acetophenones Tyrosine derivatives
9	C ₆ -C ₃	Hydroxycinnamic acid Coumarins
10	C ₆ -C ₄	Naphthoquinones
13	C ₆ -C ₁ -C ₆	Xanthenes
14	C ₆ -C ₂ -C ₆	Stilbenes
15	C ₆ -C ₃ -C ₆	Flavonoids
18	(C ₆ -C ₃) ₂	Lignans
30	(C ₆ -C ₃ -C ₆) ₂	Biflavonoids
N	(C ₆ -C ₃ -C ₆) _n	Condensed tannins

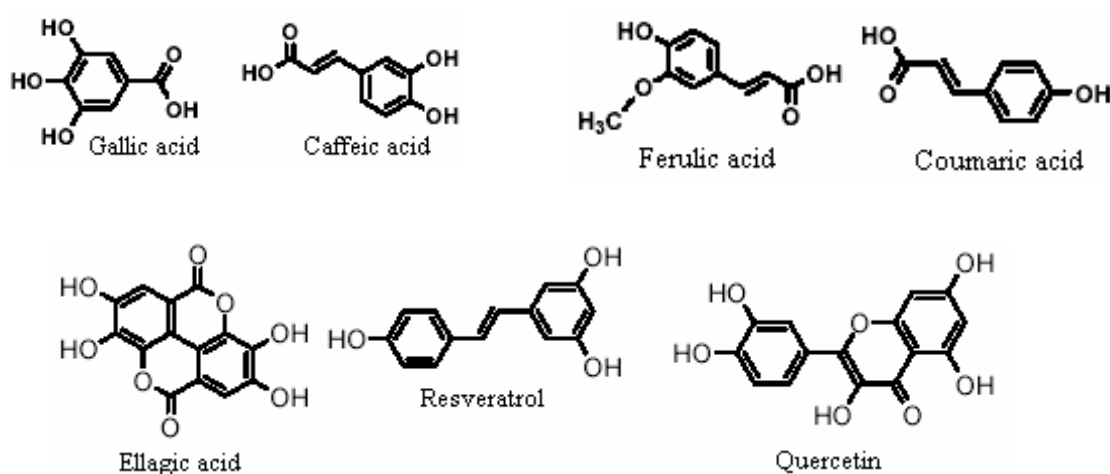


Figure 2.1. Common simple phenol and flavonoids in plants.

2.2. Flavonoids

The flavonoids are members of a class of natural compounds that recently has been the subject of considerable scientific and therapeutic interest. The flavonoids appear to have played a major role in successful medical treatments of ancient times, and their use has persisted up to now. Flavonoids are ubiquitous among vascular plants and occur as aglycones, glucosides and methylated derivatives. More than 5000 flavonoids have been described so far within the parts of plants normally consumed by humans and approximately 650 flavones and 1030 flavanols are known (Pretorius, 2003). Small amount of aglycones (i.e., flavonoids without attached sugar) are frequently present and occasionally represent a considerably important proportion of the total flavonoid compounds in the plant.

Table 2.2. Common flavonoids and common foods that contain them

Flavonoid	Foods, oils and beverages
Quercetin	onion, red apple, lettuce, broccoli, cranberry, berries, olive oil, tea, red wine
Myricetin	cranberry, grapes, red wine
Kaempferol	endive, leek, broccoli, radish, grapefruit, tea
Catechin, Epicatechin, their gallate forms	grapes, green and black tea, red wine
Cyanidin	cherry, raspberry, strawberry, grapes
Proanthocyanidin	red wine, red grapes
Hesperidin, naringin	citrus fruits
Apigenin	apple skins, celery, parsley
Resveratrol	fruit skins, berries

There is strong evidence from observational epidemiology that fruits and vegetables containing flavonoids in the diet are associated with a lower incidence of various cancers (Collins, 2005). Because of this, the idea has developed that it is the antioxidants in these foods that are the effective preventive agents. This is an attractive hypothesis; it is known that free radicals released during respiration can damage DNA, which results in mutation and consequently results in cancer. This damage can be prevented by the consumption of fruits and vegetables, which contain substantial

amounts of various natural compounds with antioxidant properties. These natural compounds scavenge free radicals and as a result reducing the degenerative effects of them. The most abundant flavonoids in fruits, vegetables and herbs are given in Table 2.2. Quercetin is the mostly seen flavonoids in apple, broccoli, berries, olive oil etc. Beverages such as teas and red wine, made from plant foods, have particularly high concentrations of certain flavonoids. Flavonoids also occur in nuts, seeds and legumes. Flavonoids have characteristic C₆C₃C₆ chemical structure (Figure 2.2).

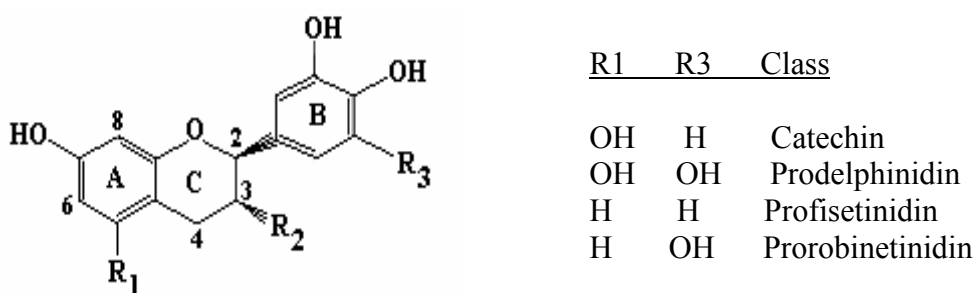


Figure 2.2. The basic unit of flavonoids.

The number of hydroxy groups and the presence of a 2,3-double bond and orthodiphenolic structure enhance antiradical and antioxidative activity of flavonoids (Tapas et al., 2008). The glycosylation, blocking the 3-OH group in C-ring, lack of a hydroxy group or the presence of only a methoxy group in B-ring has a decreasing effect on antiradical or antioxidative activity of these compounds (Tapas et al., 2008). Tannins show strong antioxidative properties because of the high number of OH groups. Some tannins in red wine or gallate esters were proved to have antioxidative effect in vivo. The numbers of hydroxy groups connected with the aromatic ring, in ortho or para position relative to each other, enhance antioxidative and antiradical activity of phenolic acids (Tapas et al., 2008).

Figure 2.3 represents major flavonoids' structures. The six-membered ring condensed with the benzene ring is either -pyrone (flavones (1) flavonols (3)) or its dihydroderivative (flavanones (4) and flavan-3-ols (5)). The position of the benzenoid substituent divides the flavonoids into two classes: flavonoids (1) (2-position) and isoflavonoids (6) (3-position). Most flavonoids occur naturally associated with sugar in conjugated form and, within any one class, may be characterized as monoglycosidic, diglycosidic, etc. The glycosidic linkage is normally located at position 3 or 7 and the

carbohydrate unit can be L-rhamnose, D-glucose, glucorhamnose, galactose or arabinose (Tapas et al., 2008).

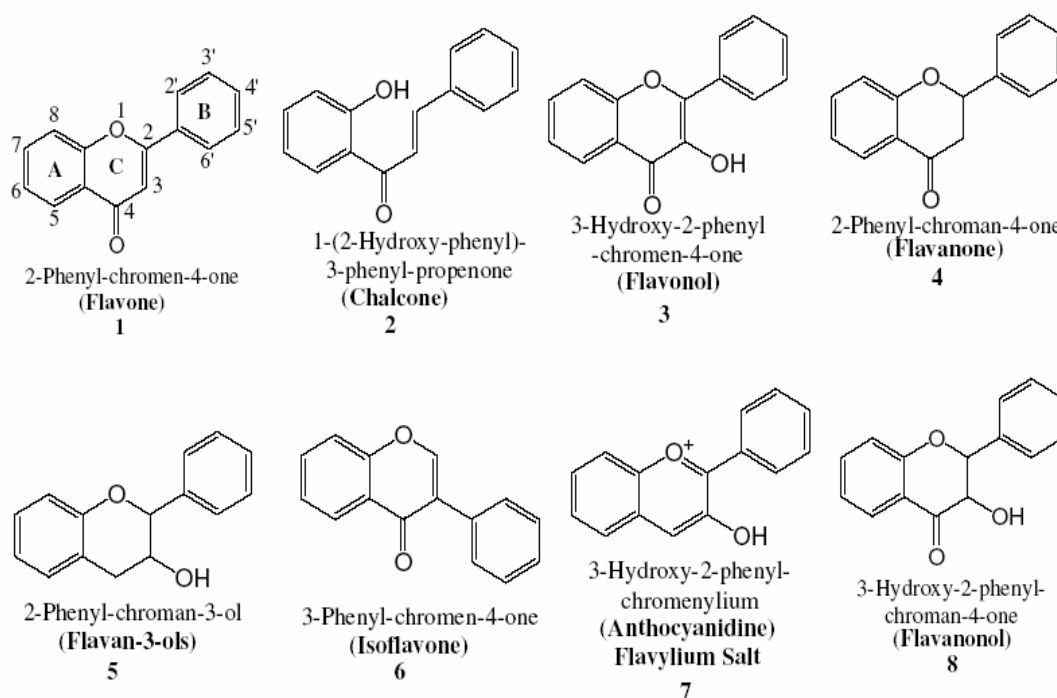


Figure 2.3. Chemical structures of some representative flavonoids.

2.3. Antioxidant Properties and Health Effects of Phytochemicals

Phytochemicals are important because of their high antioxidant activities. For this reason, they are widely used as food or dietary supplements.

Antioxidants can be classified within two classes as synthetic and natural. Among the synthetic types, the most frequently used to preserve food are butylated hydroxyanisole (BHA), butylated hydroxytoluene (BHT), propyl gallate (PG) and tert-butyl hydroquinone (TBHQ). For the same purpose, tocopherol and ascorbic acid can be widely used as natural antioxidants. Several reports reveal that BHA and BHT could be toxic (Moure et al., 2001). Additionally, the use of natural antioxidants such as ascorbic acid and tocopherols is limited because of higher manufacturing costs and lower efficiency of them (Moure et al., 2001). For these reasons, with the increasing consciousness of consumers with regard to food additive safety, a need for identifying alternative natural and probably safer sources of food antioxidants are required. The growing interest in the substitution of synthetic food antioxidants by natural ones has

focused research on vegetable sources and the screening of raw materials for identifying new antioxidants.

Beside the antioxidant capacities of them, several studies have been carried out in order to investigate their potential health effects. (Moure et al., 2001). In addition to antioxidant activity, other biological properties such as anticarcinogenicity, antimutagenicity, antiallergenicity and antiaging activity have been reported for phytochemicals. Their use as chemopreventive agents by inhibiting radical generation has been suggested since free radicals are responsible for DNA damage and radical scavengers are probably important in cancer prevention (Moure et al., 2001).

2.4. Potential Sources of Phytochemicals

The processing of plant foods results in the production of by-products that are rich sources of bioactive compounds, including phenolic compounds (Altiok, 2003). By-products of plant food processing represent a major disposal problem for the industry concerned, but they are also promising sources of compounds which may be used because of their favourable properties.

2.4.1. Grape Pomace

Phenolic compounds with antioxidant activity have been identified in several agricultural by-products, such as grape pomace. Grapes are the world's largest fruit crop with more than 60 million tons produced with sales of >US\$ 100 billion (Rayne et al., 2008), annually. About 80% of the total crop is used in wine making, and generates large quantities of wastes (grape pomace), containing grape seeds, skins and stems, represents approximately 20% of the weight of grapes processed. From these data it can be calculated that grape pomace amounts to more than 9 million tons per year (Schieber et al., 2001). Grape seed in pomace is a good source of proanthocyanidins, which exhibits high antioxidant capacity (Altiok, 2003) and produced as a dietary supplement.

Beside the seeds, grape skins in pomace represent a potentially important global source of *trans*-resveratrol. *Trans*-resveratrol, as a biologically active compound, belongs to the phytoalexins, is one of the secondary plant metabolites. Phytoalexins are

able to inhibit the progress of fungal infection, a property which has earned their inclusion in the class of plant antibiotics (Soleas et al., 1997).

There are increasing amount of publication indicating *trans*-resveratrol's biological activities, such as antiinflammatory, antimicrobial, antioxidant and mostly cytotoxic activities (Figure 2.4).

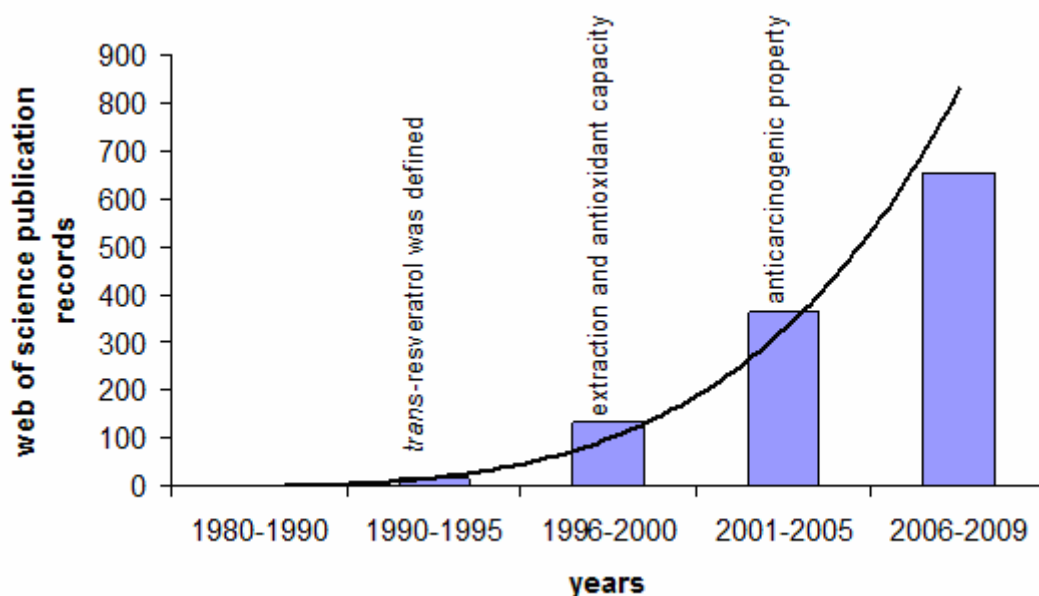


Figure 2.4. Number of publications in web of science related with the *trans*-resveratrol.

In the early years of 90s *trans*-resveratrol was firstly defined in red wines and following years in 90s, high antioxidant activity of it was investigated. Following, extensive researches had been performed on the extraction of *trans*-resveratrol from red wine and by-products of grape industry. *Trans*-resveratrol's antioxidant and vasorelexant activities (Aggarwal et al., 2004) make it effective on cardioprotective substance. Extensive research during the last two decades has suggested that, besides cardioprotective effects, it also exhibits anticancer activities. After exploring its cytotoxic activity, significant increase on researches has been seen. Resveratrol was shown to inhibit cellular processes associated with tumor initiation, promotion and progression (Jang et al., 1997). In other studies, resveratrol inhibited the proliferation of breast, oral, liver, prostate and colon cancer cell lines in a dose- and time-dependent manner (Mgbonyebi et al., 1998; Lu and Serrero, 1999; Wu, 1999; Schneider et al., 2000). In recent years, cytotoxic mechanisms of it has been tried to understand. Antitumor activity of resveratrol can be explained by the ability of it to inhibit the

cyclooxygenase (COX) activity. This inhibitory activity is relevant to cancer chemoprevention because COX catalyzes the conversion of arachidonic acid to pro-inflammatory substances such as prostaglandins, which can stimulate tumor cell growth (Pervaiz, 2004; Jang et al., 1997). Still, there is increasing amount of articles published.

Grape skin is a good source for *trans*-resveratrol, but it contains many other polyphenols including gallic acid, (+)-catechin, (-)-epicatechin, rutin and quercetin (Yu et al., 2005; Pinelo et al., 2006).

2.1.4.2. Olive Leaves

The **Olive** (*Olea europaea*) is a species of a small tree in the family Oleaceae, native to the coastal areas of the eastern Mediterranean Basin, from Lebanon, Syria and the maritime parts of Turkey and northern Iran at the south end of the Caspian Sea (wikipedia). Its fruit, the olive, is of major agricultural importance in the Mediterranean region as the source of olive oil.

The fruit is a small drupe 1–2.5 cm long, thinner-fleshed and smaller in wild plants than in orchard cultivars. Olives are harvested at the green stage or left to ripen to a rich purple colour (black olive).

The olive tree is an evergreen. It is short and squat, and rarely exceeds 8–15 meters in height. The silvery green leaves are oblong in shape, measuring 4–10 cm long and 1–3 cm wide. The trunk is typically gnarled and twisted. For careful cultivation, the trees are pruned. The pruning preserves the flower bearing shoots of the preceding year, while keeping the tree low enough to allow the easy gathering of the fruit. The pruned leaves are generally assumed as “nuisance” and are burned. Leaves are also one of the main by-products of the olive oil industry.

Olives are the most extensively cultivated fruit crop in the world. Cultivation area tripled from 2.6 to 8.5 million hectares between 1960 and 2004. The ten largest producing countries, according to the Food and Agriculture Organization, are all located in the Mediterranean region and produce 95% of the world's olives (Table 2.3.).

Olive leaves are rich in polyphenols, especially in oleuropein, rutin, verbacoside, apigenin-7-glucoside and luteolin-7-glucoside (Altıok et al., 2008; Baycin et al., 2007; Garcia et al., 2000; Savournin et al., 2001). The concentration of polyphenolic compounds in olive leaf changes depending on the quality, origin and variety (Campeol

et al., 2003) of the plant material. The divergence of content of bioactive components in the extract may also result from various factors such as cultivation areas, harvesting season, climatic conditions, collection, parts that used for extraction, washing, drying, handling, selected extraction methods, used drying method of the extract and storage conditions. These variations directly influence the biological and pharmacological activities of the extract. Therefore, in order to ensure the consistency of benefits, it is necessary to clarify the antioxidant capacity and antimicrobial activity of the extract with quantitative determination of the major bioactive components present in the extract.

Table 2.3. Olive producing countries
(Source: Wikipedia, 2010)

Rank	Country/Region	Production (in tons)	Cultivated area (in hectares)	Yield (q/Ha)
–	World	17317089	8597064	20.1
1	Spain	6160100	2400000	25.7
2	Italy	3149830	1140685	27.6
3	Greece	2300000	765000	31.4
4	Turkey	1800000	594000	30.3
5	Syria	998988	498981	20.0
6	Tunisia	500000	1500000	3.3
7	Morocco	470000	550000	8.5
8	Egypt	318339	49888	63.8
9	Algeria	300000	178000	16.9
10	Portugal	280000	430000	6.5
11	Lebanon	275000	250000	6.5

Recent experimental and theoretical studies found that OLCE (olive leaf crude extract) has anti-HIV activity by blocking the HIV virus entry to host cells (Lee-Huang et al., 2007; Bao et al., 2007). OLCE have also the antidiabetic effect in normal and streptozotocin-induced diabetic rats (Eidi et al., 2009). The oral administration of the OLCE for 14 days significantly decreased the serum glucose, total cholesterol, triglycerides, urea, uric acid, creatinine, aspartate amino transferase and alanine amino

transferase while it increased the serum insulin in diabetic rats but not in normal rats. A comparison was made between the action of olive leaves extract and glibenclamide (600 microgram/kg), a known antidiabetic drug. The antidiabetic effect of the extract was more effective than that observed with glibenclamide (Eidi et al., 2009). The antihypertensive property of OLCE was tested as a food supplement. It was clearly seen that it reduces hypertension by regulating blood pressure and also lowered cholesterol level in rats (Perrinjaquet-Moccetti et al., 2008). OLCE also exhibits the anti-atherosclerotic effect. Wang et al. (2008) explained the anti-atherosclerotic effect by the mechanism of suppressed inflammatory response. The efficacies of oleuropein on infarct size, oxidative damage and the metabolic profile in rabbits was investigated (Andreadou et al., 2006). It was concluded that, oleuropein decreased the plasma lipid peroxidation product and protein carbonyl concentrations compared with the control groups, in which these factors increased relative to baseline due to ischemia and reperfusion. Oleuropein, for 3 or 6 w, reduced the infarct size, conferred strong antioxidant protection and reduced the circulating lipids (Andreadou et al., 2006).

The nutraceutical utility of other bioactive compounds present in olive leaves in high amounts such as verbacoside, apigenin-7-glucoside and luteolin-7-glucoside has been studied. Thus, verbacoside has been used to repair brain's oxidative damage caused by heroin consumption (Zheng et al., 2005), apigenin-7-glucoside to fight against Alzheimer's (Patil et al., 2003) or liver diseases (Zheng et al., 2005) and luteolin-7-glucoside to avoid the abnormal proliferation of aortic vascular smooth muscle cells that is a common cause of pathogenesis such as atherosclerosis and restenosis (Kim et al., 2006). All these effects prove the antioxidant and nutraceutical capacities of olive leaf extracts in which bioactive compounds show a synergistic activity (Benavente-Garcia et al., 2000; Paiva-Martins et al., 2003).

OLCE shows important antimicrobial activity against *Staphylococcus aureus*, *Pseudomonas aeruginosa*, *Klebsiella pneumoniae*, *Escherichia Coli* (Bayçın, 2006), *Campylobacter jejuni* and *Helicobacter pylori* (Sudjana et al., 2009).

Bayçın, (2006), investigated also the antioxidant activity of OLCE and she found the capacity as 4.36 mmol Trolox Equivalent Antioxidant Capacity (TEAC)/g olive leaf. In another study, Briante et al., (2002), were tried to separate polyphenolic compounds from each other and collected polyphenol rich eluates. The eluates possess a higher concentration of simple phenols, characterized by a stronger antioxidant capacity, than those available in extra virgin olive oils and in many tablets of olive leaf

extracts, commercially found as dietetic products and food integrators (Briante et al., 2002).

It is important to denote that bioactive compounds in OLCE exhibit different pharmacological properties and biological activities. Thus, in order to understand which compound is responsible for the activity, separation of compounds from the crude extract is crucial. The behaviour of single compound may be differentiating from the form together with the other active compounds: they may behave as synergetic or antagonistic effect. Dang et al. (2007) were tried to enrich oleuropein from olive leaves with macroporous resin D-101. As a result, the contents of oleuropein increased from 5% to 21.6% in the solid, with 88.6% of recovery rate at optimized conditions. On the other hand, Lee et al. (2009) tried to obtain enriched-polyphenolic extract by changing the extraction solvent and concluded that antioxidant activity significantly affected by the type and amount of bioactive compounds found in the extract.

CHAPTER 3

EXTRACTION AND DETECTION OF BIOACTIVE COMPOUNDS FROM PLANTS

Solid-liquid extraction finds numerous applications in the industry. In this chapter, the extraction of bioactive compounds from plant is discussed together with the effects of extraction methods, solvent type, particle size, temperature and extraction time on the extraction efficiency of the grape skin extract and olive leaf extract. It is also important to characterize the bioactive compounds in crude extract in order to investigate the selectivity and efficiency of the extraction method and extraction parameters. For this purpose, the high performance liquid chromatography (HPLC) characterizations of major bioactive compounds in olive leaf and grape skin are also included in this chapter.

3.1. Solid-Liquid Extraction (SLE)

Solid-liquid extraction or leaching occurs with the selective dissolution of one or more solutes from a solid matrix by a liquid solvent. Most of the bulk of the biomass exists as fairly inert, insoluble, and often polymeric material, such as cellulose of plants. The first step of the extraction is therefore to release and solubilize the smaller secondary metabolites in the matrix, resulting in the initial extract. Since there are many plant secondary metabolites in different plants, to choose proper extraction method and solvent to be used and optimizing operating parameters become to be critical points. From the industrial point of view, there are some factors that should be evaluated, because they influence the rate of extraction:

- *Preparation of the solid:* In plant, the cell structure is an important factor that needs to be considered. Although the solute can be on the surface of the cell, in most of the cases it is stored in intracellular spaces, capillaries, or cell structures. This way, the success of the solvent extraction strongly depends on the solid condition. One of the pretreatment steps that must be considered is the grinding of the raw material.

Grinding before solvent extraction promotes an increase of the contact area between the solvent and the solid matrix. Besides that, in most cases this step enhances the contact between solvent and solute by breaking the cell structures.

- *Diffusion rate:* Because of the complexity of the cell structure and the existence of porous and different compartments in the cell, the diffusivity of biological materials has to be evaluated as effective diffusivity. The effective diffusivity also depends on the composition and on the position of the solute in the solid material.

- *Temperature:* Normally, elevated temperature is attractive in terms of extraction process enhancement. Higher temperatures promote an increase of the solute's solubility in the solvent, increasing the solute diffusion rate into the solvent bulk, leading to a higher mass transfer rate. However, for the extraction of phytochemicals from the plants, the use of elevated temperatures can generate undesirable reactions such as the degradation compounds and losing their biological activities.

- *Solvent choice:* Although the choice of extraction method may have a significant effect on the quality of the extract, the solvent used provides the most obvious means of influencing the qualitative composition of the extract.

Some of the general properties of the solvent that should be considered when selecting the most appropriate extraction solvent include the ability of the solvent to dissolve the target compounds, ease of removal, cost, inertness, toxicity and flammability. Table 3.1 shows the solvent characteristics that should be considered for the extraction from natural matrices.

As expected, the matrix and the target compounds have perhaps the most significant effect on the selection of suitable extraction solvent. Low-polarity solvents yield more lipophilic compounds, whereas alcohols extract both apolar and polar compounds, and water extracts only polar components from the sample. Because of the toxicity of some organic solvents, there are some restrictions to their use in industry. In terms of human consumption, the presence of some solvents, such as acetone, ethanol, ethyl acetate, 1-propanol, 2-propanol, methanol and propyl acetate are acceptable in small residual percentages, according to good manufacturing practice (Meireles, 2009). Thus, the removal of solvent from the extract is very important to achieve the limits indicated in national legislation and it should be easily removed in economic point of view.

Table 3.1. Solvent characteristics for natural product extraction

Characteristic	Effect in the Process
Selectivity	Solvent selectivity guarantees the extract purity and solubilizes the target compounds
Compatibility with solute	The solvent should not react with the target compounds
Chemical and thermal stability	The stability of the solvent at operating extraction conditions must be assured not to alter the final extract
Low viscosity	To keep the extraction rate higher, lower viscosity is necessary to increase the diffusion coefficient
Ease of recovery	Economic aspects must be considered, and lower boiling point solvents are easily recovered and reused
Low flammability	According to the process needs and safety aspects, flammable solvents must be avoided
Low toxicity	Natural products require the absence of solvent traces and toxicity, besides the worker exposition
Regulatory issues	According to the pharmaceutical and food industries, environmental regulations should be considered so as to avoid process irregularities
Low cost	Economic aspects can contribute to the final product quality

Several criteria have been used in evaluating the effectiveness of the extraction method and the suitability of a solvent for a particular extraction procedure. The most commonly encountered criterion is extraction yield, i.e. the total yield or the yield of a certain target compound or compounds. In taxonomic studies and general screening purposes, however, the qualitative composition of the extract may be the decisive factor over yield in selecting the solvent of choice. Yet another important and emerging criterion for solvent selection is based on bioactivity tests, i.e. the extracts are subjected to biological tests including antioxidant activity, antimicrobial activity and cytotoxic activity. Based on the responses in the bioactivity tests, the solvent giving the highest recoveries is chosen and the extract is further purified to isolate the active component.

- *Solid material humidity*: The water in the solid material can compete with the extraction solvent for the solute's dissolution, affecting the mass transfer. Furthermore, it causes deterioration, spoilage and consequently biological activity loss. Thus, in most of the cases the material is dried under conditions that do not cause degradation of the compounds.
- *Solvent-solid ratio*: The solvent-to-solute ratio is always an important variable for the extraction of compounds in general. This is the parameter that determines the amount of solvent used, and it is always related to economic aspects.

3.2. Mass Transfer: Equations and Kinetics

Solvent extraction is the extraction of the soluble material inside the solid matrix using a specific solvent. The extraction mechanism can be described in the following steps: First, the solvent must be transferred onto the solid surface. After that, the solvent penetrates into the solid matrix by diffusion. The solute is dissolved until a solubility limitation depending on the type and nature of the solvent. It is important to notice that the solute plus solvent form a diluted solution in any practical application. The solution containing the solute diffuses to the surface by effective diffusion. At the end, the solution is transferred from the surface to the bulk solution by natural or forced convection.

The rate of dissolution of a solute in the solvent of extraction is controlled by the rate of mass transfer of the solute from the solid matrix to the liquid. The transfer of the solute inside the solid particle occurs because of the concentration gradient in the solid-liquid interface, and it can be characterized by the effective diffusion. The equation that describes this phenomenon is based on the Fick's law and is given by;

$$\frac{N_A}{A_m} = -D_{BA} \frac{dC_A}{dz} \quad (3.1)$$

where N_A is the rate of dissolution of the solute A in the solution (kgmol/s), A_m is the area of the solid-liquid interface (m^2), D_{BA} is the diffusivity of solute in the solvent (m^2/s), C_A molar concentration of solute A in the solution (kgmol A/m^3), and z is the distance inside the porous of the solid matrix (m).

It is assumed that, on the surface of the solid particle, the transfer of solute occurs by molecular transport and there is essentially no resistance in the solid phase like as a pure material (Geankoplis C.J., 1993). In this step, the rate of mass transfer can be expressed by the following equation and it can be used for the case when the diffusion in solid is very rapid.

$$N_A = A_m k_L (C_{AS} - C_A) \quad (3.2)$$

where C_{AS} is the saturation solubility of the solute A (kgmol/m³) and k_L is mass transfer coefficient (m/s). By a material balance, the rate of accumulation of A in the solution is equal to the mass flux of A times the area.

$$\frac{VdC_A}{dt} = N_A = A_m k_L (C_{AS} - C_A) \quad (3.3)$$

Integration Eq. (3.3) with the initial condition, $C_A = C_{A0}$ at $t = 0$ to at $t = t$ $C_A = C_A$,

$$\int_{C_{A0}}^{C_A} \frac{dC_A}{C_{AS} - C_A} = \frac{A_m k_L}{V} \int_{t=0}^t dt \quad (3.4)$$

$$u = C_{AS} - C_A, \quad du = -dC_A$$

$$\int \frac{dC_A}{C_{AS} - C_A} = - \int \frac{du}{u} = -\ln u = -\ln(C_{AS} - C_A) \Big|_{C_{A0}}^{C_A} = -\ln \frac{C_{AS} - C_A}{C_{AS} - C_{A0}}$$

$$-\ln \frac{C_{AS} - C_A}{C_{AS} - C_{A0}} = \frac{A_m k_L}{V} t \Big|_0^t$$

$$\frac{(C_{AS} - C_A)}{(C_{AS} - C_{A0})} = e^{-(k_L A_m / V)t} \quad (3.5)$$

The solution approaches a saturated condition exponentially. Mass transfer rate may change depending on;

- If external surface very irregular, surface area will increase;
- If the soluble material forms a high proportion of the total solid, disintegration of the particle may occur.
- If the solid completely dissolving, the interfacial area changes markedly.

Plant material generally consists of cellulose, sugars, oily parts with lower amount of complex mixture of bioactive compounds. Thus, it is not possible to see neither the totally dissolving compound nor the high proportion of soluble material in plants.

3.3. Extraction Methods

At the present time, there are also a number of non-conventional extraction methods in use that are all, in principle, solid-liquid extractions (SLE) but which introduce some form of additional energy to the process in order to facilitate the transfer of solutes from sample to solvent. These methods include ultrasonic extraction, microwave-assisted extraction and pressurized liquid extraction. Forced-flow solid-liquid extraction techniques, such as medium-pressure solid-liquid extraction and rotation planar extraction, are methods in which the extraction solvent is forced through the sample bed either by means of pressure or by centrifugal force, respectively, thus increasing the efficiency of the extraction process (Yrjönen 2004). The main advantage of these non-conventional methods compared to conventional SLE methods is the increased extraction efficiency, which leads to increased yields and/or shorter extraction times.

3.4. Extraction of Olive Leaf Antioxidants

There is limited number of studies on the optimization of the extraction of olive leaf polyphenols. In one of the study, traditional solvent extraction method was used to extract olive leaf antioxidants. Olive leaf polyphenols were extracted with either methanol, water or various mixtures of methanol and water (Ryan et al., 2001). However, the toxicity of solvent is important point for the extracted polyphenols. For this purpose food grade ethanol should be chosen as an extraction solvent. Recently, an experimental design (i.e., 2³ full factorial design) was applied to optimize the extraction

conditions by changing the pH of the medium, the extraction time and the ethanol concentration of the solution (Mylonaki et al., 2008). They concluded that, the maximum phenolic yield was achieved by the conditions as pH 2, 60% ethanol and for 5 h extraction time. Only three levels of ethanol concentration were chosen as 40, 50 and 60% (v/v). However, in most of the studies 80% of ethanol was indicated to be the best to extract most of the polyphenolic compounds.

3.5. Extraction of Grape Skin Polyphenols

Many extraction methods were investigated in literature to extract the *trans*-resveratrol from grape and grape by-products. Table 3.1 summarizes the extraction studies of *trans*-resveratrol from grape and polyganum cuspaditum. Recently, more detailed studies have been published on effective extraction of *trans*-resveratrol.

Table 3.2. Extraction methods and optimum extraction parameters studied in literature for *trans*-resveratrol

Extraction Method	Part used	Extraction conditions	Recovery	Advantages	Disadvantages	References
Pressurized liquid extraction method	Grape	40 atm, 150 °C	2.18 mg <i>trans</i> -resveratrol/kg grape			Pineiro et al., 2006
Ultrasonic Extraction	Peanut	80% Ethanol	0.71 mg/kg peanut	Short time	Avoid toxic solvents degradation	Chukwumah et al., 2009
	Grape cane	80% Ethanol 70% Ethanol dimethylformamide DMSO	3.2 mg/g dry weight (dw) 3.4 mg/g dw 3.8 mg/g dw 3.2 mg/g dw			Rayne et al., 2008
Microwave assisted extraction	Rhizma Polygoni Cuspidati	Short time, high Temperature	94% of the total extractable resveratrol	Short time	High operating cost toxic solvent, degradation	Du et al., 2007
	Rhizma Polygoni Cuspidati	1-butyl-3-methylimidazolium bromide	92.8%			
Solvent extraction	Grape berries Leave	Chloroform:ethyl acetate Ethanol:water (4:1) Ethanol:water (4:1)	1.92 µg/g dw berry 1.87 µg/g dw berry 4.15 µg/g dw leave	Operating cost	Requirement solvent removal, avoid toxic solvent	Calzarano et al., 2008
	Leaves	Ethanol:water (4:1)	4 µg/g dw leaf			Karacabey and Mazza, 2008
	Grape canes	%50-70 Ethanol, 83 °C,	4.25 mg/g dw			Lacopini et al., 2008
	Grape varieties, various part	Ethanol:water:HCL (70:29:1)	Skin: 0.25 mg/g dw			Romero-Perez et al., 2001
	Grape skin	80% Ethanol, 60 °C	24 µg/g dw			Vatai et al., 2008
	Grape berry	40% Ethanol, 60 °C	0.21 mg/g dw			
Supercritical Liquid Extraction (SLE)	Polygonum cuspidatum	30 mPa, 50 °C,	7.1 g/kg	Safe, no requirement of solvent removal	High pressure requirement, operation cost	Yu et al., 2005
	Grape skin	250 bars, 60 °C				

These studies have mainly focused on the extraction of *trans*-resveratrol. However, it is also very important to investigate the other bioactive compounds in grape skin. Those compounds exhibit additional health benefits and also they may act synergistically together with the *trans*-resveratrol.

In solvent extraction method, to extract the polyphenols from plants, ethanol, acetone and ethyl acetate alone or with water are effectively used (Moure et al., 2001). However, ethanol and water are the most widely employed solvents for toxicological and abundance reasons, respectively. Beside this, alcohols have ability to isolate a broader spectrum of apolar and polar compounds from the material. For this purpose, ethanol is preferable solvent to extract polar polyphenolic compounds, such as organic acids, (+)-catechin and (-)-epicatechin, together with the apolar compounds, such as rutin, quercetin and *trans*-resveratrol (Chafer et al., 2005). Since the activity depends on the polyphenol compounds and the antioxidant capacity, comparative studies for selecting the optimal solvent providing maximum antioxidant activity are required for each substrate (Moure et al., 2001).

Rayne et al. (2008) investigated the effect of solvent on the extraction yield of *trans*-resveratrol (Figure 3.1).

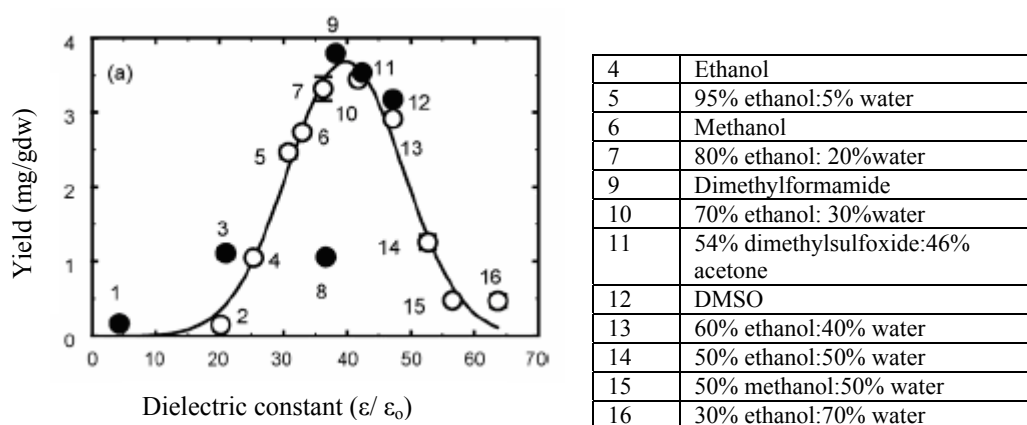


Figure 3.1. Effect of different solvents on extraction yields of *trans*-resveratrol from grape canes (Source: Rayne et al., 2008).

Although the highest extraction yield was obtained with dimethylformamide, the toxic nature of it limits the usages of it as for the solvents DMSO (dimethylsulfoxide) and methanol. Ethanol is the most appropriate solvent for the pharmaceutical applications.

Pineiro et al. (2006) studied the pressurized liquid extraction method at 40 atm and 150 °C with 3-5 cycles to extract *trans*-resveratrol from grape and 2.18 mg *trans*-resveratrol/kg grape was obtained. They claimed that extraction with pressurized liquid extraction method at high temperatures is favorable when compared with the classical extraction method since it accelerates the extraction of compounds from samples (Pinerio et al., 2006). However, Romero-Perez et al. (2001) indicated that *trans*-resveratrol decomposes at high temperature (>60 °C) in alcoholic solutions. This is also supported by the study of Liazid et al. (2007).

Despite the simple operating principle, there are several operating parameters that need to be controlled in order to obtain a sufficient extraction rate and yield. The most important parameters affecting the yield of the extraction procedure are the moisture content of the plant materials and temperature (Altiok, 2003).

Ultrasonic extraction takes advantage of the effective temperatures (which increase solubility and diffusivity) and pressures (which favor penetration and transport) at the interphase between the solvent solution subjected to ultrasonic energy and a solid matrix. Lower extraction time is the main advantage of this method. Cho et al. (2006) stated that the recovery yield of resveratrol from grape stem was significantly increased around 24-30% by comparing the traditional method ethanol/water solvent extraction.

Another way of increasing the efficiency of conventional extraction methods is to use microwave irradiation. Microwave-assisted extraction consists of heating the solvent in contact with the sample by means of microwave energy. The process involves disruption of hydrogen bonds, as a result of microwave-induced dipole rotation of molecules, and migration of the ions, which enhance penetration of the solvent into the matrix, allowing dissolution of the components to be extracted. The main advantages of microwave assisted extraction over the conventional extraction techniques are reduced solvent consumption, shorter operational times, moderately high recoveries, good reproducibility and minimal sample manipulation for extraction process. Microwave assisted extraction technique was used to extract *trans*-resveratrol from *Rhizma Polygoni Cuspidati* because the purposed technique was green, rapid and alternative to traditional method (Du et al., 2007). This method was successively used to recover 94% of the total extractable resveratrol in a short time period. However, Liazid et al. (2006) indicated that the stability of *trans*-resveratrol affected by the working temperature. It was significantly loose its stability above 100 °C. Thus, the usage of this method to

extract *trans*- resveratrol is limited because of the requirement of application of high temperature.

In recent years, the extraction method that has received increasing attention and many industrial applications in the isolation of natural products is supercritical fluid extraction (SFE), which is based on the properties of gases compressed and heated to a state above their critical pressure and temperature, at which no distinction between the gas and liquid phases can be discerned. SFE has several advantages over the conventional liquid-liquid and solid-liquid extraction techniques, e.g. the elimination of most of the organic solvents that may pose a safety risk during extraction, elimination of carry-over of the more or less toxic solvents in the final extracts, and the possibility of avoiding the detrimental effects of these solvents on the environment. The disadvantages of SFE include the low polarity of the most commonly used fluid, i.e. carbon dioxide, possible problems caused by the presence of water, unpredictability of the matrix effect and the need for specialized/expensive equipment. The practical aspects of SFE and its applications have been recently reviewed. Due to the low polarity of carbon dioxide it is best suited for the extraction of nonpolar compounds. SFE has been successfully applied to the extraction of (+)-catechin, (-)-epicatechin, rutin, quercetin and *trans*-resveratrol from grape skin (Chafer et al., 2005) by varying the pressure and temperature of the supercritical carbon dioxide. Beside this, the amount of polar modifiers, ethanol has also been found suitable for the extraction of more polar compounds such as flavanones; catechin and epicatechin.

There are many other factors such as type, species, origin, location, climate, environmental conditions, cultivation and pre- treatments of plant material directly affect the extraction yield. Beside these, the part of plant may include different type of plant secondary metabolites. For example, Careri et al. (2003) used different solvents and different parts of grape pomace to extract the *trans*-resveratrol and they noted that, highest yield of it was found at grape skin with pure acetone as an extraction solvent. Beside this, they found that grape pomace contains relatively very low amount of *trans*-resveratrol. On the other hand, Perez et al. (2001) stated that beside the importance of selection of proper solvent and part of the plant to be extracted, temperature and time had great importance during extraction. And they concluded that, the extractable *trans*-resveratrol from stem of the grape was highest with ethanol/water (80:20 v/v) solvent at 60 °C for 30 min. Although temperature generally shows a positive effect on extraction yields, elevated temperature might promote degradation of some target compounds.

3.6. Characterization of Crude Extract

Because of the wide spectrum of secondary metabolites present in many plants, there are many difficulties associated with measurements of them. Thus, many methods have been developed for the analysis of secondary metabolites such as phenolic acids, flavonoids and anthocyanidins. The majority of the methods reported for this purposes, are based on the HPLC separation of phenolics. The use of HPLC with UV and DAD detection is one of the good techniques for characterization and quantification of each phenolic compound from different samples, because HPLC with DAD detector shows good selectivity.

Grape skin contains many bioactive compounds such as *trans*-resveratrol, gallic acid, (+)-catechin, (-)-epicatechin, rutin and quercetin (Yu et al., 2005; Pinelo et al., 2006). Since gallic acid, (+)-catechin and (-)-epicatechin are polar polyphenols, they are soluble in water. On the contrary, rutin, *trans*-resveratrol and quercetin are not soluble in only water, but they are soluble in 40% ethanol (Yu et al., 2005). Thus, due to the significant differences between the polarities of polyphenols, polarity of mobile phases should be adjusted to detect polyphenols in grape skin. Gradient elution from HPLC column is favorable in this case. In literature, many studies have been performed to detect the phenolic components in plant extracts and various wavelength selections were made in HPLC methods. Phenolic acids are usually detected at 280 nm wavelength (Chafer et al., 2005; Zu et al., 2006). According to the study of Zu et al. (2006) quercetin, kaempferol were detected by HPLC-DAD system at 368 nm. On the other hand, *trans*-resveratrol and rutin are detected at 306 nm and 257 nm, respectively.

The HPLC analysis given in the Bayçın (2006) studies was used for the quantification of oleuropein and rutin. Other polyphenolic components, which are verbascoside, tyrosol, hydroxytyrosol, apigenin-7-glucoside, luteolin-7-glucoside, luteolin, and catechin, were identified according to the study of Garcia et al. (2000).

CHAPTER 4

SEPARATION OF BIOACTIVE COMPOUNDS: ADSORPTION

In this chapter, evaluating, improving and developing selective separation techniques of bioactive compounds from the olive leaf and grape skin crude extract is extensively discussed. Adsorption is the favorable technique for selective separation of active compounds. For this purpose, many adsorption studies for plant flavonoid compounds in literature are investigated and presented in this chapter. The properties of two novel adsorbents; clinoptilolite and silk fibroin, which are used to selectively separate bioactive compounds of olive leaf and grape skin in this study, are also included in this chapter. In order to understand the adsorption mechanism, the theories of solid-liquid adsorption systems are discussed and model equations are given to determine the mechanism. Additionally, dynamic column studies are mentioned and theoretical backgrounds of them are given.

4.1. Isolation or Selective Separation of Bioactive Compounds from Raw Plant Material

Plant bioactive compounds have been extensively studied and process steps in the production of them have become very important for the economy of the production process. Figure 4.1 summarizes the major process steps required for the searching, producing and selectively separating bioactive compounds from the raw plant material. After high yield extraction step, crude extracts are analyzed in order to determine their most important biological activity (i.e. antioxidant activity, antimicrobial capacity and cytotoxic activities etc.). Following the screening, further separations of bioactive compounds are performed in order to determine most bioactive compound. This step should be well developed for the selective isolation of high purity bioactive compound without losing its biological activity. Thus, isolation step has great importance, since all operating parameters (i.e. determination of high affinity adsorbent, optimising operating parameters, such as temperature, solid-liquid ratio, concentration, adsorbent

properties etc., loading & eluting parameters, and economy of the process) are investigated and it determines the parameters required for large scale production. Before the pilot-scale production of bioactive compound, column studies should be performed to optimize many operating parameters. Finally, for large scale production of high purity bioactive compound, each of these steps play crucial role for designing industrial scale production units. Final product can be used then for pharmaceutical purpose as a pure active drug compound, for food industry as a food additive/preservative and even for cosmetics' active compound.

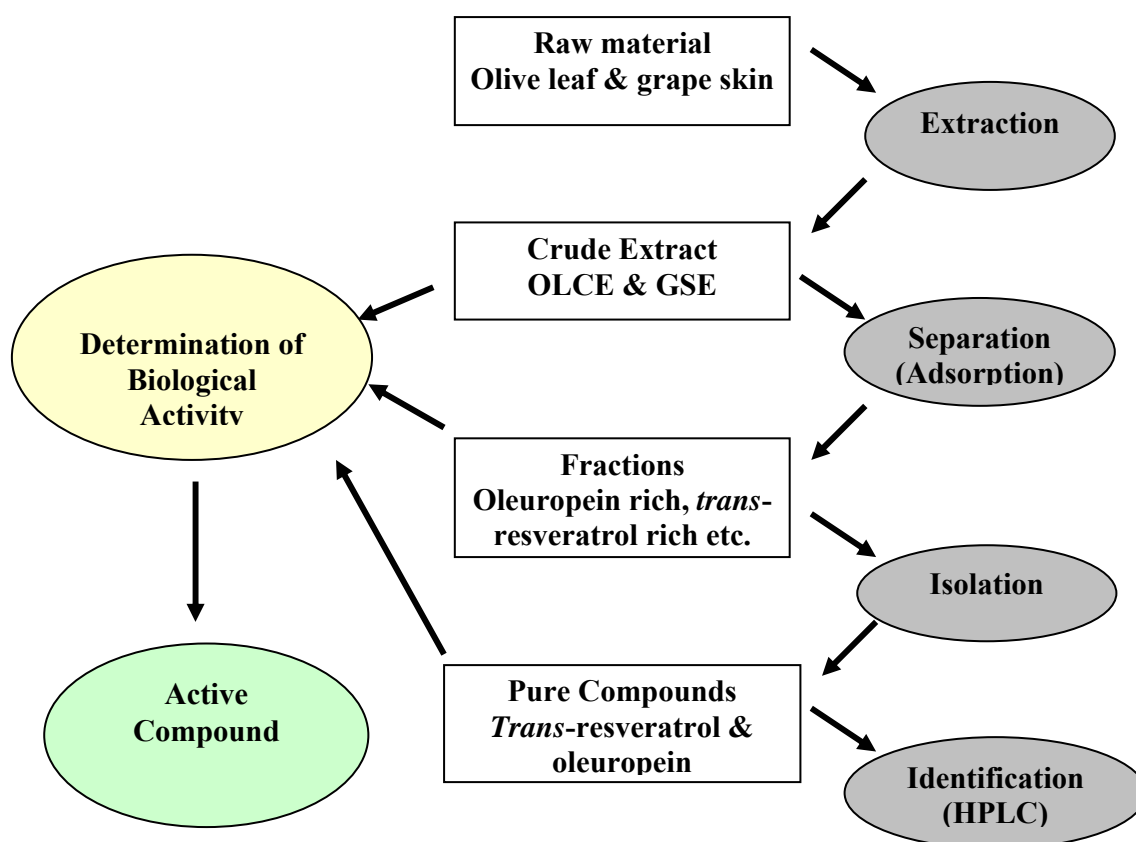


Figure 4.1. Diagram of active compound isolation procedures from raw plant material.

4.2. Adsorption

Removal of impurities is required for food, pharmaceutical or cosmetic applications. However, the simultaneous presence of different phenolic compounds could be desirable, since synergistic effects are favoured and expensive separation stages would be avoided. Several technologies have been proposed for concentration

and purification, including membrane separation, adsorption into activated carbon, solvent processing with conventional and supercritical solvents, and separation in LH-20 gels and polymeric resins.

Adsorption systems have been investigated to assess their suitability for application in the field of selective recovery of bioactive compounds. The relevant studies are summarized in Table 4.1. In almost all of the studies synthetic polymeric resins were used. Additional process step is required to recover adsorbed bioactive compounds after the adsorption process prior to use. However, with natural adsorbents it is possible to use adsorbed bioactive compounds together with adsorbents, because biosorbents also bring beneficial effects such as additional health effect, gaining controlled drug transport, prevent stability for a long time etc. So far, there is no study regarding with the adsorbents such as silk fibroin and clinoptilolite.

Table 4.1. Researches for purification and concentration of phytochemicals by selective adsorption

Studies and Adsorbed components	Adsorbent	Reference
Recovery of antioxidants from liquors obtained by pressing grape pomace	Commercial sepabeads SP700 polymeric resin	Diaz-Reinosa et al., 2010
Adsorption of rutin	Styrene-divinylbenzene copolymer Amberlite XAD16HP	Bretag et al., 2009
Selective adsorption of limonine	Amberlite XAD-8, XAD-16N, XAD-1600	Vieria et al., 2009
Adsorption of phenolic compounds from grape pomace	Charcoal	Soto et al., 2008
Adsorption of alizarin	Microporous polymeric adsorbents XAD-4, XAD-7, XAD-16	Abdullah et al., 2007
Recovery of Aroma compounds	SDVB resins, activated carbon, zeolite Y	Krings et al., 2007
Adsorptive recovery of phenolic compounds from apple juice	Polymethylmethacrylate adsorbent resin	Kammerer et al., 2007
Preparative separation of vitexin and isovitexin from pigeonpea extracts	Macroporous resins, ADS-5, 7, 8, 11, 17, 21, ADS-3, ADS-F8	Fu et al., 2007
Narirutin from citrus peels	Amberlite XAD-7 resin	Kim et al., 2007
Adsorption of Inga edulis leaves polyphenols	Macroporous resin XAD-7, XAD-16, EXA-90, EXA-118	Silva et al., 2007
Purification of commercial grape pigment	Ultrafiltration membrane	Lin R. & Barney, 2006
Luteolin separation from pigeonpea leaves	Macroporous resins	Fu et al., 2006

(Cont. on next page)

Table 4.1. (cont.)

Separation of green tea polyphenols	PA resin adsorption after ultrafiltration with CA-Ti composite ultrafilter	Li et al., 2005
Anthocyanins and hydroxycinnamates from citrus processing	Polystyrene-divinylbenzene copolymers (apolar)	Scordino et al., 2004
<i>Trans</i> -resveratrol	Cellulose cotton	Takagai et al., 2005
Immobilization of resveratrol	Monodisperse cyano-functionalized porous microspheres	Nam et al., 2005
Adsorption of aromatic compounds	Polymeric resins, XAD4	Zhang et al., 2005
Ajmalicine from <i>Catharantus roseus</i> suspension	Amberlite XAD-7HP resin	Wong et al., 2004
Cyanidin-3-glucoside	SDVB resin EXA- Amberlite XAD resins	Scordino et al., 2004
Adsorption of stevioside (sweet compound)	Amberlite XAD-7	Hafizuddin et al., 2003
Purify cauliflower extract	Amberlite XAD-2 resin	Llorach et al., 2003
Selective adsorption of limone from orange juice	Activated diatomaceous earth, granulated activated carbon, Amberlite XAD-4, XAD-7 and XAD-16	Riberio et al., 2002
Selective adsorption of berberine	Encapsulated XAD-7 with polylysine membrane	Choi et al., 1996
Recovery of Hesperidin from orange peel	SDVB resin	Di Mauro et al., 1999
Selective adsorption of flavonoid from ginkgo leaf extract	Polycarboxyl ester (XAD-7) resin	Yoon et al., 1997
Increased alkaloid (caffeine and theobromine) production using adsorption column	Amberlite XAD-4 resin	Kurata et al, 1994
Purifying anthracycline glucosides by selective adsorption	Amberlite	Oppico et al., 1989

Generally, separating flavonoids is normally carried out from the extracts by means of solid-liquid extraction or liquid-liquid extraction. After producing crude extract, liquid- liquid extraction may applicable to separate phenolic components based on their polarities. However, this separation is not particularly effective regarding reagents, solvents, energy consumption and labour intensiveness. Alternatively, the adsorption-desorption process on various adsorbents is one of the most efficient methods and can be used for the recovery and concentration of plant secondary metabolites (Fu et al., 2006).

Application of adsorption processes in pharmaceutical industry for purification purpose has become more prevalent during recent years. Adsorption is an important step in purification process in order to produce high value added products.

Another advantage of adsorption of phytochemicals is the stabilization of them during the recovery processes in order to prevent oxidation. The structure of bioactive components changes and this yields the activity loss during the processes. For example, resveratrol has two stereoisomer; *-cis* and *-trans* forms. Only *-trans* forms are plant origin. In spite of the high antioxidizing effect of resveratrol, it has some drawbacks for commercialization; it is easily degraded by sunlight, only soluble in alcoholic solvents, and difficult to stabilize in the liquid phase. Wang et al. (2002) reported that the concentration of *trans*-resveratrol in methanol was decreased to 30% within 48 h when it was exposed to sunlight. Less attention has been devoted to stabilizing the resveratrol. In order to preserve high antioxidant activity of resveratrol for a long period of time, Nam et al. (2005) investigated the immobilization of it on porous polymer particles. In their study, antioxidant activity of resveratrol was considerably decreased by time. This was explained by the conversion of *trans*-resveratrol to *cis* form and oxidation of it. And, they concluded that, it was possible to preserve antioxidant activity of resveratrol for five weeks when immobilized on polymer matrices.

Beside the stabilization, producing selective and concentrated bioactive component from extract is also important. The extract obtained from recovery processes includes various types of phytochemicals. The concentration of specific component in extract is required, since some researchers indicate that some of the components exhibit additional functionality such as antimicrobial, anticarcinogenic etc. As in the grape skin extract, further concentration process is required because of the low concentration of *trans*-resveratrol in extract. It is the similar case for most of the other recovery processes. Solid phase extraction is favourable technique to fulfill these requirements. So far, some adsorption studies have been performed especially for citrus by products. For example, the recovery of hesperidin from orange peel by concentration of extracts on styrene-divinylbenzene (SDVB) resin has been studied by Mauro et al. (1999). The adsorption and desorption on SDVB resin significantly increased the concentration of hesperidin with good yield and high purity.

Although activated charcoal was suitable to adsorb the antioxidants from hydrolysates of grape pomace, the fractions further eluted with 96% ethanol showed

activities comparable to those of the initial product, and the recovery of the adsorbed compounds was limited, probably due to irreversible adsorption (Soto et al., 2008).

4.3. Silk Fibroin

Silk synthesized by *Bombyx mori* consists of two kinds of proteins, sericin and fibroin. Fibroin is the structural fibrous protein and constitutes 70% of the intact silk, and sericin is the water-soluble glue-like protein that surrounds and binds the fibroin fibers. The silk fibroin molecule consists of heavy and light chain polypeptides of ~ 350 kDa and ~ 25 kDa, respectively (Malay et al., 2007). Silk fibroin is a protein polymer which consists of highly repetitive regions including glycine (Gly), alanine (Ala) and sericine (Ser) aminoacids. The highly repetitive primary sequence in silk fibroin leads to significant homogeneity in secondary structure, shown in Figure 4.2.

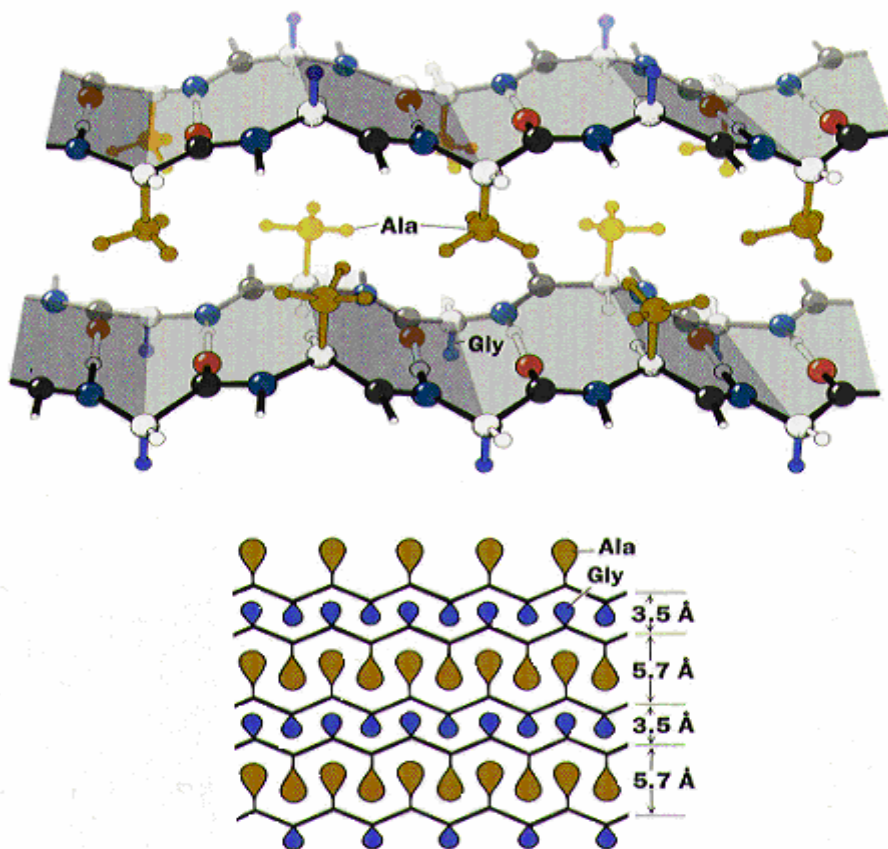


Figure 4.2. Chemical structures of silk fibroin
(Source: Serianni, 2010).

The fibroin protein consists of layers of antiparallel beta sheets. Its primary structure mainly consists of the recurrent amino acid sequence (Gly-Ser-Gly-Ala-Gly-Ala)_n.

Silk fibroin possesses a novel adsorbent property for polyphenols. Silk fibroin is an insoluble protein and has a well-defined composition, for this reason; it is preferred in many adsorption studies since 1940's. The scientists tried to enlighten the bounding mechanisms of silk fibroin and its adsorption capacity towards various compounds. There are many researches in which the silk fibroin was used as an adsorbate because of its hydrophobic character. Silk fibroin has been used as adsorbent or adsorbate in many of the studies because of its bounding mechanisms such as its hydrophobic character, insolubility in water, polar groups and basic side chains. Because of its promising health effects and bounding mechanisms, silk fibroin can be considered as a potent adsorbent for the removal of antioxidants from the crude extracts. Silk fibroin is a more suitable adsorbent for the recovery of hydrophobic polyphenols compared to the other biopolymers since it has less polar groups and more hydrophobic than others. Furthermore, because of its edible and medicinal properties, it is a valuable material for human health.

So far silk fibroin has not been used as an adsorbent for phytochemicals as it is known from the literature. Two studies of us indicate potential use of it as a novel adsorbent. Baycin, (2006), investigated the use of silk fibroin to adsorb oleuropein from olive leaf extract. In another study, Altioek et al. (2007) used silk fibroin to recover the proanthocyanidin from grape seed extract. Extraction of polyphenols from olive leaves by using different solvents and their aqueous forms, fractionation of polyphenols, especially oleuropein, were performed with silk fibroin filled column (Altioek et al., 2008).

4.4. Clinoptilolite

Zeolite is the crystalline, hydrated aluminosilicate of alkaline or alkaline earth metals, especially, sodium, potassium, calcium, magnesium, strontium and barium.

Structurally, zeolite is the "framework" aluminosilicate composed of infinitely extended three-dimensional network of AlO₄ and SiO₄ tetrahedra that form channels and interconnected voids, which are occupied by cations and water molecules. It may be

expressed in two different formulas; oxide formula and idealized formula represented as follows:

- Oxide formula: $M_{2/n}O \cdot Al_2O_3 \cdot xSiO_2 \cdot yH_2O$
- Idealized formula: $M_{x/n}[(AlO_2)_x(SiO_2)_y] \cdot wH_2O$

In the oxide formula, M represents the cation of valence n as in the idealized formula and x is generally equal to or greater than 2 since AlO_4 tetrahedra can join only to SiO_4 tetrahedra. The structural formula of a zeolite may be best expressed by the idealized formula for the crystallographic unit cell where w is the number of water molecules and the ratio y/x varies between 1 and 5 depending on the structure. The sum (x + y) represents the total number of tetrahedra, while the portion with [] defines the framework composition (Breck, 1974; Tsitsishvili et al., 1992).

The primary building unit of the zeolite framework is the tetrahedron in which the center is occupied by a silicon or aluminum atom with four oxygen atoms at the corners as shown in Figure 4.2. Each oxygen atom is shared between two tetrahedra. Hence, the tetrahedra form a continuous framework. Substitution of Si^{4+} by Al^{3+} defines the negative charge of framework, which is compensated by monovalent or divalent cations located together with water molecules in the channels. Cations in the channels can be substituted easily and therefore, they are termed exchange or extra framework cations, while Si and Al, which are not exchanged under ordinary conditions, are called tetrahedral or framework cations.

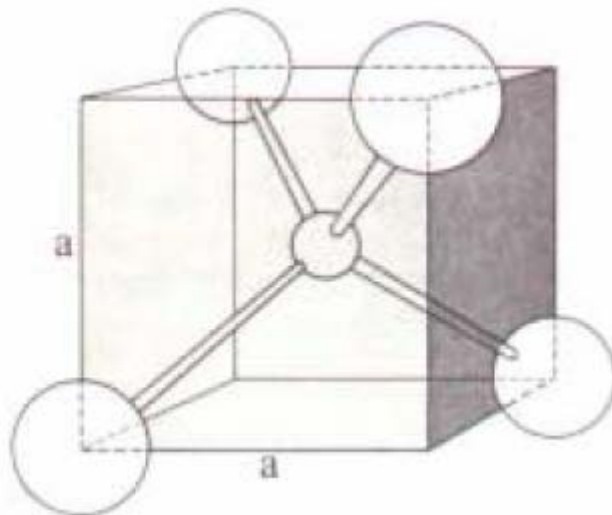


Figure 4.2. $(SiO_4)^{4-}$ or $(AlO_4)^{5-}$ Tetrahedron
(Source: Breck, 1974).

Zeolite structure can be summarized as aluminosilicate framework, exchangeable cations and zeolitic water. Aluminosilicate framework is the most stable component and defines the structure. Exchangeable cations surrounded with water molecules and oxygen atoms fill the channels and cavities in the zeolite framework and balance framework charge, while water molecules distribute the framework charge hence, act as a stabilizer (Tsitsishvili et al., 1992).

Zeolites have superior characteristics compared to the other crystalline inorganic oxide-materials. For example; they can separate molecules based on the size and configuration of the molecule relative to the size and geometry of the apertures of the zeolite structure, due to the uniform and microporous pore structure within their crystals. Thus, they act as "molecular sieves". They also adsorb molecules with permanent dipole moment with selectivity not found in other adsorbents (Breck, 1974; Moscou, 1991).

Zeolite contains many channels or cavities linked by channels. One of the characteristics that distinguish zeolites from other porous materials is their variety of pore sizes and shapes, which define the structural parameters of zeolite. Clinoptilolite crystallizes in monoclinic C2/m group with the following unit cell parameters: $a = 17.64 \text{ \AA}$, $b = 17.91 \text{ \AA}$ and $c = 7.39 \text{ \AA}$ (Joshi et al., 1997). Properties of zeolites such as ion exchange, inter-crystalline pores that discriminate molecules of different dimensions, strong acid sites have earned them extensive industrial uses. Consequently, fundamental zeolite research has become an area of great interest. The remarkable applicability of zeolites ranges from uses in biochemistry, the agroindustry, detergents, soil improvements and the energy storage. In recent years, zeolites are exciting materials for medical applications. Several biomedical applications have been reported, for example, the use of clinoptilolite as a potential adjuvant in anticancer therapy (Pavelic et al., 2001). This depends on their biological properties and long term physical-chemical stability in biological environments. One of the many exciting potential pharmacological applications of zeolites is the possible encapsulation and/or adsorption of different ions and molecules in their open framework, and the subsequent delayed release (Rivera et al., 2003). In addition, the external surface may also be exploited since it is known that the presence of surfactants on solid surfaces can induce or enhance the co-adsorption of different organic molecules. This may lead to the use of zeolites as drug delivery systems. Rivera and Farias (2003) indicate that the clinoptilolite-surfactant composites as a drug support promises new potential

application as selective adsorption of phytochemicals. Zeolites are also widely used in modern technology as selective adsorbents. It is obvious that those remarkable properties of zeolite will be utilized in the near future for the health care industries (Figure 4.3).



Figure 4.3. Biomedical effects of zeolite
(Source: Auerbach et al., 2003).

4.5. Adsorption Theory

Adsorption is mostly used to separate and to concentrate bioactive compounds of plant extracts. The cost of the final product and performance of the system determines the feasibility of the process and its efficiency. Since, bioactive compounds are widely used for the pharmaceutical industry as active drug component; the requirement of high purity final product makes the separation step as the most important

and value added production step. However, the high cost of adsorbents and process facilities used for this purpose, makes the process always in concern to control process efficiency. Therefore the sorption capacity and required contact time are two of the most important parameters to understand. The kinetics analysis is a useful tool to get the time required to reach the equilibrium regarding the completion of adsorption. The kinetic process of adsorption is explained by several mathematical models where more than one mechanism may be responsible as a rate determining step. It is required to better understand the kinetics of sorption in solid-liquid systems for the optimization and scale up of the process.

In this section sorption kinetics is briefly investigated in order to determine the mechanism of adsorption. Additionally, to determine the sorption capacity sorption equilibria between the sorbent phase and solution phase is discussed. Finally, column models are given for analyzing the breakthrough profiles.

4.5.1. Adsorption Kinetic

Several mathematical models have been proposed to analyse adsorption data, which can generally be classified as adsorption reaction models and adsorption diffusion models. Both classes should be used to describe the adsorption mechanisms. Only adsorption reaction models have been used to describe the kinetic of the sorption process. However, this situation has been criticized by Tien (2007), who is the editor of the famous journal, Separation and Purification Technology. Sorption rate should be described by a series of resistances due to external mass transfer, intraparticle diffusion and reaction. Thus, it is very important to describe the adsorption kinetics together with the adsorption diffusion models and adsorption reaction models.

When the agitation is sufficient to avoid the concentration gradient in the solutions, bulk diffusion becomes non-limiting step. Then, adsorption kinetic is mainly controlled by the following steps. These steps are shown in Figure 4.4.

1. Mass transfer from the fluid phase to the external surfaces of the sorbent particles (film diffusion resistance).
2. Pore diffusion in the fluid phase (pore diffusion resistance)
3. Adsorption reaction at the phase boundaries (surface reaction resistance)

4. Diffusion in the sorbed state (particle phase diffusion resistance or solid diffusion resistance) this can occur in a pore-surface layer.

The rate limiting step is resulted from one or combination of these steps. These steps, all of which contribute resistance to mass transfer, are those found commonly in adsorption onto porous solids and include transfer from bulk liquid to the outer surface of the particle (film diffusion resistance), movement by diffusion into the pores of the particles (pore diffusion or particle diffusion resistance) and the actual chemical or physical interaction at the binding side (surface reaction resistance).

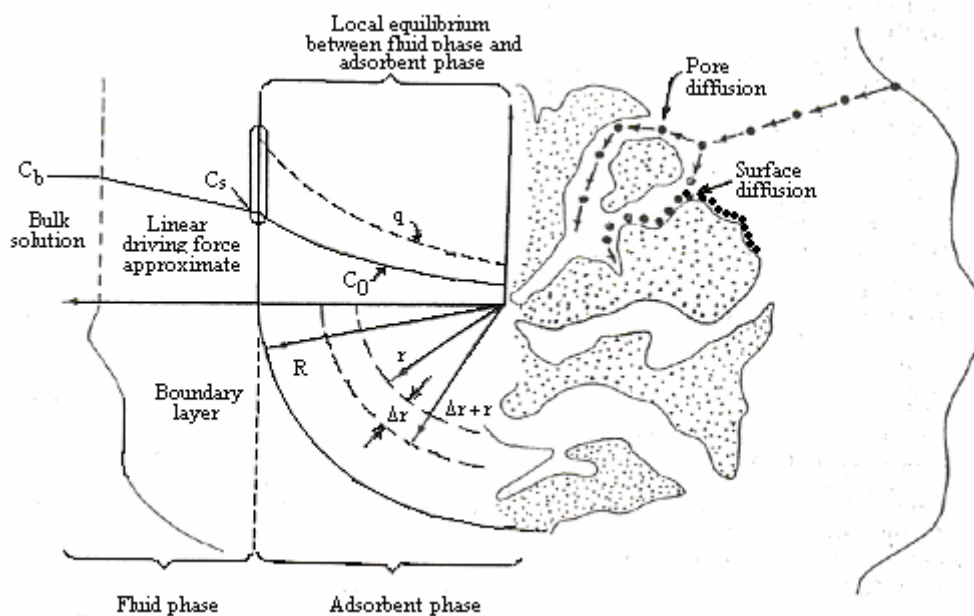


Figure 4.4. Adsorption kinetic steps.

Both micropore and macropore structure exist in the bi-porous adsorbent so at least two and three mechanisms should be considered during the sorption process. The first mechanism is related to the external mass transfer resistance associated with diffusion through the laminar fluid film surrounding to the particle. External film diffusion occurs by molecular diffusion through the boundary layer around the adsorbent particle because of a difference in concentration between the bulk fluid and the surface of the adsorbent. The external film diffusion is usually limited to the early stages of the adsorption because of the rapid decrease in the driving force. The second mechanism is related to the macropore mass transfer resistance associated with diffusion through the solution in the pores (pore diffusion) or diffusion along the

adsorbent surface (surface diffusion). Finally, the micropore diffusional resistance occurs in the sorption process. If the micropore diffusion is rapid, the uptake rate will be controlled by diffusion thorough the macropores. When the micropore diffusion is relatively slow, the distinction of the diffusional resistances is difficult. Analyzing of the ratio of the diffusion time constant can be used to distinguish the significant diffusional resistance. Varying size of the macro and micro particle provides a straightforward experimental test to determine the appropriate mechanism. When the micropore resistance is dominant, the uptake rate is independent of the particle size. On the other hand, the uptake rate strongly depends on the particle size when the macropore resistance is the rate controlling one.

In order to identify the main controlling mechanisms it is necessary to carry out the experiments to study several experimental parameters. Particle size, pH, agitation speed, temperature and initial concentration are the most important parameters that are used in the adsorption kinetic studies. The best way to determine whether the external film diffusion is the controlling step or not, is to carry out the series of batch kinetic experiments at different agitation speeds. When the agitation speed is increased, the diffusion rate of sorbate from the bulk liquid to the liquid boundary layer surrounding to the particles become higher. Under these conditions, the values of external mass transfer coefficients become larger. External mass transfer is generally the rate limiting step at the short initial period of time in the case of more than one resistances control the sorption process. The other mechanism needs to be included in the analysis of overall sorption process at later stage of the sorption.

External film diffusion is affected from changing the particle size of the adsorbent. As the particle size is decreased, the external surface area of the adsorbent increases. If the external mass transfer is the slowest step of the sorption process, reduction in the particle size increases the uptake rate. In this case, decreasing the particle size resulted in the rapid initial uptake rate and shorter time to reach equilibrium. If the macropore diffusion is the limiting step for the sorption process, greater time is required to reach equilibrium for larger particle sizes due to the requirement of the time for the diffusion to the interior of the particle. Increasing the particle size yields higher intraparticle diffusion resistance and the uptake rates become broader compared to the uptake rates for smaller particles. For the microparticle controlled sorption process, the uptake rate is independent of particle size, because there

are no diffusional resistances to the sorbate molecules at the external film and in the macropores.

Sorbate concentration affects on the uptake rates if the sorption process is controlled either by the external mass transfer or intraparticle mass transfer. If the external mass transfer is the main mechanism existing in the sorption process, increasing the initial concentration of the solution decreases the external mass transfer coefficient (k_f) and consequently decreasing the initial uptake rate. However, in case of the intraparticle mass transfer controlled sorption process, increasing the initial concentration result in the steeper uptake curve and higher intraparticle rate constant (k_d), because of higher driving force in the particle. If the adsorption is reaction controlled, the uptake rate only dependent on the sorbate concentration (Ho and McKay, 1998). The uptake rate increases by increasing the sorbate concentration in solution, because there are more sorbate molecules binding to the active sites on the sorbent surface.

pH affects not only the functional groups on the sorbent surface but also the functional properties of the sorbate. Isoelectric point (pI) is the pH at which a particular molecule or surface carries no net electrical charge. The pH value of the solution determines the ionic interactions between sorbent surface and the sorbate molecules, which is explained by the reaction controlled sorption mechanism. If the ionic interaction between the surface and sorbate is strong, the rate of reaction is faster than the other mechanisms. In this case, sorbate-sorbent reaction is not taken into consideration as rate limiting step.

Differentiation between the diffusion and the reaction controlled process is often difficult. The diffusion controlled systems are characterized by only a small dependence on temperature, while chemically controlled system is more dependent on temperature. The magnitude of the activation energy (E_a) gives an idea about the type of sorption processes. In physical sorption, equilibrium between the adsorbent surface and the adsorbate is usually rapidly attained and easily reversible, in which the energy requirements are small, because the forces involved in physical adsorption are weak. Chemical sorption is specific and much stronger forces are involved. In chemical sorption the adsorbed molecules are held on the surface by chemical bonds. In this case, the sorption energy is usually greater than 25-30 kJ/mol. However, diffusion sorption processes have lower energies.

These parameters should be well discussed by experimental studies in order to clarify which mechanism is considered as rate limiting step. In order to determine the rate limiting step, several kinetic sorption models can be used for the porous adsorbent, which is normally modeled by kinetic models as well as diffusional models. The rate controlling mechanism in the kinetic models is the solute-sorbent surface adsorption reaction, which happens at the active sites on the sorbent surface. For this reason, these models are called kinetic models. In the diffusional models, it is supposed that the rate controlling mechanism is the intraparticle diffusion taking place in the pores and can be due to the pore volume diffusion, surface diffusion or a combination of both mechanisms. Model equations, their assumptions and derivations are discussed in the following parts.

4.5.1.1. External Film Diffusion

The external fluid film resistance is significantly influenced by hydrodynamic conditions. The sorbent particle has a stagnant film of liquid, having a thickness of γ surrounding it. The transfer of solute across this film can only occur by molecular diffusion. By increasing the agitation speed, the mass transfer resistance becomes smaller due to the reduction of the film thickness, which exhibits resistance to mass transfer. Moreover, well mixed region outside of that region, there is not mass transfer resistance because of the uniform concentration distribution. Then, mass transfer resistance of the film is proportional to γ/D_{AB} , where D_{AB} is the molecular diffusion. In the case of the intraparticle controlled sorption process, mass transfer resistance exists in the particle itself. Once a solute molecule reaches to the pore at the particle surface, it must diffuse through the liquid. After reaching to the opening of a pore, solute passes through the interconnected pores, which has tortuous network, till reaching to the vacant sorption site. As sorption proceeds, solute molecules must travel farther and farther into the particle in order to find vacant sites. Thus, the process of reaching to all of the surface sites in a particle is slow one. However, external mass transfer resistance may still be large enough to have a significant effect on sorption process.

Mass transfer through the stagnant film is usually modeled with the rate law.

$$\frac{d\bar{q}}{dt} = k_f S_0 (C - C_s) \quad (4.1)$$

where \bar{q} is the average solute concentration in the solid, C is the uniform concentration of the solute in the bulk of the liquid, far from the surface, C_s is the concentration of the solute in the liquid at the particle/liquid interface, S_0 is the surface area of the adsorbent particle per unit volume of the adsorbent particle, which is $3/R_p$ for the spherical particle, and k_f is the film mass transfer coefficient. This type of rate law is often referred as a linear driving force rate law.

If the equilibrium relationship is linear ($q^* = KC$) and the bulk phase concentration C is maintained constant, Equation 4.1 can be written equivalently in the form which is given in Equation 4.2.

$$\frac{d\bar{q}}{dt} = \frac{3k_f}{KR_p} (q^* - \bar{q}) \quad (4.2)$$

Equation 4.2 can be solved by appropriate boundary conditions for a step change in concentration at time zero, which are given in Equation 4.3 and the final form of the model equation is written in Equation 4.4.

$$t < 0 \quad C = q = 0$$

$$t > 0 \quad C = C_e = \frac{q_e}{K} \quad (4.3)$$

$$\frac{\bar{q}}{q_e} = 1 - \exp\left[-\frac{3k_f}{KR_p} t\right] \quad (4.4)$$

For the porous particle, diffusion within the pores of the particle is almost always slower than diffusion in the external fluid phase. However, there would be considerable mass transfer resistance of the liquid film layer to the sorption rate, which

resists to the particle to transfer to the pore openings. This situation can also be explained by the linear driving force equation within the particle.

R_p in Equation 4.4 is the particle radius and K is the linear equilibrium constant. The linearized form of Equation 4.4 is given in Equation 4.5.

$$\ln\left(1 - \frac{\bar{q}}{q_e}\right) = -\frac{3k_f}{KR_p}t \quad (4.5)$$

The plot $\ln(1 - \bar{q}/q_e)$ against t is drawn and k_f can be determined from the slope of the curve. This equation has also known as Boyd model.

The appropriate dimensionless group characterizing film mass transfer is the Sherwood number, defined by Equation 4.6.

$$Sh = \frac{2R_p k_f}{D_{AB}} \quad (4.6)$$

For an isolated spherical particle surrounding by a stagnant fluid, the limiting value of Sh is 2 for low Reynolds numbers (Re). However, under flow conditions Sh number is a function of Schmidt (Sc) and Re numbers. There are many empirical correlations depending on the Re numbers. One of the correlations is given in Equation 4.7.

$$Sh = \frac{2R_p k_f}{D_{AB}} = 2 + 0.6Sc^{1/3} Re^{1/2} \quad (4.7)$$

4.5.1.2. Macropore Diffusion

Solute transfers from the bulk solution to the external surface of the sorbent. If the sorbent has porous structure composed of the macropores and micropores, initially, the solute diffuses throughout the macropores. Different transport mechanisms are involved in the macropore diffusion, which are pore, molecular (a), Knudsen (b) and surface diffusion (c) (Fig. 4.5). The macropore diffusion is complex quantity, since

more than one mechanism occurs simultaneously. However, molecular and surface diffusions are mostly considered mechanisms during the liquid sorption process.

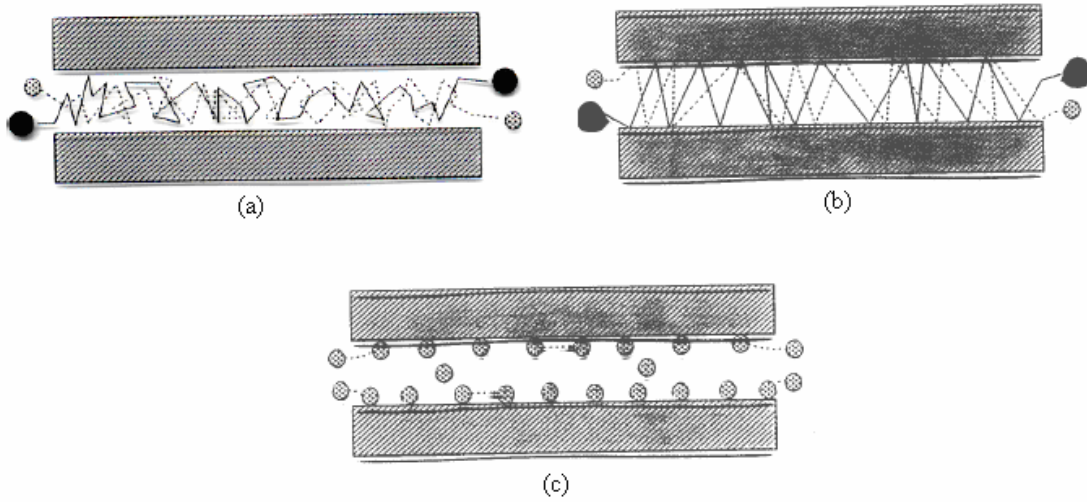


Figure 4.5. Diffusion in Macropores.

The corresponding equation for macropore diffusion control is given in Equation 4.8.

$$(1 - \varepsilon_p) \frac{\partial q}{\partial t} + \varepsilon_p \frac{\partial C}{\partial t} = \varepsilon_p D_p \left(\frac{\partial^2 C}{\partial R^2} + \frac{2}{R} \frac{\partial C}{\partial R} \right) \quad (4.8)$$

Here, pore diffusivity (D_p) is the concentration independent, because of the simplicity of the equation. If the linear isotherm relation is valid (small step change of the concentration), Equation 4.9 is simplified into;

$$\frac{\partial C}{\partial t} = \frac{\varepsilon_p D_p}{\varepsilon_p + (1 - \varepsilon_p)K} \left(\frac{\partial^2 C}{\partial R^2} + \frac{2}{R} \frac{\partial C}{\partial R} \right) \quad (4.9)$$

In Equation 4.9, $\frac{\varepsilon_p D_p}{\varepsilon_p + (1 - \varepsilon_p)K}$ term represents the effective macropore diffusivity.

Initial and boundary conditions are;

Along the radial direction, at $t=0$,

$$C(R,0)=C_0 \quad q(R,0)=q_0$$

At the surface of the particle ($R=R_p$), and at $t=t$,

$$C(R_p,t)=C_0 \quad q(R_p,t)=q_0 \quad (4.10)$$

$$\left. \frac{\partial C}{\partial R} \right|_{R=0} = \left. \frac{\partial q}{\partial R} \right|_{R=0} = 0$$

According to the boundary conditions, the solution of the Equation 4.9 yields;

$$\frac{m_t}{m_\infty} = 1 - \frac{6}{\Pi^2} \sum_{n=1}^{n=\infty} \frac{1}{n^2} \exp\left(-\frac{n^2 \Pi^2 \varepsilon_p D_p t}{R_p^2 (\varepsilon_p + (1-\varepsilon_p)K)}\right) \quad (4.11)$$

where $\varepsilon_p D_p / R_p^2 [\varepsilon_p + (1-\varepsilon_p)K]$ is the time constant for the macropore diffusion.

If the change in concentration is large, non-linearity of the equilibrium isotherm must be considered.

For a Langmuir system,

$$\frac{q^*}{q_m} = \frac{bC}{1+bC}$$

so,

$$\frac{dq^*}{dC} = \frac{bq_m}{(1+bC)^2} = bq_m \left(1 - \frac{q}{q_m}\right)^2 \quad (4.12)$$

In Equation 4.9, solute concentration in the pore liquid is very small relative to that in the sorbed phase, so $\frac{\partial C}{\partial R}$ can be replaced with the term, $\frac{\partial q}{\partial R} \left(\frac{dC}{dq^*}\right)$. Equation 4.8 is then simplified into the following equation;

$$\frac{\partial q}{\partial t} = \frac{\varepsilon_p D_p}{(1-\varepsilon_p) b q_m} \frac{1}{R_p^2} \frac{\partial}{\partial R} \left(\frac{R^2}{(1-\frac{q}{q_m})^2} \frac{\partial q}{\partial R} \right) \quad (4.13)$$

Macropore diffusion occurs by following diffusion mechanisms, which are molecular and surface diffusion. The relative importance of these mechanisms depends on the system conditions. Molecular diffusion is normally dominant in relatively large pores. Several theoretical models used for predicting molecular diffusivity in liquids. These models are Stoke-Einstein, Nernst-Einstein and Wilke-Chang. Correlations based on the equations should be considered carefully. Pore diffusion includes the diffusion of the molecules through the liquid filled pores. There is a correlation between the pore and molecular diffusion. If the pore diameter is large relative to the mean free path, the pore diffusivity is identical with the molecular diffusivity. In this case, collision between diffusing molecules in liquid occurs more frequently than collision between molecule and pore-wall. On the other hand, pore diffusion is a function of porosity and tortuosity (τ) and related equation is given as follows;

$$D_p = \frac{\varepsilon_p D_m}{\tau} \quad (4.14)$$

where D_p is pore diffusion coefficient, D_m is molecular diffusion coefficient, ε_p particle porosity and τ is tortuosity.

Knudsen diffusion becomes dominant in small pores when the collisions between the diffusing molecules and the pore walls occur more frequently than collisions between the diffusing molecules themselves. Both Knudsen and molecular diffusion involve in the movement of the sorbate through the liquid filled pores. However, additional term, which is surface diffusion, is used to explain the surface movement of molecules physically sorbed on macropore surface.

4.5.1.3. Micropore Diffusion

In macropore, large pores act as passage way for the molecules to diffuse from the surrounding environment into the interior of the particle. When the molecules are

inside the particles, they sorbed at the pore mouth of the microparticle and hence these sorbed molecules will diffuse into the interior of the microparticle. Generally, the pore size of the microparticle is close to the molecular dimensions of the sorbate and therefore, molecules inside the micropore never escape.

If the diffusion into the micropore is slow, the uptake rate is controlled by micropore diffusion. The appropriate equation for spherical sorbent particle can be given as;

$$\frac{\partial q}{\partial t} = \frac{1}{r^2} \frac{\partial}{\partial r} \left(r^2 D_c \frac{\partial q}{\partial r} \right) \quad (4.15)$$

If the uptake occurs over a small change in the adsorbed phase concentration we may assume a constant diffusivity, thus Equation 4.15 is simplified to:

$$\frac{\partial q}{\partial t} = D_c \left(\frac{\partial^2 q}{\partial r^2} + \frac{2}{r} \frac{\partial q}{\partial r} \right) \quad (4.16)$$

The initial and boundary conditions for a step change in sorbate concentration are given in Equation 17.

$$t < 0 \quad C = C_0 \quad q = q_0$$

$$t \geq 0 \quad C = C_\infty \quad q(r_c, t) = q_\infty$$

$$t \rightarrow \infty \quad C = C_\infty \quad q(r, t) = q_\infty$$

$$\left. \frac{\partial q}{\partial r} \right|_{r=0} = 0 \quad \text{for all } t \quad (4.17)$$

By applying initial and boundary conditions, Equation 4.18 can be derived for infinite case.

$$\frac{q_t}{q_\infty} = 6 \left(\frac{D_c \cdot t}{r_c^2} \right)^{1/2} \left[\frac{1}{\sqrt{\pi}} + 2 \sum_{n=1}^{\infty} i \cdot \operatorname{erfc} \left(\frac{nr_c}{\sqrt{D_c \cdot t}} \right) \right] - 3 \frac{D_c \cdot t}{r_c^2} \quad (4.18)$$

For short time [$q_t/q_\infty < 0.3$], Equation 4.18 is simplified into:

$$\frac{q_t}{q_\infty} = \frac{6}{\sqrt{\pi}} \left(\frac{D_c \cdot t}{r_p^2} \right)^{1/2} \quad (4.19)$$

For long time [$q_t/q_\infty > 0.7$], Equation 4.18 is written as follows:

$$1 - \frac{q_t}{q_\infty} \cong \frac{6}{\pi^2} \exp\left(-\frac{\pi^2 D_c t}{r_p^2}\right) \quad (4.20)$$

Equation 4.19 is used for the derivation of the Weber-Morris model, which is given in Equation 4.21.

$$q_t = k_d t^{1/2} \quad (4.21)$$

Intraparticle rate constant (k_d) in Weber-Morris is defined as;

$$k_d = \frac{6D_c^{1/2}q_\infty}{\sqrt{\pi}r_p} \quad (4.22)$$

Thus, Weber-Morris equation is valid up to $q_t/q_\infty < 0.3$.

In order to validity of the intraparticle diffusion control, Weber-Morris plot, q_t versus $t^{1/2}$, is widely used. If there is more than one resistance in the sorption process, multiple linear lines are seen in Weber-Morris model graph. If the plot of q_t versus $t^{1/2}$ gives a straight line through the origin, intraparticle diffusion is considered as the rate limiting step. If the plot does not pass through the origin, other mechanism is dominant during the sorption process. Initial period of the sorption process is much more

complex, since more than one mechanism such as external diffusion, surface diffusion and pore diffusion may be occurred.

Comparison of Micropore and Macropore Diffusion

The comparison of the micropore and macropore diffusional resistances can be investigated by their length scale and time scale of the diffusion. The diffusion process in the macropore follows the combination of the molecular and Knudsen mechanisms while the diffusion process follows an intracrystalline diffusion mechanism. The length scale of the diffusion in the macropore is the dimension of the particle, while the length scale of diffusion in the micropore is the dimension of zeolite crystal. Therefore, the magnitude of intracrystalline diffusivity is very small compared to the diffusivity in the macropore. If the time scale of the diffusion in the crystal is very long compared to that in the particle the system will be controlled by the intracrystalline diffusion because of the crystal dimension. In that case, diffusion within the macropore is very fast. Therefore the long time region of the Crank's solution is most sensitive to explain the existence of the micropore diffusion resistance.

The time scale comparison of the macropore to micropore diffusion is given in Equation 4.23.

$$\gamma = \frac{\frac{\varepsilon_p D_p}{(\varepsilon_p + (1 - \varepsilon_p)K)}}{\frac{R_p^2}{\frac{D_c}{r_c^2}}} = \frac{\text{Time scale of macropore}}{\text{Time scale of micropore}} \quad (4.23)$$

If γ is less than unity, the time scale of diffusion in the crystal is greater than that in macropore, and so micropore diffusion controls the sorption process. On the other hand, if γ is greater than unity, macropore diffusion controls the sorption process.

If the time scales of both macropore and micropore are very close to each other, it is difficult to decide which resistance controls the sorption process. In this case, both of them are involved in the process, explained by heterogeneous diffusion model. The heterogeneous diffusion model assumes that diffusion in the particle occurs by macropore diffusion through the voids of porous particle and micropore diffusion in the

crystals. Models for the heterogeneous diffusion model have been developed that assume macropore and micropore diffusion occurs in series or in parallel.

The first model is developed assuming these process occurring parallel. The differential mass balance in the solid phase;

$$\frac{\partial C}{\partial t} + \frac{\partial q}{\partial t} = \frac{1}{R_p^2} \frac{\partial}{\partial R} \left[(D_c \frac{\partial q}{\partial R}) + (D_p \frac{\partial C}{\partial R}) \right] \quad (4.24)$$

The diffusional terms in the parenthesis represents the micropore diffusion and the macropore diffusion, respectively.

A second model is developed assuming these diffusional terms occur in series. The mass balance is given in the related equation;

$$\frac{\partial C}{\partial t} + \frac{\rho(1-\varepsilon)q_0}{\varepsilon C_0} \frac{\partial q}{\partial t} = 0 \quad (4.25)$$

In the series case macropore diffusion is followed by micropore diffusion. Thus, mass balance between the macropore and micropore diffusion is given in Equation 4.26.

$$\frac{1}{R_p^2} \frac{\partial}{\partial R} (D_p \frac{\partial C}{\partial R}) = \frac{\partial C}{\partial t} + \frac{\rho(1-\varepsilon)q_0}{\varepsilon C_0} \left(3 \int_0^r \frac{1}{r_c^2} \frac{\partial}{\partial r} (D_c \frac{\partial q}{\partial r}) r^2 dr \right) \quad (4.26)$$

Homogeneous diffusion model (HSDM) assumes that the particle is a homogeneous solid through which diffusion can be modeled by solid phase diffusivity. This approach is used to differentiate diffusional mechanisms during the adsorption process, which are diffusion in the pore space, diffusion along the surface and diffusion in the solid material itself. This model describes homogeneous diffusion in a sphere, assuming a constant diffusivity, D_s , at all points in the particle and diffusion in the crystals is explained by the Fick's law. The differential mass balance in the crystals is given in Equation 4.27.

$$\frac{\partial q}{\partial t} = \frac{1}{r^2} \frac{\partial}{\partial r} \left(r^2 D_s \frac{\partial q}{\partial r} \right) \quad (4.27)$$

which is the same equation with the Crank's equation.

Crank gives an exact solution to the Equation 4.27 for the infinite bath case by assuming the constant concentration of solute at the surface. In this case D_S is concentration independent and assumed to be constant. This assumption also yields to the neglecting the external mass transfer resistance. Similar solution of the Equation 4.27 is obtained for the short term and long term region, which are given in Equation 4.19 and 4.20, respectively.

By now, the homogeneous solid diffusion model covers the micropore diffusion in the sorption process due to the active sites in the crystalline structure. However, some adsorbents, such as active carbon and zeolite, are not actually homogeneous, but rather consist of discrete pores. The adsorption of solute molecules occurs on the surface, in this case surface diffusion is considered in the homogeneous diffusion model. The subscription on the diffusivity D_S in the HSDM equation reflects surface diffusivity.

In the solution of the HSDM model, D_S is generally assumed as concentration independent. However, in reality it is well known that the D_S often exhibits fairly strong concentration dependence, and thus it varies both with the position and with time during the sorption process. Unfortunately, there is no easy theoretical way to take the concentration dependence of D_S into consideration.

Dimensionless Biot number

Biot number is used to make a comparison between the internal and external mass transfer resistances.

$$Bi = \frac{k_f r}{3\varepsilon D_p} = \frac{Sh}{6} \frac{D_m}{\varepsilon D_p} \quad (4.28)$$

where D_p is the pore diffusivity and D_m is the molecular diffusivity. For Biot number $\ll 1$, the adsorption rate is external mass transfer resistance controlled. While for $Bi \gg 100$, pore diffusion is the predominant mass transfer controlling mechanism (Maiti et al., 2009).

4.5.1.4. Adsorption Reaction Models

Adsorption reaction models have been used to describe the kinetic process of adsorption. The Lagergren rate equation (Equation 4.29) is the first order rate equation to describe the liquid-solid systems based on solid capacity.

$$\frac{dq_t}{dt} = k_1(q_e - q_t) \quad (4.29)$$

where q_e and q_t (mg/g) are the adsorption capacities at equilibrium and at time t (min), respectively. k_1 (min^{-1}) is the rate constant. After integration and applying boundary conditions $t = 0$ to $t = t$ and $q_t = 0$ to $q_t = q_t$, the integrated form of equation becomes;

$$\log(q_e - q_t) = \log q_e - \frac{k_1}{2.303} t \quad (4.30)$$

Linear driving force model is used in the cases of diffusion through a boundary liquid film controls the sorption process. The Lagergren adsorption reaction model is very similar to the linear driving force model developed for the liquid film controlled sorption. Although the constant of the rate equation in the linear driving force model (k_f) will vary inversely with the particle size and the film thickness, the rate constant k_1 of the Lagergren equation will be independent of particle diameter and flow rate (Ho et al., 2000). The rate constant only depends on the concentration of the sorbate.

The distinction between the reaction kinetic and diffusional process is often difficult to characterize, but most appropriate quantitative approach is to perform the square root of contact time analysis. A plot of the adsorbed amount against $t^{1/2}$ yields a straight line having a slope, which equals to k_d . If the straight line passes through the origin, intraparticle diffusion controls the sorption. Additional confirmation of a diffusion mechanism should be obtained by analyzing the effect of variables, such as particle size, agitation speed, concentration of the sorbate and temperature.

The rates of reaction increase more rapidly than those of diffusion processes with temperature if the reaction is the chemical. When k_d is plotted against reciprocal temperature for diffusion controlled processes the energy of adsorption is usually less

than 25-30 kJ/mol (Ho et al., 2000). The relation between the k_d and temperature is given in Equation 4.31.

$$k_d = A \exp\left(-\frac{E}{RT}\right) \quad (4.31)$$

4.5.2. Adsorption Equilibrium

One of the important parameters to evaluate the adsorption process is the equilibrium of the adsorption. An equilibrium analysis is the most important fundamental information required to evaluate the affinity or capacity of the adsorbent.

Various isotherm equations such as the Freundlich, Langmuir, Redlich-Peterson and Temkin equations have been used to describe the equilibrium characteristics of adsorption. However, in general equilibrium isotherms are described by Freundlich or Langmuir models.

The empirical Freundlich equation is expressed by:

$$q_e = k_F \cdot C_e^n \quad (4.32)$$

where q_e is the equilibrium concentration (amount of adsorbate/amount of adsorbent), C_e is the equilibrium concentration of solute in fluid phase and k_F and n are constants that are characteristic of adsorption system. The dimensions of k_F depend on the value C_e while the exponent n is dimensionless. The k_F parameter increases with the total adsorption capacity of the adsorbent to bind the adsorbate. The n value may vary along adsorption process and is related to the adsorption efficiency and also to the energy of adsorption. Favorable adsorption corresponds to n values lower than 1, while values higher than 1 indicates unfavorable adsorption.

A linearized form of Freundlich equation can be written as:

$$\ln q_e = \ln k_F + n \ln C_e \quad (4.33)$$

The k_F and n values can be obtained from the intercept and slope, respectively, from the linear regression line from a plot of $\ln q_e$ versus $\ln C_e$.

Freundlich equation is used extensively in the physical adsorption and chemical adsorption. It can be used to describe the adsorption behaviour of monomolecular layer as well as that of the multimolecular layer.

Langmuir isotherm has the following form:

$$q_e = \frac{q_{\max} k_L C_e}{1 + k_L C_e} \quad (4.34)$$

Langmuir theory assumes that sorption occurs at specific homogeneous sites within the adsorbents and there is no interaction between the sorbate molecules that are bound to the active sites. Hence, the Langmuir equation describes the adsorption behaviour of monomolecular layer.

The Langmuir and Freundlich models are used to reveal the linearity fitting and describe how solutes interact with the adsorbents.

4.5.3. Column Studies

Solid phase extraction systems are widely used to separate polyphenolic components from each others. These systems are preferably used in lab-scale analysis in order to separate components from each other prior HPLC analysis of them. From the industrial point of view, processing the recovery of biologically active components by using the adsorption techniques performed in column systems is thought to be very useful due to the adaptability of column systems to versatile process, low reagent handling and accordingly low operational costs. Thus, separation process, which is optimized by lab scale-column experiments, enlightens to process development and consequently industrial applications.

Theoretical Background of the Models for Dynamic Column Application

To understand the dynamics of a fixed-bed adsorption column, a mass balance is performed by considering a disk of cross sectional area equivalent to that of the column (A_m) but differential in thickness (Δx). The adsorbate in mobile phase flows through the disk by convection and the combined effects of molecular diffusion and axial

dispersion. The rate of convection into the disk is the interstitial velocity, that is the velocity of fluid in the void fraction, ε . This convection rate is the superficial velocity (the flow rate divided by the cross section of the column) divided by the void fraction ($= Q/ \varepsilon A$). Within the volume of disk, adsorbate may accumulate within both the mobile phase and stationary phases. The mass balance for adsorbate can be written as;
(Rate of adsorbate in)-(Rate of adsorbate out)=(Rate of accumulation of adsorbate)

$$\begin{aligned}
 & A_m \varepsilon \Delta t \left(\frac{v}{\varepsilon} C_i - D_{eff} \frac{\partial C_i}{\partial z} \right) \Big|_{z,t} - A_m \varepsilon \Delta t \left(\frac{v}{\varepsilon} C_i - D_{eff} \frac{\partial C_i}{\partial z} \right) \Big|_{z+\Delta z,t} \\
 & = A_m \varepsilon \Delta z (C_i \Big|_{t+\Delta t} - C_i \Big|_t) + A_m (1 - \varepsilon) \Delta z (q_i \Big|_{t+\Delta t} - q_i \Big|_t)
 \end{aligned} \tag{4.35}$$

C_i = inlet concentration of adsorbate in the mobile phase (mg/L)

q_i = concentration of adsorbate i in the stationary phase averaged over an adsorbent

ε : void fraction

v : mobile phase superficial velocity ($= Q/A_m$), where Q : volumetric flow rate (mL/min) D_{eff} : effective diffusivity

Dividing by $A \varepsilon \Delta x \Delta t$ and taking limit as Δx and Δt go to zero, this mass balance becomes;

$$D_{eff} \frac{\partial^2 C_i}{\partial z^2} - \frac{v}{\varepsilon} \frac{\partial C_i}{\partial z} = \frac{\partial C_i}{\partial t} + \frac{1 - \varepsilon}{\varepsilon} \frac{\partial q_i}{\partial t} \tag{4.36}$$

The initial and boundary conditions for the column initially free of adsorbate and subjected to step change in adsorbate concentration at the column inlet at time zero are given;

$$t=0, \quad C_i = q_i = 0$$

$$z=0, \quad \frac{D_{eff}}{v} \frac{\partial^2 C_i}{\partial z^2} = C_i - C_F \tag{4.37}$$

$$z=L, \frac{\partial C}{\partial z} = 0$$

where C_F is the adsorbate concentration of the feed solution.

This equation derived to model the system with theoretical rigor is differential in nature and usually require complex numerical methods to solve. Ruthven (1984) classified the useful framework for more detailed analysis of the dynamic behaviour of an adsorption system. In this classification, the nature of the mass transfer and complexity of the mathematical model required to describe the system were considered. The nature of the mass transfer is determined by the form of the equilibrium relationship (linear, favorable and unfavorable isotherms), while the complexity of the mathematical model depends on the concentration level, the choice of rate equation and the choice of the flow model (plug flow, where axial dispersion is neglected, and dispersed plug flow).

The term $\frac{\partial q}{\partial t}$ in Equation 4.38 represents the local rate of adsorption between the fluid and adsorbate phases. Various dynamic models have been derived which differ mainly in the choice of kinetic rate expression. For the simplicity of the model equation, single mass transfer resistance is assumed and can be explained either by linear rate expression or diffusion model. In case of the linear rate expression, overall effective mass transfer coefficient is the rate coefficient. However, the dominant mass transfer resistance is intraparticle diffusion, which is described by the diffusion equation with associated boundary conditions. For the realistic description of the sorption mechanism, more than one resistance should be considered in the overall mass transfer. So, two mass transfer resistances would be considered as external film resistances plus intraparticle diffusion or micropore- macropore particle diffusional resistances. Also three mass transfer resistances, including external film resistance, two intraparticle resistances (micropore-macropore), are involved in model equation. Such a model sufficiently describes almost all practical systems.

Adams-Bohart and Thomas models are used to predict the breakthrough behaviour of the dynamic studies performed in this thesis.

The Adams-Bohart Model

The following assumptions are considered in the solution of the Adams- Bohart model.

Following assumptions are made in the solution of Adams-Bohart model:

- The adsorption rate is proportional to both the residual capacity of the adsorbent and the concentration of the adsorbate
- Isothermal column
- Constant linear velocity profile
- Axial dispersion is neglected
- Irreversible equilibrium
- Adsorption can be represented by the following quasi-chemical kinetic rate expression

$$\frac{\partial q}{\partial t} = k_{AB} C_b (q_m - q) \quad (4.38)$$

At equilibrium, ($\frac{\partial q}{\partial t} = 0$) the rate equation reduces to a rectangular equilibrium relationship between the bulk fluid and the adsorbent:

$$\bar{q} = q_e = q_m \quad (4.39)$$

The Adams-Bohart model is used for the description of the initial part of the breakthrough curve (Aksu and Gönen, 2004). This model must also obey the following equation;

$$\frac{\partial C}{\partial z} = -\frac{k_{AB}}{U_0} q C_b \quad (4.40)$$

where k_{AB} is the kinetic constant (mL/ mg/ min) and U_0 is the interstitial velocity (cm/min). Some assumptions are made for the solutions of these differential equation systems: (i) the concentration field is considered to be low, e.g. effluent concentration $C < 0.15C_0$; (ii) for $t \rightarrow \infty$ $q \rightarrow N_0$, (where N_0 is the saturation concentration (mg/ mL))

(Aksu and Gönen, 2004). When the differential equation solved, the following Equation 4.43 is obtained.

$$\ln \frac{C}{C_0} = k_{AB} C_0 t - k_{AB} N_0 \frac{Z}{U_0} \quad (4.41)$$

Adams-Bohart Equation

where Z is the column bed depth (cm).

From the Equation 4.43, values describing the operational parameters of the column can be determined from a plot of $\ln C/C_0$ against t at a given bed height and flow rate.

The Thomas Model

A general analytical solution for a nonlinear (Langmuir) system has been found by Thomas. The Thomas model assumes that adsorption can be described by pseudo second order reaction rate expression;

$$\frac{\partial q}{\partial t} = k_1 C (q_m - q_i) - k_2 q_i \quad (4.42)$$

where q_m is the saturation capacity of the adsorbent, k_1 is the second order forward rate constant and k_2 is the first order reverse rate constant. At equilibrium ($\frac{\partial q}{\partial t} = 0$), Equation 4.42 results in the Langmuir isotherm:

$$q = q_e = q_m \frac{(k_1 / k_2) C_e}{1 + (k_1 / k_2) C_e} = q_m \frac{k_L C_e}{1 + k_L C_e} \quad (4.43)$$

where subscript “e” denotes an equilibrium value, and k_L is the Langmuir constant. Since $k_L = k_1/k_2$, Equation 4.43 can now be expressed in terms of a single rate constant (k_1) and the two Langmuir isotherm parameters (q_m and k_L):

$$\frac{\partial q}{\partial t} = k_1 \left[C(q_m - q) - \frac{1}{k_L} q \right] \quad (4.44)$$

Neglecting axial dispersion, the analytical solutions of Equations 4.36 and 4.44, derived by Thomas (Aksu and Gönen, 2004).

$$\frac{C}{C_0} = \frac{1}{1 + \exp\left(\frac{k_{Th}}{Q}(q_0 X - C_0 V_{eff})\right)} \quad (4.45)$$

Thomas Equation

where k_{Th} is the Thomas constant (mL/ mg/ min), X is the amount of adsorbent (g).

The linearized form of Thomas model is as follows;

$$\ln\left(\frac{C_0}{C} - 1\right) = \frac{k_{Th} q_0 X}{Q} - \frac{k_{Th} C_0}{Q} V_{eff} \quad (4.46)$$

The coefficient k_{Th} and the adsorption capacity of the bed q_0 can be determined from a plot of $\ln[(C_0/C)-1]$ against t at a given flow rate (Q).

CHAPTER 5

BIOLOGICAL ACTIVITIES OF PHYTOCHEMICALS

As already known, phytochemicals exhibit numerous health effects depending on the types and the amounts of bioactive components. There had been lots of studies investigating the antioxidant activities, antimicrobial effects, and cytotoxic properties of phytochemicals. However, recently many researchers have mainly focused on better understanding the mechanism of action of these phytochemicals in biological systems such as that of human. In this chapter, main health effects of them are summarized by explaining their mechanisms of action.

5.1. Antioxidant Activity

Antioxidative properties of polyphenols protect the tissues against free radicals. Occupational exposure to chemically and structurally diverse environmental pollutants including pesticides, toxic chemical wastes, direct and second hand cigarette smoke, gasoline exhaust, urban air pollutants ozone and radiation, and physical stress, produces free radicals. Free radicals have degenerative effects on human health, resulting in oxidative deterioration of lipids, proteins and DNA, activation of procarcinogens, inhibition of cellular and antioxidant defense systems, depletion of sulfhydryls, altered calcium homeostasis, changes in gene expression and induction of abnormal proteins, and contribute significantly to human disease (Bagchi, 2000; Bouhamidi et al., 1998). They are unstable atoms with their extra electron, which have high energy and thus are very reactive. Unstable free radicals try to become stable by transferring their energy to nearby substances and make it unstable substance. This chain reaction continues until blocking the activity of unstable substance by donating to it hydrogen ion, which can be supplied by antioxidants.

In recent years, consumers and food manufacturers have been opting for products with “all natural” labels. The volume of such products increases day by day. Consequently, a lot of emphasis is given to the identification and incorporation of novel, natural antioxidants in food products. The area of natural antioxidants developed

enormously in the past decade mainly because of the increasing limitations on the use of synthetic antioxidants and enhanced public awareness of health issues. In general, natural antioxidants are preferred by consumers because they are considered safe. Numerous reports have been published on the identification of novel, naturally occurring antioxidants from plants, animals, microbial sources, and processed food products.

Based on their function, antioxidants are classified as primary or chain breaking antioxidants, synergistic and secondary antioxidants. Primary antioxidants terminate the free-radical chain reaction by donating hydrogen or electrons to free radicals and converting them to more stable products. They may also function by addition in reactions with the lipid radicals, forming lipid-antioxidant complexes. Synthetic antioxidants, such as BHA- Butylated hydroxyanisole, BHT-Butylated hydroxytoluene, TBHQ-tert-butyl hydroquinone and tocopherols belong to this group. Many of the naturally occurring phenolic compounds like flavonoids, eugenol, and vanillin and rosemary antioxidant also have chain-breaking properties. Other group, synergistic antioxidants can be broadly classified as oxygen scavengers and chelators. They may act as hydrogen donors to the phenoxy radical, thereby regenerating the primary antioxidant. Hence, phenolic antioxidants can be used at lower levels if a synergist is added simultaneously to the food products. Secondary antioxidants such as thioldipropionic acids function by decomposing the lipid peroxides into stable end products. Compounds listed under miscellaneous antioxidants, such as flavonoids and related compounds and amino acids function as both primary antioxidants and synergists (Madhavi et al., 1996).

In the polyphenolic richness of grape skin, seeds and pulp, there are some secondary metabolites important for their antioxidant activity: (+)-catechin and (-)-epicatechin (flavan-3-ols), quercetin, and its glucoside rutin (flavonols), and *trans*-resveratrol (stilbene). Beside these grape skins also contain proanthocyanidin and the major constitutive units of them are epicatechin and epigallocatechin. Their 3-gallates are also encountered as extension units. These polyphenolic compounds are proven to be potent antioxidants and to have important biological, pharmacological and medicinal properties.

Olive leaf extract from *Olea europea* leaves mainly contain five groups of compounds. These are oleuropeosides (oleuropein and verbascoside); flavones (luteolin-7-glucoside, apigenin-7-glucoside, diosmetin-7-glucoside, luteolin and diosmetin);

flavonols (rutin); flavan-3-ols (catechin) and substituted phenols (tyrosol, hydroxytyrosol, vanillin, vanillic acid and caffeic acid) (Garcia et al., 2000).

There are main structural groups determining the antioxidative capacity of the flavonoids. These are;

- The *o*-dihydroxy (catechol) structure in the B-ring, which confers greater stability to aroxyl radicals
- The 2,3-double bond conjugated with a 4-oxo function, responsible for electron delocation from the B-ring
- 3- and 5-hydroxyl groups for maximal radical-scavenging capacity.

The main structure, which confers the antioxidant properties to the polyphenols of the olive leaf extract, is the *o*-dihydroxy (catechol) structure in the moities (Garcia et al., 2000).

Garcia et al. (2000) reported the sequence of the antioxidant capacity of the flavonoids in olive leaf extract as rutin > catechin \approx luteolin > hydroxytyrosol > diosmetin > caffeic acid > verbascoside > oleuropein > luteolin -7- glucoside \approx vanillic acid \approx diosmetin-7-glucoside > apigenin -7- glucoside > tyrosol > vanillin.

The high antioxidant capacities of rutin, catechin and luteolin show the importance of the flavonoid B-ring catechol structure (rutin, catechin, luteolin); the 3-hydroxyl free or glycosylated group (catechin and rutin); and the 2,3-double bond conjugated with a 4-oxo function (rutin and luteolin). Although the 2,3-double bond conjugated with a 4-oxo function is absent in the catechin, its antioxidant activity is nearly the same with luteolin which confirms the importance of the flavonoid B-ring catechol and free 3-hydroxyl group. The antioxidant activity of oleuropein is mainly due to the hydroxytyrosol moiety in its structure but because of its high molecular weight, its antioxidant capacity is lower than the hydroxytyrosol (Garcia et al., 2000).

5.2. Antimicrobial Activity

Antimicrobial activities of plant extracts and active components isolated from them are generally investigated against both gram negative and gram positive bacteria. So, it is important to understand the cell morphology of the bacteria in order to explain the antimicrobial mechanism.

The cell wall of gram negative bacteria has a greater complexity than the gram positive bacteria (Table 5.1).

Table 5.1. Difference between gram positive and gram negative bacteria

Component	Gram-positive bacteria	Gram-negative bacteria	
		Inner rigid wall layer	Outer wall layer
Peptidoglycan	+	+	-
Teichoic Acid	+	-	-
Polysaccharide	+	-	-
Protein	+ or -	-	+
Lipoprotein	-	+ or -	+
Lipopolysaccharide	-	-	-

Gram negative bacteria include additional outer membrane, which is composed of lipopolysaccharide and proteins, when compared with the gram positive ones. The components of the gram negative bacteria are porins, lipopolysaccharides, lipoproteins, peptidoglycan layer and periplasmic space (Figure 5.1).

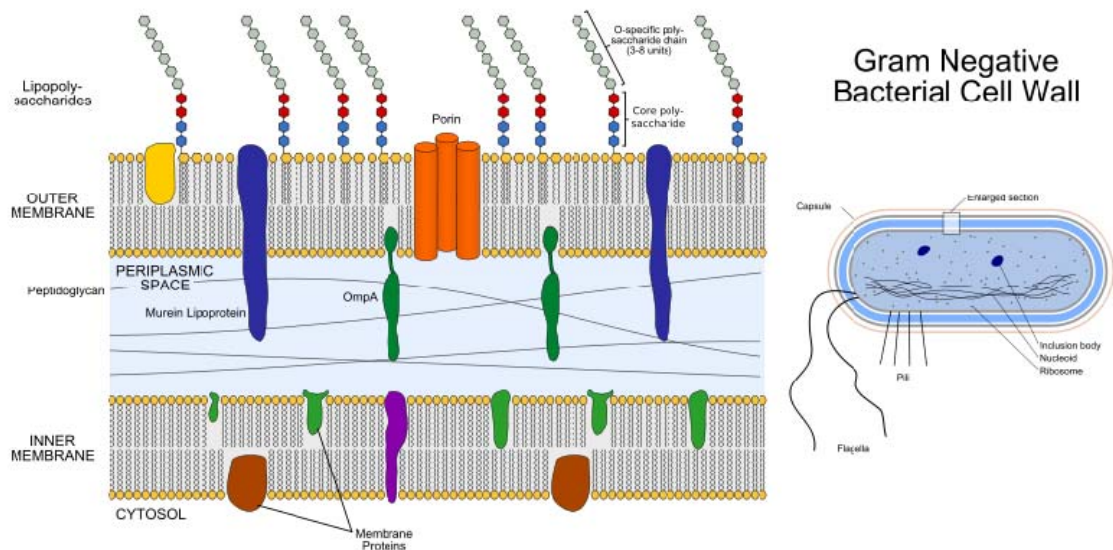


Figure 5.1. Cell wall of gram negative bacteria.

In the gram positive bacteria, such as *S. aureus* and *E. faecalis*, the cell wall is thick (15-80 nanometers) consisting of several layers of peptidoglycan. On the other

hand, gram negative bacteria such as *E. coli* and *P. aeruginosa* have a relatively thin (10 nanometers) cell wall surrounded by an outer membrane (Figure 5.2.). The membranes are a bilayered structure and a selective permeability barrier that regulates the passage of substances into and out of the cell. The outer leaflet of the membrane comprises a complex lipopolysaccharide whose lipid portion acts as an endotoxin. If endotoxin enters the circulatory system it causes a toxic reaction. This may lead to endotoxic shock, which may be fatal. This outer membrane protects the bacteria from several antibiotics, such as penicillin, dyes and detergents which would normally damage the inner membrane or cell wall.

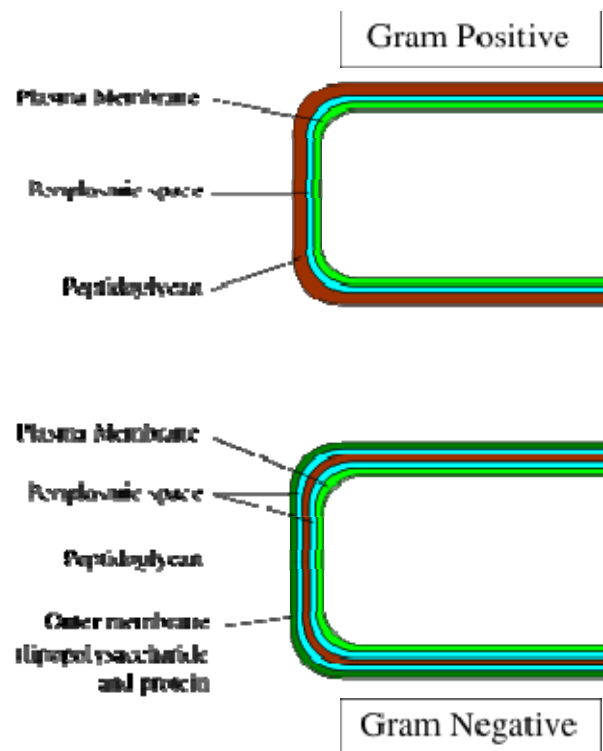


Figure 5.2. Differences of the cell wall structure of gram negative and gram positive bacteria.

Both electrostatic and hydrophobic interactions are involved in maintaining the spatial organization of the membrane components (Ingram and Buttke, 1984). It is well accepted that disorganization of the membrane by undesired or foreign substances can cause loss of either the permeability or the integrity of the membrane. This ultimately causes the death of the cell.

For many antimicrobial agents, antimicrobial actions are initiated by interactions of the biocides with the cell wall membrane of the microorganisms. The agents then penetrate into the cell and finally act at the target sites. Phenolic components from plant extracts may behave as in this direction. The phenolic compounds may produce the effect by acting extracellularly or by acting on intracellular targets. Kaur and Singh (2008), investigated that, extract of *Livistona chinensis* fruit, which contain soluble components both in polar and nonpolar solvents, cross the cell membrane first and then interact with the intercellular compartment. As the contact time between the extract and cells are increased, more -OH groups are ionized and they lead to increase in the membrane permeability of phenolic compounds and hence increase intracellular accumulation (Kaur and Singh, 2008). In another study, Kim and Fung (2004) remarked the difficulty to explain antimicrobial mechanism. However, they concluded that phenolic compounds from crude water soluble tea extracts may act on microbial cell walls or membranes, proposing that they inhibit microbial growth by change of microbial cell permeability which leads to loss of intracellular molecules such as protein, DNA, RNA and ATP.

5.3. Cytotoxic Activity

Cancer is a class of diseases in which a group of cells display *uncontrolled growth* (division beyond the normal limits), *invasion* (intrusion on and destruction of adjacent tissues), and sometimes *metastasis* (spread to other locations in the body via lymph or blood). These three malignant properties of cancers differentiate them from benign tumors, which are self-limited, and do not invade or metastasize. Most cancers form a tumor but some, like leukemia, do not.

Cancer may affect people at all ages, even fetuses, but the risk for most varieties increases with age. Cancer causes about 13% of all human deaths. According to the American Cancer Society, 7.6 million people died from cancer in the world during 2007 (Jang et al., 1997).

Nearly all cancers are caused by abnormalities in the genetic material of the transformed cells. These abnormalities may be due to the effects of carcinogens, such as tobacco smoke, radiation, chemicals, or infectious agents. Other cancer-promoting genetic abnormalities may be randomly acquired through errors in DNA replication, or

are inherited, and thus present in all cells from birth. The heritability of cancers is usually affected by complex interactions between carcinogens and the host's genome.

A diet which is rich in plant foods contains a variety of secondary metabolites and contributes to protecting the body against cancer. Secondary metabolites carried out a number of protective functions in the human body. They can boost the immune system, protect the body from free radicals and relevantly exhibit anti-carcinogenic activity by serving properties as protective agents against various pathogens and as growth regulatory molecules. Due to these physiological functions, secondary metabolites are potential anticancer drugs, since either direct cytotoxicity is affected on cancer cells or affected on tumor development.

A variety of phytochemicals, such as sulfides, isothiocyanates, glucosinolates, flavonoids, carotenoids, phenols, and diarylhepanoids, are known to mediate chemopreventive responses (Jang et al., 1997). One of the most fascinating molecules is resveratrol. Synthesis of resveratrol in grapes most likely associated with stress factor such as UV-radiation, injury or fungal invasion. This suggested that the compound was biosynthesized soon after the recognition of the pathogen by the plant. This property was the starting point of the idea about the cytotoxic property of it. Resveratrol inhibits the cyclooxygenase activity and antipromotional activity correlated with its antioxidant and antimutagen property. Furthermore, it induced phase II drug metabolizing enzymes involved chiefly in the detoxification of carcinogen metabolites (anti-initiation activity) and induced human promyelocytic leukemia cell differentiation (antiproliferation activity). Finally, antitumor and anti-inflammatory effects were observed with mouse and rat models, respectively, providing support for the physiologic significance of the *in vitro* and cell culture data. (Jang et al., 1997).

CHAPTER 6

MATERIALS AND METHODS

6.1. Materials

Grape pomace was obtained from Ege region in Turkey from Urla-İzmir and Muğla. Olive leaves used in all experiments were collected from the olive trees grown in the campus of Izmir Institute of Technology in Izmir Turkey.

Silk fibroin obtained from the Smiss Co. TM was used in this study. The particle size is lower than 20 μm and it was sterilized. So, it was directly used in adsorption studies. On the other hand, natural zeolite is obtained from the Gördes region, Turkey. For the preparation of the natural zeolite to the adsorption studies, it was crushed and sieved into 5 different particle sizes. The preparation procedure is given in Appendix A.1.3.

Polyphenolic compounds of grape skin, such as (+)-catechin, (-)-epicatechin, gallic acid, rutin, kaempferol, quercetin and *trans*-resveratrol (*trans*-3,5,4'-trihydroxystilbene) as HPLC standards were purchased from Sigma Chemical Co. Free samples of the extract obtained from *polyganum cuspaditum*, Chinese plant, was obtained from Tianjin Jianfeng Natural Product R&D Co., Ltd. (Tianjin extract), which was used to investigate the behaviour of adsorbents used in this study. The purity of it was checked by comparing the high purity (>99%) of HPLC standard. On the other hand, main phenolic compound of olive leaf, which is oleuropein, was purchased from Extrasynthese, France.

All solvents used during the HPLC study are HPLC grade. Acetic acid and acetonitrile was purchased from Merck, Darmstadt. The other reagents were analytical grade, which were ethanol, methanol and acetone supplied by Merck, having a purity of >95%.

6.2. Methods

Experimental work performed under three main groups. The first group is the pretreatment and extraction of olive leaf and grape skin antioxidants. This part includes the identification of olive leaf and grape skin phenolic compounds. Moreover, the effects of extraction methods, solvents, temperature changes on the chromatographic analysis of polyphenolic compounds are also involved. The second group consists of adsorption of olive leaf and grape skin antioxidants on silk fibroin and clinoptilolite. In this part, the methods for the characterization of bioactive compounds and the characterization of adsorbents before and after adsorption are also given. Moreover, the methods used for the determination of antimicrobial, antioxidative and cytotoxic properties of the bioactive compounds are given. The last group belongs to the dynamic adsorption studies performed with the crude extracts. The experimental procedure followed in this study is schematically represented in Figure 6.1.

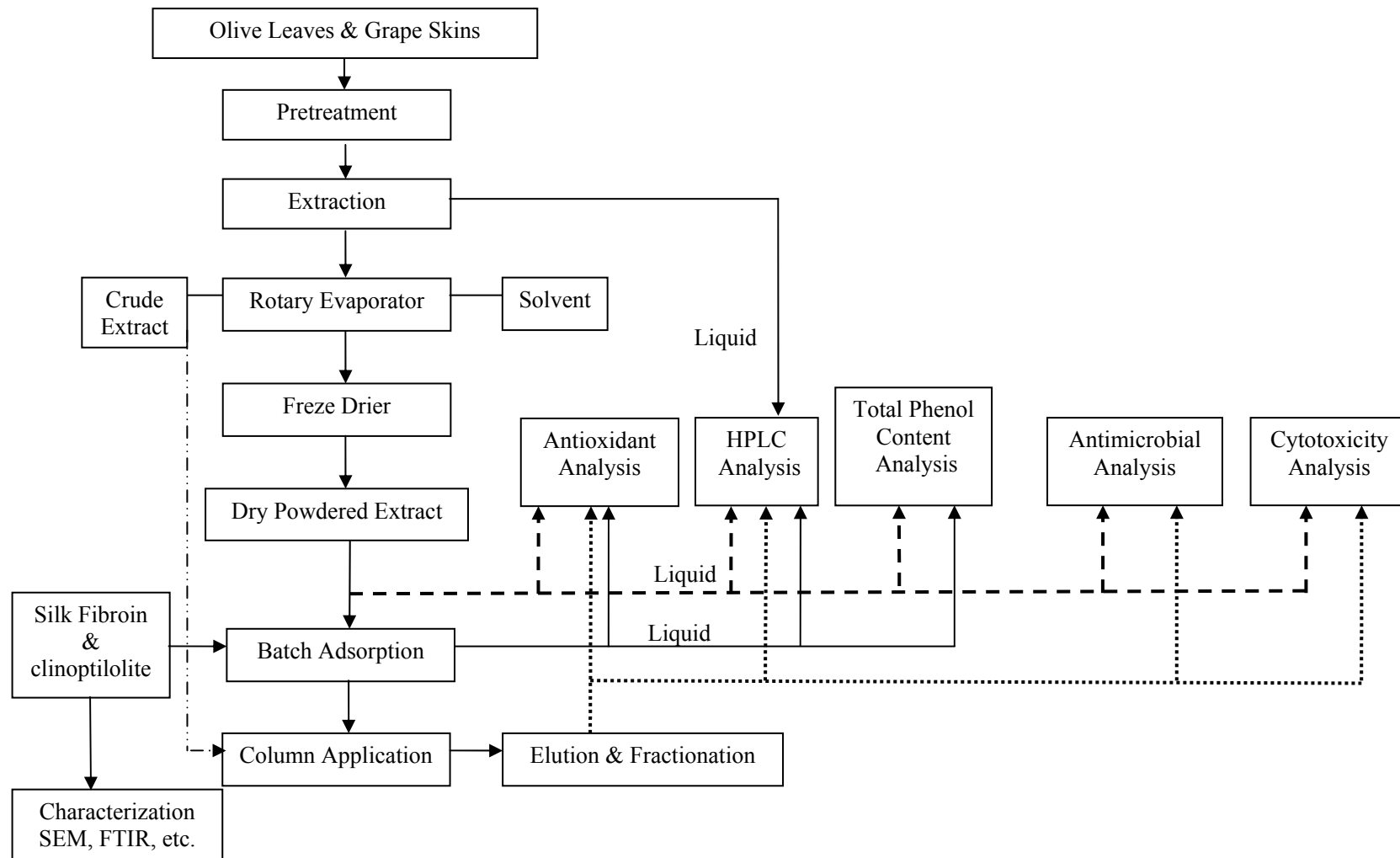


Figure 6.1. Experimental procedure of the study.

6.2.1. Pretreatments of Olive Leaf and Grape Pomace

Grape pomace was washed and seeds were separated from stems and skins. After that they were dried in an oven at 40 °C for 3 days. Skins were separated from stems and each part of grape pomace was grinded and kept in dark at 4 °C.

Olive leaves were washed and dried in an oven at 40 °C for 4 days. Dried olive leaves were grinded and kept in dark.

6.2.2. Extraction

6.2.2.1. Extraction Studies with Grape Skin

Grape seeds, skins and stems were used to determine the *trans*-resveratrol content of pomace. For this purpose, traditional liquid-solid extraction method and ultrasonic extraction method were selected. Solid liquid ratio was kept constant as 1/10 for both of the methods. In order to investigate the importance of selecting appropriate extraction solvents; pure ethanol, pure methanol, and their 20% aqueous forms were used in extraction experiments. In order to determine the effect of temperature on extraction yield of *trans*-resveratrol in solvent extraction method, 30 °C and 60 °C were chosen. In each one of the temperature conditions tested, *trans*-resveratrol content at certain times of extraction (15, 30, 60 minutes and 24hours) was determined by RP-HPLC. After applying extraction, crude extracts were centrifuged for 5 min at 5000 rpm. In case of the low concentration of *trans*-resveratrol in the extract (i.e. because of the detection limit of HPLC), 1 mL of sample was concentrated to 0.1 mL with a SpeedvacTM vacuum concentrator at 40 °C for 6 hours. After removing solvent with rotary evaporation at 40 °C, crude dry extract was obtained with freeze drier, which was applied at -52 °C and 0.2 mbar.

6.2.2.2. Extraction Studies with Olive Leaves

The solvent type is the most important factor affecting the efficiency of liquid solid extraction. For this reason, different solvents; acetone, ethanol and their aqueous

forms (10- 90%, v/v) were investigated to determine the effective extraction of polyphenolic compounds from olive leaf. Deionized water was used in all experiments. After 24 hours extraction time, the extracts were filtrated and centrifuged for 5 min at 5000 rpm. The total phenol contents and antioxidant capacities of all extracts were determined. In order to obtain dried olive leaf extract, the extraction solvent was removed by using rotary evaporator at 40 °C with a 120 rpm rotation under vacuum. Then, solvent free olive leaf extract was dried by using a freeze drier system at -52 °C and 0.2 mbar. Crude dry extract was stored in light protected glasses until further use.

The time required for the effective extraction was determined by taking samples against time and by analysing these samples for their total phenol content.

6.2.3. Identification of Bioactive Compounds

Polyphenolic compounds of olive leaf and grape skin were analyzed with HPLC. The detailed HPLC procedure was given in Appendix A.1.2. For the quantitative analysis of grape skin polyphenols, the calibration curves for gallic acid, (+)-catechin, (-)-epicatechin, *trans*-resveratrol, quercetin and kaempferol were obtained and given in Appendix C. In case of the analyzing olive leaf's polyphenols, the amount of oleuropein and rutin were calculated using the calibration curves of them (Appendix C).

Since crude extract of grape skin contains many phenolic components at different polarities, it is possible to separate them from each other by dissolving the freeze dried solvent free crude extracts with different solvents having different polarities. For this purpose, dry extract of grape skin was dissolved in water, ethanol-water solutions and pure ethanol subsequently, and it was illustrated in Figure 6.2.

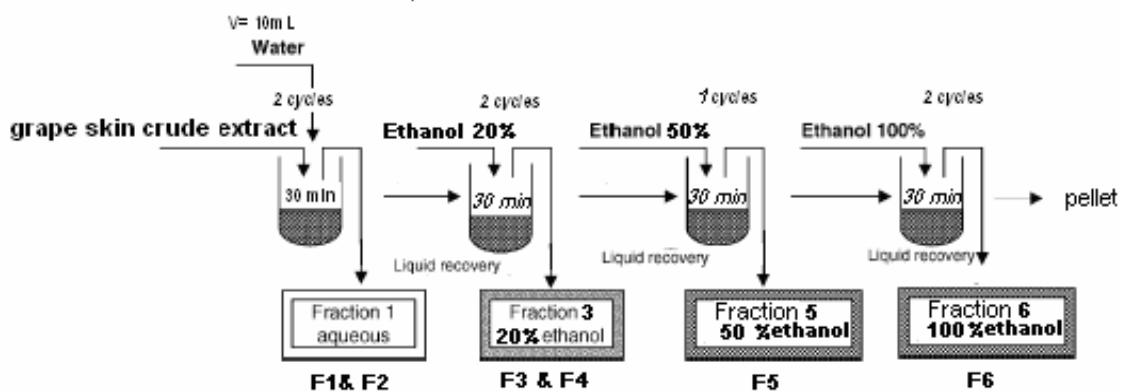


Figure 6.2. Sample preparation for HPLC analysis of grape skin crude extract fractional dissolution of polyphenolic compounds.

The fractions obtained from this procedure were qualitatively analyzed with HPLC. This procedure is very beneficial and useful in industrial scale production of bioactive compound from crude extract by decreasing the difficulties of column separation by some extent. After prior separation of bioactive compounds from crude extract, it would increase the efficiency of the column application, which is used for the selective separation of individual compound with a high purity.

6.2.4. Bioactivity Tests

Plant source phenolic compounds exhibit important biological activities and extensive researches have been performed recently in this field. Phenolic compounds may have activity either as a single compound or as synergistically by two or more compounds. Thus, separation of active compounds from crude extract has become important. For large scale production, it is also inevitable to optimize process steps.

In order to exhibit the effectiveness of the separation process, the biological activities of separated fractions such as antimicrobial activity, antioxidant activity and cytotoxic activities were studied. The methods to investigate those activities are given in Appendix (A.2.1-A.2.3).

6.2.5. Adsorption Studies

In the production of high value added products, adsorption purification process has special value for selective separation of the active compounds from the crude extract. Finding the proper low cost adsorbent; and the determination of the behaviour of the adsorbent against those polyphenolic compounds is essential; and is the most important step for the process.

6.2.5.1. Adsorbents

Adsorption studies were performed with two adsorbents: clinoptilolite and silk fibroin. The surface morphology of the adsorbents was analyzed by scanning electron microscope (SEM; Philips XL 30S FEG, FEI Company, Eindhoven, Netherlands) and prior to analysis, samples were mounted on metal grids, using double-sided adhesive tape and coated with gold under vacuum.

The change in the crystalline state was monitored by X-ray diffractometry (XRD; Xpert Pro, Philips) with CuK_α radiation for 2θ from 0 to 60° . Enrichment of the mineral was performed by the method given in the section of “purification of natural zeolite”. The size reduction procedure of the natural zeolite prior to use in the adsorption studies was given in Appendix A.1.3.

Determination of the Purity

In the determination of the purity of the mineral the method given by Nakamura et al. (1992) was applied. In this method, the summation of the seven intensities of the characteristic peaks belonging to the clinoptilolite in the range of 2θ range of 9.82° - 19.02° ($2\theta = 9.82^\circ, 11.15^\circ, 13.07^\circ, 14.89^\circ, 16.91^\circ, 17.28^\circ, \text{ and } 19.02^\circ$). The clinoptilolite purity of the samples was determined by comparing the sum of intensities with the reference Idaho samples (27031, Castle Creek, Idaho; referred as Idaho sample in this thesis), whose purity was 95%.

Inductively Coupled Plasma- Atomic Emission (ICP-AES) Analysis

Chemical analysis of the clinoptilolite rich minerals were determined by Varian ICP-AES. The borate fusion method was used in the determination of the major elements, sodium, calcium, magnesium, potassium, copper, aluminum, iron, manganese and zinc. The calibration curves of these elements were obtained with multielement standard of them. Silicon standard was used for the quantitative determination of it. 0.1 g of the sample was mixed with 1 g of lithium tetraborate until homogeneity was obtained. Then it was placed in 1000 °C furnace for 1 h. The glass bead formed was dissolved in 70 mL, 1.6 M HNO₃ and was completed to 250 mL with deionized water.

Purification of Natural Zeolite

CL5 sample was further purified in order to obtain high purity of clinoptilolite. For this purpose, 15 g of CL5 sample was shaking with 75 mL of boiling deionized water for 5 min in a beaker. After waiting for 10 min for settling, the precipitate was separated from the supernatant, which include suspended clinoptilolite. Centrifugal force was used to separate and collect the suspended clinoptilolite from water. For this purpose, subsequent centrifugation was applied at 1000 rpm, 3000 rpm and 5000 rpm. At each step, supernatant was separated from the precipitate, and precipitates were collected and purity test was applied using XRD.

6.2.5.2. Adsorption of Olive Leaf Polyphenols

Following the extraction, separations of polyphenols of olive leaf crude extract were performed by subsequent use of silk fibroin filled and clinoptilolite filled columns.

Olive leaf crude extract (OLCE) was obtained by extraction, which was performed at the following optimized conditions as given in section 7.1.2. Extraction of bioactive compounds was performed with 70% ethanol by keeping solid-liquid ratio and temperature as constant at 1/20, at room temperature, respectively. Ethanol was removed by the rotary evaporation at 40 °C. Then, extract was placed in a +4 °C to settle down the chlorophyll. Polyphenolic compounds of ethanol and chlorophyll free extract were analysed by HPLC. Oleuropein and rutin contents of the extract were

quantitatively determined using calibration curves, whereas other compounds qualitatively determined. Finally, crude dry olive leaf extract was obtained by freeze drier.

Powdered solvent free olive leaf crude extract samples as 1 g and 1.5 g were dissolved in 40 mL of deionized water at room temperature with magnetic stirring. Then, solutions were centrifuged at 5000 rpm for 5 min. Remaining water-soluble fractions in pellet were re-dissolved with 5mL of deionized water and solution was centrifuged. The supernatants were collected and completed to 50 mL with deionized water. A syringe column of 63 mm in length and 10 mm internal diameter with teflon fittings was used. After filling it with 0.2 g of powdered silk fibroin, the column was preconditioned by washing with 5 mL of deionized water, ethanol and deionized water, respectively. Then, extract solution was loaded to the preconditioned column by GilsonTM ASPEC XL liquid handling system at constant flow rate. The loading breakthrough curves of oleuropein and rutin were obtained by analyzing their concentration at the column outlet with HPLC. After saturation of column with oleuropein and rutin, the fractions were eluted by washing the column with water and then with aqueous ethanol solutions. Polyphenolic composition of these fractions, which were called as water fraction and ethanol fraction, were analyzed by HPLC. Antioxidant capacities, antimicrobial activities and cytotoxic effects of these fractions were tested according to methods given in Appendix A.2 and compared with the solvent free OLCE. For the adsorption of ethanol free OLCE by clinoptilolite, ethanol and water fractions of OLCE obtained from the silk fibroin loaded column, were used with different inlet concentrations. Samples were centrifuged at 5000 rpm for 5 min prior to adsorption experiments. Folin-ciocalteu method (App. A.1.1) was used for the determination of the total phenol content of the extract. For the adsorption kinetics, batch studies were performed in a thermoshaker at 25 °C with a solid-liquid ratio as 1/40. Samples were taken against time and were centrifuged at 3000 rpm for 5 min at 25 °C. Then, total phenol contents of the samples were determined.

The effect of initial OLCE concentration, particle size, agitation speed, temperature and the purity of the adsorbent on adsorption were investigated. The experimental conditions are given in Table 6.1.

Table 6.1. Experimental conditions for the adsorption of OLCE onto clinoptilolite at constant solid/liquid ratio (1/40)

Parameters				
Particle size (µm)	Initial concentration (mg GAEq/mL)	Agitation speed (rpm)	Purity of clinoptilolite (%)	Temperature (°C)
250-425, 106-150, 75-106, <25, <25 (clinoptilolite rich)	0.164	180	<58, 61,69, 78, 91	25
<25 (clinoptilolite rich)	0.053, 0.107, 0.187, 0.244, 0.311, 0.369, 0.909	180	91	25
<25 (clinoptilolite rich)	0.224	50-100-180	91	25
<25 (clinoptilolite rich)	0.079	180	91	10, 20, 30, 40

6.2.5.3. Adsorption of Grape Skin Polyphenols

To understand the behaviour of the both silk fibroin and natural zeolite, individual adsorption studies of each major polyphenolic standards, which are gallic acid, (+)-catechin, (-)-epicatechin, and *trans*-resveratrol, were performed in batch adsorption studies. The initial concentrations of the standard solutions were; 0.531 mg/mL gallic acid, 0.784 mg/mL, (+)-catechin, 0.802 mg/mL (-)-epicatechin and 0.091mg/mL *trans*-resveratrol. Additionally, adsorption studies were performed with the multi-compound mixtures of those standards to investigate the difference between the mono-compound and multi-compound adsorption properties of the adsorbents. Uptake curves for these adsorption studies were obtained by taking samples against time and by analyzing the samples with HPLC. In order to keep solid- liquid ratio constant, series of flasks were prepared including 0.5 g of the adsorbent. Each of these flasks was used for separate sampling at certain times and after centrifugation of the samples at 5000 rpm for 5 min, samples were analyzed with HPLC. The solid-liquid

ratio, temperature and shaking speed were kept constant during the experiments at 1/20, 30 °C and 180 rpm, respectively.

After the investigation of adsorption behaviours of both adsorbents on the adsorption of grape skin polyphenolic compounds, adsorption studies for the *trans*-resveratrol were performed because of its beneficial properties. Since the solubility of *trans*-resveratrol plays role in the adsorption, the ethanol concentration of the solution was changed from 10% to pure ethanol (by 10% increments) and adsorption experiments with both clinoptilolite and silk fibroin were performed using these solutions. The other parameters such as *trans*-resveratrol concentration (1.12 mg/mL), solid-liquid ratio (1/40), temperature (30 °C), contact time (3 hour) and shaking speed (180 rpm) were kept constant.

After the determination of appropriate composition of the solution, where the maximum adsorbed amount of *trans*-resveratrol was achieved, adsorption isotherms were obtained by changing the initial concentration of *trans*-resveratrol while considering the solubility of *trans*-resveratrol. In order to obtain the adsorption isotherm of *trans*-resveratrol on adsorbents, adsorption experiments were carried out by keeping solid-liquid ratio, temperature, shaking speed as constant. Adsorption isotherms of 51.5% pure polyganum cuspidatum's *trans*-resveratrol onto clinoptilolite and silk fibroin were obtained. Additionally, pure *trans*-resveratrol was used to obtain adsorption isotherm for clinoptilolite rich CL5 sample. In the adsorption studies, the effects of solid-liquid ratio, initial concentrations, agitation speed, temperature change, purities of *trans*-resveratrol and clinoptilolite were investigated. The experimental conditions for the adsorption studies performed with the silk fibroin and clinoptilolite are illustrated in Table 6.2 and Table 6.3, respectively.

Table 6.2. Experimental conditions for the adsorption of the grape skin polyphenols onto the silk fibroin; particle size of the silk fibroin was <20 μm

Parameters for adsorption of <i>trans</i>-resveratrol by silk fibroin				
Solid-liquid ratio	Initial concentration (mg/ mL)	Agitation speed (rpm)	Purity of <i>trans</i>-resveratrol (%)	Temperature ($^{\circ}\text{C}$)
1/40, 1/50, 1/60, 1/70, 1/80, 1/90	0.856	180	51.5	30
1/40	0.171, 0.315, 0.360, 0.635, 0.756, 0.994, 1.053, 1.176, 1.301	180	51.5	30
1/40	Varying concentrations between 0.099- 1.084	180	51.5	30, 40, 50

The solubility limits of *trans*-resveratrol in 10% and 20% ethanol solution at 30 $^{\circ}\text{C}$ and were controlled by dissolving subsequently increased amounts of *trans*-resveratrol in solution. After centrifugation of these solutions at 5000 rpm and 30 $^{\circ}\text{C}$ for 5 minutes, HPLC analyses of the solutions were performed and quantitative results were compared with the dissolved amount of *trans*-resveratrol.

After investigating the adsorption behaviour of both of the adsorbents, the selective separation of *trans*-resveratrol from the mixture of polyphenolic standards solution was tried to be performed.

Table 6.3. Experimental conditions for the adsorption of the grape skin polyphenols onto the clinoptilolite

Solid-liquid ratio	Particle size (μm)	Initial concentration (mg GAEq/mL)	Agitation speed (rpm)	Purity of clinoptilolite (%)	Purity of <i>trans</i> -resveratrol (%)	Temperature ($^{\circ}\text{C}$)
Sorption studies performed with 51.5% pure <i>trans</i>-resveratrol obtained from polyganum cuspaditum						
1/40	<25	0.099, 0.192, 0.238, 0.361, 0.572, 0.845	180	91	51.5	30
1/10, 1/20, 1/30, 1/40	45-75	0.099	180	64	51.5	30
1/40	<25	Varying concentrations	150	91	51.5	15, 25, 40
1/40	<25	0.072-0.185	150	91	51.5, 99	40
Sorption studies performed with pure <i>trans</i>-resveratrol						
1/40, 1/100, 1/120	<25	0.010- 0.084	150	91	99	30
1/120	<25	Varying concentrations	150	91	99	25-45
1/120	<25	0.038	50, 100, 150	91	99	30
1/120	Coarse, mid, fine	0.038	150	-	99	30
Sorption isotherm						
1/40	45-75		150	64	51.5	40
1/40	<25		150	91	51.5	40
1/120	<25		150	91	99	40

6.2.6. Dynamic Column Studies of Grape Skin Polyphenols

Dynamic adsorption and desorption experiments were carried out in a syringe column (63 mm length, 10 mm internal diameter) with inert supports. Column was filled with 0.2 g of silk fibroin and subsequent preconditioning was performed by washing it with 5 mL of water, 5 mL ethanol and again 5 mL of water. The mixture of polyphenols, which consists of (+)-catechin, (-)-epicatechin, gallic acid and *trans*-resveratrol in a 20% ethanol solution, was prepared with a inlet concentration of 0.249 mg/mL, 0.248 mg/mL, 0.252 mg/mL, and 0.247 mg/mL, respectively. The mixture was loaded to the preconditioned column with a constant flow rate (1 mL/min) by GilsonTM SPE system. Column effluents were analyzed with HPLC in order to determine the

breakthrough profile of the silk fibroin in the column by obtaining the loading breakthrough curves.

After saturation of the column, the fractions were eluted by washing the column with water and then with aqueous ethanol solutions. The selectivity of the silk fibroin in column was investigated. Column efficiency was also tested by two times loading and desorbing of mixture including *trans*-resveratrol, gallic acid, (+)-catechin and (-)-epicatechin.

Dynamic Column Studies Performed with the trans-Resveratrol

After investigating the performance and selective separation properties of *trans*-resveratrol from the silk fibroin loaded column, dynamic column studies were performed with *trans*-resveratrol in order to optimize the operating parameters, such as flow rate, initial concentration of the solution and adsorbent amount in the column. 51.5% pure polyganum cuspidatum *trans*-resveratrol (obtained from Tianjin) was used in studies because of the low cost and considerably high purity of it.

The experimental setup was shown in Figure 6.3.

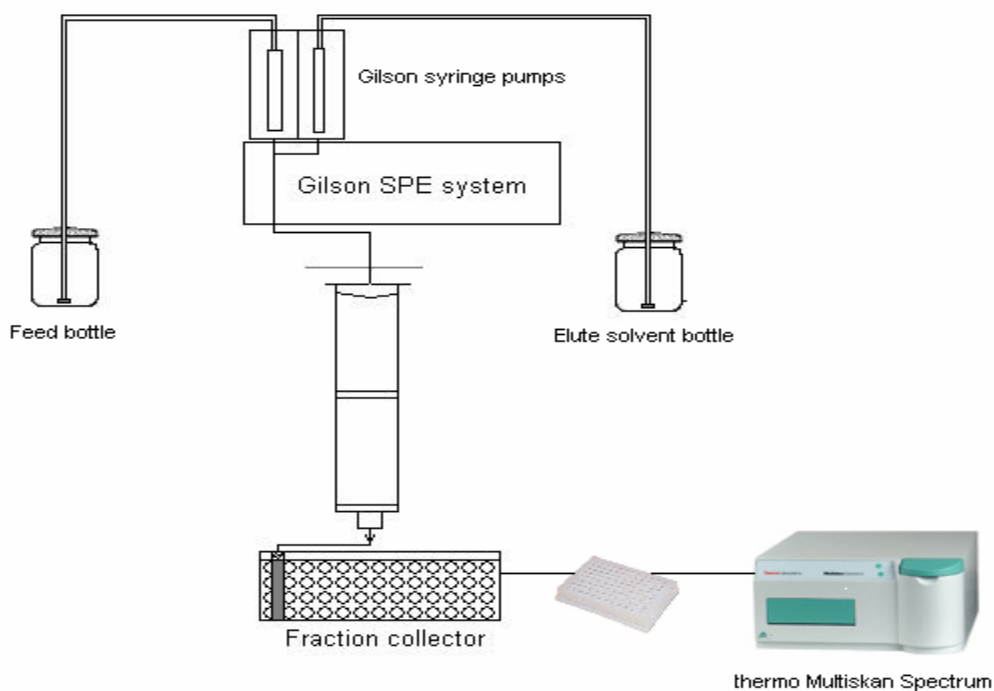


Figure 6.3. Flow scheme of the apparatus for column study.

This is developed automated system, which enables loading and desorbing of the analytes by controlling the flow rate by GilsonTM solid phase extraction (SPE) system, collecting column outlets by fraction collector on 96-well microplate and measuring absorbance with ThermoTM microplate reader.

Trans-resveratrol aqueous solution with different inlet concentrations of *trans*-resveratrol ranging from 0.0095 to 0.205 mg/mL were passed through an adsorption column packed with silk fibroin. The adsorption column was 63 mm in length and 10 mm in diameter (Figure 6.3). Samples were periodically taken from the effluent to determine the *trans*-resveratrol concentration and to calculate the dynamic adsorption capacity. Additionally, the effects of flow rate and amount of adsorbent were investigated by changing flow rates from 0.5 mL/min to 1 mL/min and changing column depths from 10 to 14 mm.

Trans-resveratrol was analysed using Thermo multiscan spectrum instrument with direct absorbance measurement at 306 nm with UV-transparent 96-well plate. Calibration curve for *trans*-resveratrol was obtained by comparing its absorbance values with HPLC analysis (Appendix A.1.6., Figure A.8) and used to determine of the solution concentration.

CHAPTER 7

RESULTS AND DISCUSSIONS

7.1. Extraction Studies

7.1.1. Extraction of Bioactive Compounds from Grape Pomace

Different parts of grape pomace were used in the extraction studies in order to determine the potential source of *trans*-resveratrol. Highest yield was obtained with grape skin as 0.156 mg/g dw. Stem of grape pomace did not a good source of *trans*-resveratrol (Table 7.1). Thus, for further studies grape skin was selected and extraction studies were performed with it.

Table 7.1. *Trans*-resveratrol content of different part of grape pomace obtained from Muğla. Solid liquid extraction was performed with a 1:10 (solute:solvent) ratio in thermostated water bath

Extracted part	Extraction conditions	<i>Trans</i> -resveratrol content (mg/g dry sample)
Skin+stem	60 °C for 30 min	0.104 (± 0.003)
Stem	60 °C for 30 min	0.022 (± 0.001)
Skin	60 °C for 30 min	0.156 (± 0.002)
Skin	60 °C for 40 min	0.081 (± 0.002)
Skin	30 °C for 30 min	-

The extraction yield of *trans*-resveratrol was decreased nearly two fold when extraction time was increased to 40 min. Thus, we can conclude that extraction time is very critical parameter that directly effects the extraction of *trans*-resveratrol, since *trans*-resveratrol is known to thermally decompose in alcoholic solution at > 60 °C

(Perez et al., 2001). Another extraction study was performed at 30 °C in spite of 60 °C, but *trans*-resveratrol was not detected in the extract.

Highest extraction yield of *trans*-resveratrol was achieved for the Urla region grape pomace as 0.227 mg/g of dry powder sample when extracted with 80% ethanol for 30 minutes at 60 °C (Table 7.2.). It was 0.156 mg/g of dry powder sample when Muğla region grape pomace was used. Thus, the origin, species, and harvest time are important parameters of *trans*-resveratrol content of grape pomace.

Table 7.2. *Trans*-resveratrol content of different part of grape pomace obtained from Urla. Solid liquid extraction was performed with a 1:10 (solute:solvent) ratio in thermostated water bath

Extracted part	Extraction conditions	<i>Trans</i> resveratrol content (mg/g dry sample)
Skin+stem	60 °C for 30 min	0.161 (± 0.001)
Stem	60 °C for 30 min	0.040 (± 0.002)
Skin	60 °C for 30 min	0.227 (± 0.001)

As an alternative to conventional solvent extraction method, ultrasonic extraction technique (US) was used to extract *trans*-resveratrol. Because of the higher yield of *trans*-resveratrol, Urla region grape skins were used. The effects of method on extraction yields of *trans*-resveratrol were compared by analyzing the crude extracts with HPLC. Additionally, effects of many parameters on extraction efficiency, such as solvent types, extraction time and temperature were investigated for both of the extraction methods.

The other bioactive compounds in grape skin also have great importance. So, it is important to determine the effect of selected extraction methods and extraction conditions on other compounds. Table 7.3 summarizes the effect of extraction methods, temperature and solvent on the polyphenolic compounds in the extract. Standard solutions of grape skin polyphenols were searched in the crude extract. The HPLC method was developed and calibration curves were obtained belonging to these standard compounds (Appendix C). The detailed HPLC method was given in Appendix A1.2.

Table 7.3. Polyphenol composition (mg/g dw) of grape skin extract extracted with different extraction methods and conditions

Phenolic Components \ Extraction condition	In thermoshaker, 30 °C, 180 rpm, 30 min, 80% ethanol	In water bath, 60 °C, 30 min,	
		80% methanol	80% ethanol
GA	0.3106	0.5007	0.2274
(+)-catechin	1.2079	1.9802	1.2745
(-)-epicatechin	0.6988	0.8402	0.3506
Rutin	0.4304	0.5522	0.2664
<i>Trans</i> -resveratrol	npd	0.2090	0.0574
Quercetin	npd	npd	npd
Kaempferol	npd	npd	npd
<i>Chromatograms were given in Appendix B</i>	App. B.1.	App.B.2.	App.B.3.
Phenolic Components \ Extraction condition		US extraction, 30 °C, 30 min,	
		80% methanol	80% ethanol
GA		0.3683	0.3366
(+)-catechin		0.5690	1.2903
(-)-epicatechin		0.8299	0.7791
Rutin		0.4137	0.4329
<i>Trans</i> -resveratrol		0.2037	0.0755
Quercetin		npd	npd
Kaempferol		npd	npd
<i>Chromatograms were given in Appendix B</i>		App. B.4.	App.B.5.

In solvent extraction method, highest *trans*-resveratrol recovery was achieved with the 80% methanol at 60 °C for 30 min as 0.209 mg/g dw (Table 7.3.). Similar results reported in the study of Romero-Perez et al. (2001). They reported that the effective extraction was attained with 80% methanol maintained at same conditions, and severe extraction conditions (higher temperature and longer extraction times) caused the degradation of *trans*-resveratrol. In the case of using 80% ethanol instead of 80%

methanol as a solvent, *trans*-resveratrol recovery decreased 4 times. In ultrasonic extraction method, similar results were seen. With the 80% methanol solution, high recovery was achieved as 0.2037 mg/g dw, which was very close to solvent extraction yield. The main advantage of this method is application of process even at lower temperature (30 °C), which is very important from the economy point of view.

To investigate the amount of quercetin and kaempferol in extract, 1 mL of the extract obtained with 80% Methanol at 30 °C for 30 min by ultrasonic extraction method, was almost dried in vacuum concentrator. Then, it was dissolved in methanol to the final volume of 200 µL. After centrifugation the sample at 5000 rpm for 5 min, the sample was injected to HPLC. The polyphenol composition of the sample is given in Table 7.4.

Table 7.4. Polyphenol composition of the extract obtained with the ultrasonic extraction method at 30 °C for 30 minutes by 80% methanol

Polyphenols	mg /g dw grape skin
Gallic acid	0.4360
(+)-catechin	0.6156
(-)-epicatechin	0.7903
Rutin	0.7431
<i>Trans</i> -resveratrol	0.1807
Quercetin	0.2093
Kaempferol	0.0790
<i>Chromatograms were given in Appendix B.6</i>	App.B.6.

Direct injection of the extract to the HPLC did not give any results belong to quercetin and kaempferol. This might be probably due to the minimum detection level limitation of the HPLC. After concentrating the extract by vacuum concentrator, both quercetin and kaempferol were detected in the extract as 0.209 and 0.079 mg/g dw of grape skin, respectively.

Rather than the *trans*-resveratrol, the effects of extraction method and extraction conditions on the other polyphenolic compounds were also investigated. It is seen that, both the type and amount of polyphenolic components in extract strongly depend on the applied extraction method. Highest yields of polyphenolic compounds including (+)-catechin, (-)-epicatechin, rutin, and gallic acid were achieved with the traditional solvent extraction method performed with 80% methanol in water bath at 60 °C for 30

min. The noticeable difference was observed for (+)-catechin, and the highest amount of it was found in the crude extract as 1.9 mg/g dw.

7.1.2. Extraction of Bioactive Compounds from Olive Leaves

In this study two solvents and their aqueous forms were used to extract phenolics from olive leaves. The total phenol content of olive leaf extract in different extraction solvent systems was compared. Figure 7.1 illustrates the effect of ethanol-water and acetone-water solvent system on extraction yield in terms of total phenol content. Data were analyzed by using Minitab Statistical software, release 14 for windows. Data belongs to the analysis of solvent effect on total phenol content were expressed as \pm standard deviation (SD). Any significant differences between solvents and samples were determined by one-way ANOVA followed by Tukey test for multiple comparison considering differences statistically significant at $P < 0.005$. The highest phenol content was obtained with 70% aqueous ethanol solution as 10.43 (± 0.35) and 90% aqueous acetone solution as 9.29 (± 0.10) in terms of mg tannic acid per gram leaf. By applying the Tukey test, in case of the 70% aqueous ethanol extraction, total phenol content of the extract was statistically significantly different than the others ($P < 0.05$).

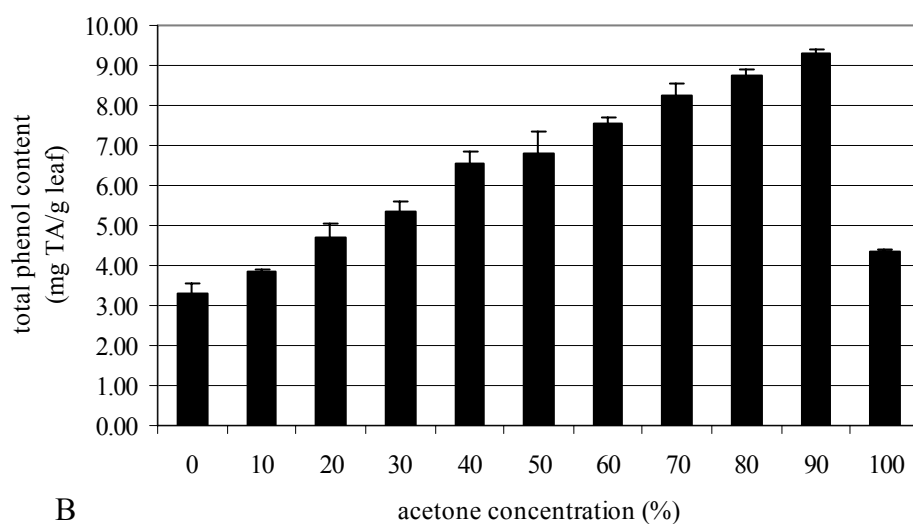
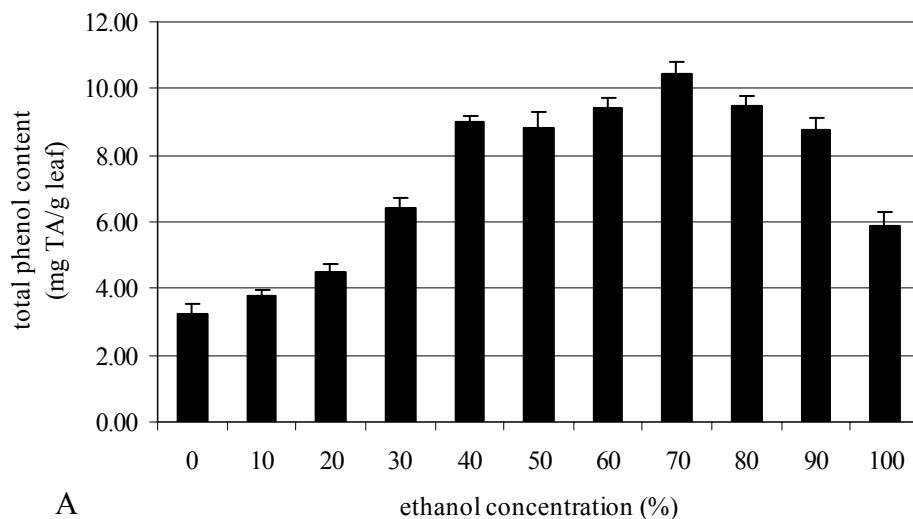


Figure 7.1. Effect of extraction solvent on total phenol content of olive leaf extract; A) ethanol-water solution; B) acetone-water solution.

The total phenol content in 70% ethanol solution was slightly higher than the total phenol content in 90% acetone solution. However, ethanol is more preferable solvent because of its nontoxic, environmentally safe and inexpensive features. Ethanol alone or acetone alone was not effective as a solvent for extraction of phenolic compounds. These results revealed that water has important role in extraction process by increasing the diffusion of extractable polyphenols through the plant tissues.

The extraction kinetics during 24 hours were investigated by taking samples against time. Extraction of polyphenolic compounds from olive leaf was performed with 70% ethanol solution. Figure 7.2 shows the change in the total phenol content during 24

hours. It was concluded that 2 hour extracting time was sufficient for obtaining most of the extractable polyphenols since the total phenol contents between 2 hours and 24 hours were not change significantly.

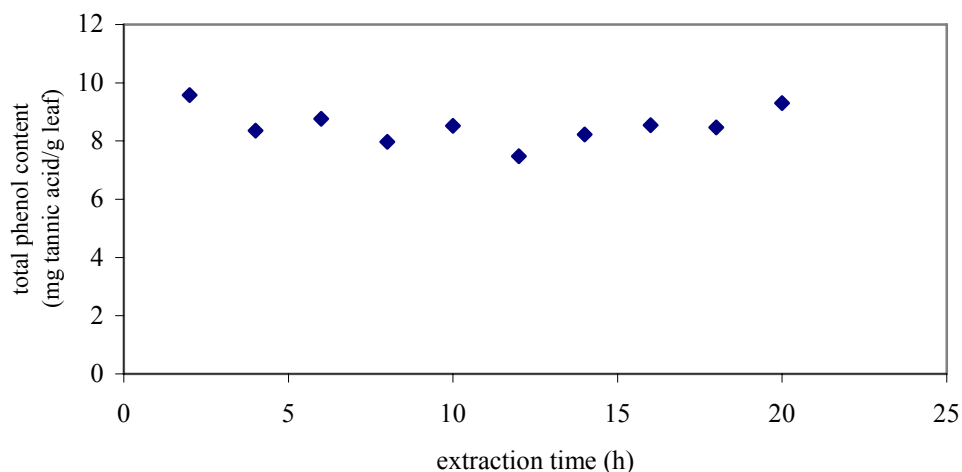


Figure 7.2. Effect of extraction kinetics in 70% ethanol solution.

Besides total phenol content, total antioxidant activity measurements were used in order to determine the effects of solvent type on the quality of extracts. The change in ethanol concentration affects the percent inhibition of ABTS radical cation (Figure 7.3). The highest inhibition percent was achieved by 70% ethanol extract, which can be explained by its high polyphenol contents as shown in Figure 7.1-A.

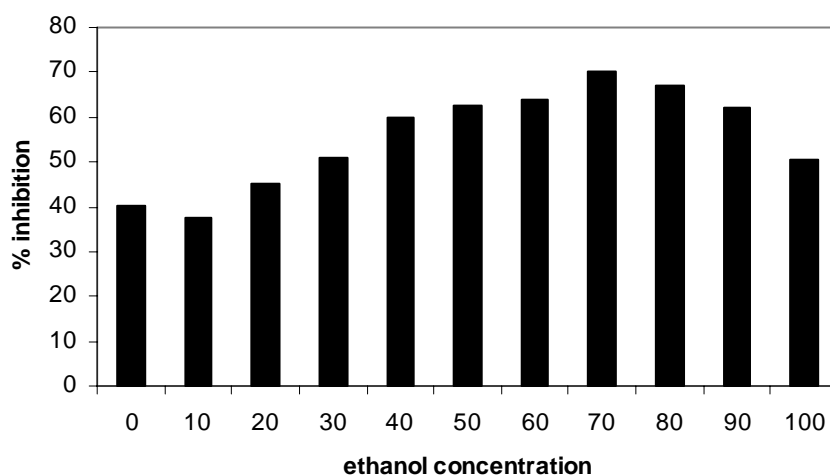


Figure 7.3. Effect of solvent type on inhibition percent of ABTS radical cation.

Figure 7.4 shows the linear correlation between the total phenol content and antioxidant capacities of extracts obtained by different ethanol concentrations with high regression coefficient as 0.968. This parallel relationship indicates the total phenol content directly affects the antioxidative activity of olive leaf extract.

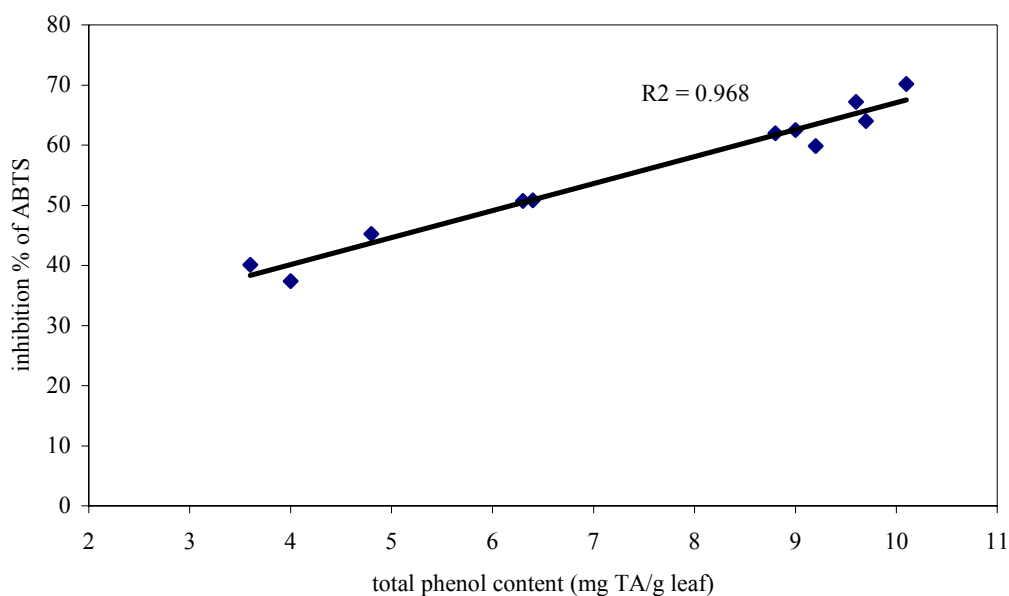


Figure 7.4. Correlation between total phenol content and inhibition percent of ABTS.

For the characterization of olive leaf extracts, quantification of the major polyphenolic compounds, oleuropein and rutin present in olive leaf extracts were determined by using HPLC analyses. The detailed HPLC method is given in Appendix A1.2.2. The crude extracts obtained from the extraction studies with different aqueous ethanol solutions were analysed to see whether the total phenol content is directly related with the oleuropein and rutin amounts. Figure 7.5 shows the effect of solvent and ethanol percentage on the extraction yield of oleuropein and rutin.

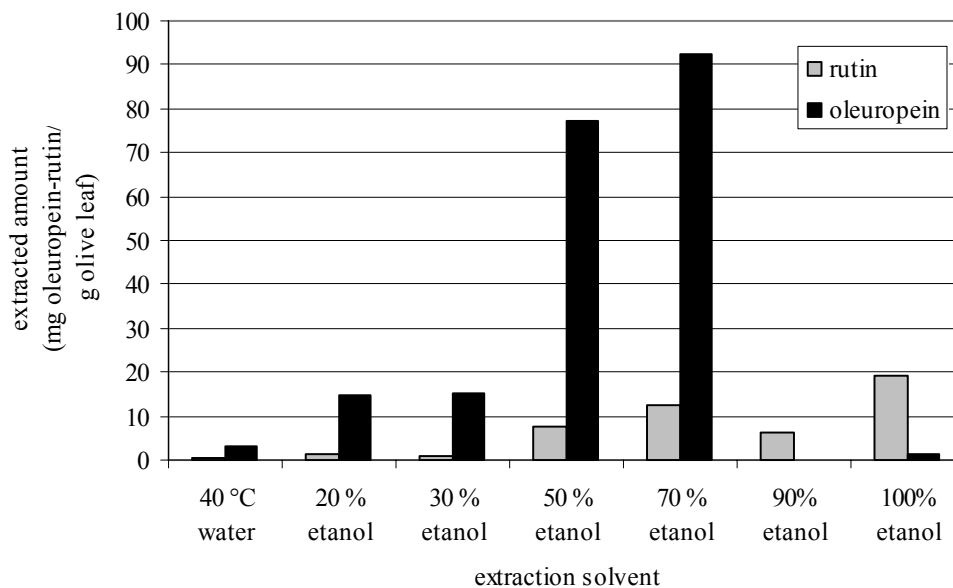


Figure 7.5. Effect of solvent on extracted amount of oleuropein and rutin per gram of olive leaf.

The highest yield of oleuropein and rutin extraction was achieved by 70% ethanol solution as expected from the results of total phenol content and antioxidant activity analyses. Although highest total phenol content was detected in 70% ethanol extract, the total phenol content of 50% ethanol extract was comparable, which were 8.83 and 10.43, respectively. However, oleuropein and rutin contents of these crude extracts were significantly different. Oleuropein content of the 70% ethanol extract was nearly 20% higher than the 50% ethanol extract.

7.2. Identification of Bioactive compounds

High performance liquid chromatography (HPLC) was used to analyse the bioactive compounds in the extracts. Different HPLC methods were used in the analysis of the olive leaf and grape skin polyphenolic compounds.

7.2.1. HPLC Analysis of Grape Skin Polyphenols

Main phenolic compounds in grape skin extract were analyzed by HPLC. C18 column showed good separation ability to phenolic components analyzed in this study

(Figure 7.6). Separation was performed by decreasing the polarity of mobile phase. So polar phenolic components, which are gallic acid, (+)- catechin and (-)-epicatechin, were detected firstly. This good separation is helpful to investigate the behaviour of the adsorbents. Calibration curves for these standard phenolic components were observed and were given in Appendix C.

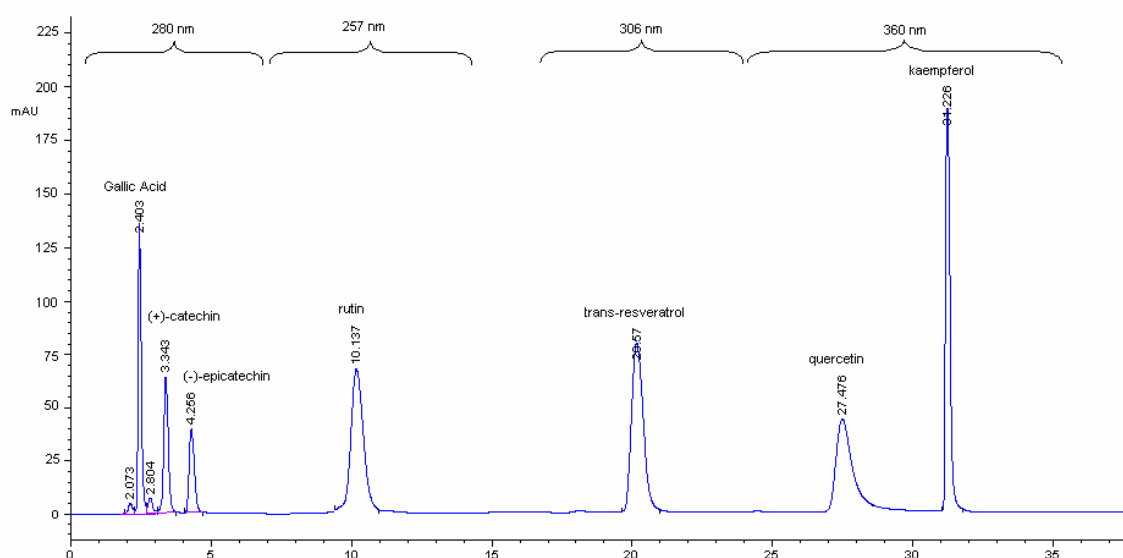


Figure 7.6. HPLC C18 column separation of the grape skin extract's main polyphenolic compounds.

7.2.2. HPLC Analysis of Olive Leaf Polyphenols

Olive leaf extract was analyzed by HPLC according to the study of Bayçın et al. (2006). The two most abundant phenolic compounds in olive leaf extract, oleuropein and rutin were identified by comparing their retention times with the corresponding standards. The other phenolic compounds found in olive leaf extract were identified by comparing their retention times with the study of Garcia et al. (2000). HPLC chromatogram of olive leaf crude extract was given in Figure 7.7.

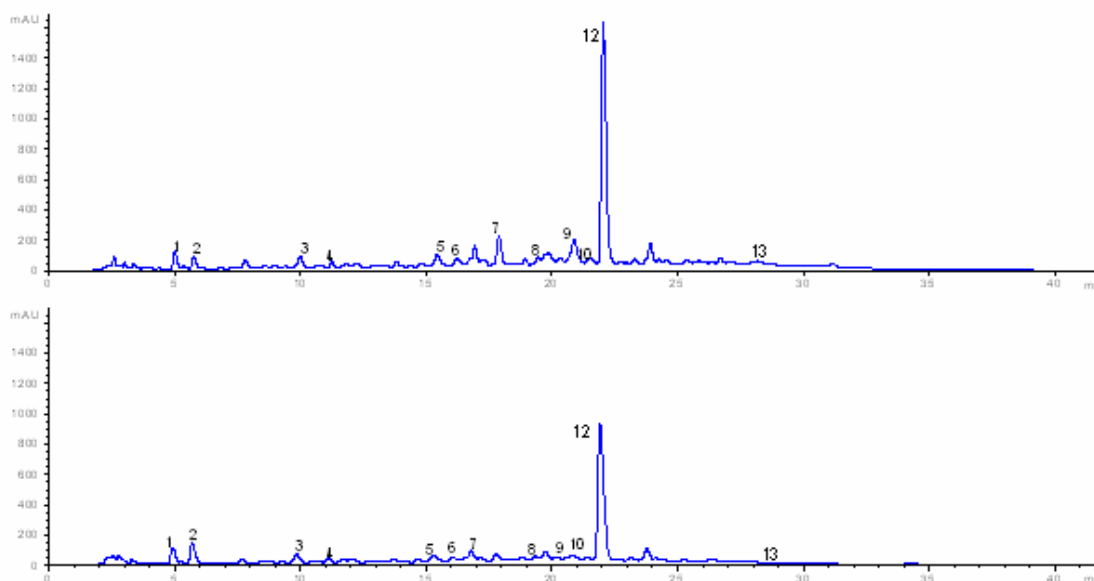


Figure 7.7. HPLC profile of olive leaf crude extracts at two initial concentrations as A: 1.5 g CE/50 mL including 228 mg oleuropein and 28.67 mg rutin B: 1 g CE/50 mL including 162 mg oleuropein ($\approx 30\%$) and 21.2 mg rutin ($\approx 5\%$).

The HPLC profile showed several peaks corresponding to different major olive leaf polyphenols identified as hydroxytyrosol, tyrosol, rutin, luteolin-7-glucoside, verbascoside, apigenin-7-glucoside, oleuropein, luteolin. The numbered peaks and abundance of the main compounds in olive leaf extract were given in Table 7.5.

Table 7.5. Peak number and abundance (peak area %) of the main phenolic compounds present in olive leaf crude extract

Phenolics	Peak #	1 g CE Peak area %
Hydroxytyrosol	1	2.27
Tyrosol	2	1.85
(+)-catechin	3	2.23
Caffeic acid	4	1.09
Vanillic acid	5	3.07
Vanillin	6	2.52
Rutin	7	4.66
Luteolin-7-glucoside	8	1.92
Verbascoside	9	6.11
Apigenin-7-glucoside	10	2.32
Diosmetin-7-glucoside	11	-
Oleuropein	12	29.43
Luteolin	13	0.81

7.3. Selective Isolation of Bioactive Compounds from Crude Extract: Adsorption

Selective separation is important process step in isolation of bioactive compounds from plant crude extract especially for the pharmaceutical industry. With this process it is possible to produce high purity value added products. So, this process step is very crucial for the production. Optimizing the process conditions and selecting most appropriate adsorbents for this purpose are the most important. In this study for selective separation of OLCE and GSCE bioactive compounds, novel adsorbents, clinoptilolite and silk fibroin were used as adsorbents. In this section the adsorption behaviour of these two adsorbents were also investigated in order to better understand the effectiveness of the adsorption.

7.3.1. Adsorbents

Morphology of Silk Fibroin (SEM Pictures)

Scanning Electron Microscopy (SEM) pictures of silk fibroin were taken in order to examine its morphology and morphological changes before and after the adsorption process. Figure 7.8 shows the SEM photomicrographs of silk fibroin.

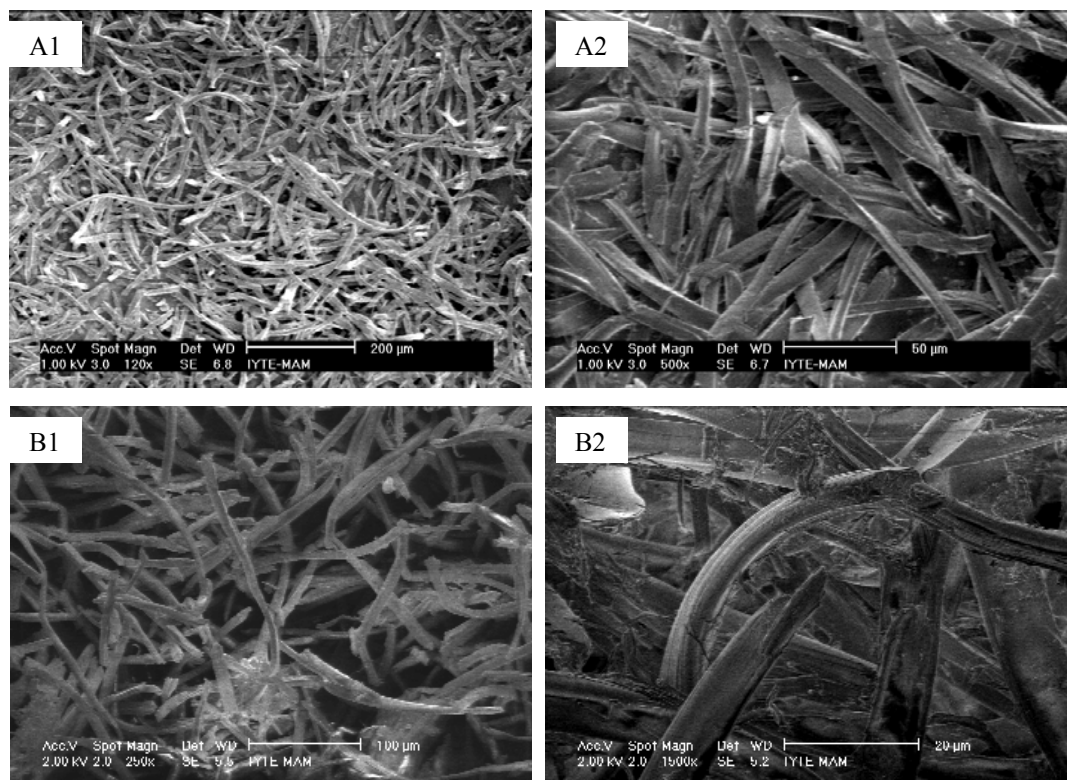


Figure 7.8. SEM photomicrographs of silk fibroin before (A1 and A2) and after adsorption (B1 and B2).

The SEM micrographs at different magnitudes show that the commercial silk fibroin was formed fibers having average 90 μm length. The most important difference in SEM micrographs was detected for the adsorption of *trans*-resveratrol on silk fibroin. After adsorption, some morphological changes were seen on the surface of the fibers (Figure 7.8-B2). Clear fibers were not seen after *trans*-resveratrol adsorption and fibers' surface was coated with *trans*-resveratrol. Interestingly, *trans*-resveratrol has crystal view in SEM micrographs (Figure 7.9). This macromolecule has average 5 μm length and 2 μm thicknesses.

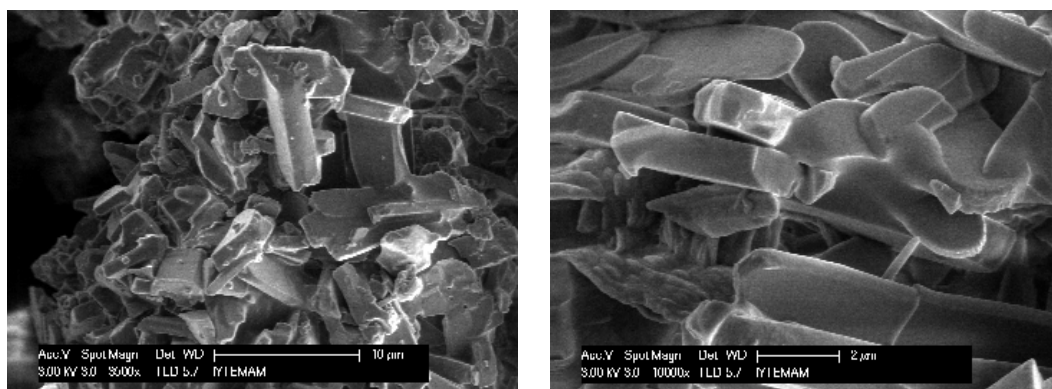


Figure 7.9. SEM photomicrographs of *trans*-resveratrol.

In case of the olive leaf crude extract and grape skin crude extract, there were not difference between the SEM micrographs taken before and after adsorption.

Digital pictures of silk fibroin before and after adsorption of *trans*-resveratrol were given in Figure 7.10. The yellowish color indicates the presence of *trans*-resveratrol on the silk fibroin.

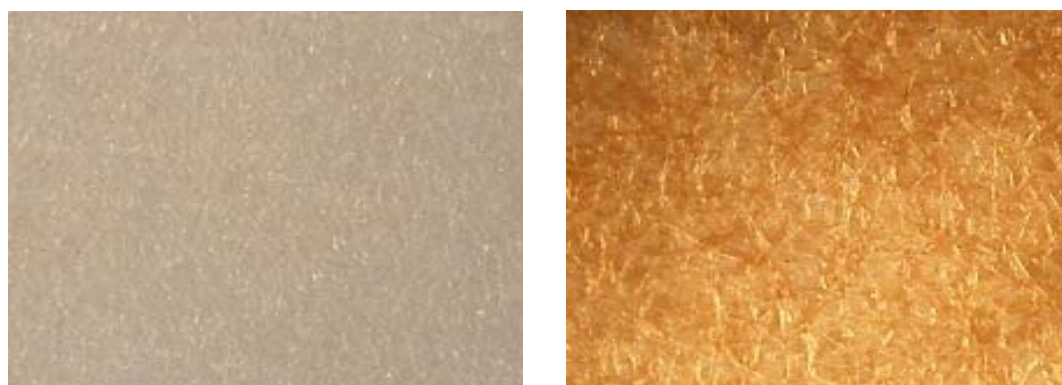


Figure 7.10. Digital images of silk fibroin before and after adsorption of *trans*-resveratrol (Olympus SZ-61, at 45x).

Characterization of Clinoptilolite

Characterization of adsorbent before the adsorption is very important. Since, clinoptilolite has different morphology and purity depends on its origin, processing steps and pretreatment procedures, it should be well characterized. For this purpose, SEM photomicrographs were taken in order to determine its particle size and to verify

tetrahedral crystal structure. Furthermore, XRD diffractograms were investigated in order to determine the purity of clinoptilolite in samples.

Morphology of Clinoptilolite (SEM Pictures)

The SEM photomicrographs of wet sieved Gördes region clinoptilolite were given in Figure 7.11. Wet sieving was effective method to separate particles having different particle size ranges. Samples through CL1 to CL5 have an order from large to small particle sizes. CL1 coded clinoptilolite sample has higher than 106 μm particle size. The other coded samples, which are CL2, CL3 and CL4 has particle size within the range of 75-106 μm , 45-75 μm and 25-45 μm , respectively. The clinoptilolite sample having a lower than 25 μm particle sizes is called as CL5. Photomicrographs in Figure 7.11 (A column) clearly show the effectiveness of the wet sieving method. Homogenous particle size distributions were seen at almost all of the photomicrographs. Although size reduction process results in the crystal loose, good hexagonal structures were seen in SEM images even at lower particle sizes (high magnification of the images: B and C column of the Figure 7.11).

The purity of clinoptilolite at Gördes region samples was analyzed by XRD (Figure 7.12). The samples obtained after wet-sieving were also analyzed in order to determine their purities.

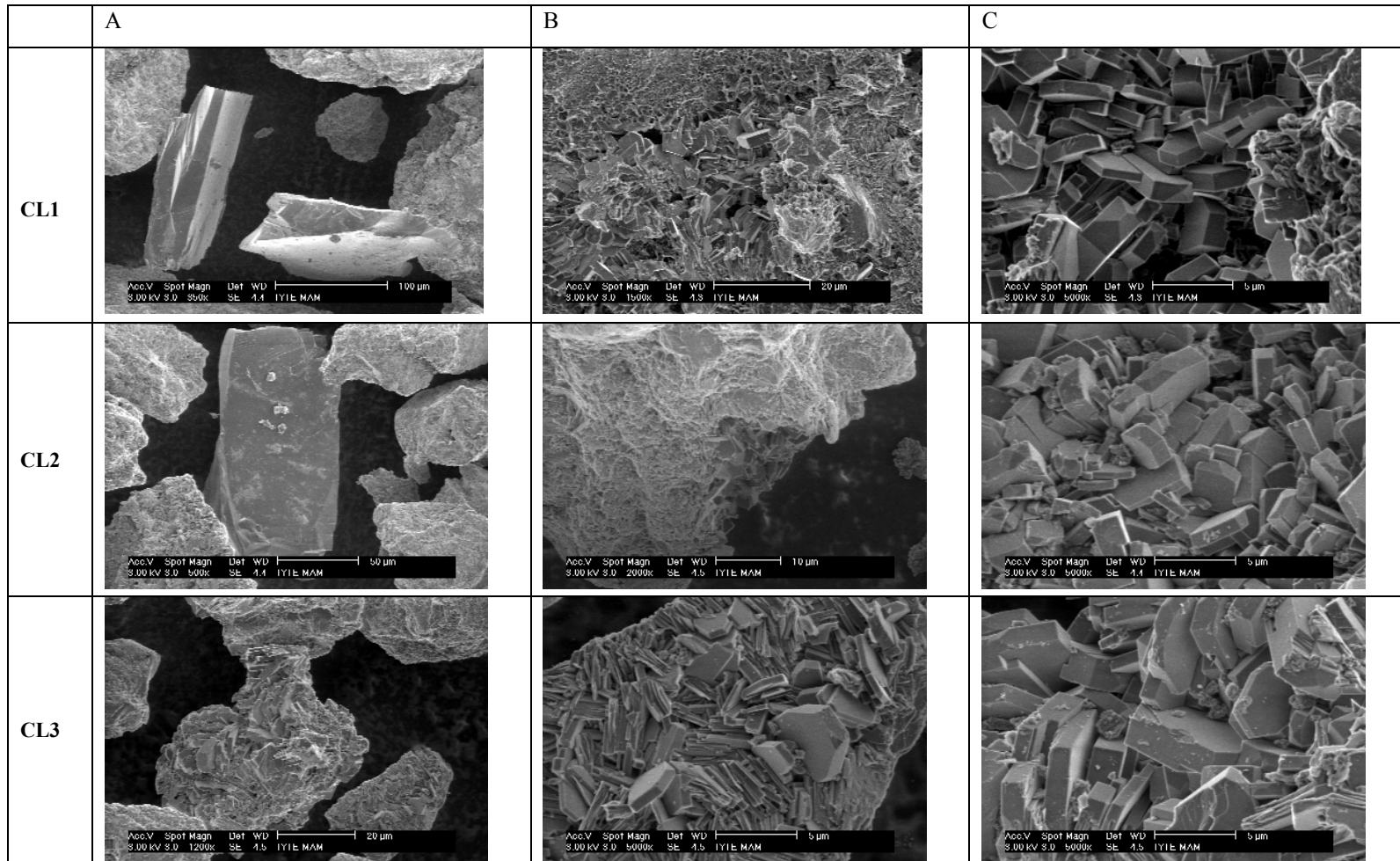


Figure 7.11. SEM photomicrographs of clinoptilolite in different scales after wet sieving into 5 different sizes.

(cont. on next page)

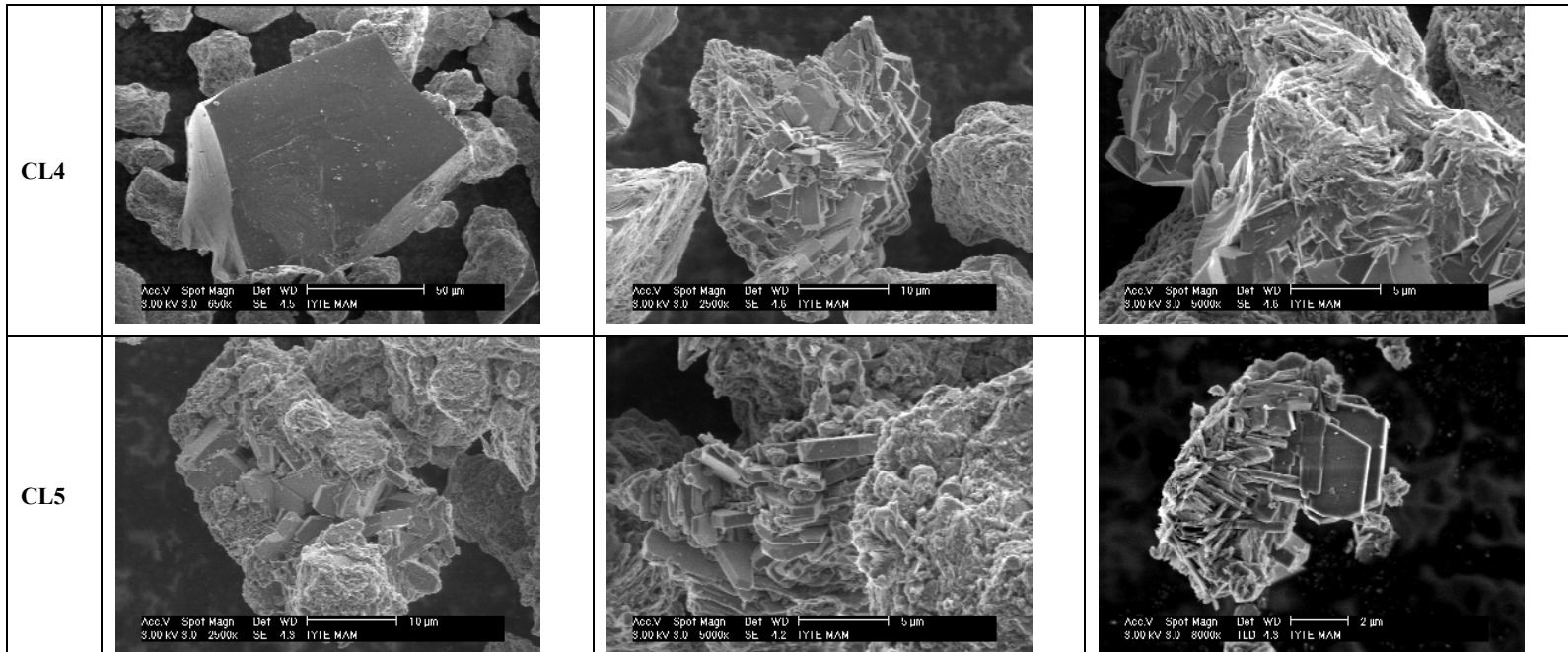


Figure 7.11. (cont.)

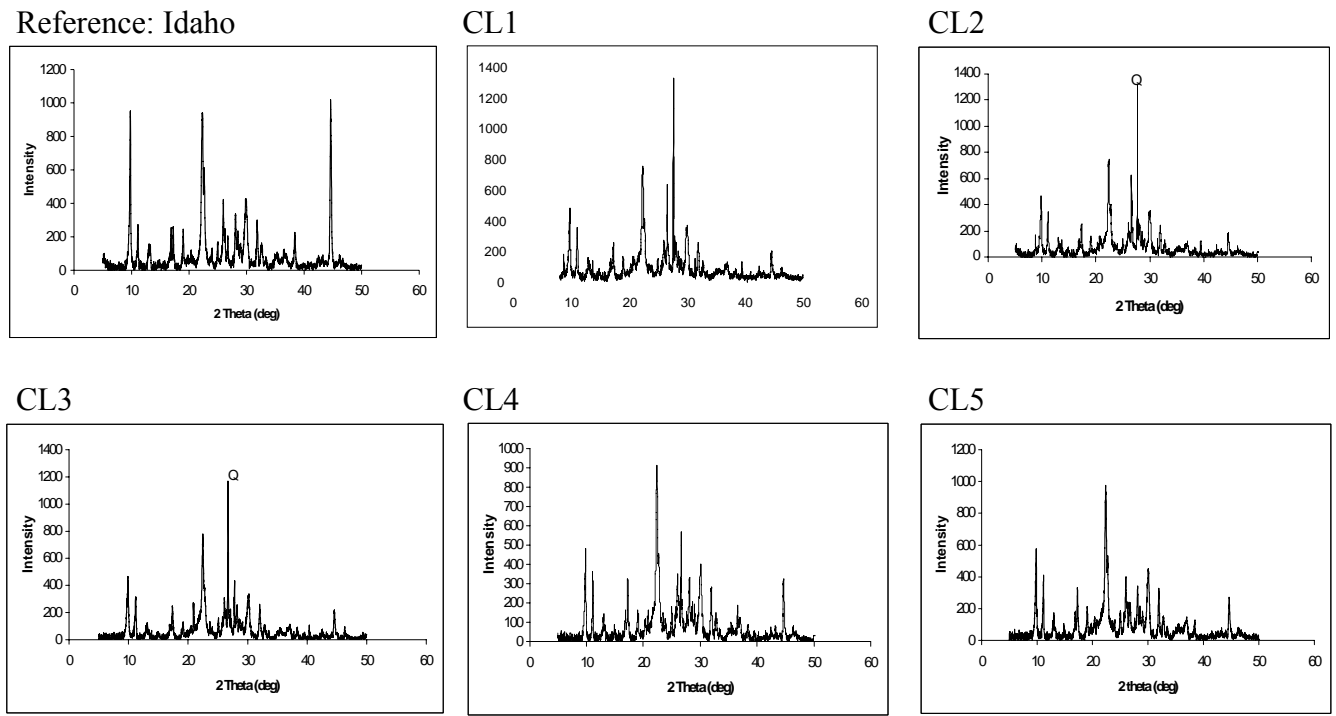


Figure 7.12. X-Ray Diffractogram of wet- sieved clinoptilolite samples.

Specific peak of quartz mineral (displayed by Q on graph) was detected in sample CL1, CL2, and CL3 by search match XPert software. Particle size lower than 25 μm , does not include quartz mineral anymore. This result is expected since quartz mineral is tough and it is not possible to reduce its particle size easily.

The purity of clinoptilolite at each sample was determined according to Nakamura et al. (1992). In this method, the diffraction intensity from clinoptilolite was calculated by the sum of seven intensities of the (9.82), (11.15), (13.07), (14.89), (16.91), (17.28), and (19.02) 2 Theta values, which are characteristic peaks for clinoptilolite. The clinoptilolite purity of the samples was determined by comparing the sum of intensities with the reference Idaho samples, whose purity was 95%. The purity of samples is given in Table 7.6.

Table 7.6. The purity of clinoptilolite in samples according to the method of Nakamura et al. (1992)

	CL1	CL2	CL3	CL4	CL5
Purity (%)	61	69	64	80	78

Sample CL5, which has a high purity of clinoptilolite, was further purified in order to obtain higher purity of clinoptilolite based on the developed method by gravitational separation by centrifugation. For this purpose, 15 g of CL5 sample was mixed with 75 mL of boiling deionized water for 5 min in a beaker. After waiting for 10 min for settling, the pellet was separated from the supernatant, which include suspended clinoptilolite. Then, the samples were centrifuged at different centrifugal speeds as 1000, 3000 and 5000 rpm. The purities of the collected samples were analyzed by XRD and their XRD diffractograms were given in Figure 7.13.

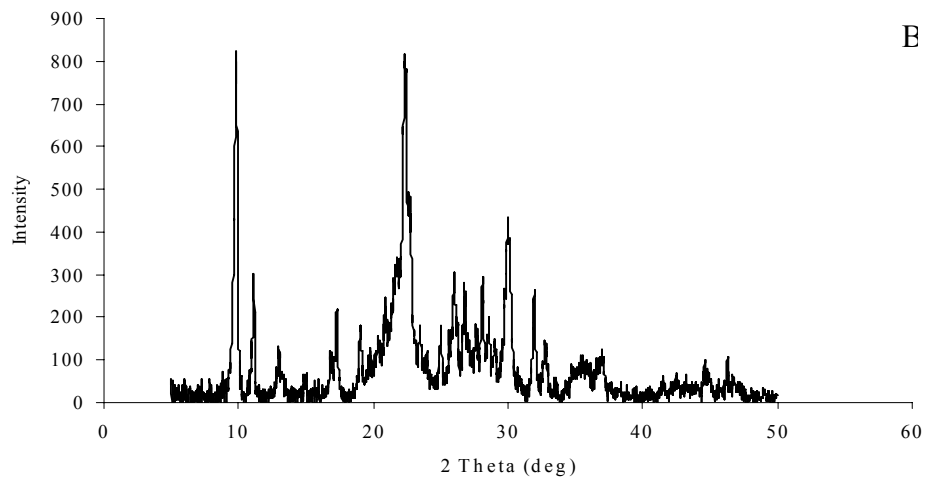
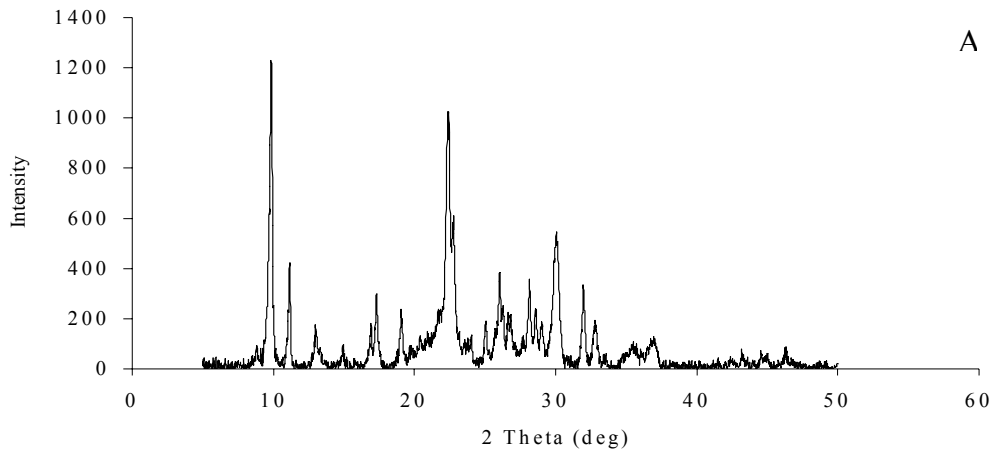


Figure 7.13. XRD Diffractogram of the separated fractions; A: 1000 rpm centrifuge pellet, B: 3000 rpm.

Clinoptilolite rich sample was obtained after separation of suspended solution with centrifuge at 1000 rpm. XRD diffractogram of it was very similar to the reference Idaho sample. The purity of samples is given at Table 7.7.

Table 7.7. The purity of clinoptilolite at samples according to the method of Nakamura et al. (1992)

	CL5-1000rpm	CL5-3000rpm	CL5-5000rpm	CL5-residue
Purity (%)	91	64	No characteristic peaks belong to the clinoptilolite	46

After separation of the clinoptilolite from the CL5 sample, 91% pure clinoptilolite was obtained by centrifugation of the sample at 1000 rpm. The purity of the clinoptilolite in the residue of the CL5 sample reduced to 46%. Clinoptilolite sample of a 91% purity was used in further adsorption studies in order to investigate the affinity of clinoptilolite to adsorb plant phytochemicals.

Chemical Analysis of Clinoptilolite Rich CL5 Sample

ICP- AES analyses of clinoptilolite rich CL5 samples were performed before and after adsorption of olive leaf extract. The results of chemical analyses of the samples are summarized in Table 7.8. The clinoptilolite rich CL5 sample was found to be rich in potassium ions. The elemental compositions before and after adsorption of the olive leaf polyphenolic compounds revealed that there was no considerable change in elemental composition of the samples. There was a slight change in the sodium ion, which reduces from 11.2 to 8.7 mg sodium/g of clinoptilolite after adsorption study. The chemical analysis revealed the Si/Al ratio of 5.19 that is typical for the clinoptilolite rich material (Breck, 1974; Tsitsishvili et al., 1992). Insignificant change was observed in the Si and Al contents of the clinoptilolite sample during the adsorption study, suggesting that the clinoptilolite structure retained its integrity.

Table 7.8. Elemental composition of clinoptilolite rich CL5 sample

Elements	(mg element/g clinoptilolite)	
	Before adsorption	After Adsorption
Al	57.6	54.5
Ca	11.5	11.9
Cu	0.1	0.1
Fe	10.2	9.4
K	45.7	44.0
Mg	2.0	2.2
Mn	0.2	0.2
Na	11.2	8.7
Si	298.7	287.1
Zn	0.0	0.0

The elemental analyses of the solutions were also performed in order to investigate the change in elemental composition of the solution. ICP-AES analyses were

performed with the solutions before and after the glycoside rich olive leaf crude extract (OLCE) fraction adsorption on the clinoptilolite rich CL5 sample. Almost all of the elements in solution were constant except sodium and potassium. Both potassium and sodium ions are increased in the solution after the adsorption experiment, which is mainly due to the releasing of them from solid to the solution.

Table 7.9 Elemental composition of solution before and after OLCE adsorption studies

Elements	OLE (ppm)	
	Before adsorption	After Adsorption
Al	1.2	1.7
Ca	7.6	7.7
Cu	0.0	0.0
Fe	0.6	0.4
K	2.1	5.2
Mg	0.2	0.5
Mn	0.0	0.0
Na	6.7	13.8
Si	5.5	5.7
Zn	0.1	0.1

7.3.2. Adsorption of Grape Skin Polyphenols on Silk Fibroin

Fractional dissolution of the powdered crude extract is very important step prior to the purification. It reduces the cost of the process by increasing the high yield of pure target compound. The fractional dissolution of the extract was performed and the extract samples coded with F1 to F6 were obtained. The qualitative analyses of these extracts were performed and phenolic compounds distributions were given in Table 7.10.

Solvents with different polarities used to dissolve grape skin crude extract lead to obtain different components. Polar fractions such as gallic acid, (+)-catechin, (-)-epicatechin were detected at fractions F1 and F2, which were obtained by dissolving crude extract with pure water (Table 7.10). In fractions 2 and 3, *trans*-resveratrol became to be detected, since *trans*-resveratrol is insoluble in water. Additional to *trans*-resveratrol there were other moderately polar undefined components.

HPLC analysis of F5 indicates that quercetin was found at fraction obtained by 50% ethanol. Other apolar phenolic components are found at F6. Because of the limit of detection rutin and kaempferol could not be detected in any fractions.

Table 7.10. Qualitative polyphenolic components detected at fractions obtained from gradient dissolutions of crude extracts

	F1& F2	F3 & F4	F5	F6
Gallic acid	+	-	-	-
(+)-catechin	+	-	-	-
(-)-epicatechin	+	-	-	-
Rutin	-	-	-	-
<i>Trans</i> -resveratrol	-	+	-	-
Quercetin	-	-	+	-
Kaempferol	-	-	-	-
Unknown Apolar components	-	-	+	+
Other unknown polar components	+	+	-	-

After investigating the fractional dissolution of crude extract, the adsorption studies were designed by using the gallic acid, (+)-catechin, (-)-epicatechin and *trans*-resveratrol standards. Kaempferol, quercetin and rutin was not expected anymore after removing the solvent from the extraction medium (i.e. these three polyphenols are precipitated in polar nature). In order to better understand the adsorption behaviour of the silk fibroin, amount of standards in model mixture were adjusted by taking into consideration of the crude extract's polyphenolic composition, which includes highest amount of *trans*-resveratrol. The phenolic composition of this extract has already given in Table 7.3.

Adsorption Kinetics

First of all, in order to determine the adsorption kinetics, batch adsorption studies were performed with each of the individual compounds found in the extract except, rutin, quercetin and kaempferol.

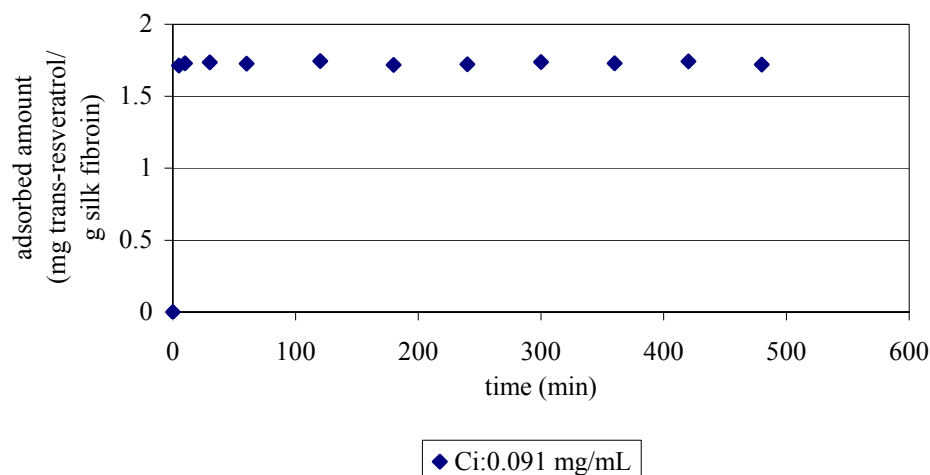


Figure 7.14. Adsorption kinetics of *trans*-resveratrol on silk fibroin, at initial concentration of 0.091 mg *trans*-resveratrol /mL 20% aqueous ethanol. Experimental conditions: S/L: 1/40; shaking speed: 180 rpm; 30 °C.

Rapid adsorption was observed for *trans*-resveratrol on silk fibroin. Within 5 min, almost all of the *trans*-resveratrol was adsorbed and there was no significant variation after 5 min (Figure 7.14).

In case of the gallic acid adsorption on silk fibroin, 120 min was required to reach the equilibrium. On the other hand, for (+)-catechin and (-)-epicatechin, the adsorption equilibrium was reached for longer adsorption time (Fig. 7.15). In the first 3 h, the adsorbed amount of them increased rapidly, after 3 h they reached equilibrium.

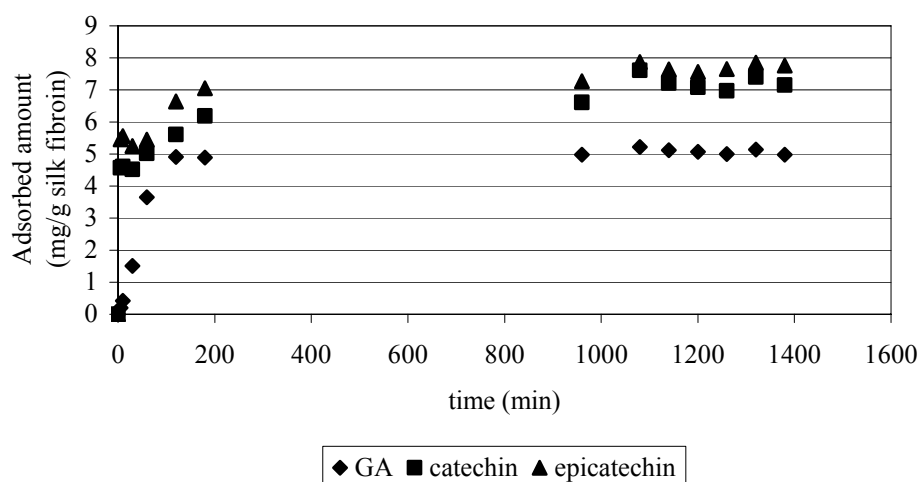


Figure 7.15. Mono-component adsorption kinetics curves for gallic acid, (+)-catechin and (-)-epicatechin on silk fibroin from 20% ethanol solution. Experimental conditions: S/L: 1/40; shaking speed: 180 rpm; 30 °C.

After pointing out the behaviours of phenolic standards, the contact time of 3 hour was selected for further studies.

Adsorption of Trans-resveratrol on Silk Fibroin

Both selective isolation and high purity production of *trans*-resveratrol is very important for serving it as a pharmaceutical compound. Thus, the adsorption ability of silk fibroin of *trans*-resveratrol was investigated in detail.

Effect of Ethanol Concentration of Solution on Adsorption of Trans-resveratrol

Ethanol concentration in the solution directly influences the solubility of *trans*-resveratrol. Thus, to achieve the maximum adsorption of *trans*-resveratrol by silk fibroin, the effect of ethanol concentration on adsorption of it was investigated.

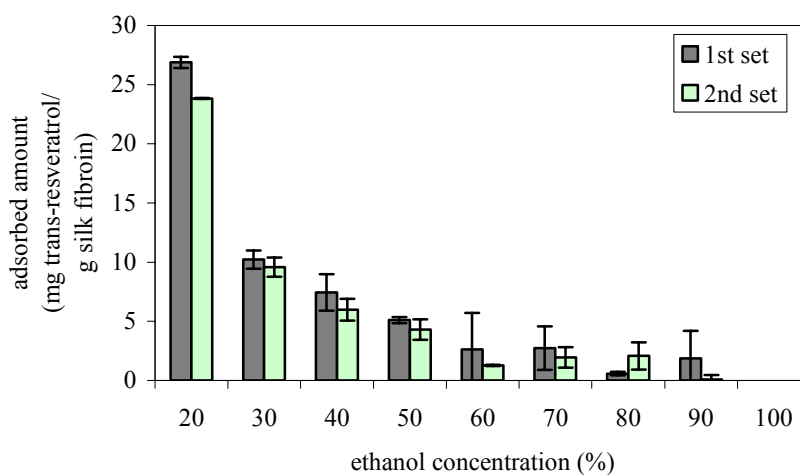


Figure 7.16. Effect of ethanol concentration on adsorption of *trans*-resveratrol on silk fibroin. Experiment conditions: T= 30 °C, contact time: 3 h, solid-liquid ratio: 1/40, shaking speed: 180 rpm.

Ethanol concentration significantly affects the adsorption of *trans*-resveratrol on silk fibroin (Figure 7.16). It was not possible to perform a study with 10% of solution's ethanol concentration, because of the solubility limitation of the *trans*-resveratrol at the selected initial *trans*-resveratrol concentration. Thus, adsorption experiments could be performed with 20% and higher percent ethanol concentrations. At higher ethanol

concentration, adsorption of *trans*-resveratrol significantly decreases. This behaviour can be explained by the dipole moments of the *trans*-resveratrol, ethanol and water, which are 1.6 debye (Erkoc et al., 2003), 1.69 debye and 1.85 debye, respectively. From the principles of like dissolves like, *trans*-resveratrol solubility would increase by increasing ethanol concentration in solution. At higher ethanol concentration *trans*-resveratrol prefers to stay in solution. However, higher adsorption efficiency from the solution having lower ethanol concentration was achieved. The adsorption mechanism of *trans*-resveratrol might be explained by the hydrogen bonds between the hydroxyl groups of *trans*-resveratrol and surface of the silk fibroin fibers. The dipole moments of the proteins on the surface of the silk fibroin might also play a role in the dipole-dipole interactions.

Effect of Solid-liquid Ratio on Adsorbed Amount of Trans-resveratrol on Silk Fibroin

The effect of solid-liquid ratio on the adsorption efficiency of the *trans*-resveratrol was investigated. For this purpose experiments were performed by keeping *trans*-resveratrol concentration constant as 0.85 mg/mL in 20% ethanol at 30 °C for 3 h.

The adsorbed amount of *trans*-resveratrol increased with decreasing solid-liquid ratio at the constant initial concentration of *trans*-resveratrol (Figure 7.17). Adsorption of *trans*-resveratrol could be achieved even from the higher volume of solution. The maximum adsorption capacity of the adsorbent could not be detected within the selected solid-liquid ratio range. Saturation of the adsorbent might be achieved at even at lower solid-liquid ratios. This property is very desirable for large scale separation process. The maximum *trans*-resveratrol adsorption capacity of the silk fibroin was found from the adsorption isotherm study as 48 milligram *trans*-resveratrol per gram of silk fibroin (Figure 7.20). To achieve the maximum adsorption capacity of the silk fibroin, solid-liquid ratio should be lowered than 0.011.

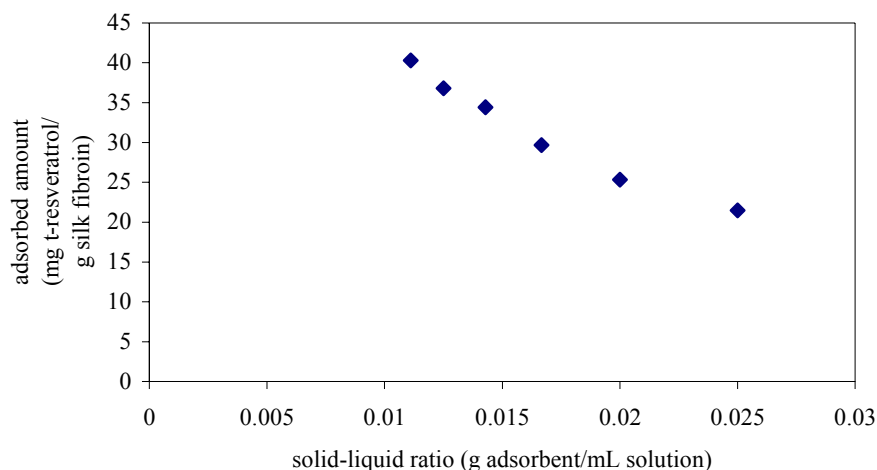


Figure 7.17. Adsorbed amount of *trans*-resveratrol at different solid-liquid ratios.

Highest extraction yield of *trans*-resveratrol was achieved as 0.2 mg/g dry grape skin. After the extraction of *trans*-resveratrol, *trans*-resveratrol concentration in the 20 % of ethanol solution was 0.05 mg/mL, which was relatively 18 times lower from the selected initial concentration. Thus, solid-liquid ratio of the process should be very low to achieve the maximum *trans*-resveratrol adsorption capacity of the silk fibroin. Solid-liquid ratio can be changed by the following ways: increasing the volume of the solution, concentrating the solution or decreasing the amount of adsorbent. However, working with very low amount of adsorbent has many disadvantages due to the homogeneity and composition of the adsorbent and its moisture content. Thus, higher volume of solution or concentric solution can be used for the effective adsorption of *trans*-resveratrol from the extract.

Adsorption Isotherm of Trans-resveratrol

After investigation of the effect of ethanol concentration on the adsorption behaviour of silk fibroin, 20% ethanol concentration was selected to obtain adsorption isotherms. For this purpose, different concentrations of *trans*-resveratrol were prepared by dissolving it in pure ethanol and adjusting the final ethanol concentration to 20% by considering its solubility concentrations (Figure 7.18). The *trans*-resveratrol concentrations of the solution were then analysed by HPLC. The HPLC results were compared with the initial dissolved amount of *trans*-resveratrol by plotting the figure

between them. Linear correlation was obtained from the plot given in Figure 7.18 within the selected concentration range upto the 1.3 mg/mL *trans*-resveratrol concentration. It was not possible to prepare higher concentration of the *trans*-resveratrol after that point. Thus, in order to obtain the adsorption isotherm, *trans*-resveratrol concentration should be within the range of soluble concentration values.

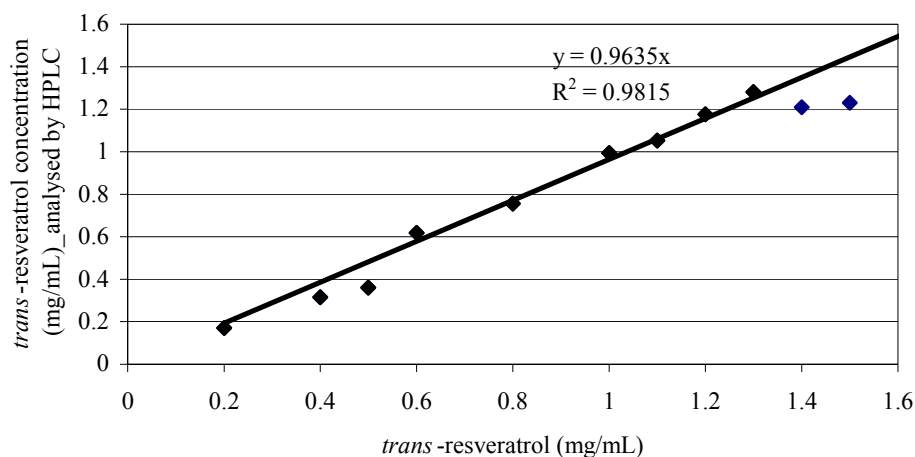


Figure 7.18. The solubility of *trans*-resveratrol in 20% ethanol solution at 30 °C.

In order to investigate the equilibrium time, kinetic analysis were performed with the solutions having low (0.091 mg/mL), middle (1.04 mg/mL) and high (1.24 mg/mL) concentrations of *trans*-resveratrol. Rapid equilibrium was achieved within 10 minutes and it was not affected from the concentration change (Figure 7.19).

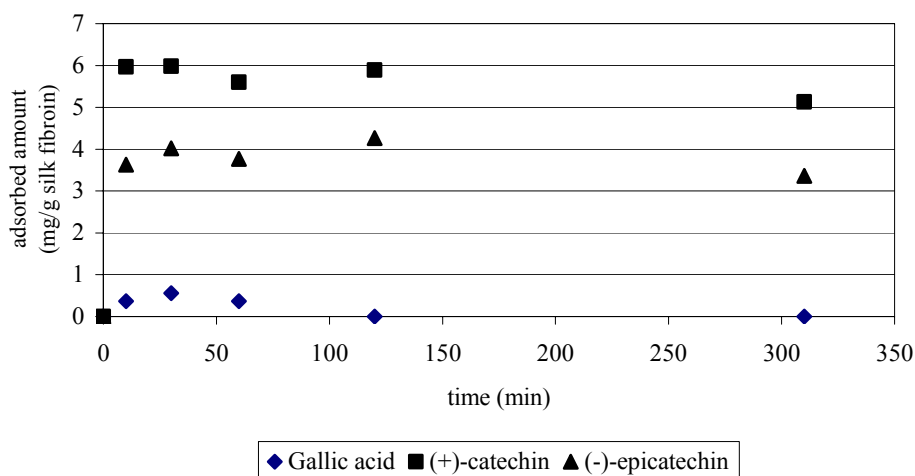


Figure 7.19. Kinetics of adsorption of *trans*-resveratrol on silk fibroin from 20% ethanol solution at 30 °C, (solid-liquid ratio: 1/40).

Then, adsorption experiments were carried out at 30 °C, 180 rpm for 3 h by keeping solid-liquid ratio as 0.025. Samples, which were taken before and after adsorption, were analyzed by HPLC. The adsorption isotherm was plotted by using the equilibrated *trans*-resveratrol amount in the solution and on the adsorbent (Figure 7.20).

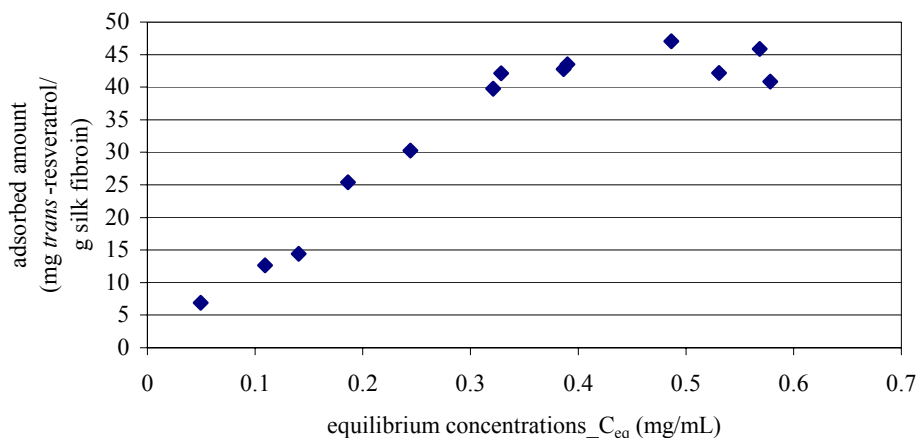


Figure 7.20. Adsorption isotherms of resveratrol on silk fibroin.

According to Figure 7.20, it can be concluded that, adsorption isotherm is 1st type adsorption. This type of adsorption can be explained by the monolayer adsorption.

Langmuir and Freundlich models were applied to equilibrium data of the adsorption isotherm.

Freundlich parameters; k_F and n were found as (Calculations are given in Appendix D.2);

$$k_F: 85.86$$

$$n: 0.805$$

$$R^2: 0.935$$

The Langmuir parameters were calculated by using the equation of the Langmuir model curve. Calculations are given in Appendix D.2.

$$q_{max} : 52.08 \text{ mg } trans\text{-resveratrol/g silk fibroin}$$

$$k_L: 0.229 \text{ mg/mL}$$

$$R^2: 0.979$$

Langmuir model best fits the equilibrium data of the adsorption isotherm having a higher correlation coefficient than the Freundlich model has. Maximum adsorption

capacity was calculated as 52.08 mg *trans*-resveratrol/g silk fibroin by using the Langmuir equation which is very approximate to the experimental value.

Multi-component Adsorption of Grape Skin Polyphenols on Silk Fibroin

The adsorption behaviour of the mixture of phenolic compounds including GA, (+)-catechin, (-)-epicatechin, rutin and *trans*-resveratrol was investigated (Figure 7.21). Although gallic acid is adsorbed by the silk fibroin as a single component, it was not adsorbed by the silk fibroin together with the other grape skin polyphenolic compounds. There was a slight change in the concentration of (+)-catechin, which reduces from 0.104 to 0.082 mg/mL. Higher amount of adsorption is detected for (-)-epicatechin and rutin in which the concentration reduces from 0.065 to 0.025 mg/mL and 0.098 to 0.012 mg/mL, respectively. Almost all of the *trans*-resveratrol was adsorbed by the silk fibroin from the solution and it did not affected from the other polyphenolic compounds found in the solution. Thus, adsorption of *trans*-resveratrol from the crude extract could be effectively performed.

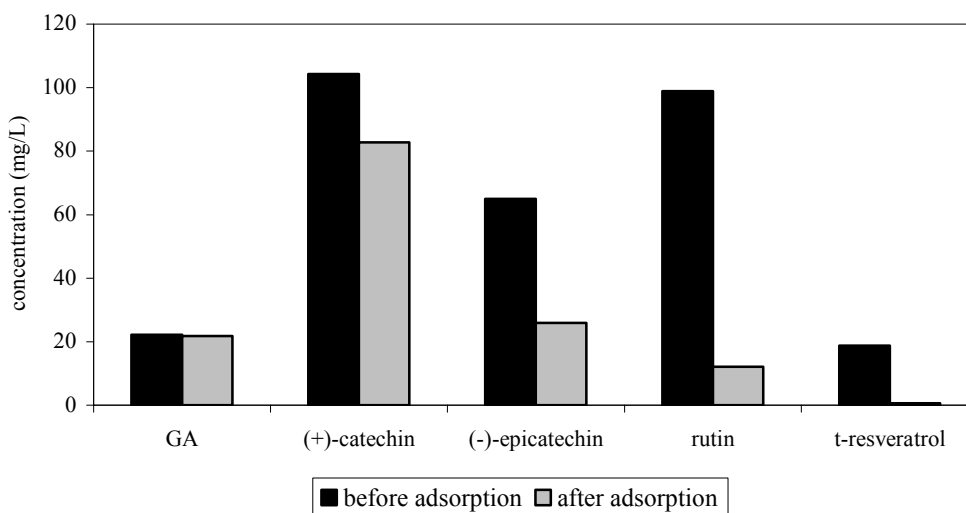


Figure 7.21. Adsorption of phenolic compounds mixtures on silk fibroin in a batch study by adjusting the solid-liquid ratio as 1/40 for 3 h at 30 °C.

In order to clarify the selective adsorption behaviour of silk fibroin, batch adsorption studies were performed by eliminating the *trans*-resveratrol and rutin from the mixture. Adsorption behaviour of silk fibroin to gallic acid, (+)-catechin and (-)-

epicatechin was followed during 5 hours (Figure 7.22). Similar result was obtained for gallic acid, in that silk fibroin did not adsorb gallic acid from the mixture. It is also clear that, its adsorption was eliminated by the presence of (+)-catechin or (-)-epicatechin rather than *trans*-resveratrol. We can conclude that gallic acid does not compete with the *trans*-resveratrol.

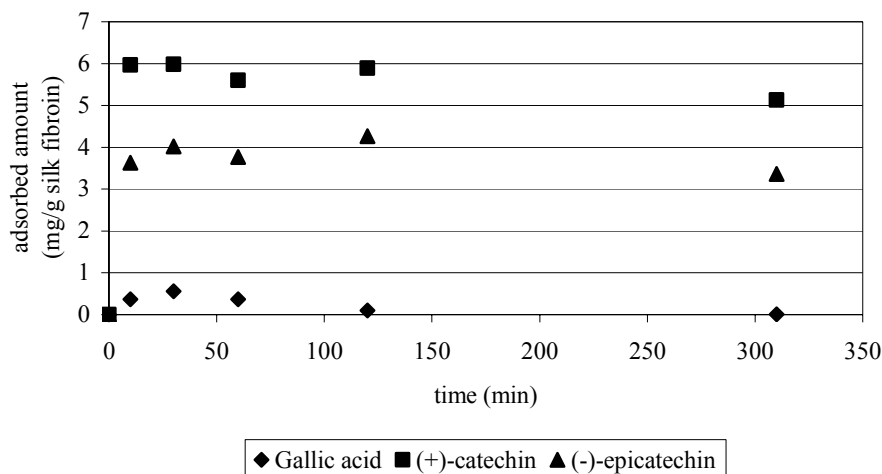


Figure 7.22. Adsorption behaviour of silk fibroin on the three phenolic compounds; gallic acid, (+)-catechin and (-)-epicatechin in 20% of ethanol solution (T: 30 °C, solid-liquid ratio: 1/40).

Effect of Temperature on Adsorption Isotherm

The effect of temperature on the adsorbed amount of *trans*-resveratrol is shown in Figure 7.23. It is expected higher adsorption capacity at low temperatures. However, the temperature change did not affect the adsorption capacity of the silk fibroin. Thus, for the economical point of view of the process, adsorption of *trans*-resveratrol can be performed at room temperature.

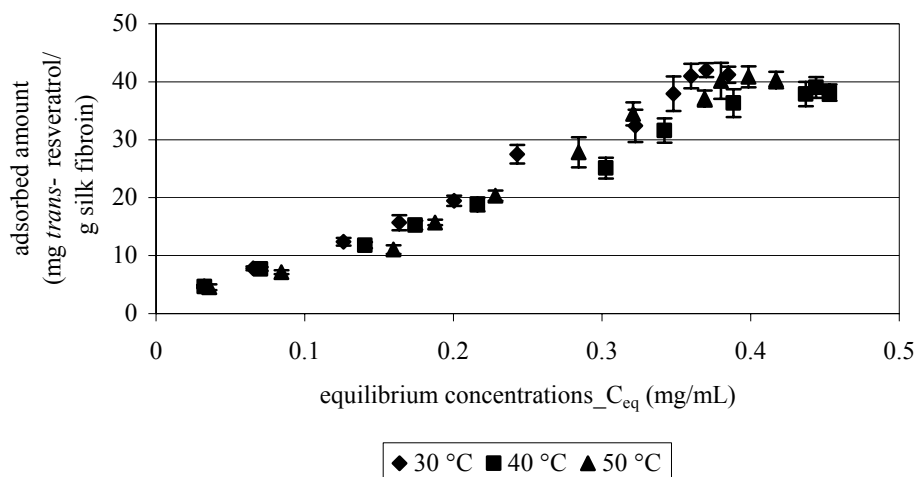


Figure 7.23. Effect of temperature on the adsorption isotherm of *trans*-resveratrol on silk fibroin. Experimental conditions: S/L: 1/40, shaking speed: 180 rpm.

7.3.3. Adsorption of Grape Skin Polyphenols on Clinoptilolite

Clinoptilolite has favourable application areas including adsorption. However, so far there is limited number of studies related with the adsorption of plant polyphenolic compounds. Only the study of Göktaş et al. (2007) indicated the adsorption of ginkgo biloba extracts's flavonoid aglycons, which are quercetin and kaempferol, on clinoptilolite. She concluded that clinoptilolite can be used for this purpose. Recently, beneficial health effects of clinoptilolite on human health, such as essential nutrients and elements supplementation, removing heavy metals and toxic substances from blood, cancer prevention role have extensively discussed. Moreover, it can be used for controlled drug carrier system. In order to understand the adsorption behaviour of clinoptilolite on *trans*-resveratrol, several studies were performed and discussed in this section.

Adsorption Kinetics

The adsorption behaviour of 51.5 % pure *trans*-resveratrol on clinoptilolite was followed for 24 h. The adsorption occurred significantly in the first 3 hours and adsorbed quantity remains almost constant with slight fluctuations thereafter (Figure 7.24). Consequently, 3 hour was sufficient for the adsorption of *trans*-resveratrol.

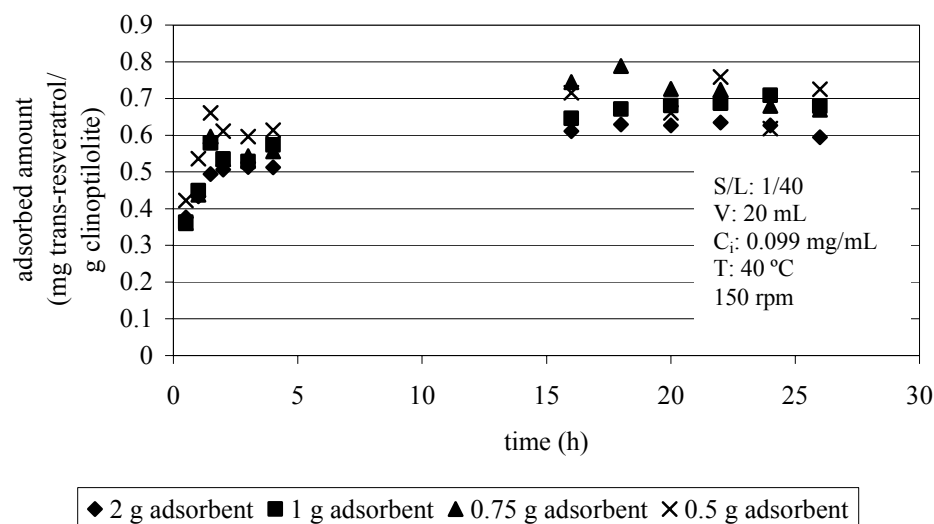


Figure 7.24. Adsorption kinetics of polyganum cuspaditum's *trans*-resveratrol (51.5% pure) on different amount of CL3 clinoptilolite sample (purity: 64%).

The effect of time on the adsorption of 51.5 % pure *trans*-resveratrol and pure *trans*-resveratrol by clinoptilolite rich CL5 sample are shown in Figure 7.25 and Figure 7.26, respectively.

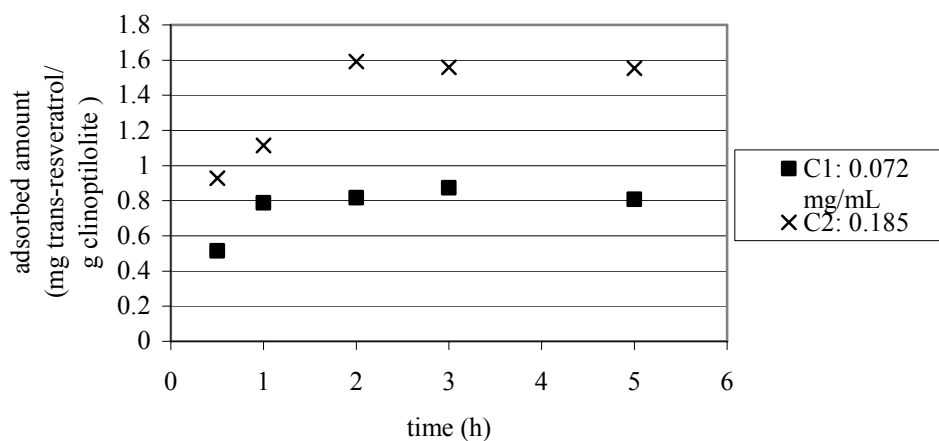


Figure 7.25. Adsorption kinetics of polyganum cuspaditum's *trans*-resveratrol (51.5 % pure) on clinoptilolite rich CL5 sample (purity: 91%). S/L: 1/40, T: 40 °C, 150 rpm.

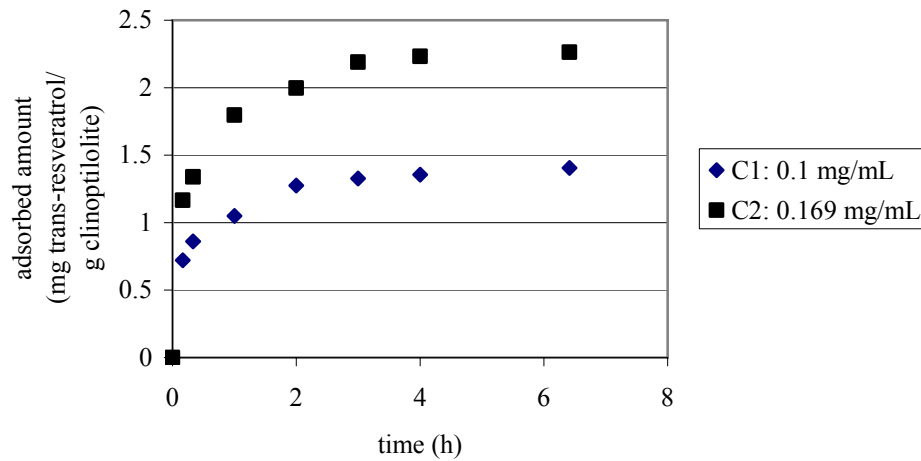


Figure 7.26. Adsorption kinetics of high purity *trans*-resveratrol on clinoptilolite rich CL5 sample. S/L: 1/40, T: 40 °C, 150 rpm.

Equilibrium was attained after 3 hours of contact time even for different purities of the clinoptilolite and the sorbate.

Changing the solid-liquid ratio affected the adsorbed amount of *trans*-resveratrol. As solid-liquid ratio decreases, adsorbed amount of *trans*-resveratrol increases (Figure 7.27).

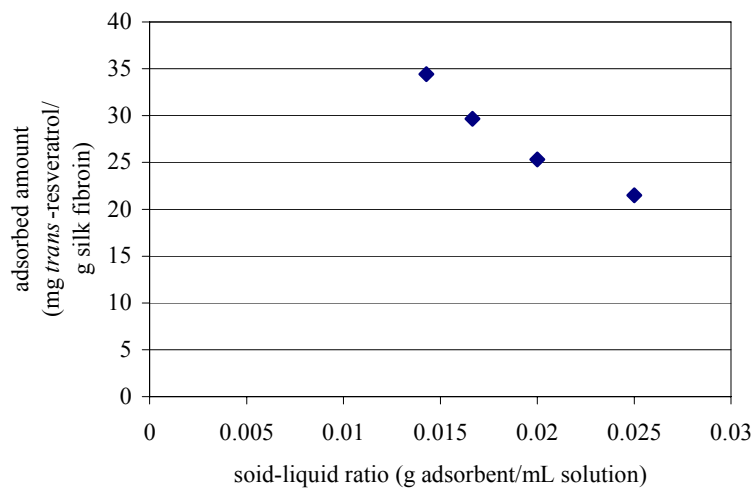


Figure 7.27. Adsorbed amount of *trans*-resveratrol on clinoptilolite at different solid-liquid ratios.

The saturation capacity of the adsorbent still could not be achieved within the selected solid-liquid ratios. The maximum adsorbed amount of clinoptilolite can be found by the isotherm study.

The adsorption behaviours of clinoptilolite to other polar phenolic components (GA, (+)-catechin and (-)-epicatechin), were also investigated. Figure 7.28 indicates that there are no affinities of clinoptilolite for the adsorption of polar components.

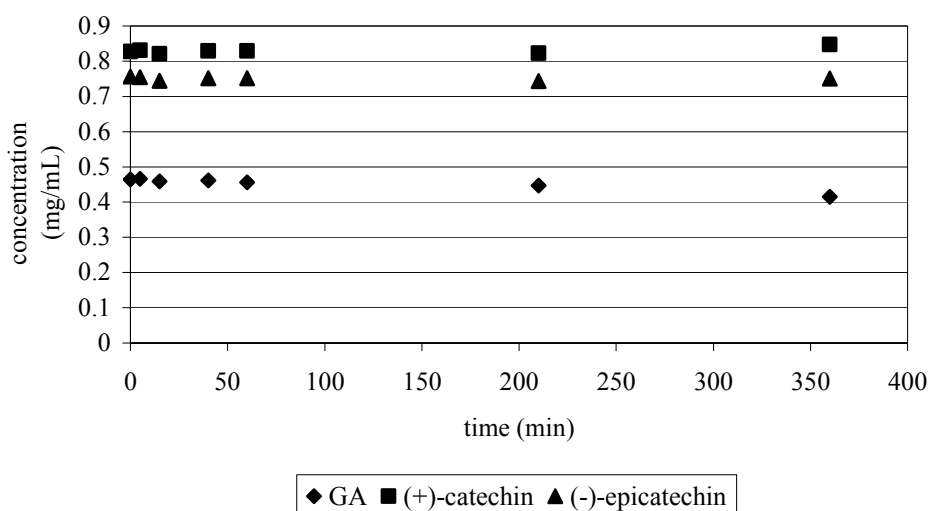


Figure 7.28. Change in concentrations of GA, (+)-catechin and (-)-epicatechin in liquid during the adsorption studies performed with clinoptilolite (Solid-liquid ratio: 1/20, 40 °C).

Effects of Ethanol Concentration in Solution on the Adsorption of Trans-resveratrol on Clinoptilolite

The effect of ethanol concentration on the amount of adsorbed *trans*-resveratrol by clinoptilolite was investigated by changing the ethanol concentration of the solution. Figure 7.29 indicates that similar results were obtained as in the *trans*-resveratrol-silk fibroin adsorption experiments.

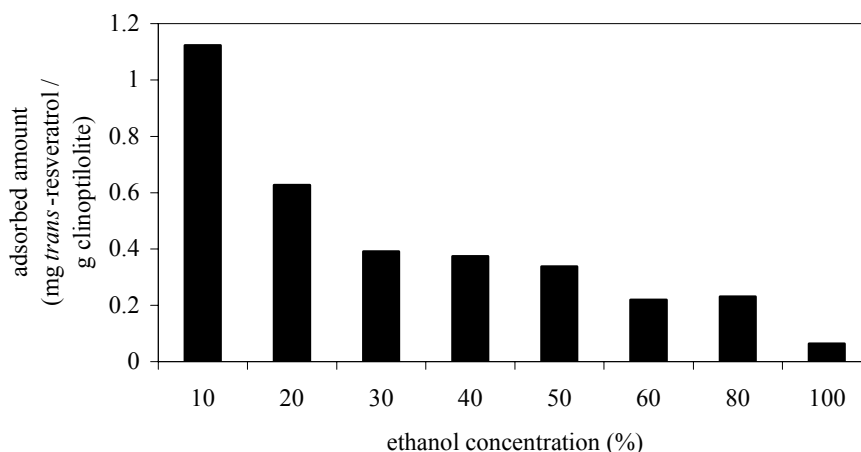


Figure 7.29. Effect of ethanol concentration on adsorption of *trans*-resveratrol on clinoptilolite (Experiment conditions; T: 30 °C, adsorption time: 3 h, solid-liquid ratio: 0.025).

Adsorbed amount of clinoptilolite significantly decreased by increasing the ethanol concentration of the solution.

Adsorption Isotherm

Adsorption isotherms of both standard *trans*-resveratrol (Sigma) and 51.5% pure *trans*-resveratrol (polyganum cuspaditum's *trans*-resveratrol supplied from Tanjin) on CL3 (particle size: 25-45 μm) and clinoptilolite rich CL5 (particle size: <25 μm) clinoptilolite samples were obtained by changing the initial concentration of *trans*-resveratrol in 10 % ethanol solution. Because of the solubility limit of *trans*-resveratrol, it should be checked within the concentration ranges, which were used to obtain adsorption isotherms. The concentrations of the solutions were verified by the HPLC analysis and linear correlations were achieved within the selected concentration ranges (Figure 7.30). *Trans*-resveratrol was soluble upto the concentration value of 0.6 mg per mL of 10 % ethanol solution. Thus, the solutions' *trans*-resveratrol concentrations were adjusted upto the limiting value to obtain the adsorption isotherm.

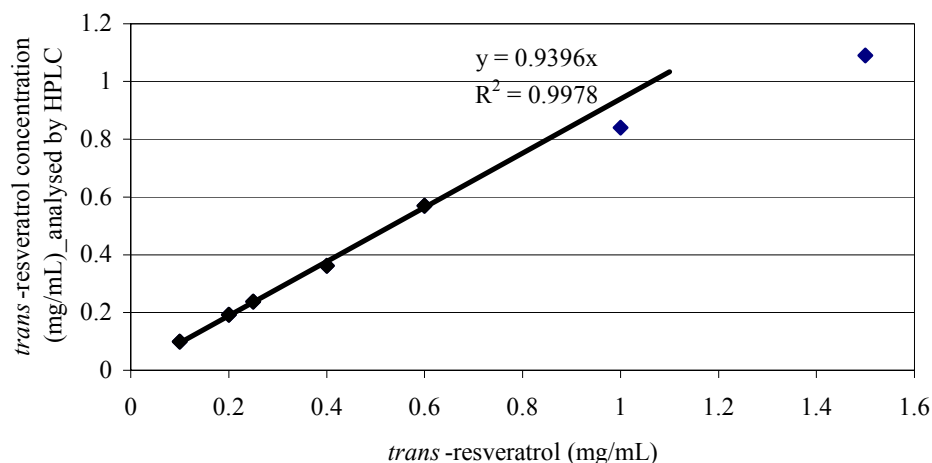


Figure 7.30. Solubility of *trans*-resveratrol in 10 % of ethanol within the range of selected concentrations.

Adsorption isotherm of 51.5% pure *trans*-resveratrol is given in Figure 7.31. Maximum *trans*-resveratrol adsorption capacity of the clinoptilolite was found as 1.6 mg *trans*-resveratrol per gram of adsorbent, which was lower than the value obtained for the silk fibroin.

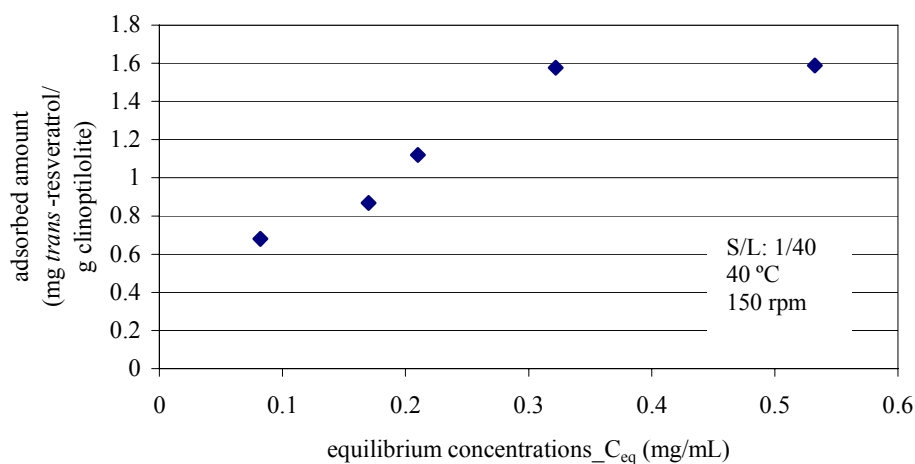


Figure 7.31. Adsorption isotherm of *trans*-resveratrol on CL3 clinoptilolite.

In order to understand the effect of purity and particle size on the sorption capacity, another sorption studies were performed by changing the adsorbent. Instead of the CL3 sample, clinoptilolite rich CL5 sample was used to obtain adsorption isotherm. Saturation capacity of clinoptilolite increased to 1.98 mg *trans*-resveratrol per gram of

adsorbent (Figure 7.32) by decreasing the particle size to lower than 25 μm and increasing the clinoptilolite purity to 91%. Both particle size and clinoptilolite purity of the samples might influence the sorption capacity.

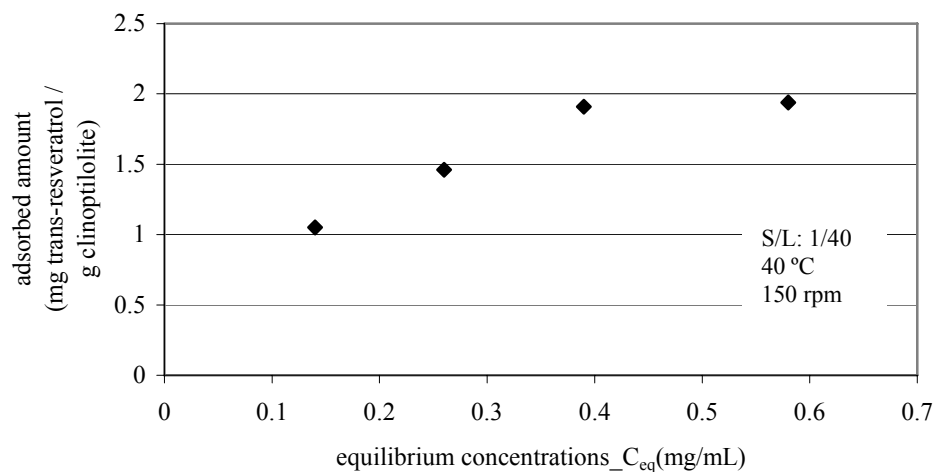


Figure 7.32. Adsorption isotherm of 51.5 % pure *trans*-resveratrol on clinoptilolite rich CL5 sample.

Another important parameter to affect on the maximum sorption capacity of the clinoptilolite is the *trans*-resveratrol purity. For this purpose Sigma standard of *trans*-resveratrol was used to obtain adsorption isotherm of it on the clinoptilolite rich CL5 sample. *Trans*-resveratrol purity significantly affected the maximum sorption capacity. 2.4 mg of *trans*-resveratrol was adsorbed per gram of adsorbent (Figure 7.33), which was 1.3 times more than the sorption capacity obtained with the *trans*-resveratrol having 51.5% purity.

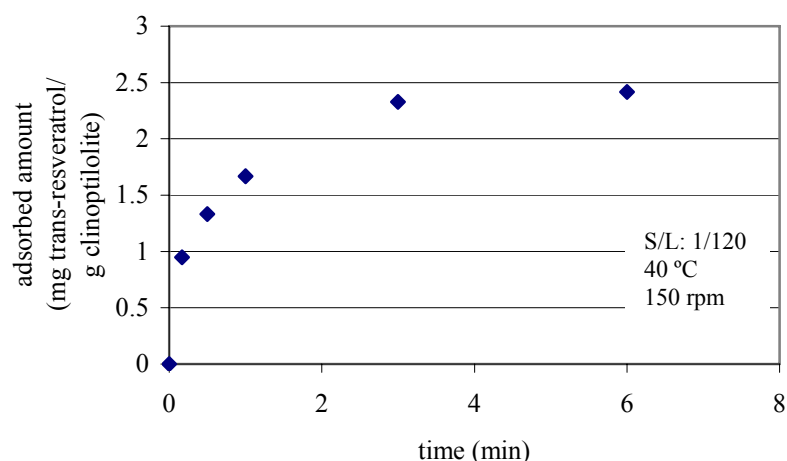


Figure 7.33. Adsorption isotherm of pure *trans*-resveratrol standard on clinoptilolite rich CL5 sample.

Freundlich and Langmuir models were applied to explain the adsorption behaviour of the clinoptilolite using the Equations 4.32 and 4.34, respectively. Model constants were shown in Table 7.11.

Table 7.11. Isotherm model constants

Adsorbent	<i>Trans</i> -resveratrol	<u>Freundlich Model</u>			<u>Langmuir Model</u>		
		k_F	n	R^2	q_{max}	k_L	R^2
CL3	51.5 %	3.385	0.506	0.914	1.89	6.75	0.988
Clinoptilolite rich CL5	51.5 %	4.503	0.447	0.935	2.16	8.22	0.993
Clinoptilolite rich CL5	Pure	7.064	0.301	0.926	2.66	28.92	0.988

p.s. Freundlich parameters; k_F and n and Langmuir parameters; q_{max} and k_L were calculated from the model curves given in Appendix D.2.

Langmuir model best fits the equilibrium data of the adsorption isotherm having a higher correlation coefficient than the Freundlich model. Maximum adsorption capacity was calculated as 2.66 milligram pure *trans*-resveratrol per gram of clinoptilolite rich CL5 sample by using the Langmuir equation. Results show that either the maximum adsorption capacity or adsorption affinity constant (k_L) increased with increasing both of the sorbent's and sorbate's purities.

Effect of Temperature on Adsorption Isotherm

The effect of temperature change on the adsorbed amount of *trans*-resveratrol is shown in Figure 7.34. It can be seen that a rise in temperature causes fluctuations on adsorbed amount of *trans*-resveratrol.

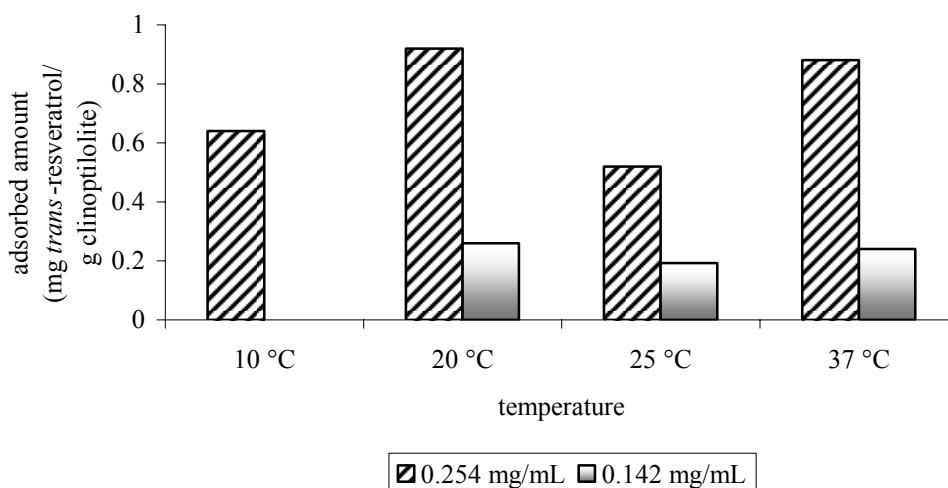


Figure 7.34. Effect of temperature on adsorbed amount of *trans*-resveratrol (Experiment conditions; solid-liquid ratio: 0.025, *trans*-resveratrol concentrations: 0.254 and 0.142 mg/mL, contact time: 24 hours).

To better understand the reason of this different trend, sorption isotherms were obtained at three different temperatures. Effects of initial concentrations on the adsorption kinetics at these three temperatures were shown in Figure 7.35 A, B and C. Rapid increase in adsorbed amounts of *trans*-resveratrol occurred within 15 minutes. An asymptotic trend with slow progress of adsorption was seen thereafter, despite different initial *trans*-resveratrol concentrations and temperatures used in the sorption studies. It was not possible to analyse the initial period of the sorption process clearly because of the time requirement for analysing *trans*-resveratrol content of the solution. It was seen that, 3 hour contact time was required to reach equilibrium. Saturation of the clinoptilolite was achieved at high initial *trans*-resveratrol concentrations (0.604 and 0.380 mg *trans*-resveratrol/mL). The maximum adsorption capacity of the clinoptilolite was found as 1.90 milligram *trans*-resveratrol per gram of clinoptilolite. A clear difference could not be detected between the adsorption capacities of clinoptilolite at these temperatures (Figure 7.36).

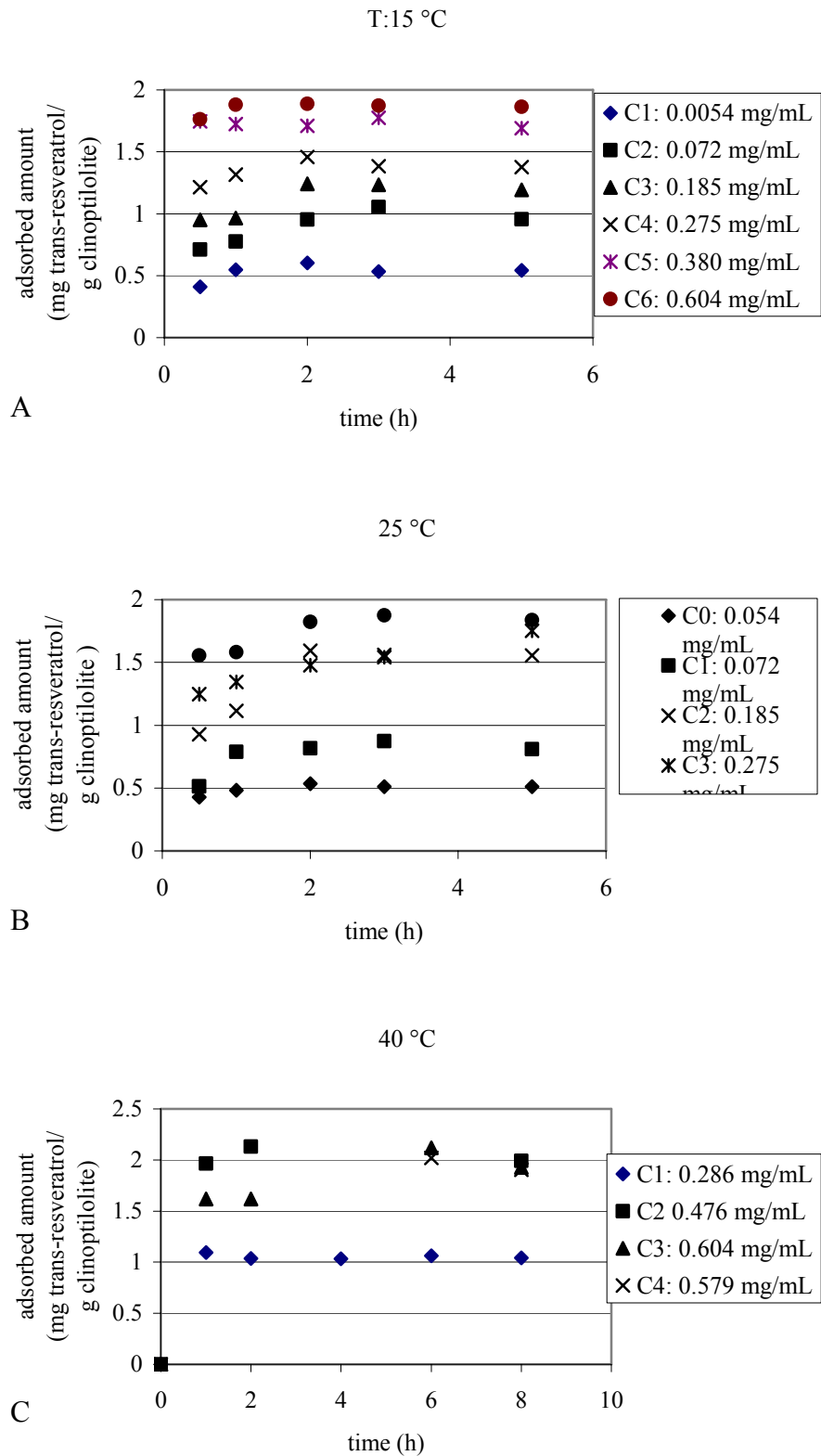


Figure 7.35. Effects of initial 51.5% pure *trans*-resveratrol concentrations on the adsorption kinetics; A: 15 °C; B: 25 °C and C: 40 °C. Experimental conditions: S/L: 1/40; shaking speed: 150 rpm, clinoptilolite rich CL5 sample.

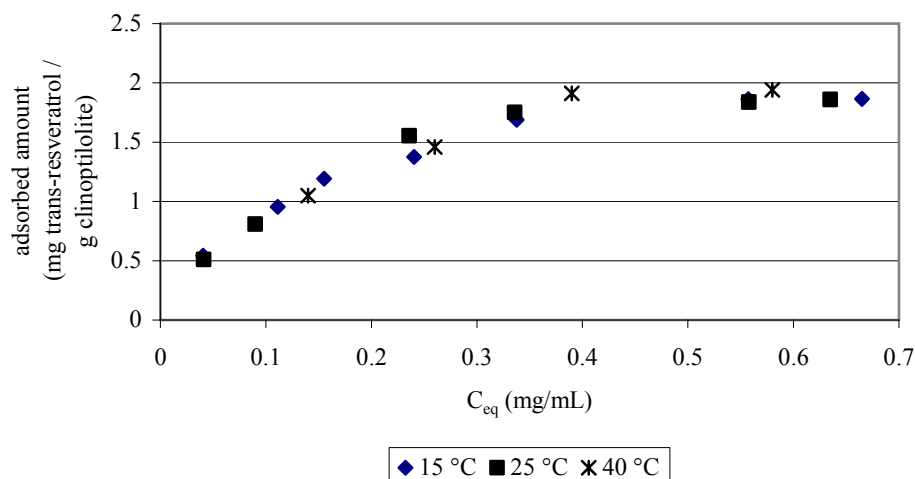


Figure 7.36. Effect of temperature on adsorption isotherm. Experimental conditions: S/L: 1/40; shaking speed: 150 rpm, clinoptilolite rich CL5 sample, 51.5% *trans*-resveratrol.

The effect of purity of *trans*-resveratrol on the adsorption kinetics and capacity of the clinoptilolite rich CL5 sample was also investigated by using pure Sigma standard *trans*-resveratrol instead of 51.5% *trans*-resveratrol. Similarly, 3 hour contact time was required to reach equilibrium (Figure 7.37). Only the saturation capacity of clinoptilolite was changed to 2.4 mg *trans*-resveratrol per gram of clinoptilolite. This was probably because of the purity of *trans*-resveratrol, which affected on the diffusivities of the molecules. Polyganum cuspidatum extract having 51.5% *trans*-resveratrol also includes many compounds, which may have different diffusivities and affinities to the adsorbent. Thus, these compounds might compete with the *trans*-resveratrol during the sorption process.

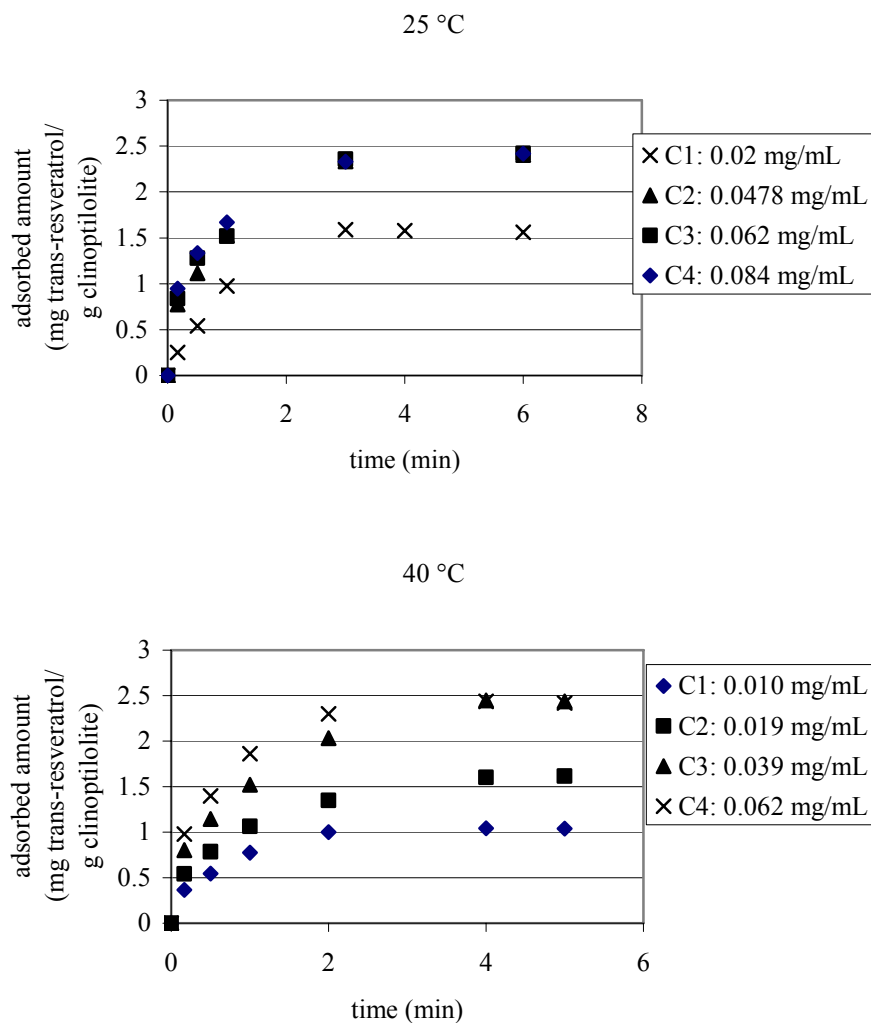


Figure 7.37. Effects of initial pure standard *trans*-resveratrol concentrations on the adsorption kinetics at two temperatures as 25 °C and 40 °C. Experimental conditions: S/L: 1/120; shaking speed: 150 rpm, clinoptilolite rich CL5 sample.

The effect of temperature change on the sorption capacity of clinoptilolite rich CL5 sample was also investigated using pure *trans*-resveratrol. A clear difference could not be detected between the adsorption capacities of clinoptilolite at these temperatures (Figure 7.38).

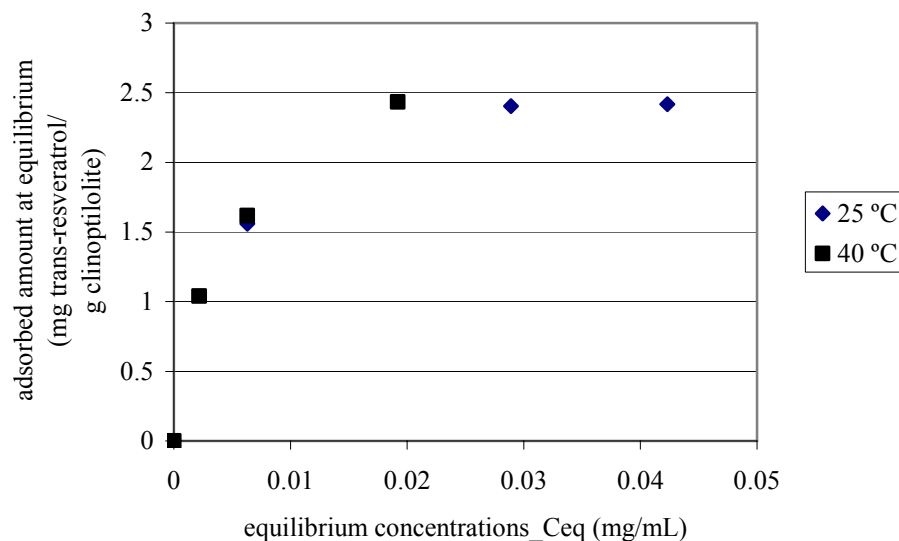


Figure 7.38. Effect of temperature on adsorption isotherm. Experimental conditions: S/L: 1/120; shaking speed: 150 rpm, clinoptilolite rich CL5 sample, pure *trans*-resveratrol.

Effect of pH on the Sorption

First the pH of the pure and 51.5 % pure polyganum cuspaditum's *trans*-resveratrol solutions was measured. Although pH of the pure *trans*-resveratrol solution was 8.1, 51.5 % pure polyganum cuspaditum's *trans*-resveratrol and grape skin crude extract's solutions were 6.8 and 4.3, respectively. This result indicates that other polyphenolic compounds significantly affect the solution pH. In order to see the effect of pH on the sorption, *trans*-resveratrol pH was reduced to 3.77 and 5.82 with 0.1 M nitric acid. Also, the pH of the grape skin crude extract was increased to 8.14 with 0.2 M NaOH. The sorption studies with these solutions were performed and results are illustrated in Figure 7.39.

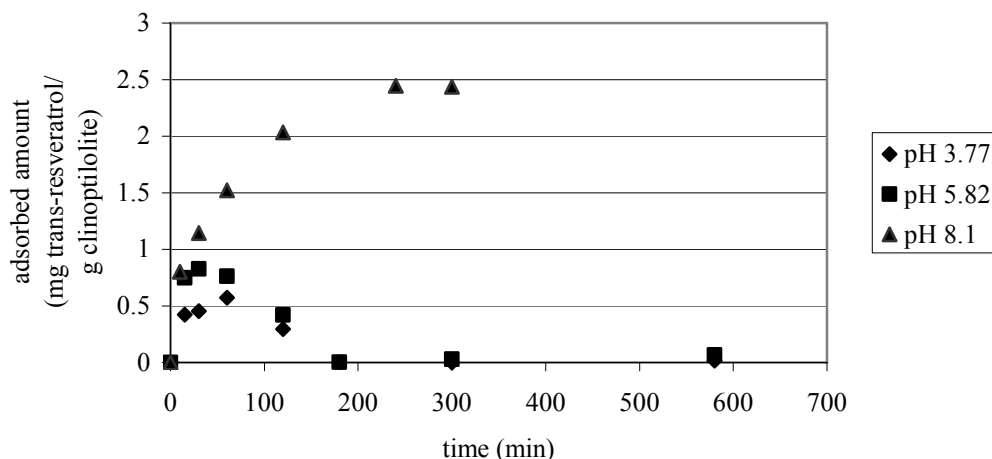


Figure 7.39. The effect of *trans*-resveratrol solution's pH on the adsorption of *trans*-resveratrol by clinoptilolite. Experimental conditions: S/L: 1/120; 30 °C; C_i : 0.038 mg/mL; shaking speed: 150 rpm, clinoptilolite rich CL5 sample.

Figure 7.39 shows that the adsorption capacity of *trans*-resveratrol onto clinoptilolite affected from the pH of the solution. Adsorbed amount of *trans*-resveratrol was 2.4 mg/g clinoptilolite when the pH of the solution was 8.1. From Figure 7.39, it can be seen that the shape of adsorbed amount versus time plots of *trans*-resveratrol onto clinoptilolite at pH 3.77 and 5.82 are quite similar in comparison to that at pH 8.1. Adsorbed amount of *trans*-resveratrol from the acidic solutions increased within 60 minutes. However, sorbed *trans*-resveratrol released thereafter.

The pH change during the sorption process was also investigated in order to explain the effect of pH on the sorption kinetics. Figure 7.40 shows the effect of pH change on the sorption kinetics of *trans*-resveratrol.

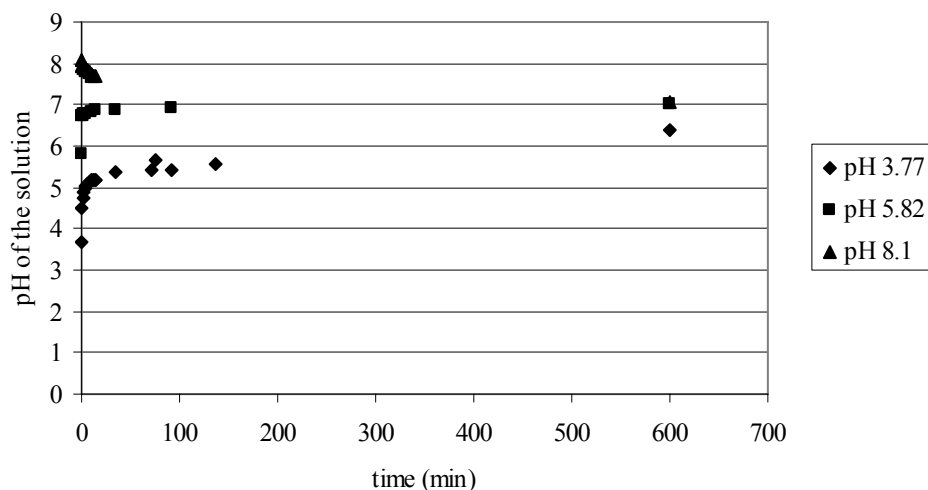
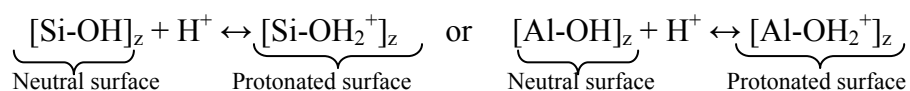


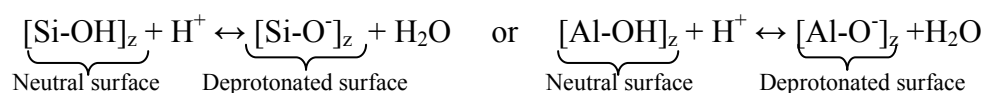
Figure 7.40. pH change during the adsorption of *trans*-resveratrol.

As seen from the Figure 7.40, the pH of the solution sharply increased within 30 minutes and then tends to reach neutral pH. This can be explained with the dissociation of outer-sphere complexes on the clinoptilolite surface in acid and the tendency to gain protons from acidic solution (Polatoglu and Ozkan, 2010). In acidic solution protonation of neutral surface can be explained by the following reaction;



As a result of this reaction, pH of the solution increases to the neutral pH values. In the basic solutions, clinoptilolite decreases the pH of the solution by the deprotonation of the surface represented below. The adsorption of *trans*-resveratrol onto the clinoptilolite surface would be the physical adsorption between the –OH groups of *trans*-resveratrol and –OH groups on the clinoptilolite surface. Initially, sorption of *trans*-resveratrol occurred and adsorbed amount of it increased within first hour. However, H⁺ ions also sorbed onto the clinoptilolite surface. Within first hour of the sorption process, adsorbed amount of *trans*-resveratrol onto the clinoptilolite from the solution of pH 5.82 was higher than the pH 3.77. This is because of the number of H⁺ ions in the solution. Hence, there was a competition between the H⁺ ions and *trans*-resveratrol. Additionally, after one hour of the adsorption, the sorbed *trans*-resveratrol released to the solution and H⁺ ions replaced onto the surface of the clinoptilolite, because, the pH of the solution tended to increase.

The highest sorption of *trans*-resveratrol was obtained from the solution having a pH 8.1. At the basic pH of the solution, clinoptilolite decreases the pH of the solution. Polatoglu and Ozkan (2010) reported that clinoptilolite is effective on the decreasing of pH of the solution while ineffective on the equilibrium pH (about 8.5). Because of the deprotonation of the clinoptilolite surface, solution pH decreases. The following reaction may explain this behaviour;



As a result of this reaction, clinoptilolite acquires an overall negative charge, due to the increasing of both Si-O⁻ and Al-O⁻ groups and a decrease in the solution pH is observed (Polatoglu and Ozkan, 2010). Since the pH of the pure *trans*-resveratrol solution was close to the neutral equilibrium pH, adsorbed amount of *trans*-resveratrol was high (Figure 7.39) and did not change with time.

In the case of the grape skin crude extract, the sorption of *trans*-resveratrol was very low, which might be because of the initial pH of the solution (4.36) and other polyphenolic compounds exist in the extract. The pH of the solution was changed to 6.98 within 10 hours.

Effect of Agitation Speed

Agitation speed influences in the distribution of the *trans*-resveratrol in the bulk solution but can also act on the formation of the external boundary film. The varying of the agitation speed is usually used to confirm the absence of significant external resistance. For this purpose the effect of agitation speed on the adsorption kinetics was investigated. Three agitation speeds were tested and results are illustrated in Figure 7.41.

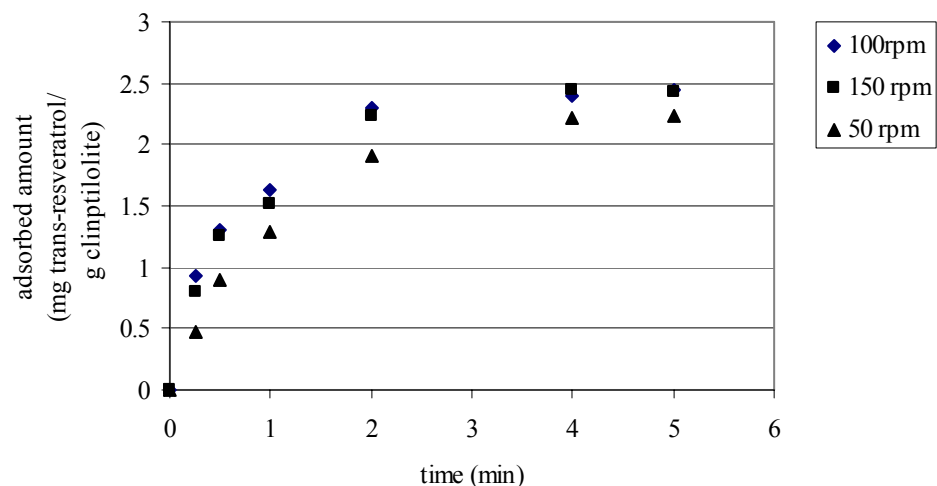


Figure 7.41. Effect of agitation speeds on *trans*-resveratrol adsorption onto clinoptilolite rich CL5 sample. Experimental conditions: C_i : 0.034 mg/mL; S/L: 1/120; 30 °C.

It is clear from the Figure 7.41 that after 100 rpm change in the agitation speeds was ineffective on the adsorption kinetics of pure *trans*-resveratrol onto clinoptilolite.

Effect of Particle Size

To investigate the effect of particle size of the clinoptilolite on pure *trans*-resveratrol adsorption, three ranges of particle sizes were used and results are shown in Figure 7.42. In order to eliminate the effect of purity, coarse particle was manually crushed into two different particle sizes and called as mid and fine samples.

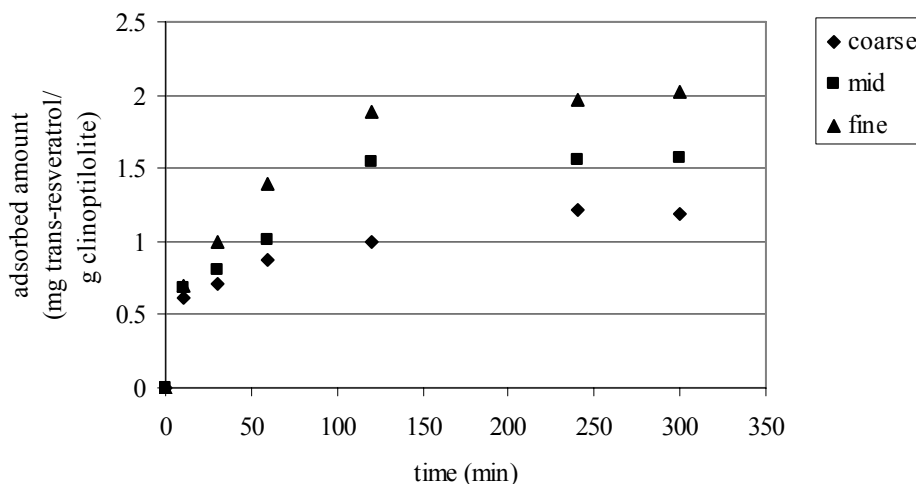


Figure 7.42. Effect of particle size on pure *trans*-resveratrol adsorption onto clinoptilolite. Experimental conditions: S/L: 1/120; Ci: 0.038 mg/mL; 150 rpm; 30 °C.

Particle size of the clinoptilolite significantly affected the adsorbed amount of the *trans*-resveratrol. As particle size decreases the adsorbed amount of *trans*-resveratrol increases. Thus, it would be possible to imply that the *trans*-resveratrol adsorption was limited by the external surface and external surface area was increased by decreasing the particle size. Additionally, since the intraparticle diffusion is dependent on the particle sizes, decreasing particle size would be yielded to more active sites, which were not accessible in large particles. Also, the uptake rate was increased by decreasing the particle size, which indicated the existence of intraparticle diffusion.

Mechanism of Adsorption

Considering the relatively small pore size of clinoptilolite (0.4- 0.7 nm), most of the *trans*-resveratrol reaction must take place at the external surface and at the surface of the macropores' cavities of the adsorbent. Because, Bonora et al. (2000) reported that, smallest size of *trans*-resveratrol was found as 1.15 nm, which is relatively large than the pore size of the clinoptilolite. Thus, it is not possible to diffuse *trans*-resveratrol molecule in micropores. The equilibrium data was analysed by external mass transfer equations. Boyd model was applied to investigate the external film mass transfer coefficient (k_f), for which sample calculation was given in Appendix D.1.

Furthermore, pore diffusion model was applied to determine the macropore diffusivities, which was given in Appendix D.3.

Adsorption of the *trans*-resveratrol on the clinoptilolite surface might occur either physically or chemically. In order to determine the controlling mechanism, the effect of temperature on adsorption capacity should be considered. Since there was no effect of temperature on the adsorption capacity of the *trans*-resveratrol, the mechanism of the adsorption can be explained by the physisorption. In the physical adsorption, hydrogen bonding, Van-der-Waals forces, electrostatic interactions, and hydrophobic interactions should be considered. Hydrophobic interactions can be explained by the adhesion between the nonpolar molecules and nonpolar adsorbent surface. Since *trans*-resveratrol has hydrophobic characteristic, hydrophobic interactions and hydrogen bonds may play a role in the bonding mechanism. It was clearly seen that by increasing the ethanol concentration of the solution, adsorption of the *trans*-resveratrol significantly eliminated. *Trans*-resveratrol preferred to stay in the solution because of the dipole moments of the solution. However, by increasing the dipole moment of the solution (decreasing the ethanol concentration), relatively high amount of *trans*-resveratrol was sorbed by the clinoptilolite. Both of the hydrogen bonds and hydrophobic interactions between the *trans*-resveratrol and clinoptilolite surface might be play a role in the sorption process.

Various kinetic models have been reported in literature to describe the sorption behaviour. Each model has specific limitations due to the related assumptions. Figure 7.37 indicates that the adsorption of *trans*-resveratrol was very fast within the first 15 minutes. Steep slope of these curves indicate instantaneous adsorption which may be due to the Si-OH or Al-OH groups presents at the outer surface of the clinoptilolite. Therefore, the adsorption of *trans*-resveratrol might be taken place probably via surface adsorption until all of the active sites were occupied in this region. Active sites in the pores are also involved in the later stages and proceeds in the inner parts of the particle. Considering the intraparticle mass transfer fractional uptake versus square roots of time, $t^{0.5}$ curves were evaluated (curves are given in Appendix D.4) in the calculations of k_d . Close to the equilibrium attainment portion of the uptake curve k_d was calculated from the slope.

The intraparticle or macropore diffusivities were determined from the time constant. The fractional uptakes (m_t/m_∞) versus time graphs were plotted and long term solution of Equation 4.11 was performed. The long term solution of Equation 4.11 is

given in Appendix D.3 and sample calculation is performed. The plots required for the solution of macropore diffusivities were also given in Appendix D.3. The effect of changing initial *trans*-resveratrol concentrations and two temperatures on macropore diffusivity is given in Table 7.12.

Table 7.12. Macropore diffusivities for the adsorption of *trans*-resveratrol onto the clinoptilolite rich CL5 sample.

T (°C)	Concentration	slope	$D_p * 10^{11}$ (m^2/sec)	R^2	$k_f * 10^3$ (m/sec)	k_d [$mg/(gmin^{1/2})$]
25	0,02	-0.0152	0.280	0.99	0.407	0.008
	0,0478	-0.0158	0.292	0.99	0.551	-
	0,0625	-0.0159	0.293	0.99	0.500	0.024
	0,0838	-0.0179	0.309	0.99	0.424	0.026
40	0,008	-0.0195	0.359	0.98	0.513	0.009
	0,0197	-0.0205	0.377	0.98	0.465	0.021
	0,0395	-0.0246	0.453	0.99	0.558	-
	0,0618	-0.0292	0.538	0.99	0.595	0.03

Table 7.12 shows that the intraparticle diffusion coefficient, D_p , increases with increasing initial concentration of the solution. This situation is expected, because increasing the concentration of the sorbate molecule increases the driving force in the macropores and there are more sorbate molecules binding to the active sites on the surface. Higher diffusivities are observed in the case of increasing the temperature of the solution. Since adsorption of *trans*-resveratrol onto the clinoptilolite is physisorption, low activation energy is enough for the mobility of the *trans*-resveratrol molecules on the surface of the macropores. Increasing the temperature of the solution would increase the mobility of the *trans*-resveratrol in the macropores and this is clearly seen in the diffusivity values obtained at high temperature. k_d value increases nonlinearly with the initial concentration of the solution. This situation is explained by the Al-Ghouti et al. (2009), in that, if the relationship between the initial concentration and k_d is not linear, pore diffusion limits the adsorption process.

External mass transfer coefficients (k_f) are also illustrated in Table 7.12. It was not possible to see any trend either by changing the initial concentrations of the solution and temperature. The k_f values were changed from 0.420 to 0.550 10^{-3} m/s.

The macropore diffusivities were in the magnitude of 10^{-11} , which was relatively low when compared with the external mass transfer coefficient (k_f). The Biot number

can be calculated from the Equation 4.28 and Biot number was found $\gg 100$ (around 2500), which indicates pore diffusion is the dominant mass transfer controlling mechanism.

To illustrate the effect of the clinoptilolite particle size on *trans*-resveratrol adsorption, three ranges of the particle size, coarse, mid and fine (having a average particle size 420 μm , 212 μm and 58.5 μm , respectively) were used and the macropore diffusivities are given in Table 7.13. The plots used in calculation of diffusivities are given in Appendix D.3.

Table 7.13. Macropore diffusivities for the adsorption of *trans*-resveratrol onto the clinoptilolite rich CL5 sample, effect of particle size

T (°C)	Particle size	slope	$D_p * 10^{11}$ (m^2/sec)	R^2	$k_f * 10^3$ (m/sec)	k_d [$\text{mg}/(\text{gmin}^{1/2})$]
30	Coarse	-0.0124	99.9	0,99	6.584	0.022
	Mid	-0.0143	29.6	0,81	3.832	0.024
	Fine	-0.0123	1.9	0,90	0.902	0.035

Table 7.13 shows that the intraparticle diffusion coefficient increases with increasing particle size. This behaviour is expected due to the decrease in the surface area available for adsorption with larger particle size. Consequently, the number of available site for adsorption reduced the molecules then tends to adsorb on the surface and diffuse into the particle more readily. From the plot of the k_d versus reciprocal square of the particle diameter, there observed an increase in k_d (as seen in Figure D.17 in Appendix D.4). This situation is expected if the intraparticle diffusion is rate limiting step in adsorption. Theoretically, the k_d and the adsorption capacity are related to available adsorbent surface area, which increases as particle size decreases.

In addition, it is clear that increasing the particle size resulted in an increase in the external mass transfer coefficient, k_f (Table 7.13). Fewer shears exists between the single particle and the surrounding liquid in the case of smaller particle size. This behaviour is different for a large particle size in which the large particle size tend to resist motion due to its own moment of inertia and therefore relatively more shear will exist between larger particles and the liquid. Moreover, it might be explained by the fact that for a small particle a large external surface area is presented to the solute molecules and as a result increasing the mass transfer (Al-Ghouti et al., 2009).

Agitation speed influences in the distribution of the *trans*-resveratrol molecules in the bulk solution but can also act on the formation of the external boundary film. The varying agitation speed is usually used to confirm the absence of significant external resistance. Increasing the agitation speed decreases the film resistance to mass transfer surrounding the adsorbent particle (Al-Ghouti et al., 2009). Three agitation speeds, 50, 100 and 150 rpm, were tested in order to investigate the kinetic of the sorption process and results are given in Table 7.14. The effect of agitation speed on the intraparticle diffusion coefficient can be seen from Table 7.14. Slight changes in intraparticle diffusion coefficients indicate that D_p increased with the increase in the agitation speed. This can be explained by decreasing the external film resistance at the initial period of the sorption process. It is possible to support this situation, since external mass transfer coefficient also increased by increasing the agitation speed. It can be attributed to decrease in boundary layer thickness around the clinoptilolite particles being a result of increasing the degree of mixing. This indicates that the external mass transfer may play a role in the adsorption of *trans*-resveratrol onto clinoptilolite. The value of k_d increased with increasing the agitation speed. This may be related to decrease in the boundary layer thickness and the increase in the mobility of the *trans*-resveratrol molecules in the pores.

Table 7.14. Macropore diffusivities for the adsorption of *trans*-resveratrol onto the clinoptilolite rich CL5 sample, effect of agitation speed

T (°C)	Agitation speed	slope	$D_p * 10^{11}$ (m ² /sec)	R ²	$k_f * 10^3$ (m/sec)	k_d [mg/(gmin ^{1/2})]
30	50	-0.013	0.24	0,99	0.32	0.026
	100	-0.015	0.28	0,81	0.37	0.033
	150	-0.018	0.33	0,90	0.46	0.043

Modification of the Clinoptilolite

In order to increase the hydrophobic character of the clinoptilolite, clinoptilolite rich CL5 sample was subjected to the acid treatment. The morphological changes were analysed by SEM and XRD and results were given in Appendix A.4 and A.5. The molarity of the acid solution significantly affected to the crystal morphology of the clinoptilolite, which was degredated with 5M and 8M HCl solution. However,

dealumination of the clinoptilolite was effectively achieved by high molar HCl concentration. Elemental analyses were also performed by the EDX mod of the SEM and results were tabulated in Table 7.15.

Table 7.15. Elemental analysis of the acid treated clinoptilolite sample performed by EDX.

	Al	Si	Na	K	Si/Al
Not treated	8.39	36.86	1.05	4.98	4.39
1M HCl	6.25	40.42	0.74	3.42	6.46
3M HCl	5.64	40.83	0.83	1.67	7.23
5M HCl	4	43	0.51	1.34	10.75
8M HCl	1.36	45.04	0.41	0.42	33.11

The treatment of clinoptilolite with HCl causes dealumination (hydrolysis of Al-O-Si bonds) by the exchange of the cations by hydronium ions (H_3O^+) (Özkan and Ülkü, 2005). Removing Al ions from the clinoptilolite opens the pores and eases sorbate to reach the active sorption sites. Additionally, dissolving of some amorphous materials that block the pores of clinoptilolite is another consequence from the acid modification (Allen et al., 2009). Si/Al ratio determines the hydrophobic character of the clinoptilolite sample. Ruthven (1984) indicates that the transition from hydrophilic to hydrophobic normally occurs at a Si/Al ratio between 8 and 10. Dealumination of the clinoptilolite was achieved by the acid treatment and 10.75 Si/Al ratio was achieved by the 5 M HCl treatment.

Adsorption studies were performed with those acid treated clinoptilolite samples after washing them with deionized water till pH of the water equals to 6.5, which is the pH of the deionized water. Parallel to the increment of the Si/Al ratio, adsorption of *trans*-resveratrol was increasing except 8 M acid treated clinoptilolite (Figure 7.43). The trend in raising the adsorbed amount of *trans*-resveratrol was due to the increasing of the hydrophobic character of the clinoptilolite. However, economy of the acid treatment process and the capacity of treated clinoptilolite sample should be considered in parallel. Although, adsorption capacity of 5 M acid treated clinoptilolite sample was doubled, acid treatment process would not be feasible because of the difficulties in acid treatment process.

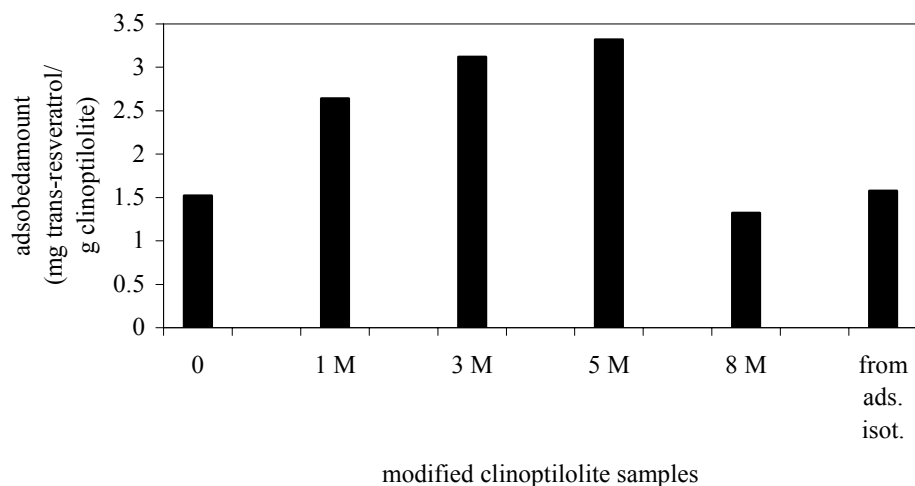


Figure 7.43. Adsorption of *trans*-resveratrol by acid treated clinoptilolite samples; adsorption studies were performed with solid-liquid ratio 1/40, at 35 °C during 24 hours.

Column Studies

Column studies were performed with the model solutions including gallic acid, (+)-catechin, (-)-epicatechin and *trans*-resveratrol. The loading was performed at room temperature with a flow rate of 1mL/min. Column effluents were collected against time and were analysed by HPLC in order to determine the effluents compositions. Figure 7.44 to 7.46 belongs to the saturation of column with each of the standard components. In Figure 7.33_A, sorption profiles of all flavonoids were shown. Sorption profiles of gallic acid, (+)-catechin and (-)-epicatechin are given separately in Figure 7.44_B and Figure 7.45_C-D, respectively. On the other hand, *trans*-resveratrol sorption profile is given in Figure 7.46, for which highest affinity was seen and breakthrough profile was obtained.

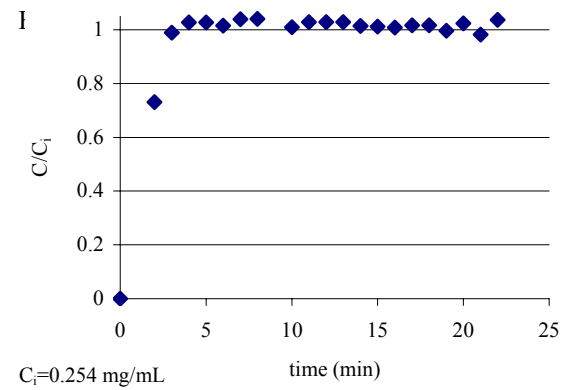
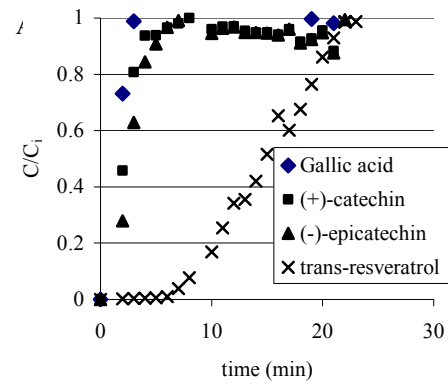


Figure 7.44. Concentration changes at column outlets relative to inlet concentrations of each compounds; A: for all polyphenols, B: for gallic acid.

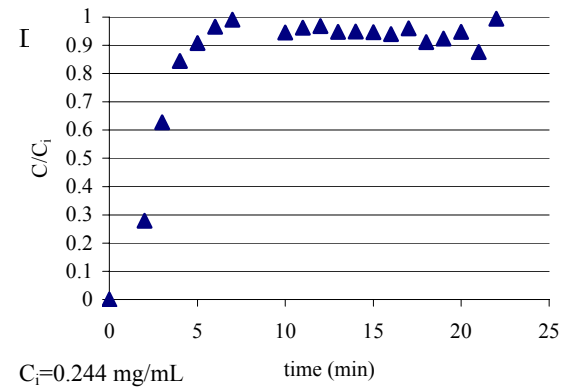
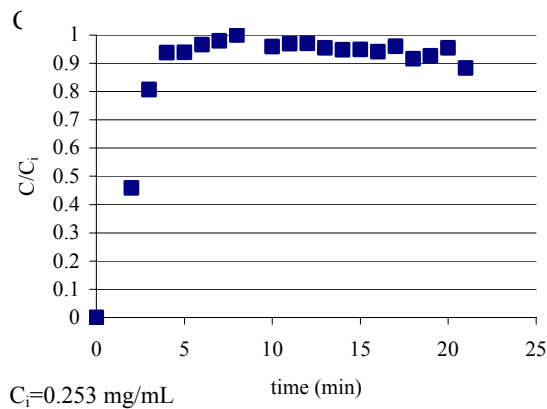


Figure 7.45. Concentration changes at column outlets relative to inlet concentrations of each compounds; C: (+)-catechin, D: (-)-epicatechin.

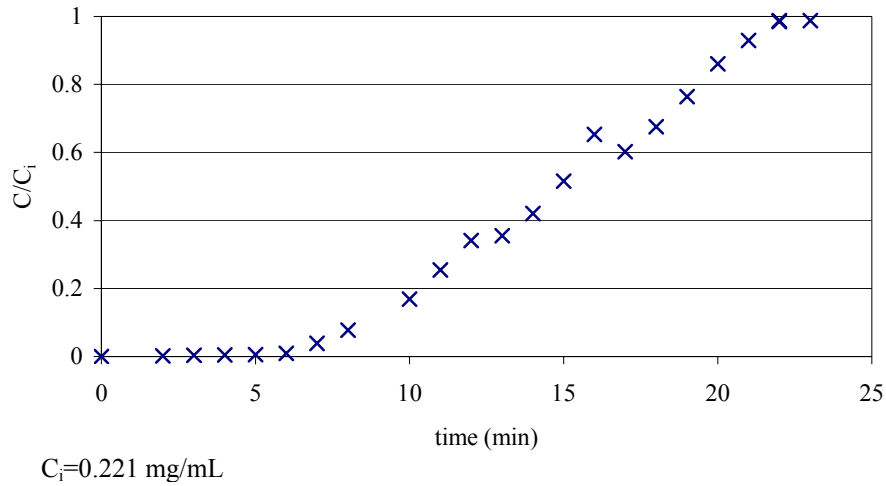


Figure 7.46. *Trans*-resveratrol concentration changes relative to inlet concentration at column outlets.

Trans-resveratrol was selectively adsorbed by the column. Silk fibroin does not show affinity to adsorb gallic acid from the mixture. (+)-catechin and (-)-epicatechin were detected in column effluents after 5 minutes passing of the mixture solution. In the multicomponent adsorption studies of grape skin polyphenols, the adsorption of gallic acid was eliminated at the presence of (+)-catechin and (-)-epicatechin. Similar situation was observed by the column study. Almost all effluents included gallic acid, whose concentration was equal to inlet concentration of it. Flow rate is important parameter, because it directly affects the contact time of mixture with adsorbent. According to kinetic studies of gallic acid, (+)-catechin and (-)-epicatechin, 120 min contact time was required to reach equilibrium. However, quick flow through the column limits the adsorption of these phenolic components. In the case of the *trans*-resveratrol, which is significantly adsorbed by the adsorbent, the saturation of the column was achieved within 22 minutes.

The following mass balances were used to quantify the capacity of adsorption as well as the ratios of adsorption.

Total adsorbed amount by column:

$$q = \frac{(C_i - C_o) * V}{w} \quad (7.1)$$

where q is the amount of adsorbate adsorbed by column (mg adsorbate/g adsorbent), C_i and C_o denote the initial concentration of the adsorbate in the aqueous phase (mg/mL) and column outlet concentration, respectively. V is the volume of analyte solution (mL) passed through the column and w is the dry weight (g) of the adsorbent.

Desorption evaluation:

$$D = C_d * V_d \quad (7.2)$$

where D is the amount of desorbed compound (mg); C_d the concentration of the analyte in the desorption solution (mg/mL); V_d the volume of the desorption solution (mL).

Table 7.16 indicates the adsorbed amounts of polyphenolic components from working solution on silk fibroin. Silk fibroin in column did not show any affinity to gallic acid, and all amount of gallic acid passed through the column without any change. However, silk fibroin in column had high affinity to adsorb the *trans*-resveratrol and 56% of total loaded *trans*-resveratrol was loaded to the column. Around 18% of the other polyphenols in working solution was also adsorbed by the silk fibroin in column.

Table 7.16. Adsorbed and desorbed amounts of polyphenols from the silk fibroin filled column and effect of eluting solvent on the polyphenolic compositions

		Gallic Acid	(+)-catechin	(-)-epicatechin	<i>Trans</i> -resveratrol
Adsorbed amount (%)		≈0	7.8	10.5	56.1
Total desorption (%)		0	95	84	92
Eluted amount (%)	Water elutions	0	97.76	96.99	9.95
	10% Ethanol	0	2.23	3.00	2.06
	40% Ethanol	0	0	0	79.72
	50% Ethanol	0	0	0	1.02
	60% Ethanol	0	0	0	0.16
	100% Ethanol	0	0	0	0.07

After the loading of the column, separation of these polyphenols is important. For this purpose, elution of loaded compounds were performed initially with water and

followed by solutions with increased ethanol concentrations from 10 to 100. It is expected that, polyphenolic compounds in working solution having polar nature would be eluted with water and nearly all polyphenols except *trans*-resveratrol was eluted from column by passing 6 mL of water. Only 10% of *trans*-resveratrol was eluted with water (Table 7.16), which would be the excess amount of it.

Dipole moments of the water, *trans*-resveratrol and ethanol are 1.85 debye, 1.6 debye (Erkoc et al., 2003) and 1.69 debye, respectively. Dipole moments of the solution are decreased by increasing the ethanol concentration of the solution. The most appropriate elution condition to elute *trans*-resveratrol from the column was achieved with 40% ethanol solution. Sorption of *trans*-resveratrol might probably be explained by the physical adsorption, since nearly 90% of sorbed *trans*-resveratrol was eluted from the silk fibroin filled column by just changing the dipole moment of the eluting solvent. Only *trans*-resveratrol was eluted from the column with 6 mL of 40% ethanol (Table 7.16), so the purity of *trans*-resveratrol in these fractions was very high (Table 7.17). Further elutions contain trace amount of *trans*-resveratrol. The purities of other fractions are shown in Table 7.17. Almost all polar polyphenols were eluted with water.

Table 7.17. Purity of eluted fractions

		% Ethanol Fractions			
		0	10	40	60
Component	GA	-	-	-	-
	(+)-Catechin	26.4	2.23	-	-
	(-)-Epicatechin	44.4	3.96	-	-
	<i>Trans</i> -resveratrol	28.78	93.17	≈99	≈99

In order to determine the column efficiency, second run was performed with pre-used column after conditioning of it with conditioners, which are the same with previously mentioned ones. Figure 7.47 indicates that, column performance was similar with previous run. However, in this case, small amount of gallic acid was adsorbed by the silk fibroin in column.

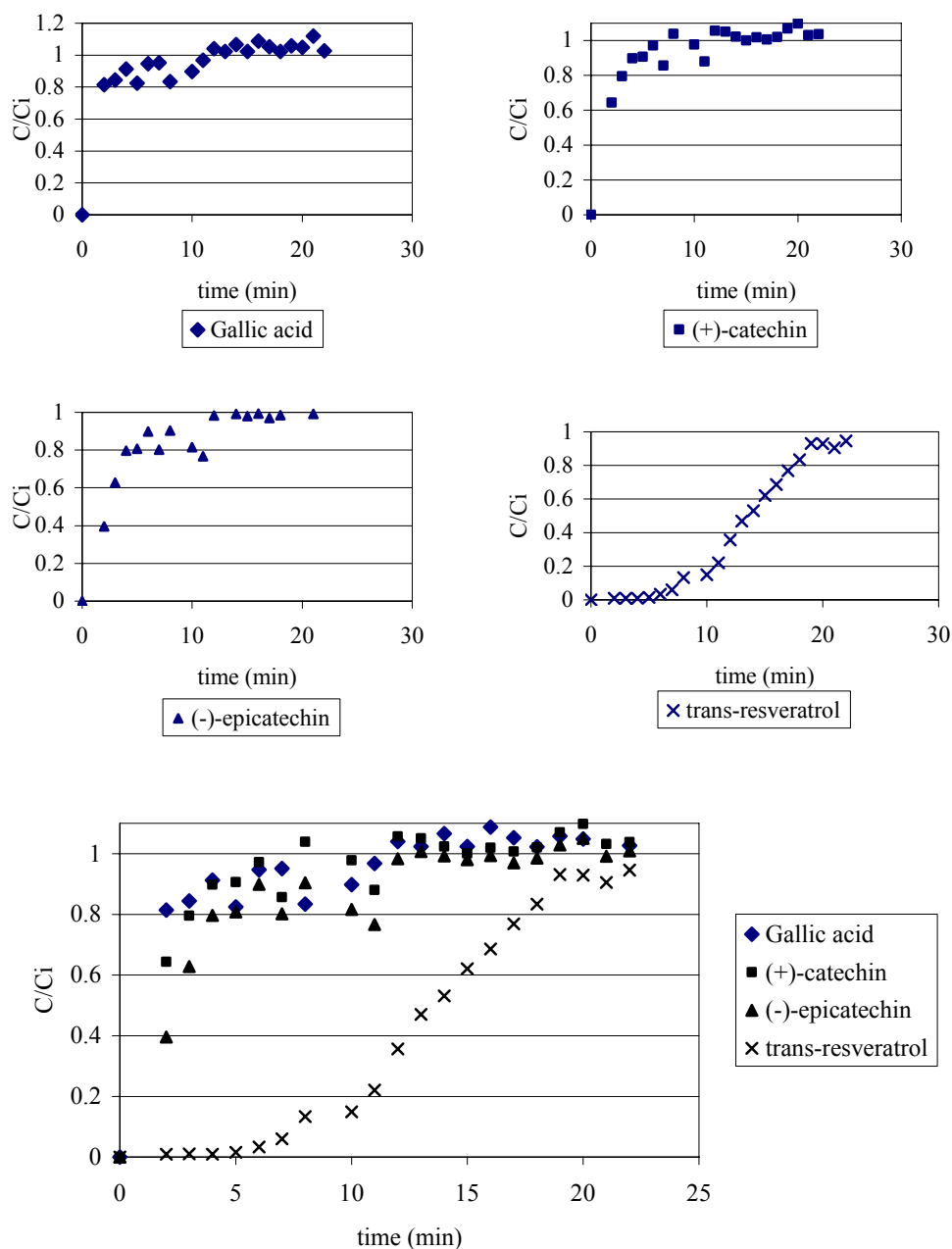


Figure 7.47. Second loading of column with polyphenols' standards mixtures.

By comparing the decreasing of the hold up amount of (+)-catechin in column with the one for the gallic acid, we can conclude that gallic acid competes with the (+)-catechin. This result was also supported with the batch adsorption studies. There was not significant difference between the hold up amounts of (-)-epicatechin and *trans*-resveratrol within two loading performances of the column (Table 7.18).

Table 7.18. Adsorbed and desorbed amounts of polyphenols from the silk fibroin filled column and effect of eluting solvent on the polyphenolic compositions (belongs to secondly used column)

		Gallic Acid	(+)-catechin	(-)-epicatechin	<i>Trans</i> -resveratrol
Adsorbed amount (%)		2.19	3.09	10.97	60.83
Total desorption (%)		100	100	91	93.8
Eluted amount (%)	Water elutions	99.4	90.06	84.61	10.76
	10% Ethanol	0.24	5.32	7.2	2.23
	40% Ethanol	0.24	4.76	8.1	86.22
	100% Ethanol	0	0	0.02	0.74

Similar to the first column performance, high purity of *trans*-resveratrol was eluted from silk fibroin filled column with 40% ethanol solution. Nearly all of the loaded *trans*-resveratrol (86%) was eluted from the column with a high purity (Table 7.19).

Table 7.19. Purity of eluted fractions from second loading column

		Ethanol % Fractions			
		0	10	40	
				1 st elution	Other elution
Component	GA	20.38	0.3	0	-
	(+)-Catechin	28.14	20.7	2.7	-
	(-)-Epicatechin	32.36	35	5.7	-
	<i>Trans</i> -resveratrol	16.56	43.7	91.4	≈99

As a conclusion, silk fibroin can effectively be used in order to separate polyphenols according to their polarities.

For dynamic column application, it is very important to determine the effect of many parameters such as flow rate, inlet concentrations of the components, adsorbent amount in column etc. for large scale application of the process and for the economy of the process. For this reason *trans*-resveratrol was used in further column studies in order to optimize the working conditions.

Dynamic Column Studies Performed with the *Trans-resveratrol*

Trans-resveratrol was analyzed with Thermo Multiscan Spectrum by comparing the absorbance values with HPLC results. Calibration curve of *trans-resveratrol* was given in Appendix C.4.

Effect of Liquid Flow Rate

The break point is the point on the S-shaped curve at which the solute concentration reaches its maximum allowed value (usually 5% of its influent value). The column saturation point is defined where the effluent concentration reaches 100% of its influent value.

The results for different flow rates of solution are plotted for a bed height of 14 mm, which includes 0.2 g of adsorbent, and an inlet adsorbate concentration of 0.1 mg/mL in Figure 7.48.

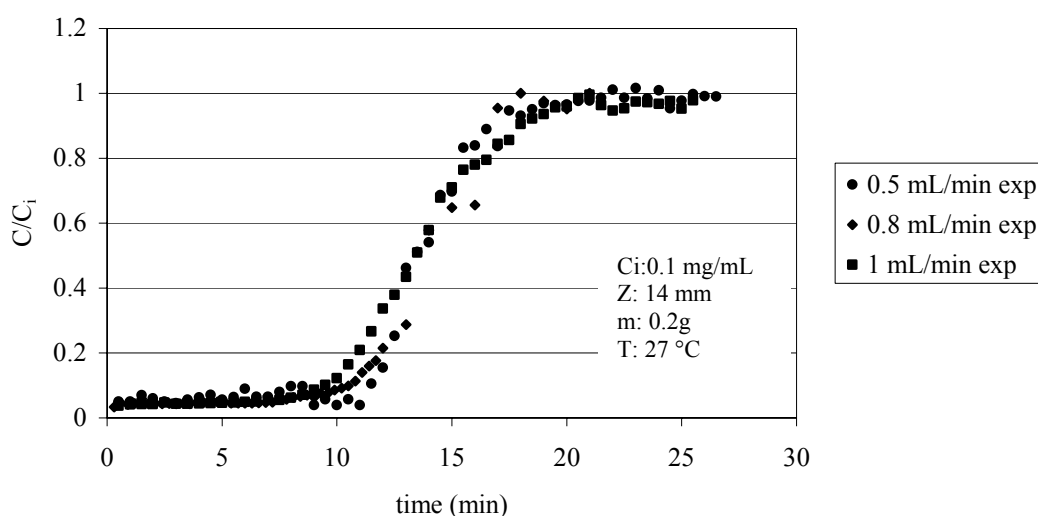


Figure 7.48. Effect of flow rates on breakthrough curve.

Figure 7.48 shows that as the flow rate decreases from 1.0 to 0.5 mL/min, the breakthrough curve was sharpened. On the other hand, the break point times were 11.5, 10.5 and 9.5 minutes for flow rates as 0.5, 0.8 and 1 mL/min, respectively. Longer time was required to reach breakthrough point for lower flow rates. However, for the effective column separation, sharper breakthrough profile is desired.

Effect of Inlet Concentration

The effect of inlet adsorbate concentration on effluent concentration is shown in Figure 7.49. During these simulations other parameters such as bed height and flow rate are kept constant as 14 mm and 1 mL/min, respectively.

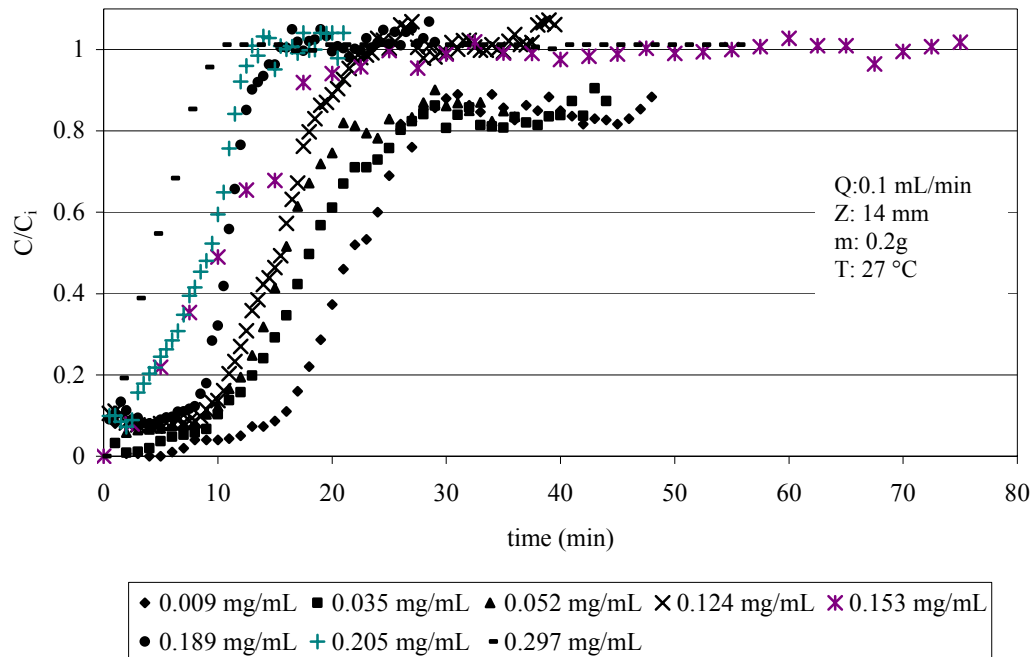


Figure 7.49. Effect of influent concentration on breakthrough curve.

Figure 7.49 indicates that longer time was required to reach $C/C_i=1.0$ for lower inlet concentration of *trans*-resveratrol (for the solutions having influent concentrations as 0.009, 0.035, and 0.052 mg/mL). For the inlet concentrations of *trans*-resveratrol (C_i : 0.124, 0.153, 0.189 and 0.205 mg/mL), good S-shape breakthrough profiles were obtained. As expected, at lower *trans*-resveratrol concentrations, greater processing times were required for the effluent concentration to reach a value equal to the inlet concentration. However, it was significantly different in case the highest inlet concentration of *trans*-resveratrol (0.297 mg/mL). Breakthrough time could not be detected and saturation of the column was achieved within very short time period.

It was observed that as the inlet adsorbate concentration increases from 0.009 to 0.297 mg/mL, the break point time decreases from 16 minutes to seconds. For larger influent concentration, steeper breakthrough curves were obtained, because higher inlet

concentration provides an important driving force for the sorption of the *trans*-resveratrol in column. *Trans*-resveratrol concentration of the solution affected the uptake rate, which was increase by increasing the inlet concentration. That is why the equilibrium is attained faster for the values of higher adsorbate concentration.

Normalization of the Breakthrough Data

Effects of flow rates and inlet concentrations of the *trans*-resveratrol feed solution on breakthrough profiles were investigated. The breakthrough data were analyzed by normalizing the data. For this purpose, normalization of the breakthrough data was performed by multiplying the flow rate (Q), time and the concentration at time t (C_t) in order to obtain the amount of sorbate passed through the column. The normalized breakthrough curves were given in Figure 7.50 and Figure 7.51.

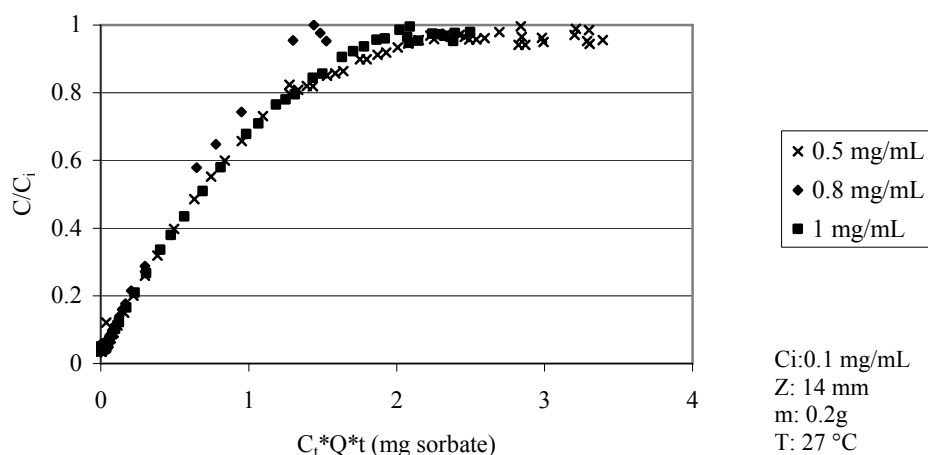


Figure 7.50. Normalized breakthrough data obtained by changing the flow rates.

Figure 7.50 indicates that the amount of sorbate passed through the column is not affected from the flow rates. After eliminating the effects of flow rates, almost similar plots were obtained from the each of the experiments. It is expected that if the sorption is controlled by the external film mass transfer, changing the flow rate should affect these profiles. Thus, external film mass transfer does not control the sorption of *trans*-resveratrol on silk fibroin. Similar conclusion was obtained from the batch kinetic study. Changing the shaking speed did not have influence on the sorption kinetics of *trans*-resveratrol.

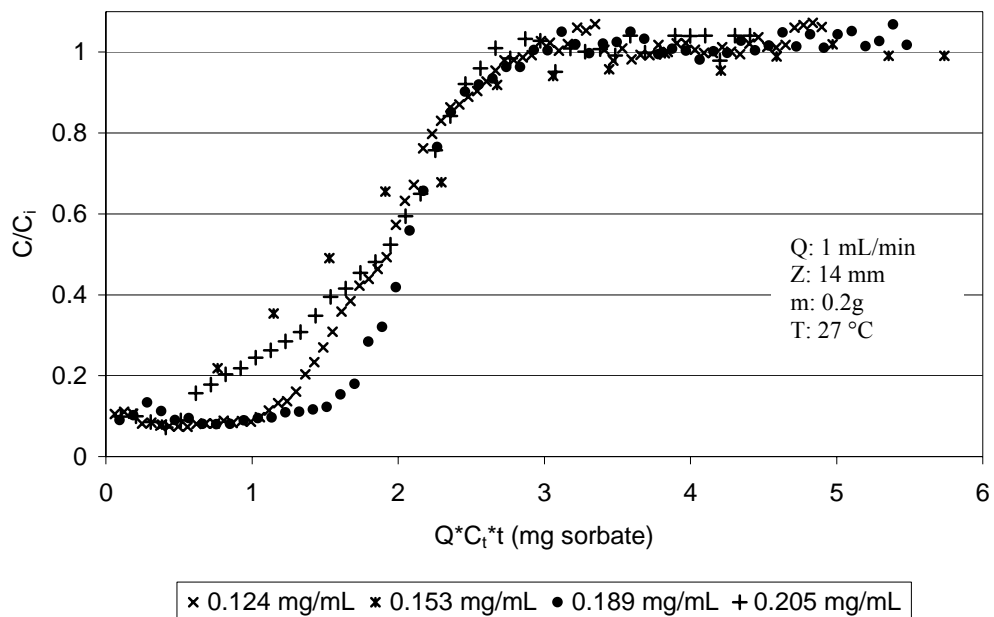


Figure 7.51. Normalized breakthrough data obtained by changing the inlet concentrations of the sorbate.

After normalization of the breakthrough data, the amount of adsorbate passed through the column was quite constant. This result supports the validity of the experimental studies. Although, changing the inlet concentration and flow rates directly affects on the breakthrough shapes by effecting on the breakthrough time and saturation time, final adsorption capacity would be a constant value. For the large scale operations, the breakthrough time and saturation time becomes very important parameters and it is required to shorten the time difference to increase the column performance.

Effect of Bed Height

The effect of bed height on the effluent adsorbate concentration is presented for flow rate of 1 mL/min and inlet adsorbate concentration of 0.035 mg/mL in Figure 7.52. It was observed that as the bed height increases from 10 to 14 mm (amount of silk fibroin was 0.15 and 0.2 grams, respectively), the break point time increased from 4 to 8 min. From Figure 7.52, as the bed height increases, *trans*-resveratrol had more time to contact with silk fibroin that resulted in higher removal efficiency of *trans*-resveratrol in column. So the higher bed column results in decrease in the solute concentration in the effluent at the same time. The slope of breakthrough curve decreased with increasing

bed height, which resulted in a broadened mass transfer zone. High uptake was observed at the highest bed height due to an increase in the binding sites for the adsorption.

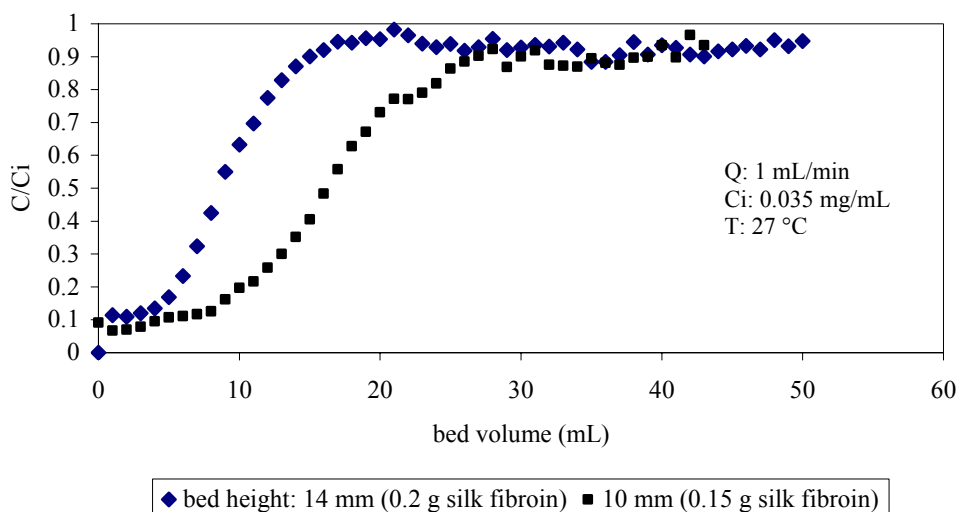


Figure 7.52. Effect of bed height on breakthrough curves. Flow rate: 1 mL/min and C_i : 0.035 mg/mL.

Column Regeneration and Performance

Trans-resveratrol adsorbed dynamically by silk fibroin filled column and then was washed with water. After that, the elution of *trans*-resveratrol was performed by ethanol-water solution: 10%, 20%, 30%, 40%, 50%, 60% and 96%. Figure 7.53 indicates the elution performance of *trans*-resveratrol with elution solvents. Water and 10% of ethanol fraction contains *trans*-resveratrol because excess *trans*-resveratrol was washed out. Most of the adsorbed *trans*-resveratrol was eluted successfully by 40% of ethanol solution.

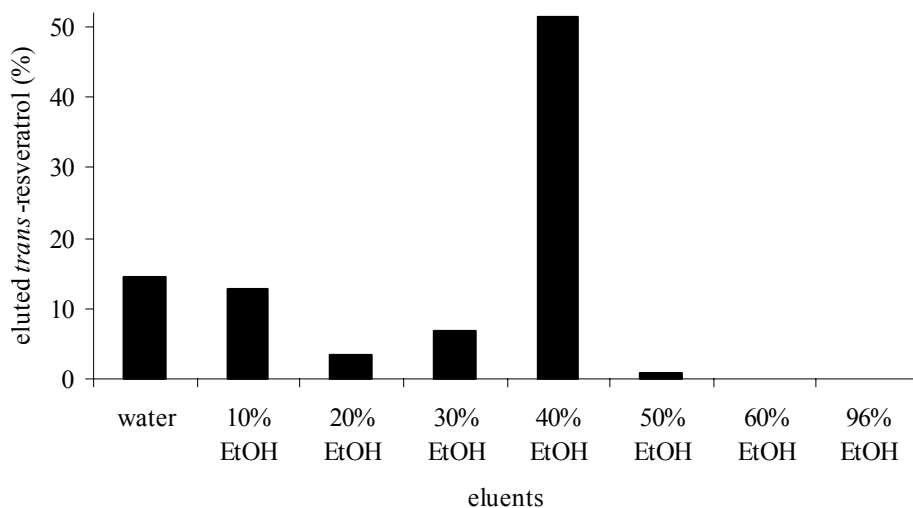


Figure 7.53. Percentage distribution of trans-resveratrol at eluted fractions.

Thus, after washing column with 10 mL of water, elutions of sorbed polyphenols were performed with 15 mL of 40% ethanol for further dynamic column studies (Fig. 7.54). After that, column was washed with 10 mL of ethanol and water for the regeneration. The flow rate during elution was kept constant as 1 mL/min.

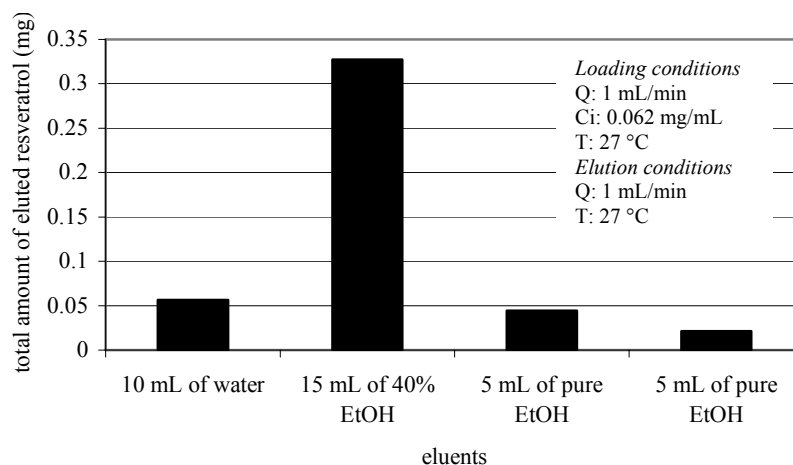


Figure 7.54. Elution of trans-resveratrol with different ethanol solutions.

In order to efficient desorption with 40% ethanol elution solvent, trans-resveratrol content of eluents were analyzed. Figure 7.55 indicates that 8 mL of 40% ethanol was sufficient to desorb most of the adsorbed trans-resveratrol on silk fibroin in

column. This study was performed for 3 times and at each cycle similar behaviour was obtained.

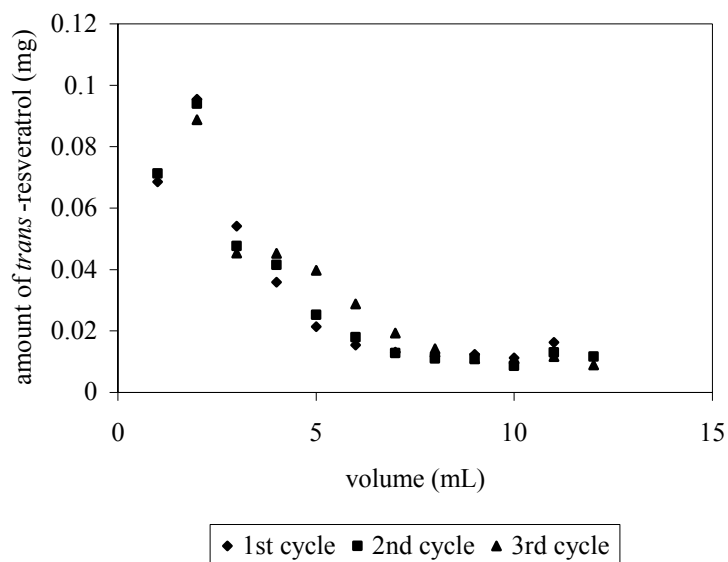


Figure 7.55. Elution of *trans*-resveratrol by 40% ethanol from column filled with silk fibroin and elution performance.

In order to examine the effect of regeneration on column performance, several times of adsorbate loading was performed to the preconditioned silk fibroin filled column. Column was initially conditioned by subsequent washing with the deionized water, ethanol and deionized water. The initial concentration of *trans*-resveratrol was 0.063 mg/mL and flow rate was kept constant at 1mL/min. It can be noticed that breakthrough curves in the first cycle do not have an expressed S-shape. In the second cycle, after regeneration, the curves assume the typical S-shape and show agreement for further cycles (Fig. 7.56). This may be explained by establishment of stable condition and better contact of solid and liquid phases.

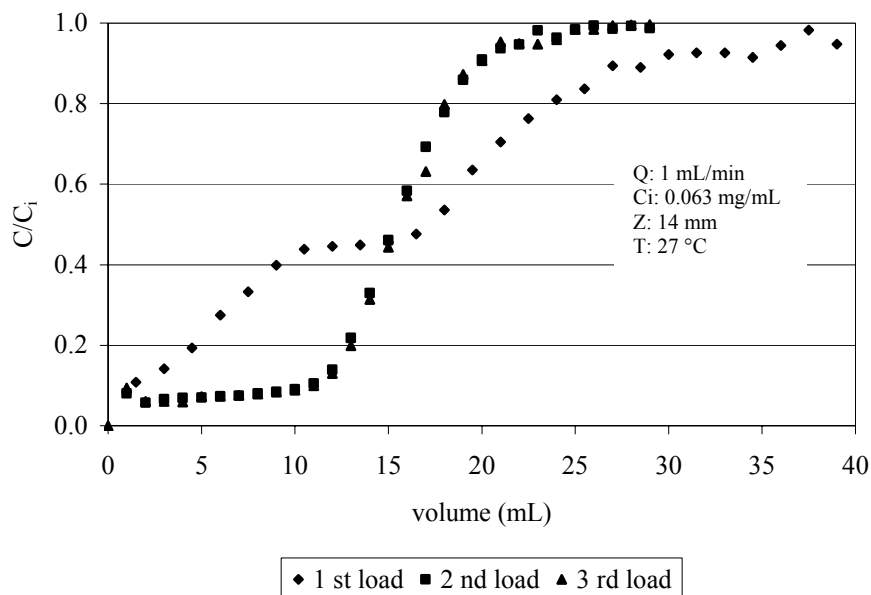


Figure 7.56. Effect of regeneration on column performance.

Quantitative Interpretation of Breakthrough Curves

Application of Adams-Bohart Model to Experimental Breakthrough Curves

Adams-Bohart model was applied to both the breakthrough curves obtained by changing flow rates and initial concentrations of *trans*-resveratrol. There are good agreements between the theoretical breakthrough curves and experimental ones especially up to the C/C_i values 0.6 (Figure 7.57 and Figure 7.58).

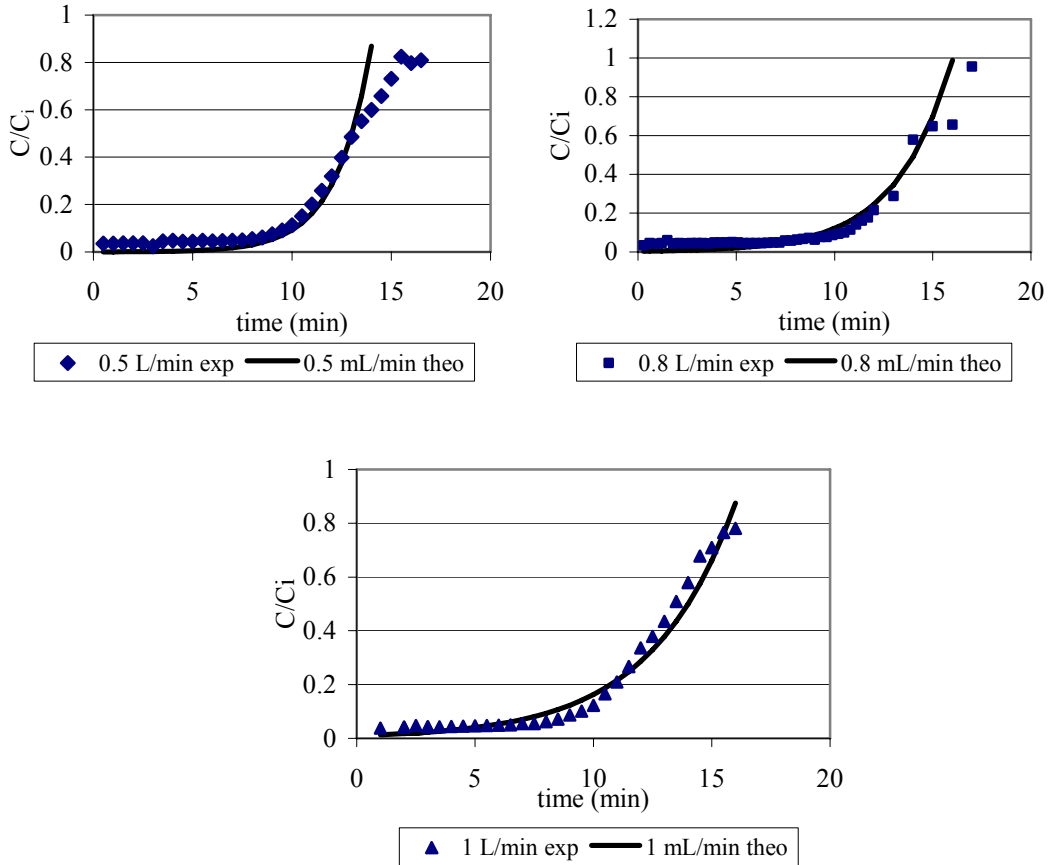


Figure 7.57. Application of Adams-Bohart model to investigate the effect of flow rate on breakthrough curve.

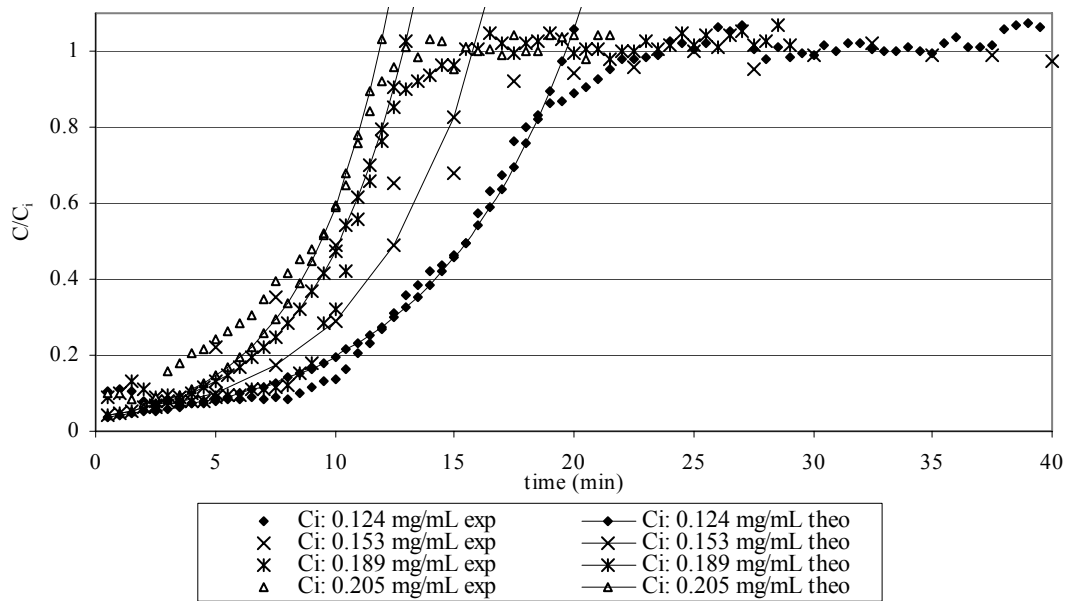


Figure 7.58. Application of Adams-Bohart model to investigate the effect of inlet concentration on breakthrough curve.

After applying Adams-Bohart equation to the experimental data for varying flow rates and inlet phenol concentrations, saturation concentration (N_0) and k_{AB} were calculated by minimizing the sum of squares of error (SSE) between the theoretical and experimental C/C_i values (Table 7.20). Squares of errors were calculated by the following equation.

$$SE = \left[\left(\frac{C}{C_i} \right)_{theo} - \left(\frac{C}{C_i} \right)_{exp} \right]^2 \quad (7.3)$$

Solver was used in excell to minimize the SSE. The summation of the squares of errors were performed until the C/C_i value equals to 1. Initial guess of N_0 and k_{AB} values were made and the values of SSE were minimized by changing the values of N_0 and k_{AB} . Solver determines the parameters with a minimum SSE values. The correlation coefficient of the experimental and theoretical C/C_i were calculated and given in Table 7.20.

Table 7.20. Parameters predicted from the Adams-Bohart model

C_i (mg/mL)	Q (mL/min)	k_{AB} (mL/mg/min)	N_0 (mg/mL)	R^2	SSE
0.102	0.5	2.96	7.1	0.973	0.143
0.102	0.8	3.04		0.963	0.116
0.102	1.0	3.06		0.971	0.163
0.124	1.0	2.41		0.998	0.0628
0.153	1.0	1.17		0.891	0.171
0.189	1.0	2.08		0.983	0.095
0.205	1.0	1.24		0.994	0.056

Saturation concentration in the Adams-Bohart model is remains constant, which indicates sorption of trans-resveratrol on silk fibroin did not affect by changing the flow rates and inlet concentration of the solution. On the other hand, Adams-Bohart rate constant (k_{AB}) was almost remained constant by changing the flow rate, which indicates that external film mass transfer is not control the sorption of trans-resveratrol on silk

fibroin. However, the values of k_{AB} were influenced by increasing initial concentration of the solution.

Application of the Thomas Model

The resulting breakthrough curves obtaining according to the Thomas model are shown as solid lines in Figures 7.59 and 7.60 in comparison with the experimental data. In particular, Thomas model predicts the initial and ascending portion of a breakthrough curve. This result has importance since the initial portion of breakthrough curve determines the useful dynamic column capacity. Thomas model overestimates the saturation point when compared with the experimental values.

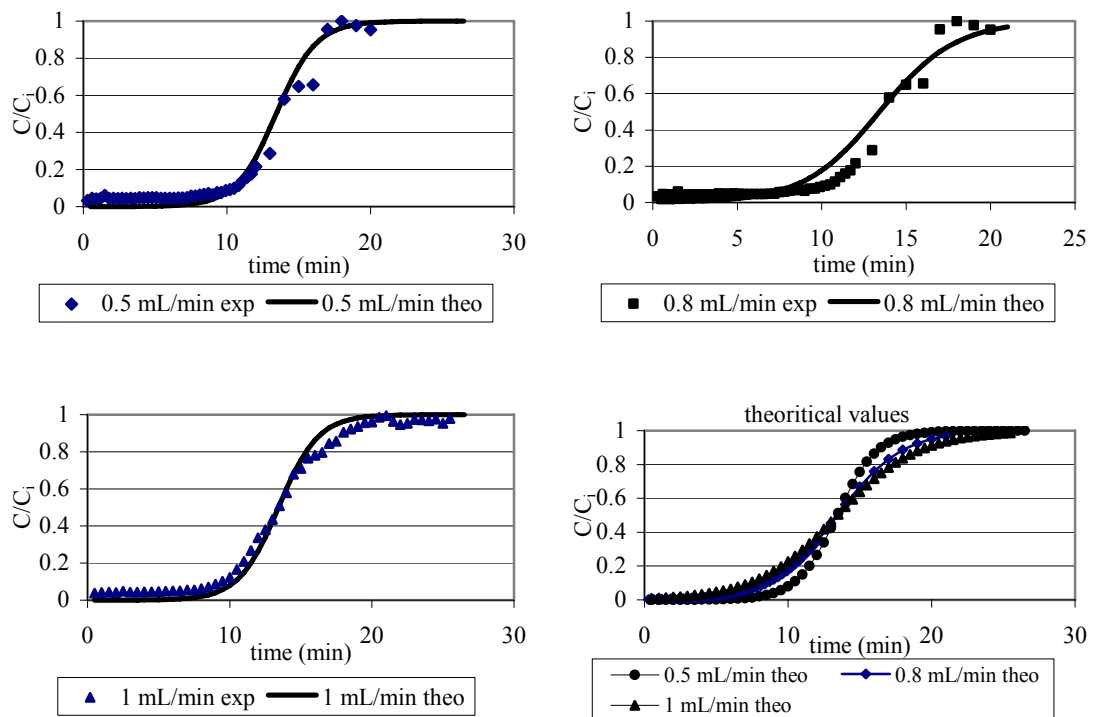


Figure 7.59. Application of Thomas model to investigate the effect of flow rates on breakthrough curve.

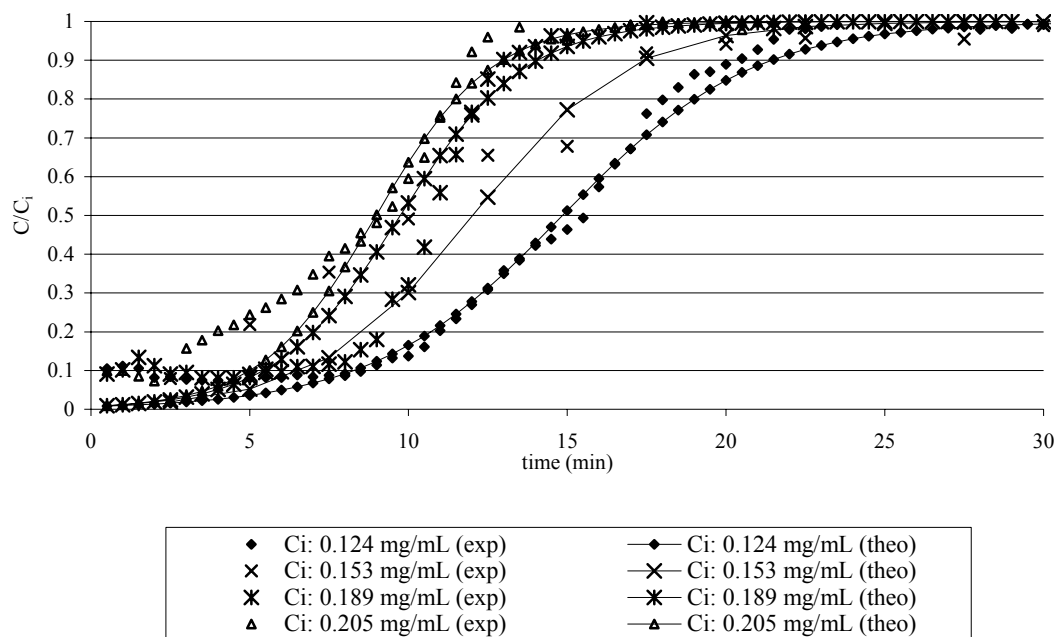


Figure 7.60. Application of Thomas model to investigate the effect of inlet concentration on breakthrough curve.

All of the parameters affected on the breakthrough profiles were investigated together in order to determine the maximum column adsorption capacity. For this purpose, theoretical values were calculated by the Thomas model and squares of error were calculated. The summation of the squares of errors was performed. k_{Th} and q_0 were the variables which were tried to be determined by minimizing the sum of square of errors. Microsoft Office Excel Solver was used to determine the Thomas constant (k_{Th}) and q_0 . k_{Th} and q_0 were found as 2.51 mL min/ mg and 8.33 mg *trans-resveratrol*/ 0.2 g adsorbent. From the batch experiments maximum adsorption capacity was found as 41 mg *trans-resveratrol*/ g of silk fibroin. The column capacity was 41.6 mg *trans-resveratrol* per gram of silk fibroin, which was close to the batch adsorption capacity, but was lower than the capacity determined by the Langmuir isotherm (52 mg *trans-resveratrol*/ g of silk fibroin).

The correlation between the theoretical and experimental breakthrough data was performed and given in Table 7.21.

Table 7.21. Thomas model parameters and correlations between the theoretical and experimental values

Initial concentration (mg/mL)	Flow Rate (mL/min)	R ²	Thomas kinetic constant (k_{Th})	Column adsorption capacity (q_0)
0.100	0.5	0.981	2.51	8.33
0.100	0.8	0.971		
0.100	1.0	0.979		
0.124	1.0	0.972		
0.153	1.0	0.984		
0.189	1.0	0.940		
0.205	1.0	0.973		

7.3.4. Adsorption and Selective Separation of Olive Leaf Crude Extract (OLCE) Polyphenols on Silk Fibroin

Adsorption of olive leaf extract polyphenols by silk fibroin filled column was performed to selectively separate the bioactive compounds.

The selective accumulation of rutin and oleuropein on the hydrophobic silk fibroin revealed the presence of interaction between silk fibroin and polyphenols during the adsorption process. The other polyphenols in olive leaf extract such as verbascoside, apigenin-7-glucoside, luteolin-7-glucoside which have closer retention times to retention time of rutin and oleuropein, were also adsorbed on silk fibroin. However, the amount of these antioxidants in olive leaf extract and the adsorbed amount of them on silk fibroin are less compared to the adsorbed amount of oleuropein and rutin.

The comparison of HPLC chromatograms given in Figure 7.61 A and B indicated that, initially both oleuropein and rutin were rapidly adsorbed on the silk fibroin from initial extract solution. The first effluent was almost free of them as seen from Figure 7.61 A. As the crude extract solution was further loaded to the column, the silk fibroin was progressively saturated with oleuropein and rutin, therefore the amounts of both polyphenols started to increase until the saturation of silk fibroin was achieved (Figure 7.61 C and D).

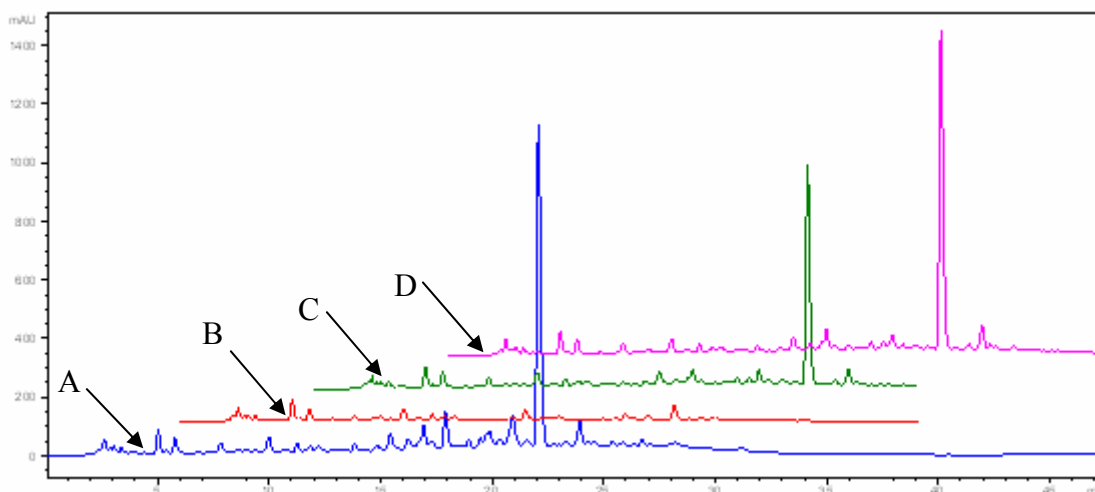


Figure 7.61. HPLC chromatogram of A: initial solution; B: 1st effluent; C: 8th effluent; D: 12th effluent of the silk loaded column.

Amount of adsorbed analytes (q) were calculated as follows:

$$q = \frac{\sum_{i=1}^n C_o - nC_i}{w} \quad (7.1)$$

where C_i denotes the inlet concentration of the analytes in the aqueous phase, n is the number of loading of analyte solution (1mL volume of each) and w is the dry weight of the adsorbent. The results obtained by this formula are listed in Table 7.22.

Table 7.22. Amount of adsorbed oleuropein and rutin (q) at different concentrations of loading

	1g OLCE/ 50 mL dw	1.5 g OLCE/ 50 mL dw
<u>Oleuropein</u>		
C_i (g/L)	3.24	4.56
q (mg/g silk fibroin)	96.41	101.17
<u>Rutin</u>		
C_i (g/L)	0.424	0.573
q (mg/g silk fibroin)	15.48	12.09

dw: deionized water

1g and 1.5 g of OLCE were dissolved in 50 mL of deionized water. So, initial oleuropein and rutin concentrations of the solution were changed. It is clearly seen that, amount of adsorbed oleuropein on the silk fibroin increases with increasing initial concentration of loading solution. This situation is attributed to the existence of a dynamic equilibrium in the column system. However, in case of the rutin adsorption, adsorbed amount of rutin decreases with increasing initial concentration of rutin in loading solution.

After reaching to the saturation of column, elutions of different fractions were performed first with deionized water and then 40% aqueous ethanol solution. HPLC results of eluted fractions with deionized water are given in Figure 7.62.

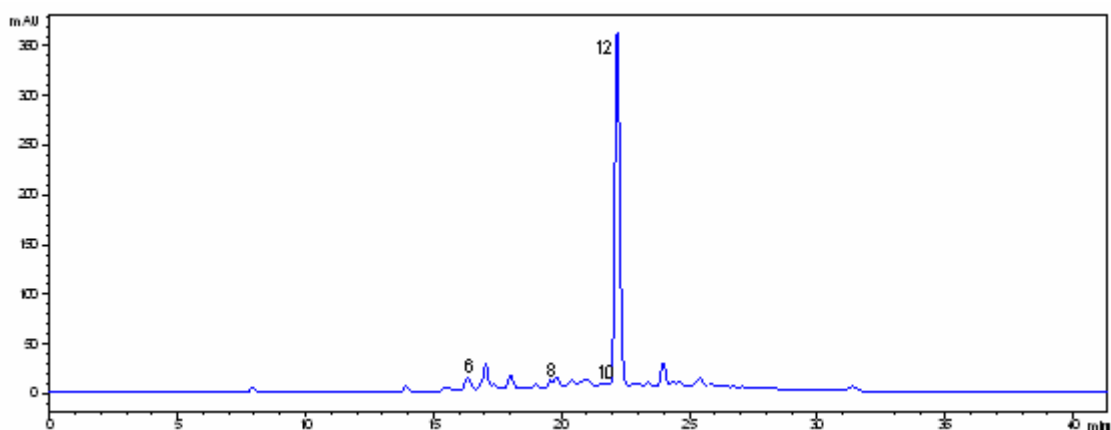


Figure 7.62. HPLC chromatogram of eluted fraction with deionized water.

Ten milliliters of water was enough to elute all oleuropein from the column. It can be clearly seen that purity of oleuropein increases.

The other remaining fractions were eluted with 40% ethanol solution from the silk fibroin filled column (Figure 7.63).

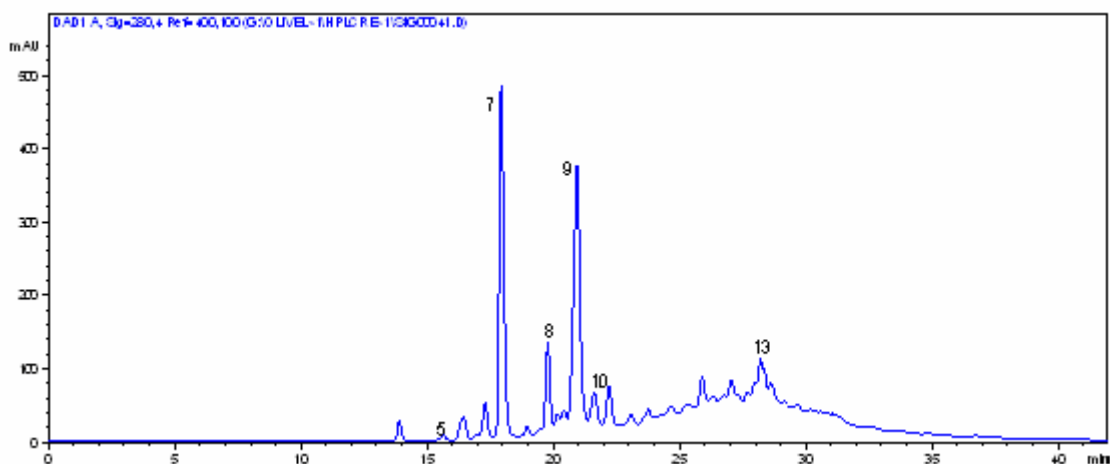


Figure 7.63. HPLC chromatogram of eluted fraction with 40% Ethanol.

Based on the sharp peaks at 18 min, 20 min and 21 min at chromatogram, it can be concluded that several other components found in crude extract solution are strongly adsorbed on silk fibroin. These peaks belong to the rutin, luteolin-7-glucoside and verbascoside, respectively (Table 7.23).

Table 7.23. HPLC profile of phenolics eluted from column with water and 40% ethanol solution

Phenolics	peak #	Water elution Peak area %	40% Ethanol elution Peak area %
Hydroxytyrosol	1	-	-
Tyrosol	2	-	-
Catechin	3	-	-
Caffeic acid	4	-	-
Vanillic acid	5	-	0.26
Vanillin	6	4	-
Rutin	7	-	13.84
Luteolin-7-glucoside	8	-	4.29
Verbascoside	9	-	15.46
Apigenin-7-glucoside	10	2.3	2.99
Diosmetin-7-glucoside	11	-	-
Oleuropein	12	62	-
Luteolin	13	-	7

7.3.5. Adsorption of Olive Leaf Polyphenols on Clinoptilolite (Clinoptilolite Rich CL5)

Figure 7.64 shows the HPLC chromatogram of OLCE in water, which was obtained after removing ethanol with rotary evaporator. The numbered peaks' list and abundance of main compounds in OLCE are shown in Table 7.24.

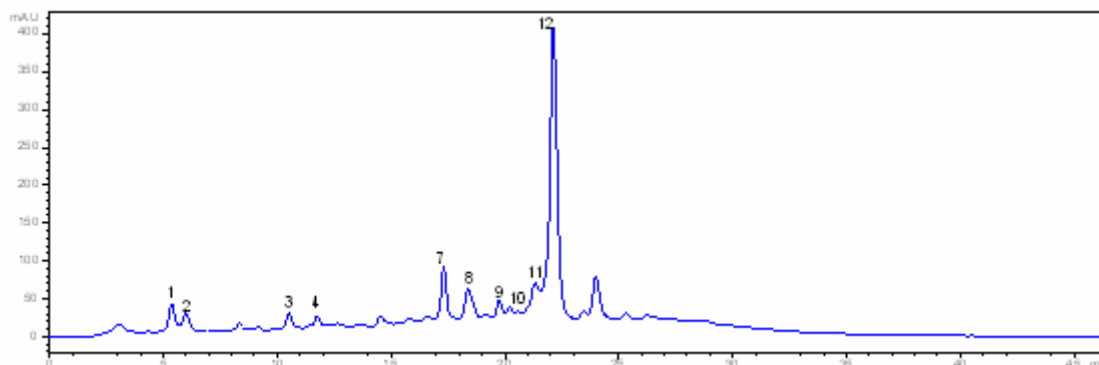


Figure 7.64. HPLC chromatogram of OLCE dissolved in water (10 mg/mL of deionized water). Oleuropein and rutin content of OLCE was found as 244.5 mg and 45.75 mg, respectively.

Table 7.24. Peak number and abundance (peak area %) of the main phenolic compounds present in olive leaf crude extract

Phenolics	peak#	1 g CE Peak area %
Hydroxytyrosol	1	3.77
Tyrosol	2	2.58
Catechin	3	1.96
Caffeic acid	4	1.74
Vanillic acid	5	-
Vanillin	6	-
Rutin	7	7.00
Luteolin-7-glucoside	8	5.93
Verbascoside	9	2.85
Apigenin-7-glucoside	10	1.25
Diosmetin-7-glucoside	11	6.72
Oleuropein	12	41.15
Luteolin	13	-

It is clearly seen that, OLCE includes many phenolic compounds and those phenolic compounds have different character. In order to understand the behaviour of the clinoptilolite, 1mL of condensed crude extract was 5 times diluted with deionized water and contact with the clinoptilolite at 25 °C and 180 rpm. The solid-liquid ratio was 1/40. Figure 7.65 indicates the difference in HPLC chromatograms of OLCE after adsorption study.

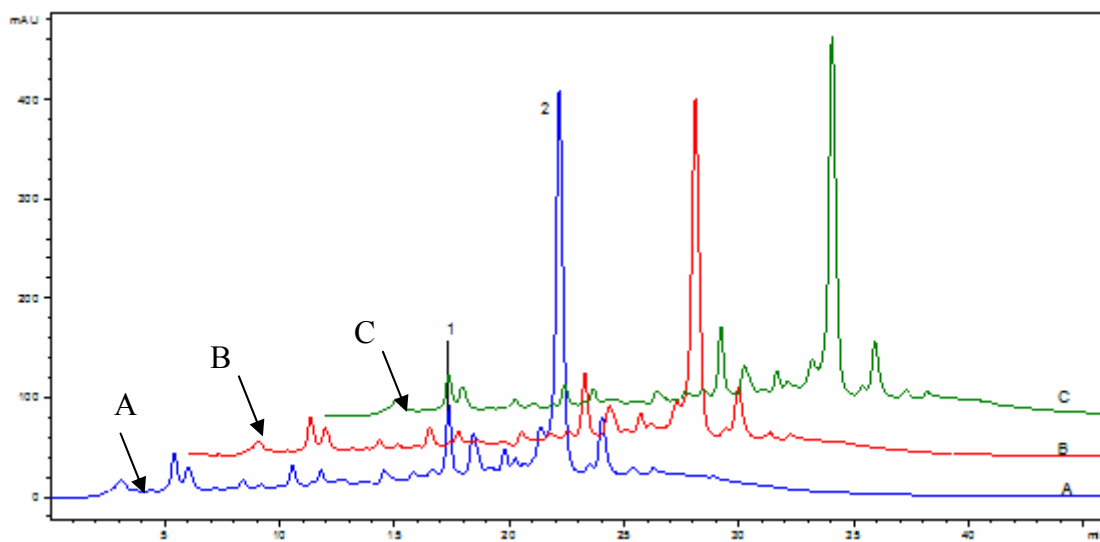


Figure 7.65. HPLC chromatograms of solution A: before adsorption, B: sample taken after 1 h during the adsorption study and C: sample taken after 5 h during the adsorption study.

There is a not clear difference between the HPLC chromatograms of the solutions. The main peaks belonging to the rutin (1) and oleuropein (2) do not change significantly. However, in order to see the differences in other phenolic compounds' peaks, magnified version of chromatograms should be drawn (Figure 7.66).

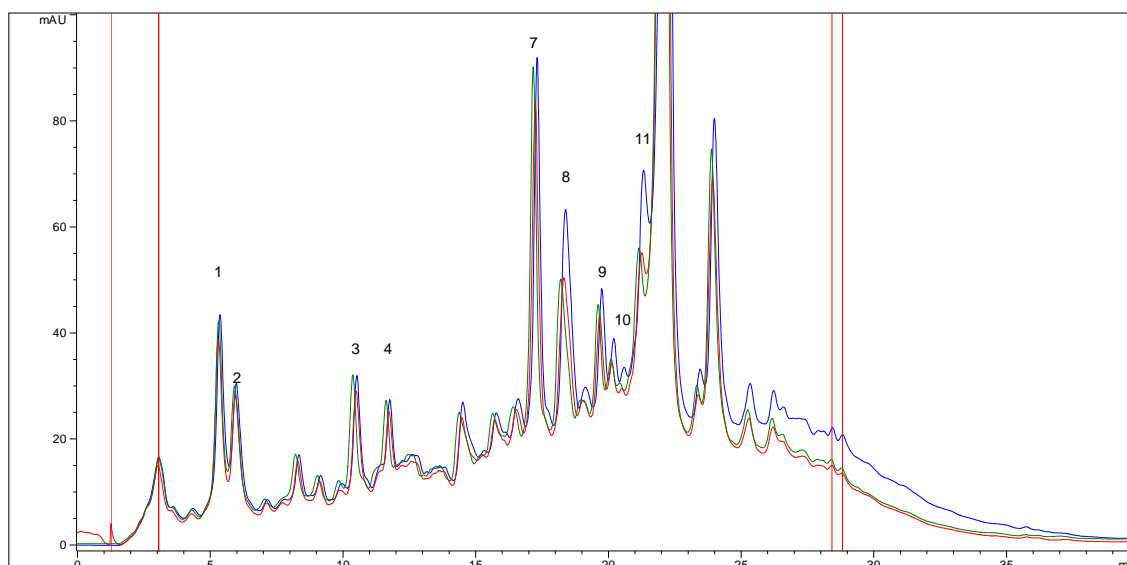


Figure 7.66. Overlaid HPLC chromatograms of OLCE solutions before and after adsorption study (blue: before adsorption, green and red: after adsorption).

Peaks 8, 10, 11, which are luteolin-7-glucoside, apigenin-7-glucoside and diosmetin-7-glucoside, respectively, have changed during the adsorption. Also, important changes in peaks are seen after the certain retention time (24 minutes). The common property of adsorbed fraction is to be glucoside forms of phenolic compounds.

To clarify the adsorption property of clinoptilolite, oleuropein free fraction obtained from desorption of extract on silk fibroin with 40 % ethanol was used. Ethanol was removed by rotary evaporator and solution was centrifuged at 5000 rpm for 5 min prior to the adsorption study. Most of the polyphenolic compounds were adsorbed on pure clinoptilolite (Figure 7.67). So, further adsorption studies were performed with oleuropein and rutin free fraction.

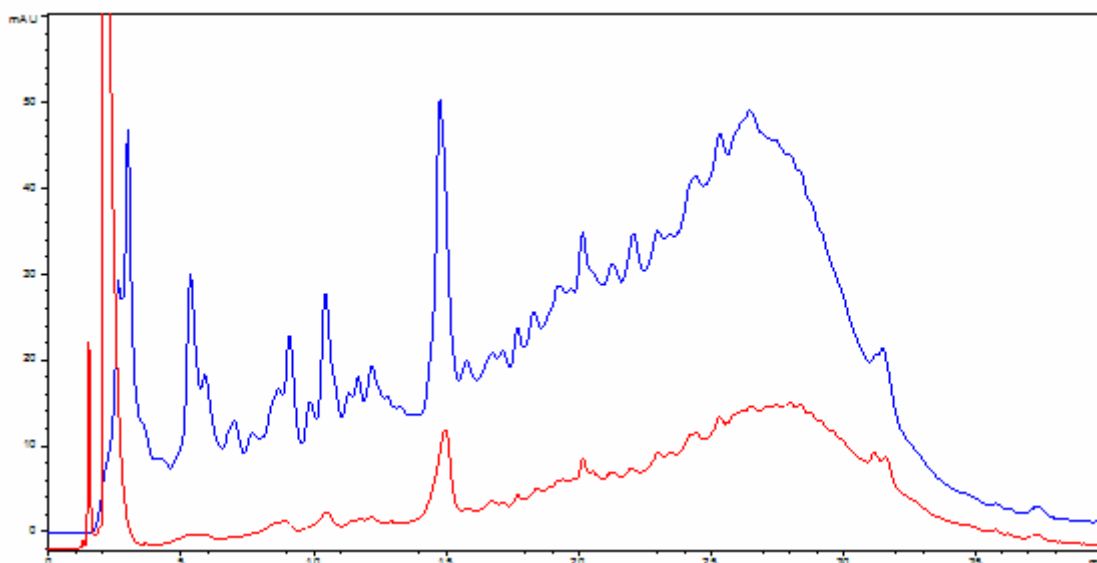


Figure 7.67. HPLC chromatograms of oleuropein and rutin free solutions: before (blue) and after (red) adsorption study performed with pure clinoptilolite (T: 25 °C, solid-liquid ratio: 1/40 and at 180 rpm).

Adsorption Kinetics

Rapid adsorption of OLCE was occurred by clinoptilolite (Figure 7.68). Equilibrium was achieved within 5 minutes. So, sampling times were shortened and another experiment was performed to see the adsorption kinetic within 10 minutes (Figure 7.69).

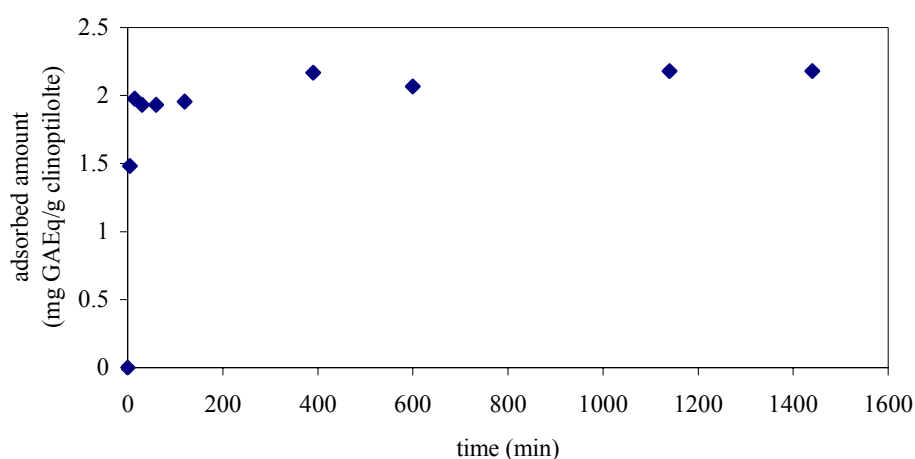


Figure 7.68. Adsorption kinetics of OLCE on purified clinoptilolite rich CL5 sample (<25 μ m). Ci: 0.205 mg GA Eq/mL .

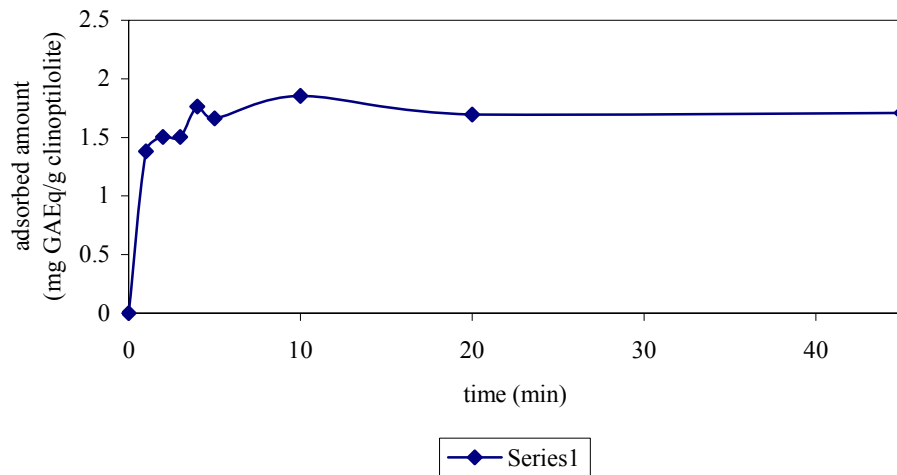


Figure 7.69. Adsorption kinetics of OLCE on purified clinoptilolite rich CL5 sample (<25 μm) within 10 minutes. Ci: 0.188 mg GA Eq/mL.

The effect of temperature on adsorption of OLCE on clinoptilolite was given in Figure 7.70.

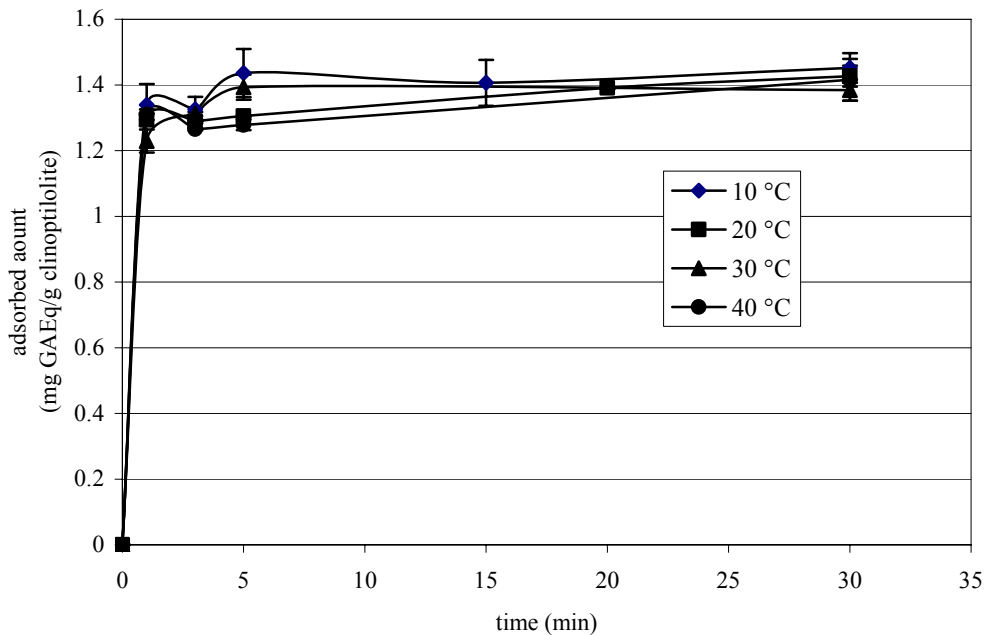


Figure 7.70. Effect of temperature on adsorption of OLCE on purified CL5 clinoptilolite (<25 μm). Ci: 0.079 mg GA Eq/mL.

A clear difference could not be seen between adsorption kinetics of clinoptilolite at these four temperatures. For this reason, to obtain adsorption isotherm, batch adsorption studies were performed at 25 °C. Samples were taken at against time in order

to prove that equilibrium concentrations. The change in concentration of the solution was given in Figure 7.71.

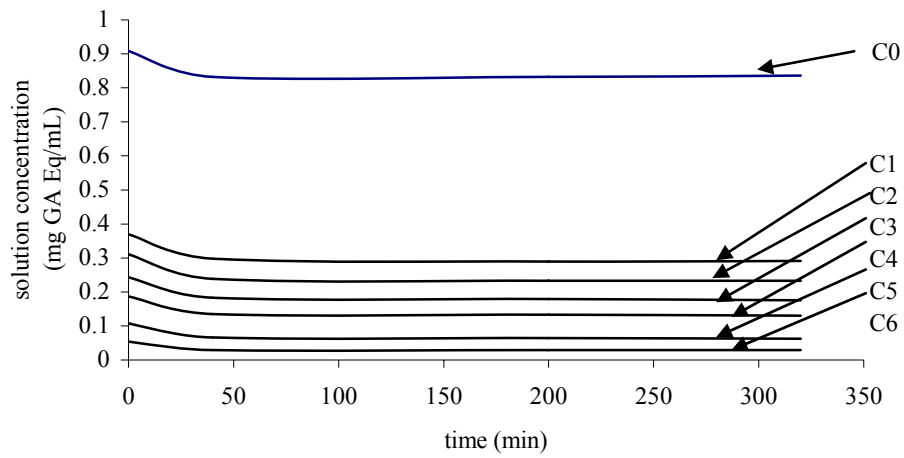


Figure 7.71. Solution concentration within 320 minutes.

Concentration of the solution did not change significantly, so equilibrium concentrations were used to obtain adsorption isotherm. Figure 7.72 also shows the HPLC chromatograms of the solution after reaching equilibrium.

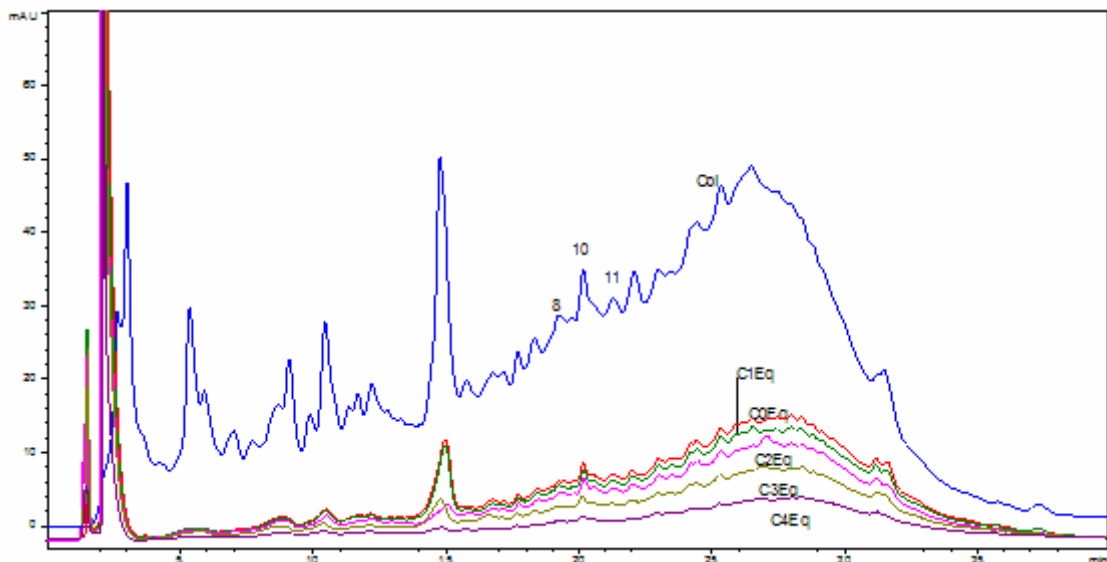


Figure 7.72. HPLC chromatograms of oleuropein and rutin free OLCE fraction; C_{0i} : chromatogram of selected initial C_0 concentration, the others are HPLC chromatograms for different initial concentration of solution (C_0 to C_4) after reaching equilibrium.

Adsorption isotherm of OLCE on clinoptilolite was given in Figure 7.73.

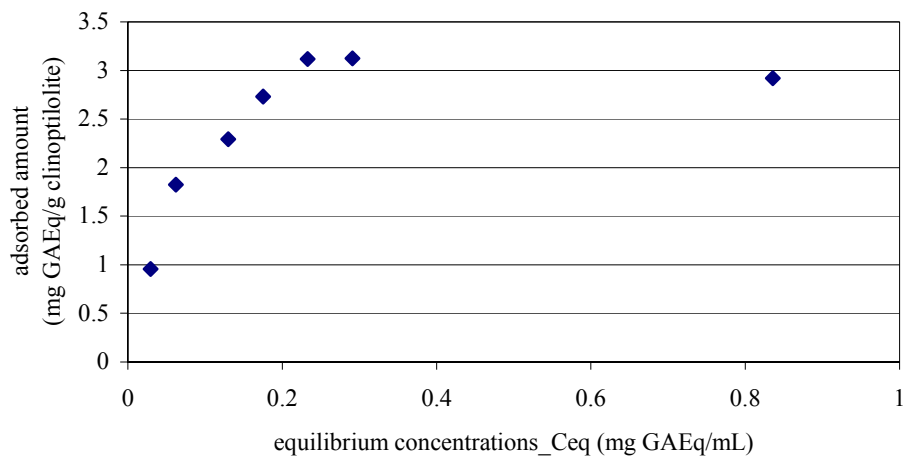


Figure 7.73. Adsorption behaviour of OLCE at different initial concentration.

Freundlich and Langmuir models were applied to explain the adsorption behaviour of the clinoptilolite.

Freundlich parameters; k_f and n were found as (Appendix D.2);

k_f : 6.41

n : 0.507

R^2 : 0.955

The Langmuir parameters were calculated by using the equation of the Langmuir model curve (Appendix D.2).

q_{max} : 3.99 mg GAEq OLCE/g clinoptilolite

k_L : 11.14 mg GAEq OLCE / mL

R^2 : 0.975

Langmuir model best fits the equilibrium data of the adsorption isotherm having a higher correlation coefficient than the Freundlich model. Maximum adsorption capacity was calculated as 3.99 mg GAEq OLCE/ g clinoptilolite by using the Langmuir equation which is very approximate to the experimental value.

The effect of particle size on adsorption of OLCE was studied. It is expected to increase adsorption capacity by decreasing the particle size. However, changing particle size yields different impurities of clinoptilolite sample. Purity of the clinoptilolite is another important parameter that could directly affect the adsorption of OLCE. Figure

7.74 shows the effect of particle size on adsorption capacity of OLCE. According to the XRD analysis, the purity of the clinoptilolite in samples was given just above the bars.

Purity of the clinoptilolite significantly affects the adsorption capacity of OLCE. It is clearly seen when compared the adsorption capacities of the clinoptilolite having a <25 μm particle size. Purified clinoptilolite adsorbed nearly 50% more OLCE polyphenols when compared with the not purified sample. Adsorbed amount of OLCE was increased by decreasing particle size and increasing purity of the sample except the adsorbent having a particle size 75-106 μm . It is very difficult to obtain homogeneous adsorbent including the similar framework and extraframework cations, and impurities. Thus, this behaviour can be explained by the inconsistent sorbent property.

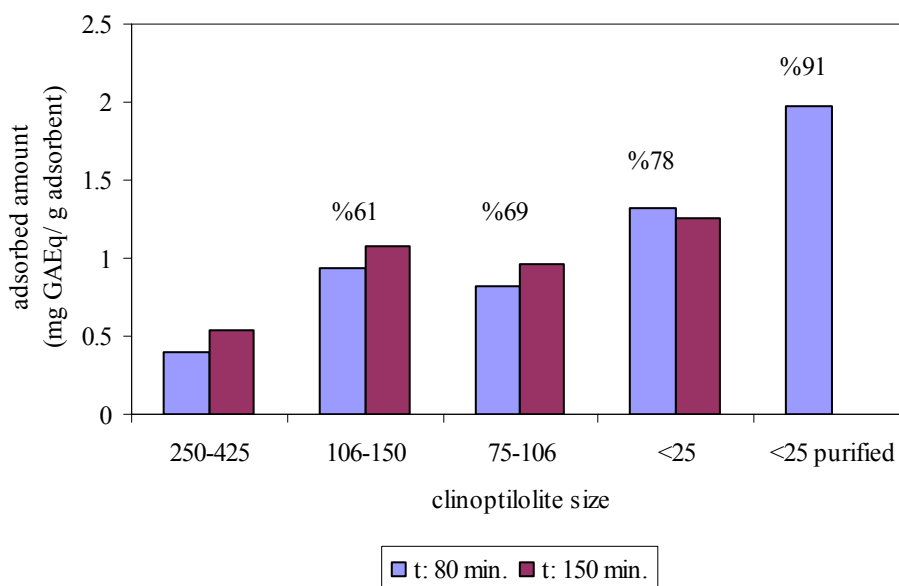


Figure 7.74. Effect of particle size on adsorption capacity of OLCE.

In order to determine the effect of particle size on adsorption by eliminating the effect of purity, clinoptilolite sample having a particle size within the range of 250-425 μm was grinded into three different sizes. Figure 7.75 shows that adsorbed amount was increased by decreasing the particle sizes.

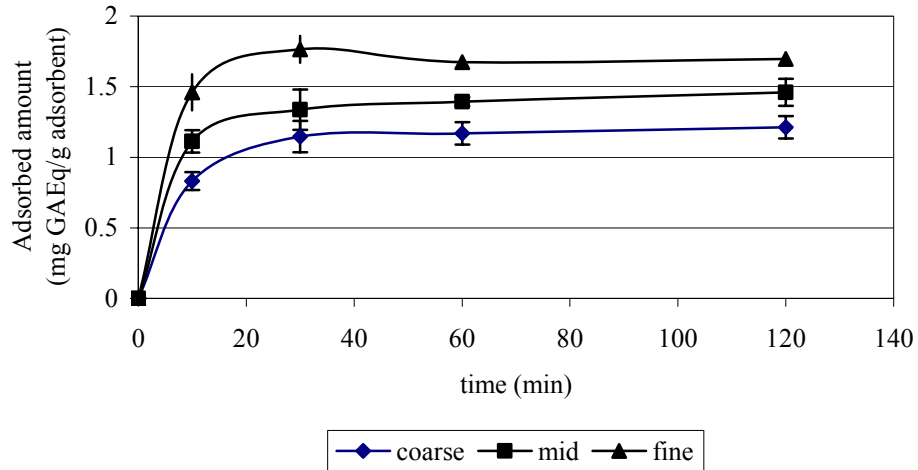


Figure 7.75. Effect of particle size on adsorption of oleuropein and rutin free OLCE fraction.

The effect of agitation on adsorption of OLCE was studied at three different shaking speeds. The sorption of OLCE fraction was so rapid that clear difference was not observed (Figure 7.76). Adsorbed amount of oleuropein and rutin free OLCE fraction was very close at equilibrium. However, at the initial period of sorption, adsorbed amount was lower at lower shaking speeds. This is because of the external film resistance at the initial period of sorption.

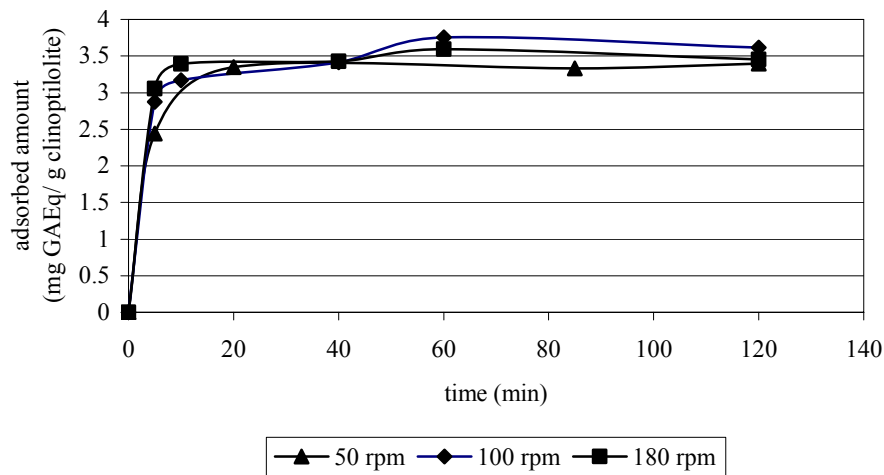


Figure 7.76. Effect of agitation on adsorption of oleuropein and rutin free OLCE fraction (T: 25 °C, C_i : 0.224 mg GA Eq/ mL of deionized water, solid-liquid ratio: 0.025).

7.4. Biological Activities

Antioxidant capacity, antimicrobial and cytotoxic effects of the crude extracts and isolated fractions were given in the following sections.

7.4.1. Antioxidant Capacity of crude extracts and fractions

Antioxidant capacities of crude extracts and isolated fractions were measured and compared with the rutin, oleuropein and *trans*-resveratrol standards. ABTS method was used to determine the antioxidant capacities of the extracts and the plots between the concentration versus % inhibition and time versus absorbance were given in Appendix E. Both of the crude extracts exhibit high antioxidant activities, which make them potent antioxidant source (Table 7.25). However, the importance of fractionation is clearly seen that, water fraction (rich in oleuropein and rutin) obtained from silk fibroin filled column has highest antioxidant capacity as 29.1 mg trolox/mg dry extract among the all fractions. This result is also supported by analyzing the standard compounds of rutin and oleuropein, which are high antioxidant capacity around 35 TEAC. Moreover, we can conclude that, after column separation of OLCE, high purity of oleuropein and rutin rich fraction was obtained, because its antioxidant activity is very close to the antioxidant activities of standards.

Table 7.25. Antioxidant capacities of polyphenolic compounds of standards and isolated fractions from crude extract

Standard Compounds	Antioxidant capacity_ TEAC value (mg trolox/ mg extract)
Rutin	35.23
Oleuropein	34.95
<i>Trans</i> -resveratrol	50.92
Fractions	
Olive leaf crude extract (OLCE)	7.91
Grape skin crude extract (GSCE)	7.29
Water fraction of OLCE (rich in oleuropein and rutin)	29.1
Ethanol fraction of OLCE (rich in glucosides)	5.85

7.4.2. Antimicrobial activities of crude extracts and fractions: MIC Values

Freeze dried grape skin extract obtained with the ultrasonic extraction method was dissolved in DMSO having a *trans*-resveratrol content as 0.510 mg/g dw. The results observed confirmed that most of the microorganisms were not inhibited effectively by the crude extract of grape skin. On the other hand, after selective separation of *trans*-resveratrol from the extract with a silk fibroin filled column, effective inhibition on both gram positive and gram negative bacteria were achieved. The MIC values of recovered *trans*-resveratrol are given in Table 7.26.

Table 7.26. MIC results for extract and isolated fractions

		MIC values (mg/mL)			
		Recovered <i>trans</i> -resveratrol	Grape skin extract	Olive Leaf Extract	
				Crude Extract	Water Fraction (Oleuropein and rutin rich fraction)
Microorganism	<i>E. coli</i>	3.125	not inhibited		
	<i>E. coli</i> (pathogen)	0.39	6.25	6.25	12.5
	<i>Salmonella</i>	0.39	3.125	6.25	12.5
	<i>L. monocytogenes</i>	0.39	not inhibited		
	<i>S. carnosus</i>	0.39	not inhibited		
	<i>S. aureus</i>	0.39	6.25	50	
	<i>L. plantarum</i>	0.39	not inhibited		

According to the results shown in Table 7.26, recovered *trans*-resveratrol from the grape skin extract exhibited inhibition against most of the microorganism with a low MIC values as 0.39 mg/mL except natural *E. coli*. High concentration of *trans*-resveratrol is required to inhibit natural *E. coli*. This property is very important, since natural *E. coli* is naturally found in human intestinal system.

On the other hand, MIC values of olive leaf crude extract were found 6.25 mg/mL for *E. coli* and *Salmonella*. Although, water fraction of OLCE exhibits high

antioxidant activity, 12.5 mg/mL of concentration is required to achieve same inhibition on these microorganisms. Polyphenols may show synergistic activity and in olive leaf crude extract, probably synergistic effect was effective against those microorganisms, because of the lower MIC value.

7.4.3. Cytotoxic Activity

It is important to determine the cytotoxic activities of crude extracts on cancer cell lines. MCF 7 and PC3 cell lines were used in order to determine cytotoxic activities olive leaf extract and grape skin extract. Furthermore, after the fractionation, fractions were analyzed to determine the activity of isolated compounds.

Crude extracts did not inhibit cancer cells. However, isolated of active compound exhibit significant effects on both cancer cells (Figure 7.77).

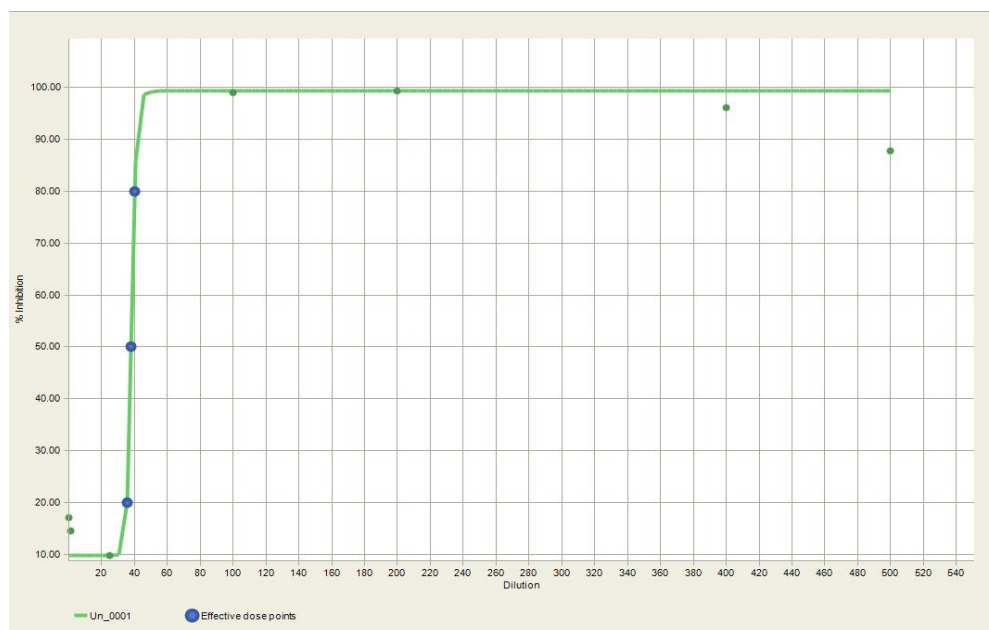


Figure 7.77. Sample graph for determination of IC50 values of purified *trans*-resveratrol against MCF7 cell line.

Table 7.27 indicates that recovered *trans*-resveratrol effectively inhibits both PC3 and MCF7 cancer cell lines with a small dose. This result exhibits the importance of the purification processes. On the other hand, although olive leaf crude extract did

not show any inhibition activity, isolated ethanol fraction, which mainly include verbascoside, luteolein and glucosides, showed inhibition on only PC3 cell lines.

Table 7.27. IC50 values of crude extracts and isolated fractions

		IC50 values ($\mu\text{g}/\text{mL}$)			
		Recovered <i>trans-resveratrol</i>	Grape skin crude extract	Olive Leaf Extract	
				Crude Extract	Ethanol Fraction
Cell line	<u>PC3</u>				
	<i>24 hours</i>	37.81	-	-	179.77
	<i>48 hours</i>	27.68	-	-	178.05
	<u>MCF7</u>				
	<i>24 hours</i>	34.85	-	-	-
	<i>48 hours</i>	31.41	-	-	-

CHAPTER 8

CONCLUSIONS

Grape pomace and olive leaves are the potential source for bioactive flavonoid compounds, which have favorable properties such as, antioxidant, antimicrobial activities and cytotoxic effects. Selective recovery of these valuable substances from the by-product of the agro-industries in Turkey is very important; in order to produce high value added products.

Grape skin is the potential source for *trans*-resveratrol, which is one of the important phytochemicals. For this purpose extraction studies were performed and highest *trans*-resveratrol yield was obtained as 0.201 mg/g dw, by ultrasonic extraction method. Because of the significant cytotoxic activity of *trans*-resveratrol, recovery of it from the crude extract of grape skin is very important. For this purpose, the adsorption behaviours of silk fibroin and clinoptilolite on *trans*-resveratrol were observed. Analytical grade pure *trans*-resveratrol, 51.5% pure polyganum cuspaditum's *trans*-resveratrol and crude grape skin extract were used in batch adsorption studies to investigate the effect of adsorbent property on sorption kinetics and capacity. Although, high sorption capacity of silk fibroin (45 mg *trans*-resveratrol/g silk fibroin), cost of the adsorbent should be considered. Since clinoptilolite is abundant in Turkey, adsorption of *trans*-resveratrol onto clinoptilolite would be feasible even having a low adsorption capacity (2.49 mg *trans*-resveratrol/g clinoptilolite). The modified form of clinoptilolite may be used for higher adsorption capacity of *trans*-resveratrol. The results of kinetic studies indicate that sorption of *trans*-resveratrol onto clinoptilolite was particle controlled mechanism and intraparticle diffusion controls the sorption process. Adsorption almost completed within three hours, which was very fast. The purity of clinoptilolite had significant effect on the sorption kinetics and capacity. Around 14% increment in the adsorption capacity was observed in the case of using the clinoptilolite rich CL5 sample (91% purity). Clear differences could not be detected between the adsorption capacities of both of the adsorbents by changing the solution temperature. However, since the mechanism of adsorption of *trans*-resveratrol on

adsorbents was physisorption, low activation energy was enough for the mobility of the molecule on the surface of the adsorbent.

Oleuropein and rutin are the main polyphenolic compounds of olive leaf, and around 13% oleuropein and 0.2% rutin containing olive leaf extract was obtained with solid-liquid extraction method at optimized extraction parameters. It was found that silk fibroin can be used as a potential adsorbent for the recovery of polyphenols from crude extract. Rutin and oleuropein were effectively adsorbed by silk fibroin with a 15 and 96 mg/g adsorption capacity, respectively. We explored that; clinoptilolite rich natural zeolite selectively adsorbed the glycosidic form of luteolein, apigenin and diosmetin and virgin clinoptilolite rich mineral (61%) and purified form of it (91%) was used for this purposes.

Column separation of olive leaf and grape skin polyphenolic compounds were performed with a silk fibroin filled column. The selective separation of *trans*-resveratrol from the mixture of polyphenolic standards solution was tried to be performed and high purity of *trans*-resveratrol was also isolated from the column. Because of the selective adsorption property of silk fibroin, dynamic column studies were performed with silk fibroin filled syringe column. The effects of inlet concentration, flow rate and amount of adsorbent were investigated by evaluating the breakthrough curves obtained for *trans*-resveratrol. Oleuropein was eluted from the silk fibroin filled column with a high purity. At the same time, fraction rich in rutin, luteolein-7-glucoside, verbascoside, apigenin-7-glucoside was obtained.

In order to exhibit the effectiveness of the separation process, the biological activities of separated fractions_ antimicrobial activity, antioxidant activity and cytotoxic activities_ were studied. High amount of crude extracts were required to inhibit the pathogenic microorganisms. However, significant inhibition effects were achieved with the very low concentrations of the isolated fractions. Crude extracts did not inhibit cancer cells. We found that *trans*-resveratrol effectively inhibits both PC3 and MCF7 cancer cell lines with a small dose. On the other hand, although olive leaf crude extract did not show any inhibition activity, isolated ethanol fraction, which mainly include verbocroside, luteolein and glucosides, showed inhibition on only PC3 cell lines.

REFERENCES

- Abdullah, M.A.; Chiang, L.; Nadeem, M. Comparative Evaluation of Adsorption Kinetics and Isotherms of a Natural Product Removal By Amberlite Polymeric Adsorbent. *Chemical Engineering Journal*. **2007**, 146, 370-376.
- Aggarwal, B.B.; Bhardwaj, A.; Aggarwal, R.S.; Seram, N.P.; Shishodia, S.; Takada, Y. Role of Resveratrol in Prevention and Therapy of Cancer: Preclinical and Clinical Studies. *Anticancer Research*. **2004**, 24, 21-38.
- Aksu, Z.; Gönen, F. Biosorption of Phenol by Immobilized Activated Sludge in a Continuous Packed Bed: Prediction of Breakthrough Curves. *Process Biochemistry*. **2004**, 39, 599-613.
- Al-Ghouti, M.A.; Khraisheh, M.A.M.; Ahmad, M.M.; Allen, S. Adsorption Behaviour of Methylene Blue onto Jordanian Diatomite: A Kinetic Study. *Journal of Hazardous Materials*, **2009**, 165, 589-598.
- Allen, S.J.; Ivanova, E.; Koumanova B. Adsorption of sulfur dioxide on chemically modified natural clinoptilolite. Acid modification. *Chemical Engineering Journals*, **2009**, 152, 389-395.
- Altıok, E. Production of Grape Seed Proanthocyanidins, Izmir Institute of Technology, Izmir, Turkey, 2003.
- Altıok, E.; Bayçın, D.; Bayraktar, O.; Ülkü, S. Isolation of Polyphenols from the Extracts of Olive Leaves (*Olea Europaea L.*) by Adsorption on Silk Fibroin. *Separation and Purification Technology*, **2008**, 62, 342-348.
- Altıok, E.; Ülkü, S.; Bayraktar, O. Recovery of Proanthocyanidin from Waste of Turkish Traditional Product, Pekmez (Molasses). *Food Science and Technology Research*, **2007**, 13, 321-326.
- Andreadou, I.; Iliodromitis, E.K.; Mikros, E.; Constantinou, M.; Agalias, A.; Magiatis, P.; Skaltsounis, A.L.; Kamber, E.; Tsantili, A.; Kremastinos, D. The Olive Constituent Oleuropein Exhibits Anti-Ischemic, Antioxidative, and Hypolipidemic Effects in Anesthetized Rabbits, *Journal of Nutrition*, **2006**, 136, 2213-2219.
- Auerbach, S.M.; Carrado, K.A.; Dutta, P.K. *Handbook of Zeolite Science and Technology*, Section 22, Marcell Dekker Inc., New York, 2003.

- Balasundram, N.; Sundram, K.; Saman, S., Phenolic Compounds in Plants and Agri-industrial by-Products: Antioxidant Activity, Occurrence, and Potential Uses. *Food Chemistry*, **2006**, 99, 191-203.
- Bao, J.; Zhang, D.W.; Zhang, J.Z.H.; Huang, P.L.; Huang, P.L.; Lee-Huang, S. Computational Study of Bindings of Olive Leaf Extract (OLE) to HIV-1 Fusion Protein gp41, *FEBS Letters*, **2007**, 58, 2737-2742.
- Bayçın, D. Adsorption of Olive Leaf antioxidants on Silk Fibroin, Izmir Institute of Technology, İzmir, Turkey, 2006.
- Baycin, D.; Altıok, E.; Ülkü, S.; Bayraktar, O. Adsorption of Olive leaf (*Olea europea* L.) Antioxidants on Silk Fibroin. *Journal of Agriculture and Food Chemistry*, **2007**, 55, 1227-1236.
- Bagchi, D.; Bagchi, M.; Stohs, S. J.; Das, D. K.; Ray, S. D.; Kuszynski, C. A.; Joshi, S. S.; Pruess, H.G. Free Radicals and Grape Seed Proanthocyanidin Extract: Importance in Human Health and Disease Prevention. *Toxicology*, **2000**, 148, 187-197.
- Benavente-Garcia, O.; Castillo, J.; Lorente, J.; Ortuno, A.; Del Rio, J.A. Antioxidant Activity of Phenolics Extracted from *Olea europaea* L. Leaves. *Food Chemistry*, **2000**, 68(4), 457-462.
- Bonora, M.; Brustolon, M.; Storaro, L.; Casagrande, M.; Biglino, D.; Itagaki, Y.; Segre, U.; Lenarda, M. EPR of Trans-Stilbene Radical Cations Formed in Zeolite Cavities: A New Approach to Study the Zeolite Void Space. *Physical Chemistry Chemical Physics*, **2000**, 2, 4823-4828.
- Bouhamidi, R.; Prevost, V.; Nouvelot, A. High Protection by Grape Seed Proanthocyanidins (GSPC) of Polyunsaturated Fatty Acids against UV-C Induced Peroxidation. *Plant Biology and Pathology*, **1998**, 321, 31-38.
- Breck, D.W. *Zeolite Molecular Sieves Structure, Chemistry and Use*, Wiley-Interscience, New York, 1974.
- Bretag, J.; Kammerer, D.R.; Jensen, U.; Carle, R. Adsorption of Rutin onto a Food Grade Styrene-Divinylbenzene Copolymer in a Model System. *Food Chemistry*, **2009**, 114, 151-160.

- Briante, R.; Patumi, M.; Terenziani, S.; Bismuto, E.; Febbraio, F.; Nucci, R. Olea Europaea L. Leaf Extract and Derivatives: Antioxidant Properties. *Journal of Agricultural and Food Chemistry*, **2002**, 14, 4934-4940.
- Careri, M.; Corradini, C.; Elviri, L.; Nicoletti, I.; Zagnoni, I. Direct HPLC Analysis of Quercetin and Trans-Resveratrol in Red Wine, Grape, and Winemaking Products. *Journal of Agricultural and Food Chemistry*, **2003**, 51, 5226-5231.
- Calzarano, F.; Agostino, V.; Carlo, M. Trans-Resveratrol Extraction from Grapevine: Application to Berries and Leaves from Vines Affected by Esca Proper. *Analytical Letters*, **2008**, 41(4), 649-661.
- Campeol, E.; Flamini, G.; Cioni, P.L.; Morelli, I.; Cremonini, R.; Ceccarini, L. Volatile Fractions from Three Cultivars of *Olea europea* L. Collected in Two Different Seasons. *Journal of Agricultural and Food Chemistry*, **2003**, 51, 1994-1999.
- Chafer, A.; Pascual-Marti, M.C.; Salvador, A.; Berna, A. Supercritical Fluid Extraction and HPLC Determination of Relevant Polyphenolic Compounds in Grape Skin. *Journal of Separation Science*, **2005**, 28, 2050-2056.
- Cho, Y.J.; Hong, J.Y.; Chun, H.S.; Lee, S.K.; Min, H.Y. Ultrasonic-Assisted Extraction of Resveratrol from Grapes. *Journal of Food Engineering*, **2006**, 77, 725-730.
- Choi, J.W.; Yoo, D.; Lee, W.H.; Pedersen, H. Selective Adsorption of Plant Metabolite on Encapsulated Adsorbent: Local Thermodynamic Equilibrium Model. *Journal of Fermentation and Bioengineering*, **1996**, 81, 47-54.
- Chukwumah, Y.C.; Walker, L.T.; Verghese, M.; Ogutu, S. Effect of Frequency and Duration of Ultrasonication on the Extraction Efficiency of Selected Isoflavones and Trans-Resveratrol from Peanuts. *Ultrasonic Sonochemistry*, **2009**, 16, 293-299.
- Collins, A.R. Antioxidant Intervention as a Route to Cancer Prevention. *European Journal of Cancer*, **2005**, 41, 1923-1930.
- Dang, J.Z.; Zhang, X.S.; Huang, X.Y.; Feng, L.X. Study on the Enrichment of Oleuropein from *Olea Europaea* Leaves with Macroporous Resin D-101. *Zhong Yao Cai*, **2007**, 30, 454-457.

- Di Mauro, A.; Fallico, B.; Passerini, A.; Rapisarda, P.; Maccarone, E. Recovery of Hesperidin from Orange Peel by Concentration of Extracts on Styrene-Divinyl Benzene Resin. *Journal of Agricultural and Food Chemistry*, **1999**, 47, 4391-4397.
- Diaz-Reinoso, B.; Lopez, N.G.; Moure, A.; Dominguez, H.; Parajo, J.C. Recovery of Antioxidants from Industrial Waste Liquors Using Membranes and Polymeric Resin. *Journal of Food Engineering*, **2010**, 96, 127-133.
- Du, F.Y.; Xiao, X.H., Li, G.K. Application of Ionic Liquids in the Microwave-Assisted Extraction of Trans-Resveratrol from Rhizma Polygoni Cuspaditi. *Journal of Chromatography A*, **2007**, 1140, 56-62.
- Eidi, A.; Eidi, M.; Darzi, R. Antidiabetic Effect of Olea Europaea L. in Normal and Diabetic Rats, *Phytotherapy Research*, **2009**, 23, 347-350.
- Erkoc, S.; Keskin, N.; Erkoc, F. Resveratrol and its Analogues Resveratrol-Dihydroxyl Isomers: Semi Empirical SCF-MO Calculations, *Journal of molecular structure: THEOCHEM*, **2003**, 63, 67-73.
- Fu, Y.; Zu, Y.; Liu, W.; Efferth, T.; Zhang, N.; Liu, X.; Kong, Y. Optimization of Luteolin Separation from Pigeonpea [Cajanus Cajan (L.) Millsp.] Leaves by Macroporous Resins. *Journal of Chromatography A*, **2006**, 1137, 145-152.
- Fu, Y.; Zu, Y.; Liu, W.; Hou, C.; Chen, L.; Li, S.; Shi, X.; Tong, M. Preparative Separation of Vitexin and Isovitexin from Pigeonpea Extracts with Macroporous Resins. *Journal of Chromatography A*, **2007**, 1139, 206-213.
- Garcia, O.B.; Castillo, J.; Lorente, J.; Ortuno, A.; Del Rio, J.A. Antioxidant Activity of Phenolics Extracted from Olea Europaea L. Leaves. *Food Chemistry*, **2000**, 68, 457-462.
- Geankoplis, C.J. *Transport Processes and Unit Operations*, Prantice Hall, 1993.
- Göktaş, S.; Ülkü, S.; Bayraktar, O. Clinoptilolite Rich Mineral as a Novel Carrier for the Active Constituents Present in Ginkgo Biloba Leaf Extract. *Applied Clay Science*, **2007**, 40, 6-14.

- Hafizuddin, W.M.; Yussof, W.; Sarmidi, M.R. Equilibrium and Kinetic Modelling of the Adsorption of Steoviside on Amberlite XAD-7 Beads. *Proceeding of International Conference on Chemical and Bioprocess Engineering*, University of Malaysia., **2003**, 103-110.
- Ho, Y.S.; Ng, J.C.Y.; McKay, G. Kinetics of Pollutants Sorption by Biosorbent: Review. *Separation and Purification Methods*, **2000**, 29, 189-232.
- Ho, Y.S.; McKay G. Sorption of Dye from Aqueous Solution by Peat. *Chemical Engineering Journal*, **1998**, 70, 115-124.
- Ingram, L.; Buttke, T.M. Effects of Alcohols on Microorganisms. *Advances in Microbial Physiology*, **1984**, 25, 253-300.
- Jang, M.; Cai, L.; Udeani, G.O.; Slowing, K.V.; Thomas, C.F.; Beecher, C.W.W.; Fong, H.H.S.; Farnsworth, N.R.; Kinghorn, A.D.; Mehta, R.G.; Moon, R.C.; Pezzuto, J.M. Cancer Chemopreventive Activity of Resveratrol, a Natural Product Derived from Grapes. *Science*, **1997**, 275, 218-238.
- Joshi, M.S.; Hoshi, A.L.; Choudhari, A.L.; Kasture, M.W. Structural Studies of Natural Heulandite using Infrared Spectroscopy. *Materials Chemistry and Physics*, **1997**, 48, 160-163.
- Kammerer, D.R.; Saleh, Z.S.; Carle, R. Stanley, R.A. Adsorptive Recovery of Phenolic Compounds from Apple Juice. *European Food Research and Technology*, **2007**, 224(5), 605-631.
- Karacabey, E.; Mazza, G. Optimization of Solid-Liquid Extraction of Resveratrol and Other Phenolic Compounds from Milled Grape Canes. *Journal of Agricultural and Food Chemistry*, **2008**, 56, 6318-6325.
- Kaur, G.; Singh, R.P. Antibacterial and Membrane Damaging Activity of Livistona Chinensis Fruit Extract. *Food and Chemical Toxicology*, **2008**, 46, 2429-2434.
- Kim, M.R.; Kim, W.C.; Lee, D.Y; Kim, C.W. Recovery of Narirutin by Adsorption on a Non-Ionic Polar Resin from a Water-Extract of *Citrus Unshiu* Peels. *Journal of Food Engineering*, **2007**, 78, 27-32.

- Kim, T.J.; Kim, J.H.; Jin, Y.R.; Yun, Y.P. The Inhibitory Effect and Mechanism of Luteolin 7-Glucoside on Rat Aortic Vascular Smooth Muscle Cell Proliferation. *Archives of Pharmacal Research*, **2006**, 29, 67-72.
- Kim, S.; Fung, D.Y.C. Antimicrobial Effect of Crude Water Soluble Arrowroot (Puerariae Radix) Tea Extracts on Food-Borne Pathogens in Liquid Medium, *Letters in Applied Microbiology*, **2004**, 39, 319-325.
- Krings, U.; Kelch, M.; Berger, R.G. Adsorbents for the Recovery of Aroma Compounds in Fermentation Process. *Journal of Chemical Technology and Biotechnology*, **2007**, 58, 293-299.
- Kurata, H.; Kawai, A.; Seki, M.; Furusaki, S. Increased Alkaloid Production in a Suspension Culture of Coffea Arabica Cells Using an Adsorption Column for Product Removal. *Journal of Fermentation and Bioengineering*, **1994**, 78, 117-119.
- Lacopini, P.; Baldi, M.; Storchi, P.; Sebastiani, L. Catechin, Epicatechin, Quercetin, Rutin and Resveratrol in Red Grape: Content, In Vitro Antioxidant Activity and Interactions. *Journal of Food Composition and Analysis*, **2008**, 21, 589-598.
- Lee, O.H.; Lee, B.Y.; Lee, J.; Lee, H.B.; Son, J.Y.; Parks, C.S.; Kim, Y.C. Assessment of Phenolics-Enriched Extract and Fractions of Olive Leaves and Their Antioxidant Activities. *Bioresource Technology*, **2009**, 100, 6107-6113.
- Lee-Huang, S.; Huang, P.L.; Zhang, D.; Lee, J.W.; Bao, J.; Sun, Y.; Chang, Y.T.; Zhang, J.Z.H.; Huang, P.L. Discovery of Small-Molecule HIV-1 Fusion and Integrase Inhibitors Oleuropein and Hydroxytyrosol: Part I. Integrase Inhibition. *Biochemical and Biophysical Research Communications*, **2007**, 354, 872-878.
- Liazid, A.; Palma, M.; Briqui, J.; Barroso, C.G. Investigation on Phenolic Compounds Stability During Microwave-Assisted Extraction. *Journal of Chromatography A*, **2007**, 1140, 29-34.
- Li, P.; Wang, Y.; Runyu, M.; Zhang, X. Separation of Tea Polyphenol from Green Tea Leaves by a Combined CATUFM-Adsorption Resin Process. *Journal of Food Engineering*, **2005**, 67(3), 253-260.
- Lin R.; Barney, H.W. Purification of Commercial Grape Pigment. *Journal of Food Science*, **2006**, 45, 297-306.

- Llorach, R.; Espin, J.C.; Tomas-Barberan, F.A.; Ferreres, F. Valorization of Cauliflower (*Brassica Oleracea* L. Var. *Botrytis*) By-Products as a Source of Antioxidant Phenolics. *Journal of Agricultural and Food Chemistry*, **2003**, 51, 2181-2187.
- Lu, R.; Serrero, G. Resveratrol, A Natural Product Derived from Grape, Exhibits Antiestrogenic Activity, and Inhibits the Growth of Human Breast Cancer Cells. *Journal of Cellular Physiology*, **1999**, 179, 297-304.
- Madhavi, D.L.; Despande, S.S.; Salunkhe, D.K. Food Antioxidants Technological, Toxicological, and Health Perspectives, Marcel Dekker Inc., New York, **1996**, pg. 65- 97.
- Maiti, A.; Sharma, H.; Basu J.K.; De, S. Modeling of Arsenic Adsorption Kinetics of Synthetic and Contaminated Groundwater on Natural Laterite. *Journal of Hazardous Material*, **2009**, 172, 928-934.
- Malay, Ö.; Bayraktar, O.; Batigün, A. Complex Coaservation of Silk Fibroin and Hyaluronic Acid. *International Journal of Biological Macromolecules*, **2007**, 40, 387-393.
- Mauro, A.D.; Fallico, B.; Passerini, A.; Rapisarda, P.; Maccarone, E. Recovery of Hesperidin from Orange Peel by Concentration of Extract on Styrene-Divinylbenzene Resin. *Journal of Agricultural and Food Chemistry*, **1999**, 47, 4391-4397.
- Meireles, M.A.A. Extracting Bioactive Compounds for Food Products: Theory and Applications. Taylor & Francis Group, USA, 2009, 137-151.
- Mgbonyebi, O.P.; Russo, J.; Russo, I.H. Antiproliferative Effect of Synthetic Resveratrol on Human Breast Epithelial Cells. *International Journal of Oncology*, **1998**, 12, 865-874.
- Moure, A.; Cruz, J.M.; Franco, D.; Dominguez, J.M.; Sinerio, J.; Dominguez, H.; Nunez, M.J.; Prajo, J.C. Natural Antioxidants from Residual Sources. *Food Chemistry*, **2001**, 72, 145-171.
- Mylokani, S.; Kiassos, E.; Makris, D.P.; Kefelas, P. Optimization of the Extraction of Olive (*Olea Europaea*) Leaf Phenolics Using Ethanol/Water- Based Solvent Systems and Response Surface Methodology. *Analytical and Bioanalytical Chemistry*, **2008**, 392, 977-985.

- Moscou, L. The Zeolite Scene., Introduction to Zeolite Science and Practice, van Bekkum, H., Flenigen, E. M., Jansen, J. C., Elsevier, Amsterdam, (1991), pp. 1-11.
- Nakamura, T.; Ishikawa, M.; Hiraiwa, T.; Sato, J. X-Ray Diffractometric Determination of Clinoptilolite in Zeolite Tuff Using Multiple analytical Lines. *Analytical Sciences*, **1992**, 8,539-543.
- Nam, J.B.; Ryu, J.H.; Kim, J.W.; Chang, I.S.; Suh, K.D. Stabilization of Trans-Resveratrol Immobilized in Monodisperse Cyano-Functionalized Porous Polymeric Microspheres. *Polymer*, **2005**, 46, 8956-8963.
- Oppico, E.; Varenio, C.; Rosa, O.G. Process for Purifying Anthracyclinone Glycosides by Selective Adsorption on Resins. U.S. Patent 4861870, 1989.
- Ozkan-Cakicioglu, F.; Ulku, S. The Effect of HCl Treatment on Water Vapor Adsorption Characteristics of Clinoptilolite Rich natural Zeolite. *Microporous and Mesoporous Materials*, **2005**, 77, 47-53.
- Paiva-Martins, F.; Gordon, M.H.; Gameiro, P. Activity and Location of Olive Oil Phenolic Antioxidants in Liposomes. *Chemistry and Physics of Lipids*, **2003**, 124, 23-36.
- Patil, S.C.; Singh, V.P.; Satyanarayan, P.S.V.; Jain, N.K.; Singh, A.; Kulkarni, S.K. Protective Effect of Flavonoids against Aging- and Lipopolysaccharide-Induced Cognitive Impairment in Mice. *Pharmacology*, **2003**, 69, 59-67.
- Pavelic, K.; Hadzija, M.; Bedrica, L.; Pavelic, J.; Dikic, I.; Katic, M.; Kralj, M.; Bosnar, M.H.; Kapitanovic, S.; Krizanac, S.; Stojkovic, R.; Jurin, M.; Subotic, B.; Colic, M. Natural Zeolite Clinoptilolite: New Adjuvant in Anticancer Therapy. *Journal of Molecular Medicine*, **2001**, 78, 708-720.
- Perez, A.I.R.; Raventos, R.M.L.; Lacueva, C.A.; Torre-Boronat, M.C. Method for the Quantitative Extraction of Resveratrol and Piceid Isomers in Grape Berry Skins: Effect of Powdery Mildew on the Stilbene Content. *Journal of Agricultural and Food Chemistry*, **2001**, 49, 210-215.
- Perrinjaquet-Moccetti, T.; Busjhan, A.; Schmidlin, C.; Schmit, A.; Bradl, B.; Aydogan, C. Food Supplementation with an Olive (*Olea Europaea* L.) Leaf Extract Reduces Blood Pressure in Borderline Hypertensive Monozygotic Twins. *Phytotherapy. Research*, **2008**, 22, 1239-1242.

- Pervaiz, S. Chemotherapeutic Potential of the Chemopreventive Phytoalexin Resveratrol. *Drug Resistance Update*, **2004**, 7, 333-344.
- Pinelo, M.; Arnous, A.; Meyer, A.S. Upgrading of Grape Skins: Significance of Plant Cell-Wall Structural Components and Extraction Techniques for Phenol Release. *Trends in Food science and Technology*, **2006**, 17, 579-590.
- Pineiro, Z.; Palma, M.; Barroso, C.G. Determination of Trans-Resveratrol in Grapes by Pressurised Liquid Extraction and Fast High Performance Liquid Chromatography. *Journal of Chromatography A*, **2006**, 1110, 61-65.
- Polatoglu, I; Ozkan-Cakicioglu, F. aqueous Interactions of Zeolitic Material in Acidic and Basic Solutions. *Microporous and Mesoporous Materials*, **2010**, 132, 219-225.
- Pretorius, J.C. Flavonoids: A Review of Its Commercial Application Potential as Anti-Infective Agents. *Current Medicinal Chemistry-Anti Infective Agents*, **2003**, 2, 335-353.
- Rayne, S.; Karacabey, E.; Mazza, G. Grape Cane Waste as a Source of Trans-Resveratrol and Trans-Viniferin: High-Value Phytochemicals with Medicinal and Anti-Phytopathogenic Applications. *Industrial Crops and Products*, **2008**, 27(3), 335-340.
- Riberio, M.H.L.; Silveria, D.; Dias, S.F. Selective Adsorption of Limonine and Naringin from Orange Juice to Natural and Synthetic Adsorbents. *European Food Research and Technology*, **2002**, 215, 462-471.
- Rivera, A.; Farias, T. Clinoptilolite-Surfactant Composites as Drug Support: A New Potential Application. *Microporous and Mesoporous Materials*, **2003**, 80, 337-346.
- Rivera, A.; Farrias, T.; Ruiz-Salvador, A.R.; Menorval, L.C. Preliminary Characterization of Drug Support Systems Based on Natural Clinoptilolite. *Microporous and Mesoporous Materials*, **2003**, 61, 249-259.
- Romero-Perez, A.I.; Lamuela, R.M.; Andres, C.; Torre, M.C. Method for the Quantitative Extraction of Resveratrol and Piceid Isomers in Grape Berry Skins: Effect of Powdery Mildew on the Stilbene Content. *Journal of Agricultural and Food Chemistry*, **2001**, 49, 210-215.

- Ruthven, D.M. *Principles of Adsorption and Adsorption Processes*. Wiley-Interscience, New York, 1984.
- Ryan, D.; Lawrence, H.; Prenzler, P.D.; Antolovich, M.; Robards, K. Recovery of Phenolic Compounds from *Olea Europaea*. *Analytica Chimica Acta*, **2001**, 445, 67-77.
- Savournin, C.; Baghdikian, B.; Elias, R.; Dargouth-Kesraoui, F.; Boukef, K.; Balansard, G. J. Rapid High-Performance Liquid Chromatography Analysis for the Quantitative Determination of Oleuropein in *Olea europaea* Leaves. *Journal of Agricultural and Food Chemistry*, **2001**, 49, 618-621.
- Schieber, A.; Stintzing, F.C.; Carle, R. By-Products of Plant Food Processing as a Source of Functional Compounds-Recent Developments. *Trends in Food Science & Technology*, **2001**, 12, 401-413.
- Schneider, Y.; Vincent, F.; Durantou, B.; Badolo, L.; Gosse, F.; Bergmann, C.; Seiler, N.; Raul, F. Anti-Proliferative Effect of Resveratrol, a Natural Component of Grapes, and Wine, on Human Colonic Cancer Cells. *Cancer Letters*, **2000**, 158, 85-91.
- Scordino, M.; Mauro, A.; Passerini A.; Maccarone, E. Adsorption of Flavonoids on Resins: Cyanidin 3-Glucoside. *Journal of Agricultural and Food Chemistry*, **2004**, 52, 1965-1972.
- Serianni A.S., <http://www.nd.edu/~aseriann/silk.gif>, June 2010.
- Silva, E.M.; Pompeu, D.R.; Larondelle, Y.; Rogez, H. Optimisation of the Adsorption of Polyphenols from *Inga Edulis* Leaves on Macroporous Resins Using Experimental Design Methodology. *Separation and Purification Technology*, **2007**, 53, 274-280.
- Soleas, G.J.; Diamandis, E.P.; Goldberg, D.M. Resveratrol: A Molecule Whose Time Has Come? And Gone?. *Clinical Biochemistry*, **1997**, 30, 91-113.
- Soto, M.L.; Moure, A.; Domínguez, H.; Parajó, J.C. Charcoal Adsorption of Phenolic Compounds Present in Distilled Grape Pomace. *Journal of Food Engineering*, **2008**, 84, 156-163.

- Sudjana, A.N.; Dorazio, C.; Ryan, V.; Rasool, N.; Ng, J.; Islam, N.; Riley, T.V.; Hammer, K.A. Antimicrobial Activity of Commercial *Olea Europaea* (Olive) Leaf Extract. *International Journal of Antimicrobial Agents*, **2009**, 33, 461-463.
- Takagai, Y.; Kubota, T.; Kobayashi, H.; Tashiro, T.; Takahashi, A.; Igarashi, S. Adsorption and Desorption Properties of Trans-Resveratrol on Cellulose Cotton. *Analytical Sciences*, **2005**, 21, 183-186.
- Tapas, A.R.; Sakarkar, D.M.; Kakde, R.B. Flavonoids as Nutraceuticals: A Review. *Tropical Journal of Pharmaceutical Research*, **2008**, 7, 1089-1099.
- Tien, C. Remarks on Adsorption Manuscripts Received and Declined: An Editorial. *Separation and Purification Technology*, **2007**, 54, 277-278.
- Tsitsishvili, G.V.; Andronikashvili, T.G.; Kirov, G.N.; Filizova, L.D. Natural Zeolites, Ellis Horwood, New York, 1992.
- Vatai, T.; Skerget, M.; Knez, Z. Extraction of Phenolic Compounds from Elder Berry and Different Grape Marc Varieties Using Organic Solvents and/or Supercritical Carbon Dioxide. *Journal of Food Engineering*, **2008**, 90, 246-254.
- Vieira, S.I.; Dias, S.; Ribeiro, M.H. Bitterness Reduction of Limonin by Selective Adsorption onto New Polymeric Adsorbents. *New Biotechnology*, **2009**, 25, S186-S187.
- Wang, Y.; Catana, F.; Yang, Y.; Roderick, R.; Breemen, R.B. An LC-MS Method for Analyzing Total Resveratrol in Grape Juice, Cranberry Juice and in Wine. *Journal of Agricultural and Food Chemistry*, **2002**, 50, 431-435.
- Wang, L.; Geng, C.; Jiang, L.; Gong, D.; Liu, D.; Yshimura, H.; Zhong, L. The Anti-Atherosclerotic Effect of Olive Leaf Extract is Related to Suppressed Inflammatory Response in Rabbits with Experimental Atherosclerosis. *European Journal of Nutrition*, **2008**, 47, 235-243.
- Wikipedia, The Free Encyclopedia, <http://en.wikipedia.org/wiki/Olive>, June 2010.
- Wong, P.L.; Royce A.J.; Lee-Persons C.W.T. Improved Ajmalicine Production and Recovery from *Catharanthus roseus* Suspensions with Increased Product Removal Rates. *Biochemical Engineering Journals*, **2004**, 21, 253-258.

- Wu, J.M. Differential Effects on Growth, Cell Cycle Arrest, and Induction of Apoptosis by Resveratrol in Human Prostate Cancer Cell Lines. *Experimental Cell Research*, **1999**, 249,109–115.
- Yrjönen, T. Extraction and Planar Chromatographic Separation Techniques in the Analysis of Natural Products. University of Helsinki, Finland. 2004.
- Yoon, S.Y.; Choi, W.J.; Park, M.; Yang, J.W. Selective Adsorption of Flavonoid Compounds from the Leaf Extract of Ginkgo Biloba L. *Biotechnology Techniques*, **1997**, 11, 553-556.
- Yu, W.; Shu, B.; Zhao, Y. Supercritical CO₂ Extraction of Resveratrol and Its Glucoside Piceid from Chinese Traditional Herb *Polygonum Cuspidatum*. *Journal of the Science of Food and Agriculture*, **2005**, 85, 489-492.
- Zhang, W.; Chen, J.; Pan, B.; Zhang, Q. Binary Competitive and Cooperative Adsorption of Aromatic Compounds on Polymeric Resins. *Chinese Journal of Polymeric Science*, **2005**, 23, 6-9.
- Zheng, Q.; Zhang, Y.; Zheng, R.; Guo, D.; Li, C. Effects of Verbascoside and Luteolin on Oxidative Damage in Brain of Heroin Treated Mice. *Pharmacie*, **2005**, 60, 539-543.
- Zheng, Q.S.; Sun, X.L.; Xu, B.; Li, G.; Song, M. Mechanisms of Apigenin-7-Glucoside as a Hepatoprotective Agent. *Biomedical and Environmental Sciences*, **2005**, 18, 65-70.
- Zu, Y.; Li, C.; Fu, Y.; Zhao, C. Simultaneous Determination of Catechin, Rutin, Quercetin, Kaempferol and Isorhamnetin in the Extract of Sea Buckthorn (*Hippophae Rhamnoides* L.) Leaves by RP-HPLC with DAD. *Journal of Pharmaceutical and Biomedical Analysis*, **2006**, 41, 714-719.

APPENDIX A

METHODS AND BIOLOGICAL ACTIVITY TESTS

A.1. Methods

A.1.1. Total Phenol Analysis

Folin- ciocalteu method was used to determine the total phenol content of the extracts. Lyophilized crude extract of olive leaf and grape skin was dissolved in water and ethanol, respectively. Liquid extracts obtained after centrifugation and after the solvent removal were also analyzed after centrifugation of the samples at 5000 rpm for 5 min. 500 μ L of sample was mixed with the 2.5 mL of Folin-ciocalteu reagent (1:10 dilution with deionized water) and left to stand 2.5 min at room temperature and then 2 mL of sodium carbonate solution (7.5% in deionized water) was added. After incubating 1 h at room temperature in a dark place, the absorbances were measured at 725 nm by UV spectrophotometer (Perkin Elmer and Thermo Microplate reader). The total phenol content of the sample was given according to calibration curve obtained with the gallic acid and tannic acid.

Calibration Curve of Gallic Acid Standard

0.5 mg/mL stock standard of gallic acid was prepared by firstly dissolving 250 mg of dry gallic acid in 10 mL of ethanol and then diluting to 500 mL with distilled water. The solution was kept in the 4 °C. The standard concentrations that were prepared for calibration curve are 0.02-0.03-0.04-0.05 and 0.06 mg/mL.

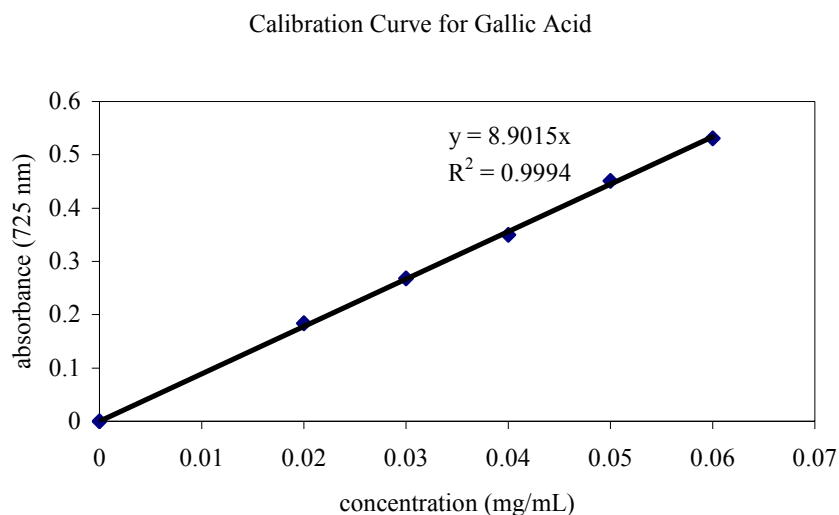


Figure A.1. Calibration curve of gallic acid standard which is used for expression of total phenol contents as gallic acid equivalents.

Calculation of Total Phenol Contents in Gallic Acid Equivalent

$$\text{GAEq}(\text{mg GA/g sample}) = \frac{A \cdot \text{DF} \cdot V_{\text{solv}}(\text{mL})}{[\text{slope of cal. curve} \cdot \text{sample amount}(\text{g})]}$$

In this equation:

GA: gallic acid

A: absorbance of working solution

V: solvent volume for dissolving extract, mL

Sample amount: weighted extract, g

DF: dilution factor

A.1.2. HPLC Analysis

A.1.2.1. HPLC Analysis of Grape Skin Polyphenols

In order to qualify and quantify the bioactive polyphenolic compounds in grape skin, high performance liquid chromatography (HPLC) analysis of the samples was performed. Prior to the injection, samples were filtered through 0.45 μm syringe filter. Agilent 1100 series of HPLC having a Lichrosphere C18 analytical column (i.e. column length: 250 mm, column diameter: 4mm, particle size: 5 μm) was used. GilsonTM solid

phase extraction unit was connected to the HPLC and atomization was achieved. The detection of polyphenolic compounds were achieved with diode array detector and HPLC program is given in Table A.1.

Table A.1. HPLC elution program for the grape skin polyphenols

Time (min)	Mobile Phase A (%) (5.5% acetic acid)	Mobile Phase B (%) (20% A in acetonitrile)
0	83.5	16.5
13	82	18
15	82	18
17	77	23
25	75	25
27	68.5	31.5
30	0	100
40	0	100
45	83.5	16.5
50	83.5	16.5

Stock solutions of gallic acid, (+)-catechin (-)-epicatechin standards were prepared in water; *trans*-resveratrol was prepared in 20% EtOH and quercetin, kaempferol and rutin standards were prepared in methanol. In order to obtain calibration curves of each polyphenolic standards, series of dilutions of stock solutions were prepared. While gallic acid, (+)-catechin and (-)-epicatechin, were detected at 280 nm, *trans*-resveratrol and rutin were detected at 306 nm and 256 nm, respectively. The remaining less polar standards, quercetin and kaempferol were detected at 368 nm.

A.1.2.2. HPLC Analysis of Olive Leaf Polyphenols

The HPLC analysis given in the study of the Baycin et al. (2007) was used for the quantification of oleuropein and rutin. Other polyphenolic components, which are verbascoside, tyrosol, hydroxytyrosol, apigenin-7-glucoside, luteolin-7-glucoside, luteolin, and catechin, were identified according to the study of Garcia et al. (2000).

The linear gradient elution system was used with the mobile phase given in Table A.2.

Table A.2. HPLC elution program for the olive leaf polyphenols

Time (min)	Mobile Phase A (%) (5.5% acetic acid)	Mobile Phase B (%) (20% A in acetonitrile)
0	95	5
20	75	25
40	50	50
50	20	80
60	5	95

A.1.3. Preparation Procedure of Natural Zeolite

Clinoptilolite is a mineral obtained from the Gördes region. It should be well characterized before used, so pretreatment procedure was applied to obtain a clinoptilolite rich adsorbent, which is given in Figure A.2.

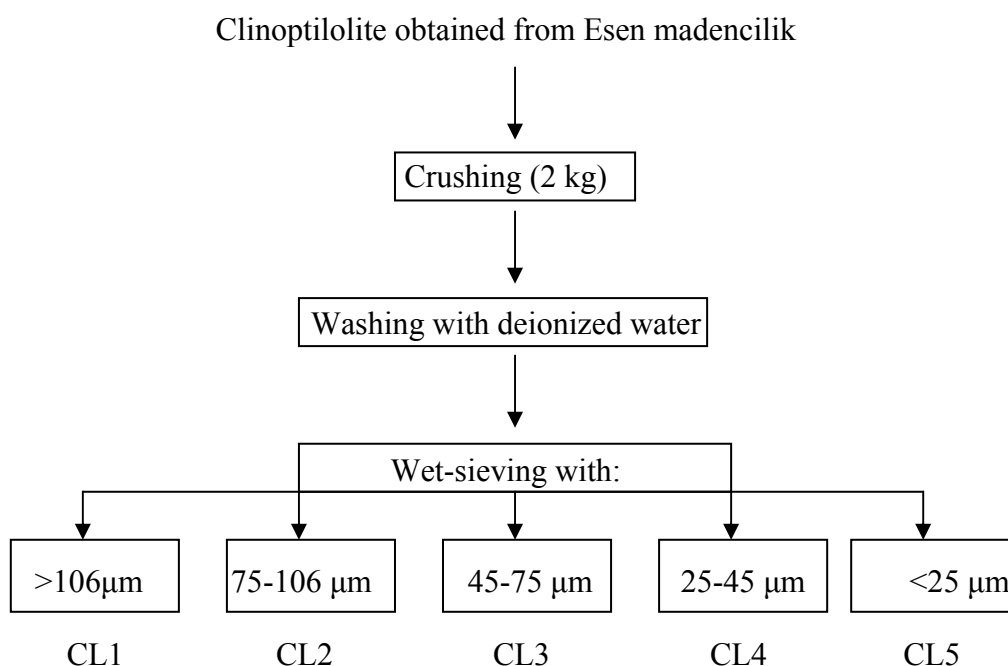


Figure A.2. Flow chart for the preparation steps of clinoptilolite for adsorption; wet-sieving was applied to separate the clinoptilolite based on their particle sizes, the advantage of wet sieving is to remove impurities, such as clay, extra- framework cations etc.

The samples (CL1-CL5) were analyzed with SEM and XRD to determine the crystallinity and purity of the clinoptilolite.

A.1.4. Modification of Clinoptilolite

Dealumination of clinoptilolite rich CL5 sample was achieved by treating 5 g of CL5 with 100 mL of 1, 3, 5, and 8 M of HCl solution in a thermostated bed at 100 °C for 3h. Then samples were washed until the pH of the washing solution equals to 6.4, which is the pH of the deionized water. The infrared spectra of zeolites were taken by using KBr pellet technique with Shimadzu IR 470 spectrometer. Additionally SEM photomicrographs and EDX analysis of samples were taken in order to see the morphology of the samples. Finally X-Ray diffractograms of samples were analysed to see the crystals of the clinoptilolite.

The FTIR spectra of the representative acid treated zeolites are shown in Figure A.3. For the zeolites prepared the strong bands at 1056 and 470 cm^{-1} , assigned to a T–O asymmetric stretching and T–O bending vibrations of the internal tetrahedra, respectively (Özkan and Ülkü, 2005). The effect of dealumination was observed with the shift in the wave numbers of the IR bands. Figure Ab.3 shows the change in the spectrum with the HCl treatment. As seen from the figure the position of the vibrations at 1066 cm^{-1} (the asymmetric stretching mode involving mainly the tetrahedral atoms) is very sensitive to the dealumination degree and this zeolitic band shifted to 1100 cm^{-1} depending on the increase in HCl concentration from 1 M to 8 M and dealumination degree. Beside, the band at 614 cm^{-1} was lost its intensity as parallel to increase in the HCl concentration. The shifting of the 1056 cm^{-1} wave number of Al–O–Al bond to the higher values is attributed to the dealumination of zeolite framework and the change in the bond strength and Si–O–Si angle (Özkan and Ülkü, 2005).

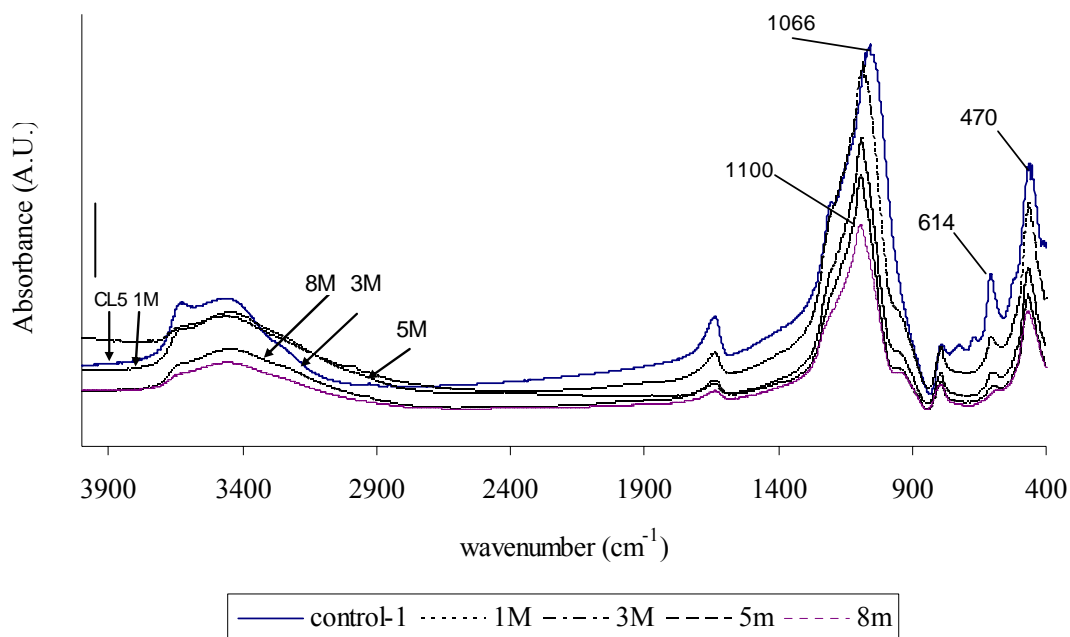


Figure A.3. FTIR spectra of CL5 (control-1) and acid treated samples (1M, 3M, 5M, and 8M).

The results of the X-Ray diffraction study (Figure A.4) showed that the characteristic (9.82), (11.15), (13.07) 2 Theta intensity values were significantly affected from the acid treatment. Almost all of the characteristic peaks were disappeared at the 8 M HCl treated samples. 8 M acid treatment destructed the structure of the clinoptilolite. The intensities of the 9.82 2 theta were decreased by increasing the concentration of HCl, but that characteristic bond was seen even at the 5 M HCl treated sample.

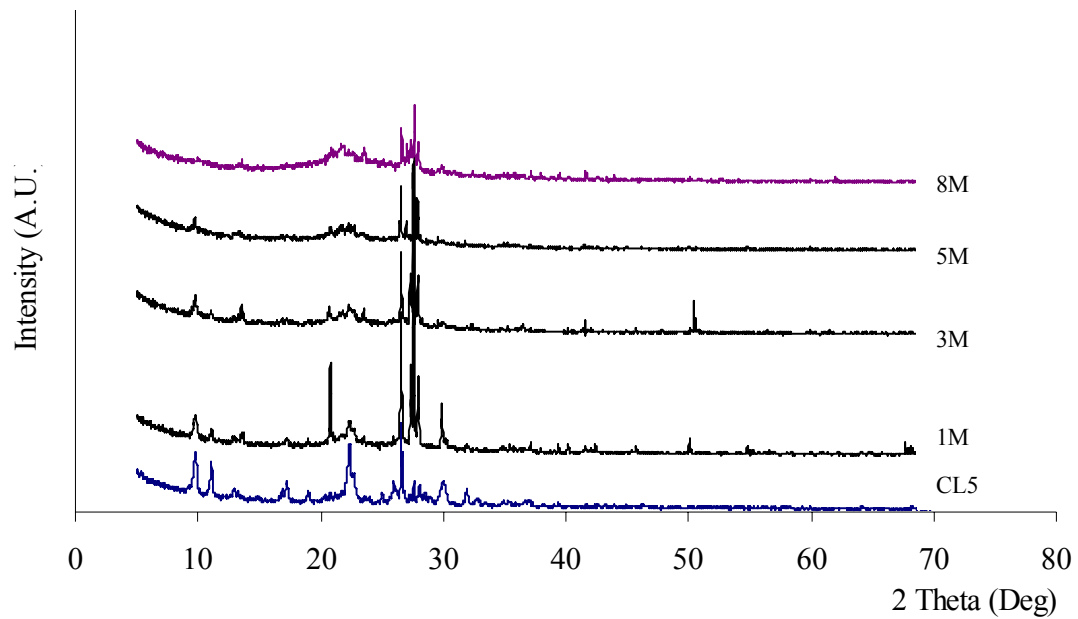
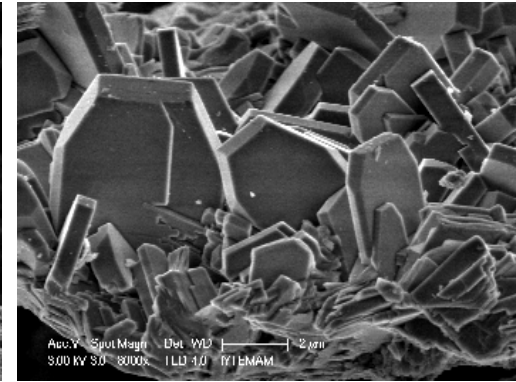
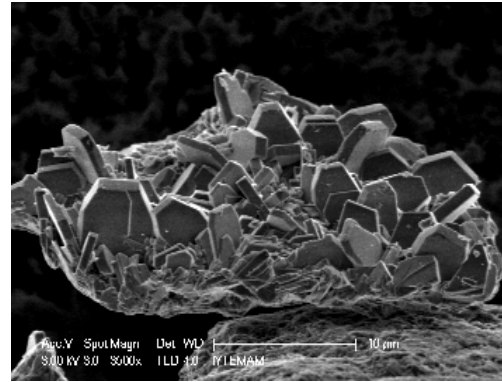
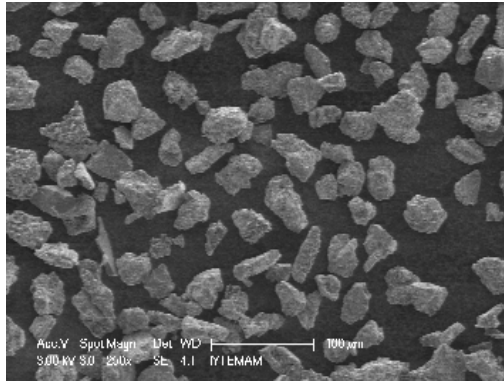


Figure A.4. XRD Diffractogram of the CL5 and acid treated samples.

The SEM photomicrographs of acid treated samples were given in Figure A.5.

Not
treated



1M HCl

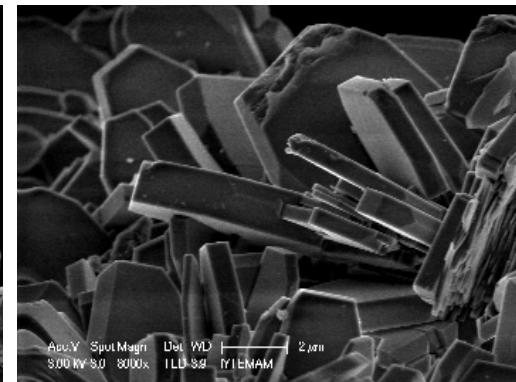
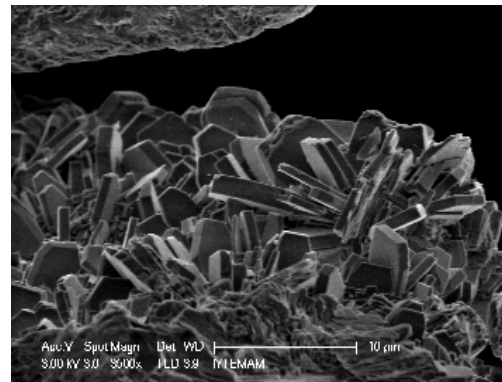
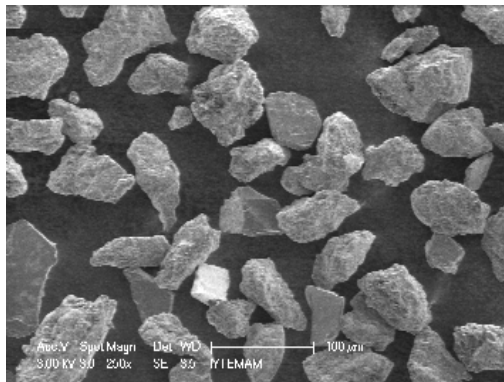
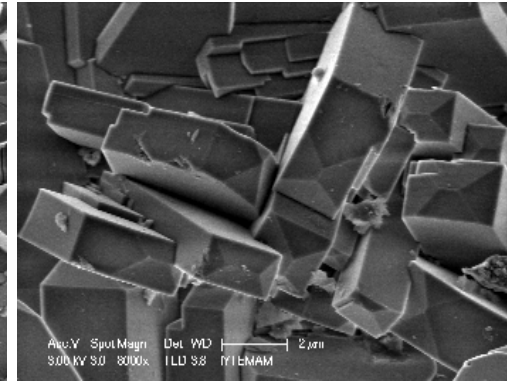
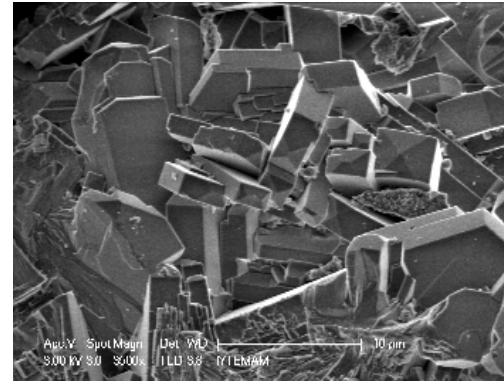
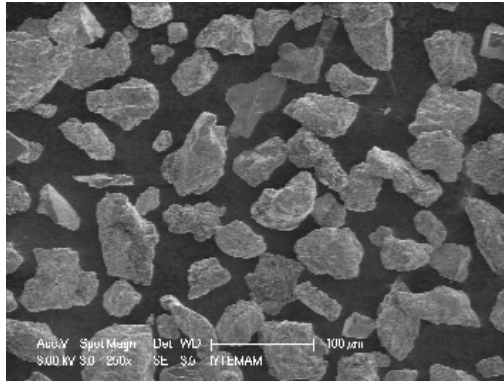


Figure A.5. SEM photomicrographs of CL5 and acid treated samples.

3M HCl



5M HCl

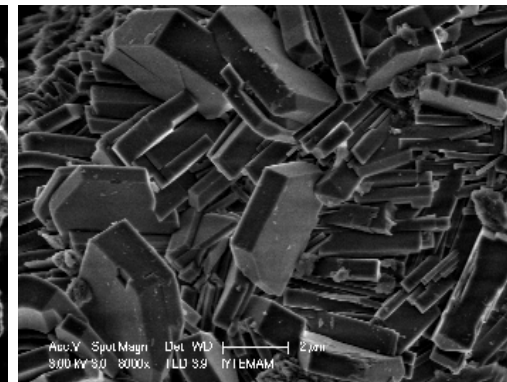
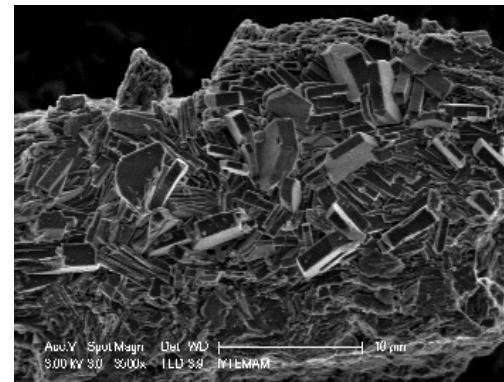
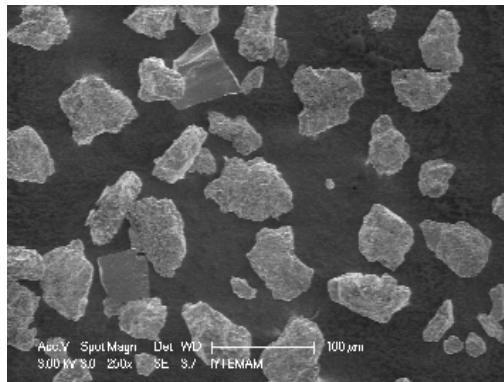


Figure A.5. (cont.)

(Cont. on next page)

8M HCl

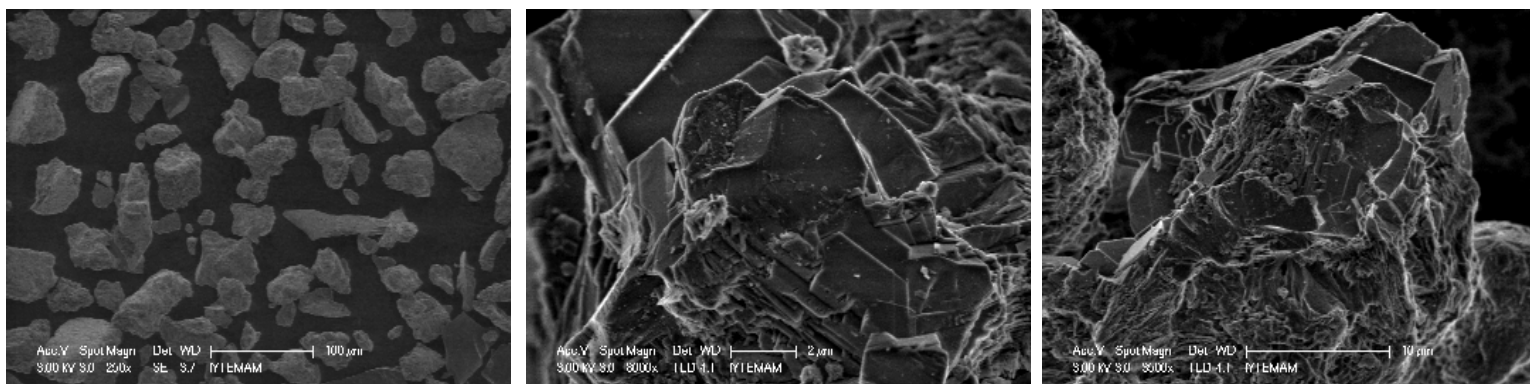


Figure A.5. (Cont.)

A.1.5. Purity Test for the Tianjin *trans*-Resveratrol

The purity of the Tianjin extract was determined by comparing the HPLC calibration curves obtained for the high purity (>99%) sigma *trans*-resveratrol HPLC standard and for the Tianjin *trans*-resveratrol.

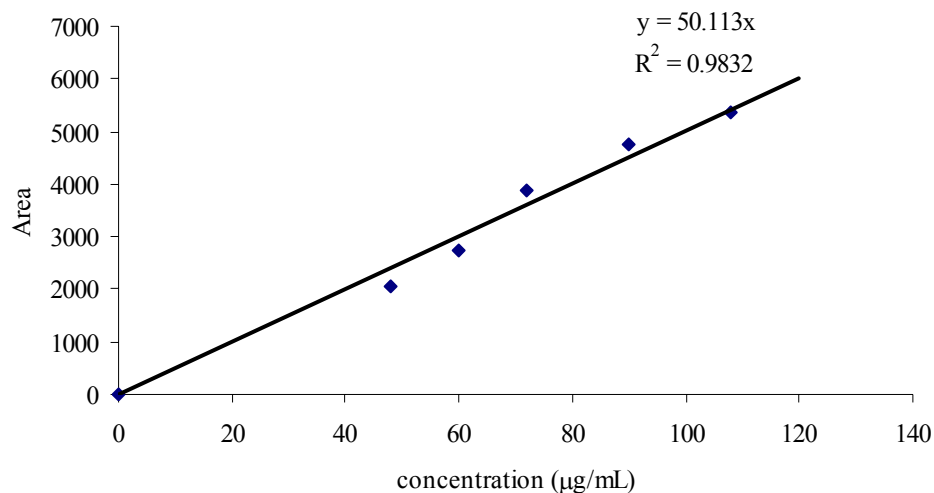


Figure A.6. Calibration curve obtained with Tianjin *trans*-resveratrol.

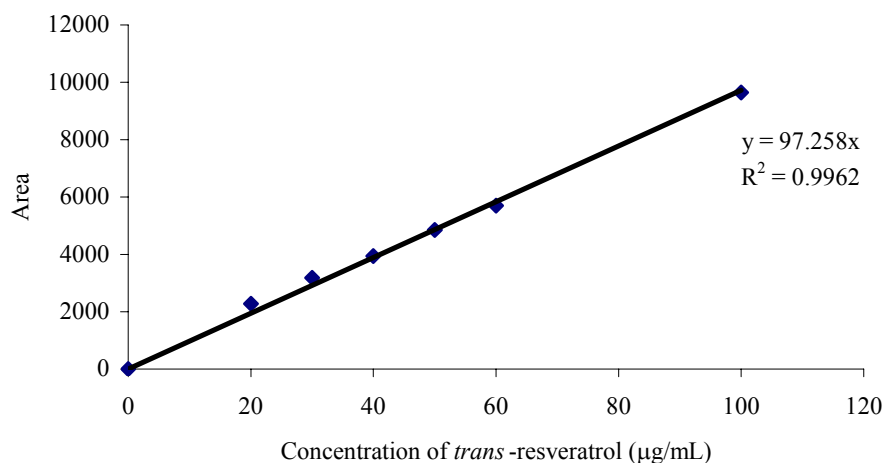


Figure A.7. Calibration curve obtained with HPLC standard of *trans*-resveratrol (Sigma).

$$\text{Purity of Tianjin } \textit{trans}\text{-resveratrol} = \frac{m_1}{m_2} * 100 = \frac{50.113}{97.258} * 100 = 51.5\%$$

A.1.6. Detection of *trans*-Resveratrol by Direct Absorbance Measurement with UV-Transparent 96-Well Plate

This rapid measurement method was developed in order to determine the *trans*-resveratrol concentration in solution. Absorbance values were recorded at 306 nm, at which peak maxima were obtained. Thus, calibration curve for *trans*-resveratrol was obtained by changing the initial concentration of the solution. Validation of the concentrations were performed by HPLC analysis.

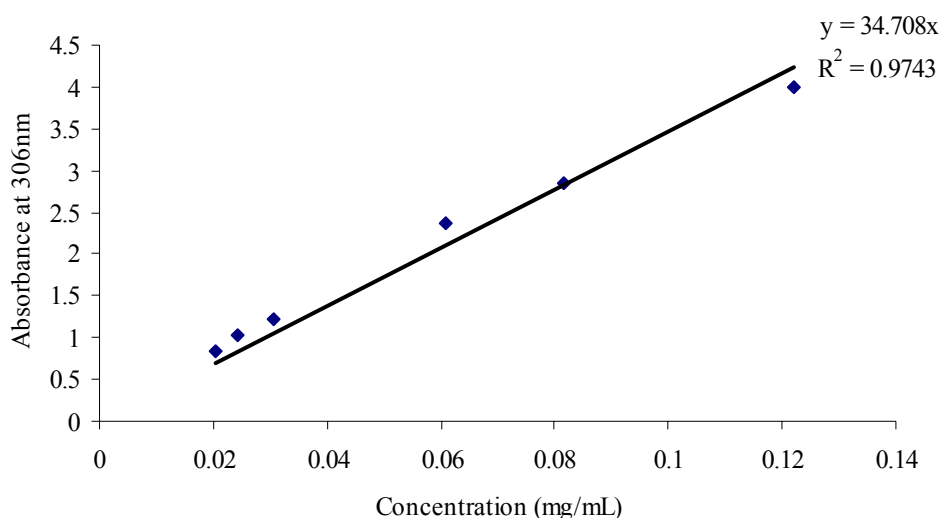


Figure A.8. Calibration curve for *trans*-resveratrol, HPLC analysis of each concentration was performed for validation.

A.2. Biological Activity Tests

A.2.1. Antioxidant Activity Measurement

A number of assays have been introduced for the measurement of the total antioxidant activity of body fluids, food extracts, and pure compounds (Altiok, 2003). In this study, the used method was based on the ability of olive leaf and grape skin antioxidants to scavenge the $ABTS^{\cdot+}$ (ABTS radical cation) compared with a standard antioxidant (Trolox) in a dose-response curve.

ABTS was dissolved in water to a 7 mM concentration was reacted with 2.45 mM potassium persulfate solution to form $ABTS^{\cdot+}$. The mixture was kept in the dark at

ambient temperature for 12-16 hours in order to complete the reaction. While studying phenolic compounds, the ABTS^{•+} solution was diluted with ethanol to an absorbance of 0.70 (±0.02) at 734 nm and equilibrated at 30 °C. On the other hand, stock solutions of phenolics in ethanol were prepared as they produced inhibition between 20% - 80%.

20 µL of phenolic compounds was added to 2 mL of diluted ABTS^{•+} solution and the absorbance was taken at each 1 minute during 6 minutes at Thermo microplate reader. All samples were analyzed at least three times at different concentrations. The percentage inhibition of absorbance at 734 nm was calculated and the trolox equivalent antioxidant capacity (TEAC) value was derived (Altiok, 2003).

Antioxidant activity measurements were evaluated by comparing the slopes of the concentration versus percentage inhibition (%) curves with the one observed for the standard trolox.

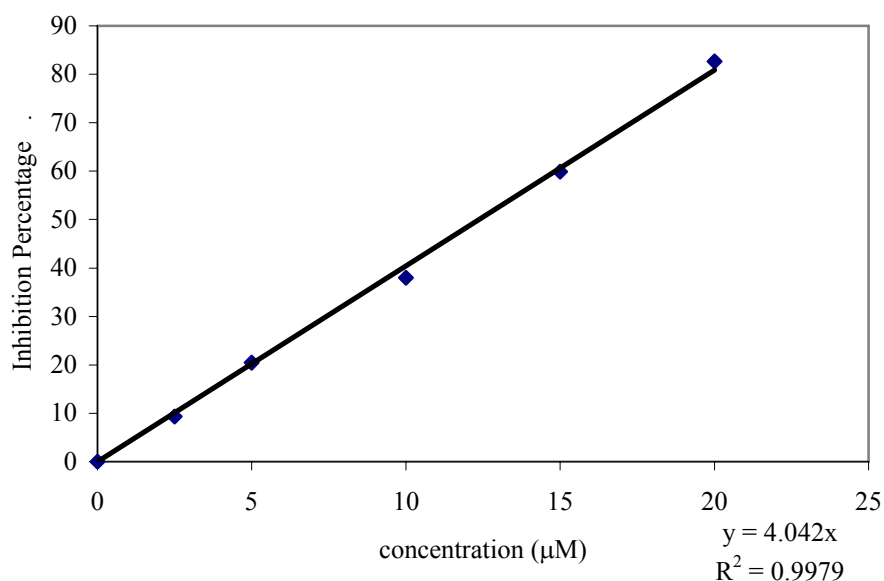


Figure A.9. Calibration curve for trolox.

Following formula was used to determine the antioxidant capacity of sample based on the trolox standard curve;

$$\text{Antioxidant capacity (mg trolox/mg sample)} = \frac{S_{\text{sample}} * DF}{S_{\text{trolox}} * M_w * C * 10^4}$$

where;

S_{sample} : slope of the sample (slope of the concentration vs. % inhibition graph)

DF: Dilution factor

C: Initial concentration of the sample (mg/mL)

S_{trolox} : slope of trolox curve

M_w : Molecular weight of trolox (= 250.3)

A.2.2. Antimicrobial Test; Determination of Minimum Inhibition Concentration (MIC) values

Antimicrobial activity of crude extracts and purified fractions were performed against gram negative (*Escherichia coli* and *Salmonella typhimurium*) and four gram positive bacteria (*Staphylococcus aureus*, *Staphylococcus carnosus*, *Listeria monocytogenes* and *Lactobacillus plantarum*).

In this study, a serial 2-fold dilution method was performed to determine the MIC's of the extracts. Firstly, extract was dissolved (in case of freeze dried powdered extract) in a DMSO (dimethyl sulfoxide-99.5% from Amersco) with a concentration of 100 mg/mL and filtered with a 0.45 μm syringe filter in order to obtain bacteria free solution. Then, two fold dilution of extract was carried out by using sterile deionized water under aseptic conditions. After that, 100 μL of each dilutions and 95 μL nutrient broth (it was MRS broth for *L. plantarum*) were added in each well of 96 well microplate. Each well was inoculated with 5 μL of 6 h incubated bacterial suspensions. Negative control was performed with serial dilutions of DMSO (50%). It was observed that there was any effect on microbial growth of 25% DMSO in solution (Kacar, 2007). The microplate was incubated at 37 $^{\circ}\text{C}$ for 24 h and turbidity of the solution was determined by a Varioscan microplate reader at 620 nm with 30 min intervals. Also, the growth curve of each bacterium was obtained (Figure A.10). It was clearly observed that 6 h subculture time was enough for the inoculum, at that time all of the microorganisms were at their logarithmic phase.

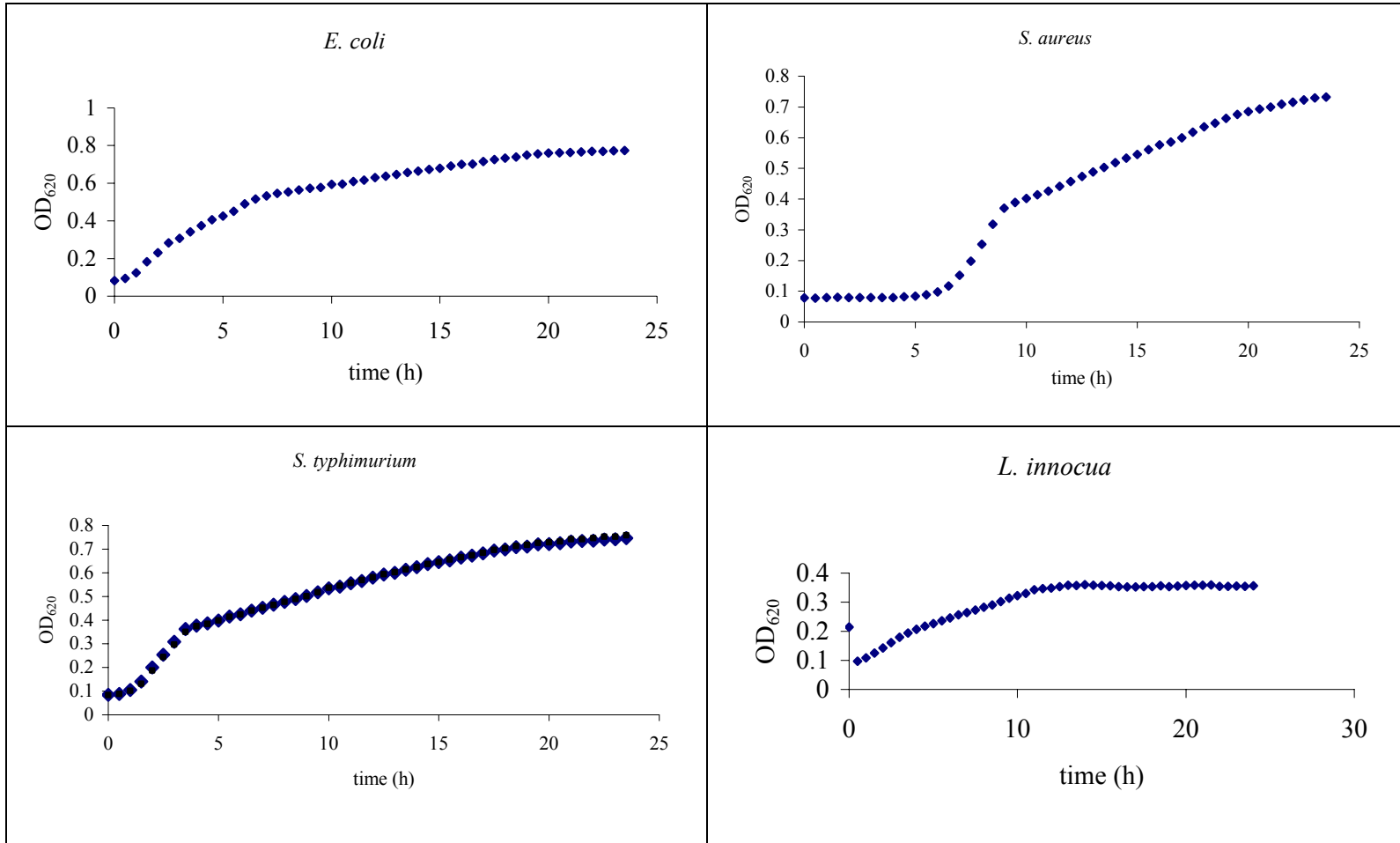


Figure A.10. Growth curves of microorganisms.

(Cont. on next page)

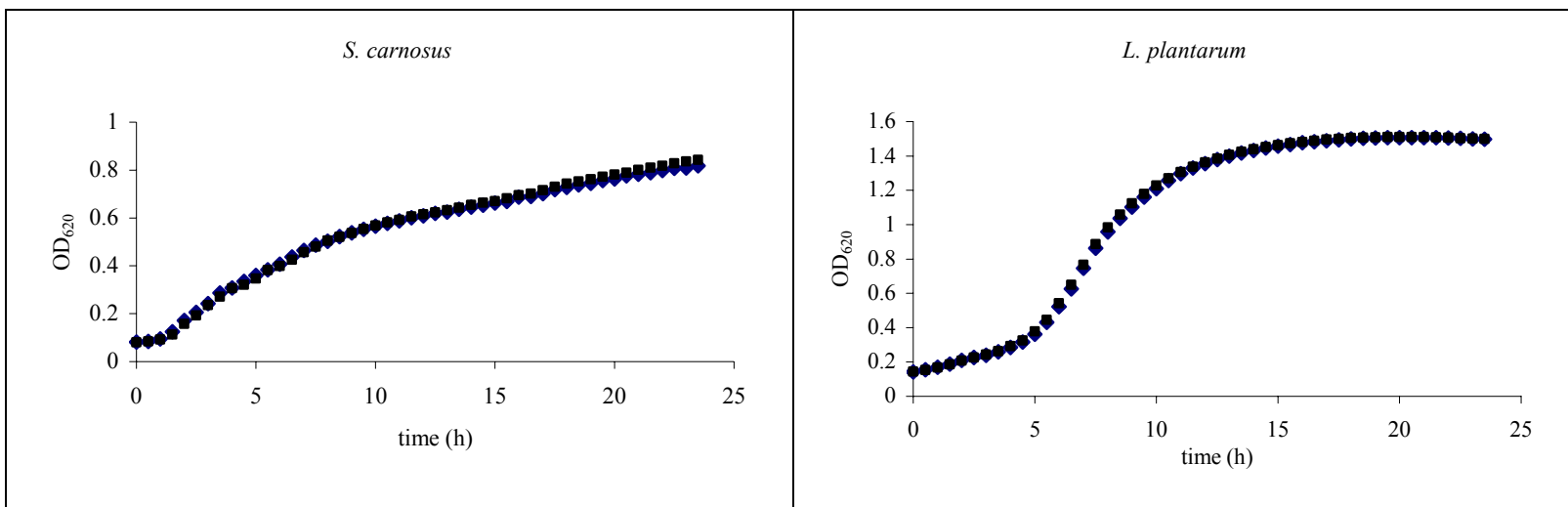


Figure A.10. (Cont.)

A.2.3. Cytotoxic Activity Test: MTT Assay

Cytotoxic activity of crude extract and purified fractions were obtained. Human Prostate Cancer (PC3) cell line was kindly provided by BIOMAM. Cells were maintained in Dulbecco's modified Eagle's medium (DMEM) containing 5% fetal bovine serum (FBS) (BIO-IND), 50 µg/mL gentamicin sulfate, 250 µg/mL Fungizone Amphotericin B (GIBCO Invitrogen), incubated at 37 °C in the dark with 5% CO₂ humidified incubator and passaged when they reached 80-85% confluency. Cells used in experiments were maintained from 10-20th passages. Human breast cancer (MCF7) cell line was also used to determine the inhibition efficiency of extracts.

To investigate the cytotoxic activity of the extracts, 95µL of cell suspension was inoculated into 96-well microculture plates at 1×10^4 cells density per well in culture media containing FBS, fungizone, gentamicin sulfate. Extracts were dissolved in dimethyl sulfoxide (DMSO) (Sigma Chemical Co.), filter sterilized, diluted at the appropriate concentrations with the culture medium. In all well, 1% DMSO concentration was fixed. Dilutions of extracts were freshly prepared before each experiment. After 24 h cultivation for cell attachment, extracts were added at final concentration 0.1 µg/mL, 1 µg/mL, 25 µg/mL, 100 µg/mL, 200 µg/mL, 400 µg/mL, 900 µg/mL for triplicate assay. Cells were treated with the extracts for 24 hours, 48 hours and cytotoxic effects were determined by tetrazolium (3-{4,5-dimethylthiazol-2-yl}-2,5-diphenyl tetrazolium bromide) (Sigma Chemical Co.) based colorimetric assay. This method depends on the cleavage of tetrazolium salt to purple formazan crystals by mitochondrial enzymes of metabolically active cells. Briefly; 4 hours before the end of each incubation period, medium of the cells was removed and wells were washed by pre-warmed phosphate-buffered saline (PBS) to remove any trace of extracts and to prevent colour interference while optical density determination. MTT stock solution (5 mg/mL) was diluted at 1:10 ratio into complete culture media, 100 µL of MTT dilution was added into each well and incubated. After 3.5 hours plates were centrifuged at 1200 rpm for 10 minute at room temperatures to avoid accidental removal of formazan crystals. Crystals were dissolved with 100 µL DMSO.

The absorbance was determined at 540 nm. Results were represented as percentage viability and calculated by the following formula:

$$\% \text{ viability} = 100 - [(OD_s - OD_B / OD_c - OD_B) \times 100]$$

OD_B indicated the optical density of blank, OD_s indicated the optical density of sample and OD_c indicated the optical density of control.

APPENDIX B

HPLC CHROMATOGRAMS FOR EXTRACTION EFFICIENCY

The effects of solvent type, extraction methods, types and origins of the grapes were investigated. The quantitative HPLC characterizations were performed and HPLC chromatograms of samples were given in the following Figures B1 to B6. In these figures, numbered peaks indicate the polyphenolic compounds, whose list is given below:

<u>Peak number</u>	<u>Polyphenol name</u>
1	Gallic acid
2	(+)-catechin
3	(-)-epicatechin
4	rutin
5	<i>trans</i> -resveratrol
6	quarcetin
7	kaempferol

In Figures B1 to B6, five chromatograms are given. In the chromatogram A, overall view of HPLC profile of the sample is given. For this purpose, chromatograms, which were obtained at different wavenumbers, were overlaid. On the other hand, these chromatograms are separately given and letter indicators of them are: B: 280 nm detection; C: 257 nm detection; D: 306 nm detection and E: 368 nm detection.

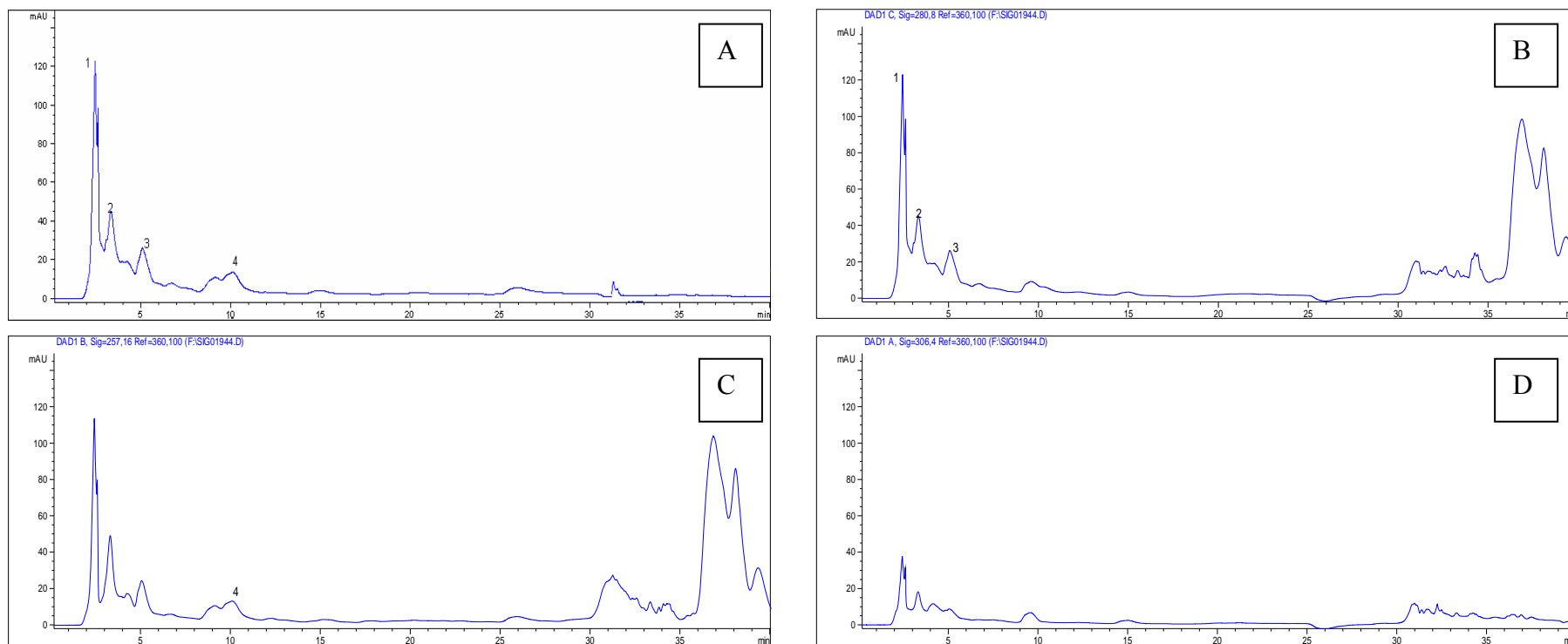


Figure B.1. Extraction conditions: solvent extraction (80% EtOH), in thermoshaker, at 180 rpm. and 30 °C, for 30 minutes. HPLC chromatogram at 368 nm is not given here.

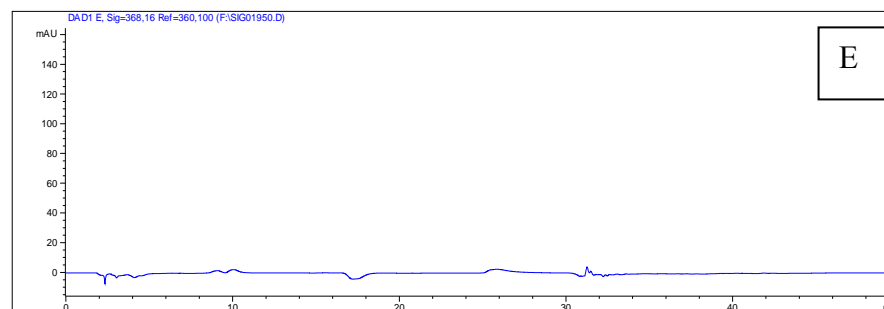
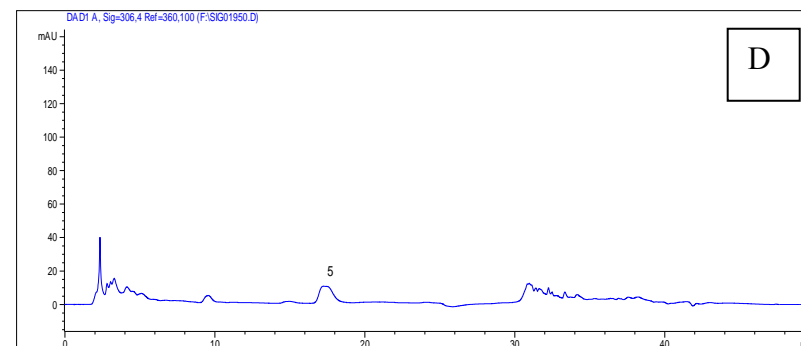
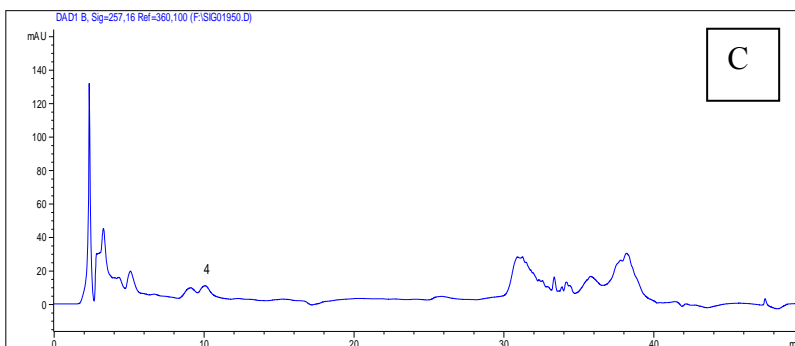
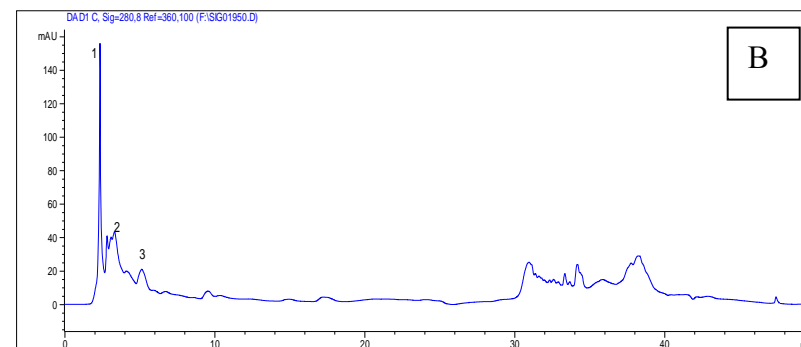
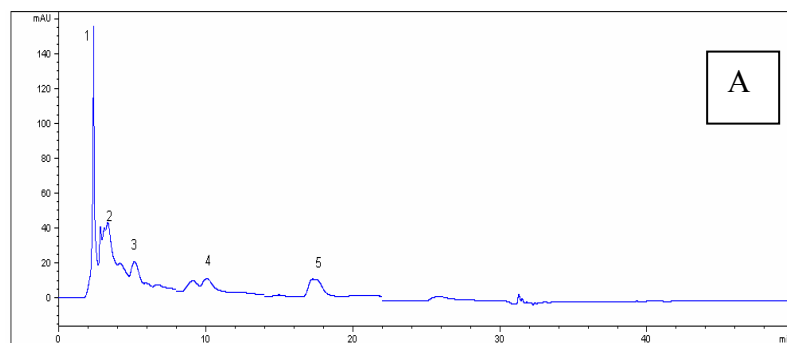


Figure B.2. Extraction conditions: solvent extraction (80% MeOH), in thermostated bath, at 60 °C, for 30 minutes.

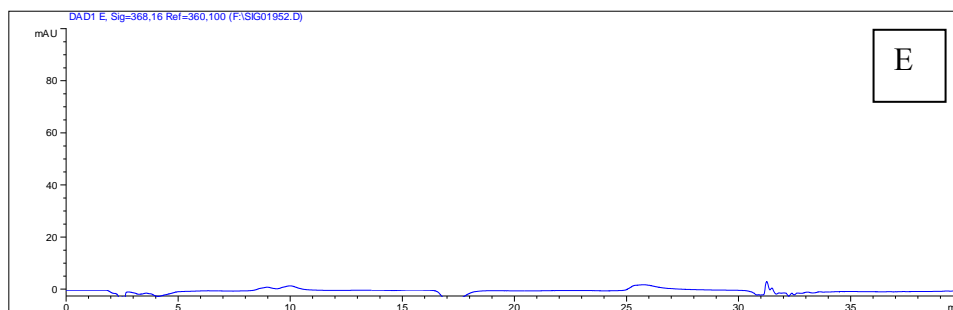
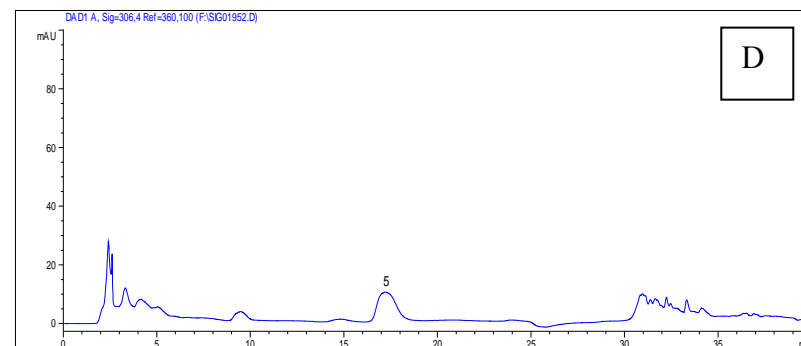
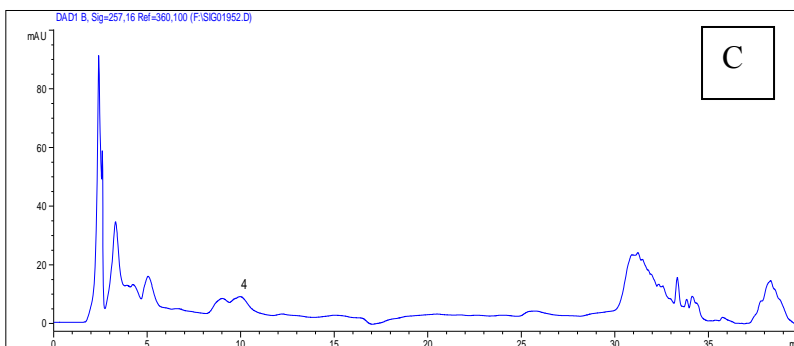
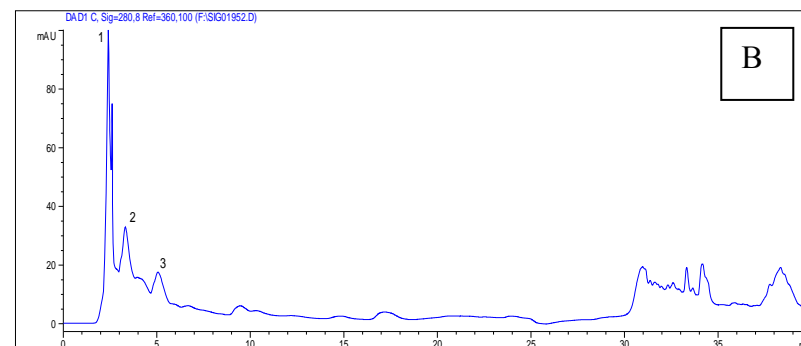
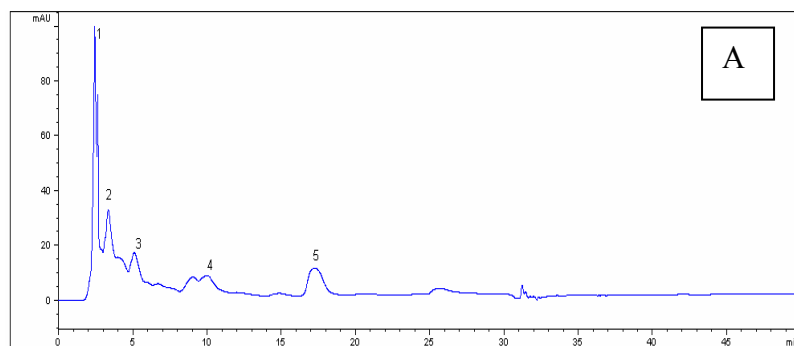


Figure B.3. Extraction conditions: solvent extraction (80% EtOH), in thermostated bath, at 60 °C, for 30 minutes.

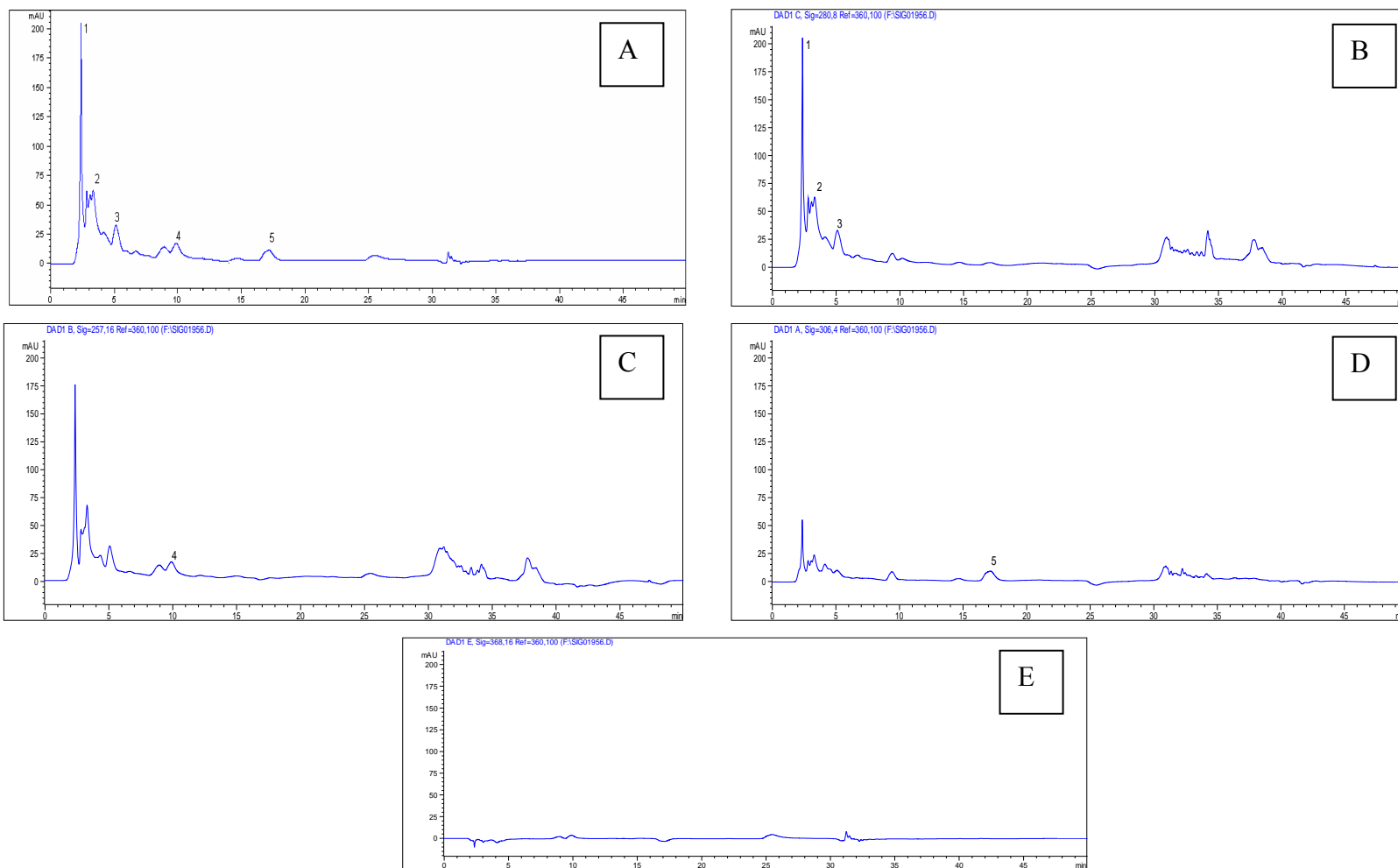


Figure B.4. Extraction conditions: Ultrasonic extraction (80% MeOH), in thermostated bath, at 60 °C, for 30 minutes.

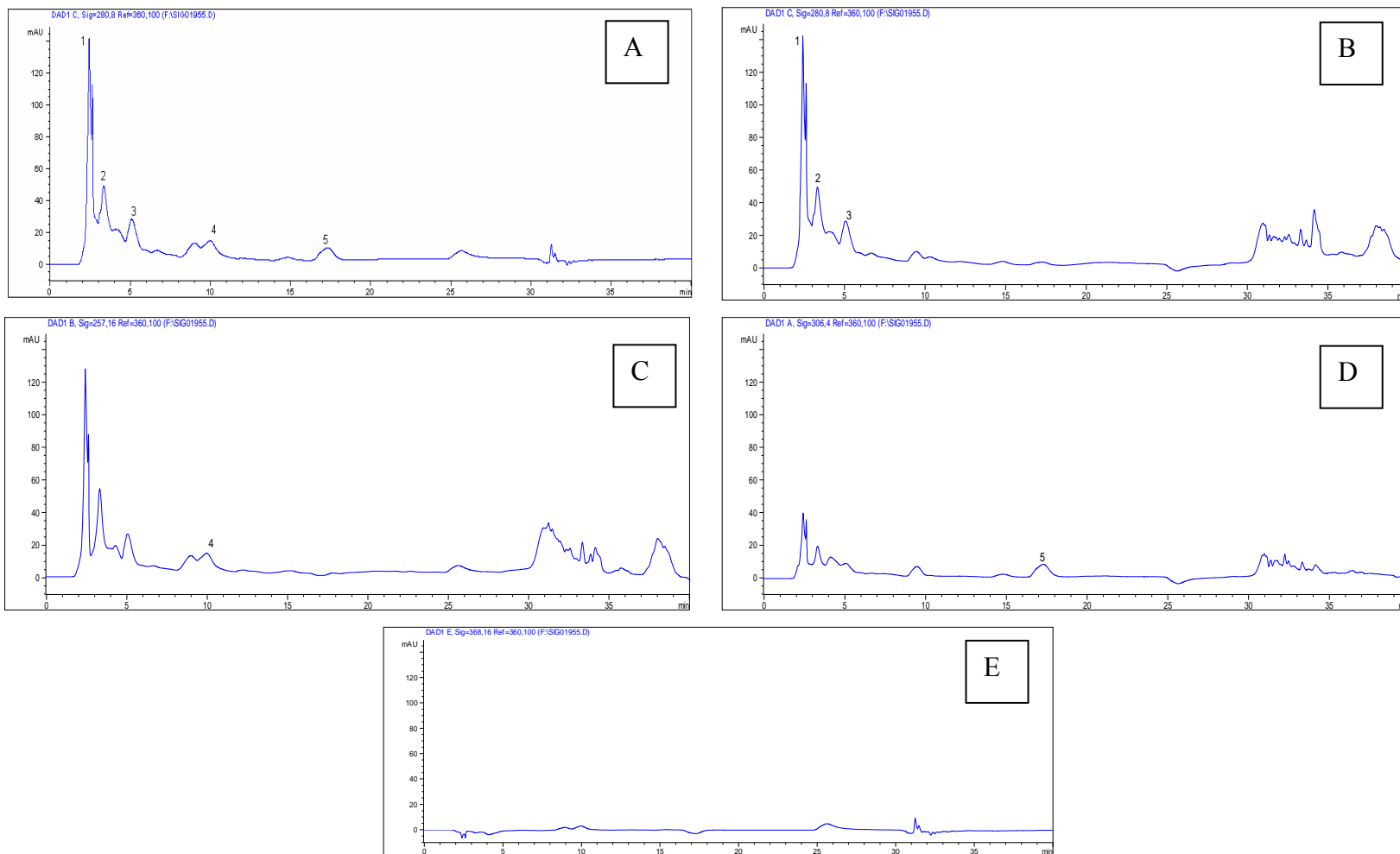


Figure B.5. Extraction conditions: Ultrasonic extraction (80% EtOH), in thermostated bath, at 60 °C, for 30 minutes.

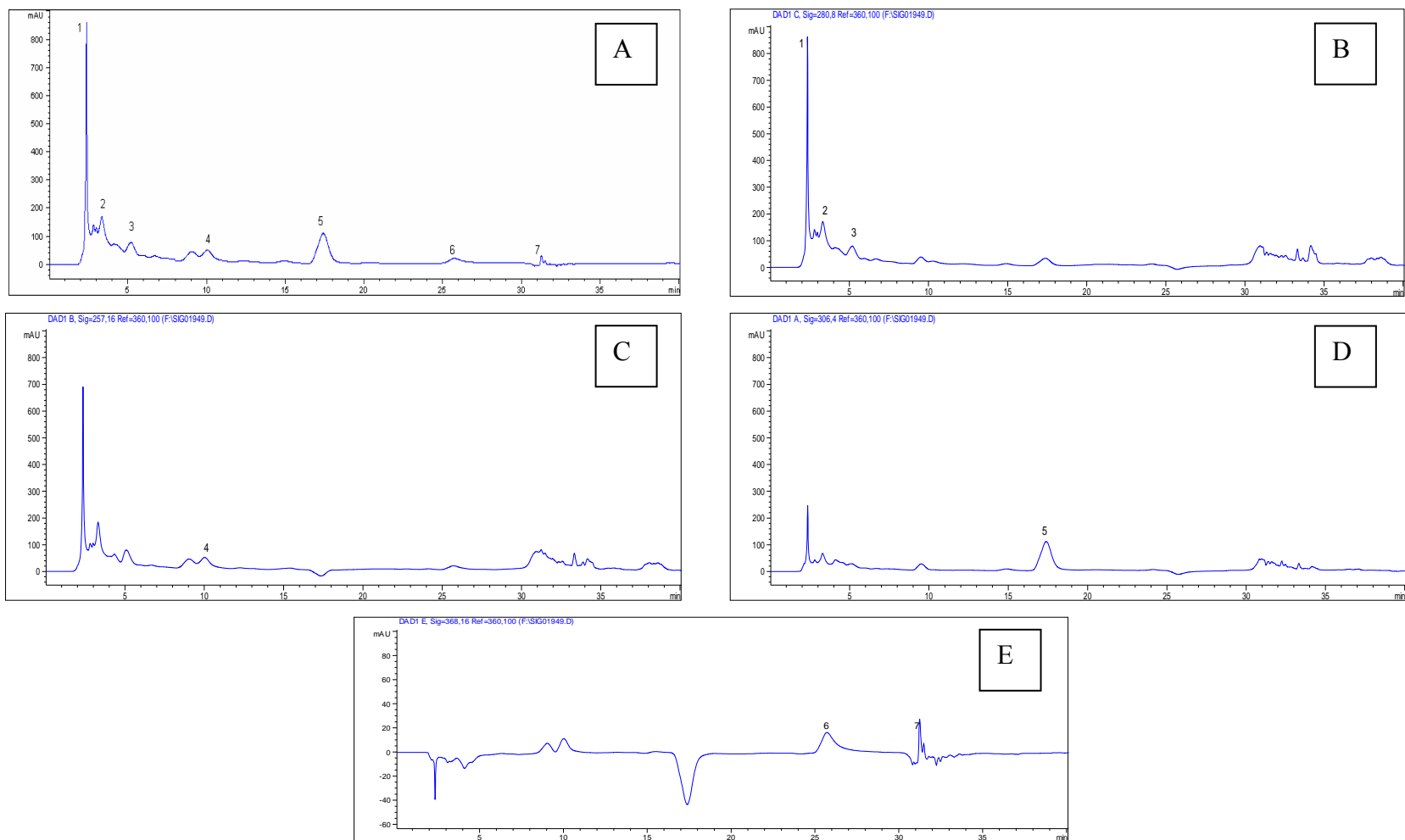


Figure B.6. Extraction conditions: Ultrasonic extraction (80% MeOH), in thermostated bath, at 60 °C, for 30 minutes. Concentrated extract.

APPENDIX C

HPLC CALIBRATION CURVES

Calibration curves of relevant flavonoid standards were used for the quantitative analyses of them in experiments. For this purpose, gallic acid, (+)-catechin and (-)-epicatechin were dissolved in deionized water, whereas rutin, trans-resveratrol, quercetin and kaempferol standards were dissolved in methanol. External calibrations for these standards were performed by preparing each of these standards at different concentrations. Each sample was injected to the HPLC after the filtration of solutions with 0.45 μm microfilters. The area versus concentration curves were plotted to form a calibration curve.

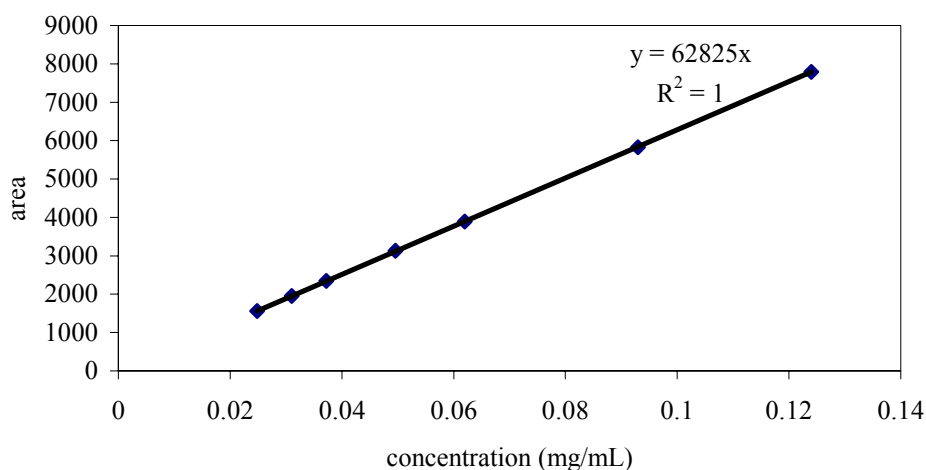


Figure C.1. Calibration curve for gallic acid.

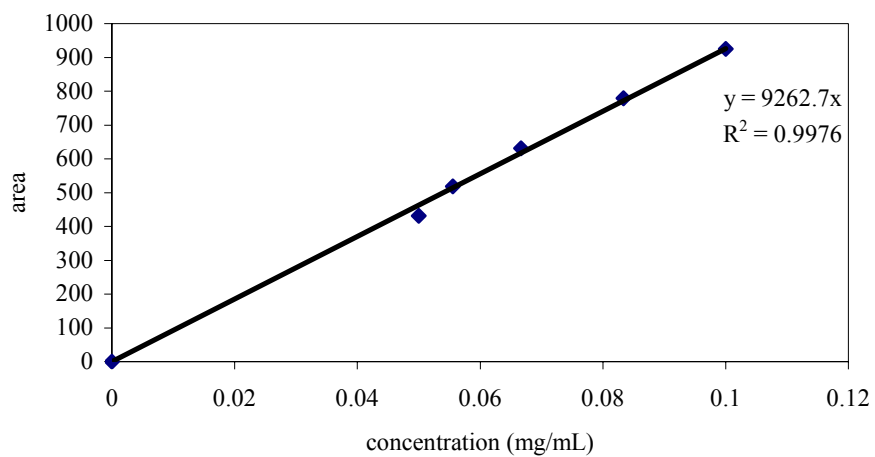


Figure C.2. Calibration curve for (+)-catechin.

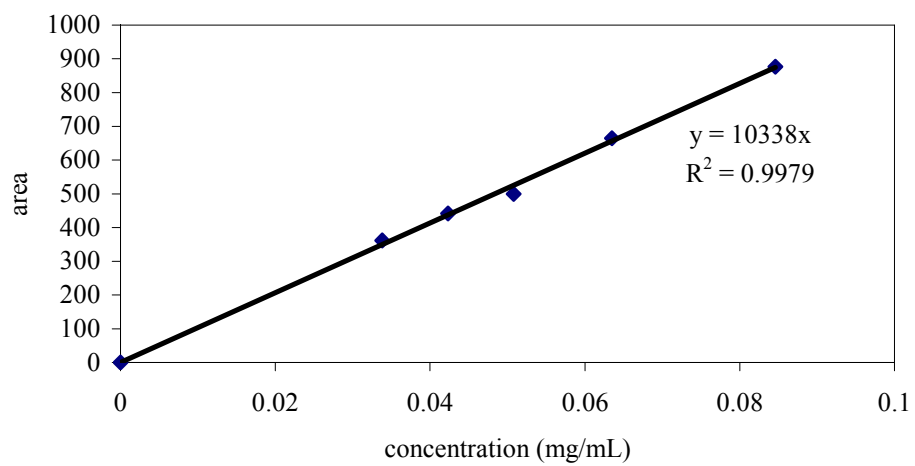


Figure C.3. Calibration curve for (-)-epicatechin.

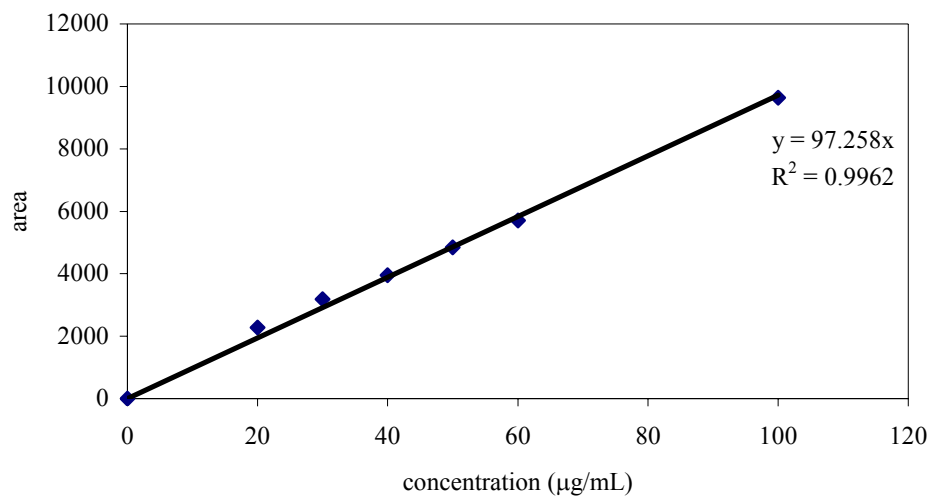


Figure C.4. Calibration curve for *trans*-resveratrol.

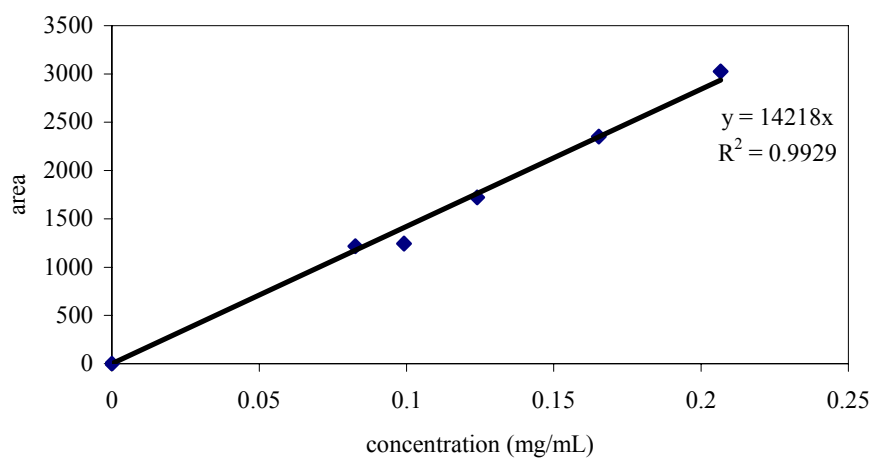


Figure C.5. Calibration curve for rutin.

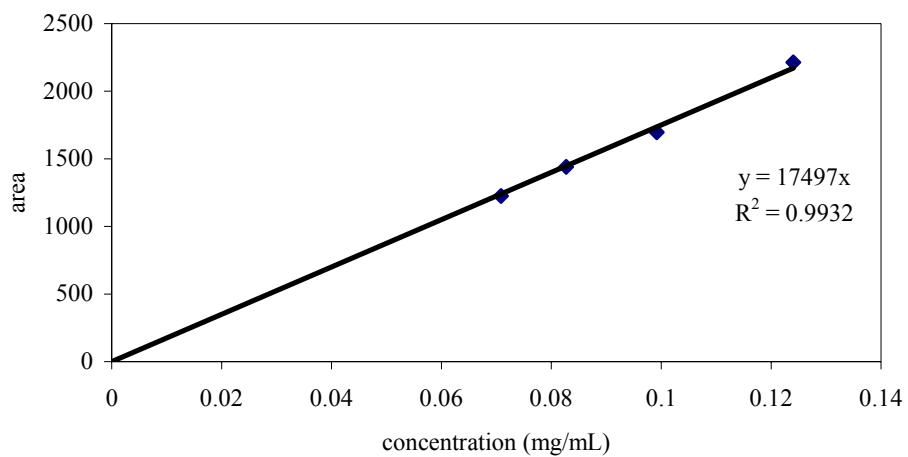


Figure C.6. Calibration curve for quercetin.

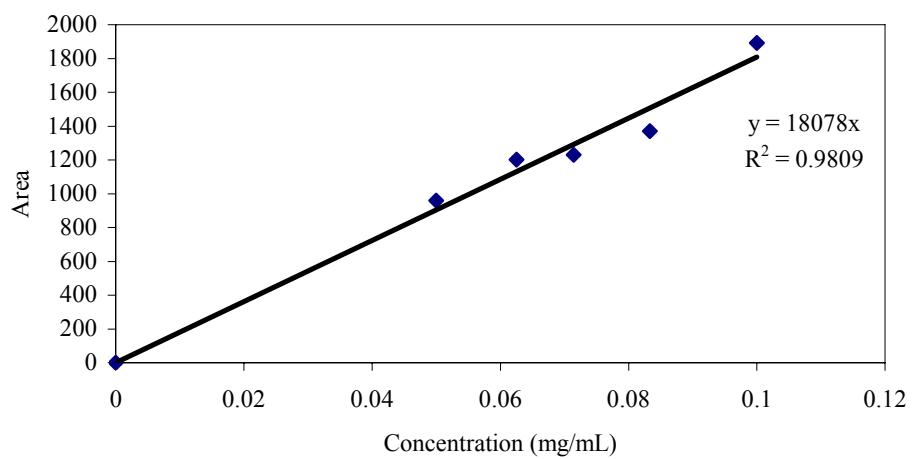


Figure C.7. Calibration curve for kaempferol.

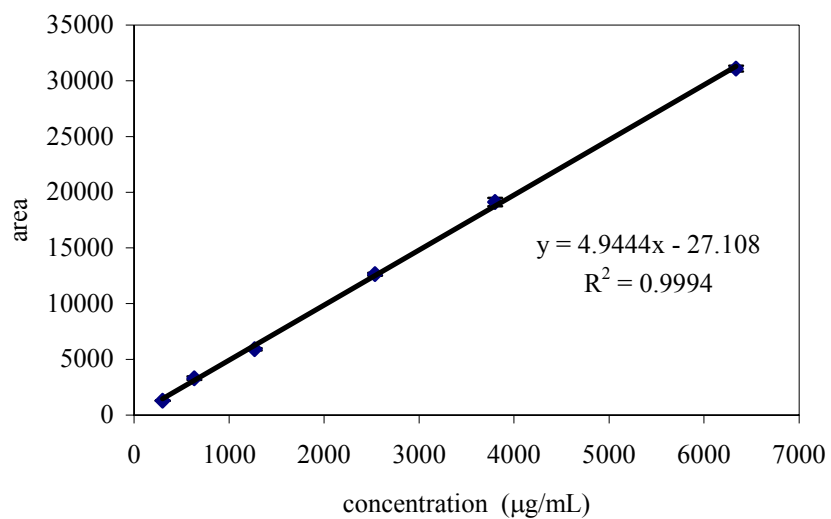


Figure C.8. Calibration curve for oleuropein
(Source: Bayçın, 2006).

APPENDIX D

THEORETICAL EVALUATIONS OF ADSORPTION DATA

D.1. Adsorption Kinetic Models

Determination of External Mass Transfer Coefficient

Boyd Model was applied to the adsorption kinetic data collected from the study of *trans*-resveratrol adsorption on clinoptilolite. The model is given by the following equation.

$$\frac{\bar{q}}{q_e} = 1 - \exp\left[-\frac{3k_f}{KR_p}t\right]$$

$$1 - \frac{\bar{q}}{q_e} = \exp\left[-\frac{3k_f}{KR_p}t\right]$$

after taking the ln of the both sides;

$$\ln\left(1 - \frac{\bar{q}}{q_e}\right) = -\frac{3k_f}{KR_p}t$$

is obtained.

The plot $\ln\left(1 - \frac{\bar{q}}{q_e}\right)$ against t is drawn and k_f can be determined from the slope of

the curve.

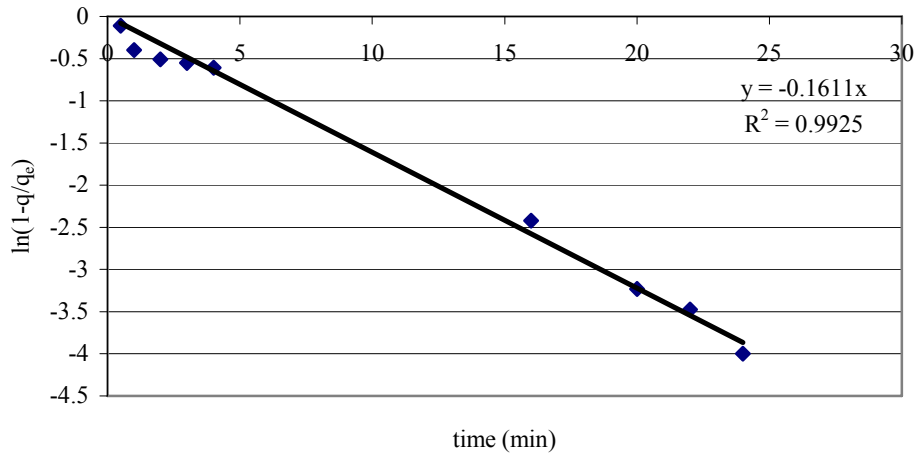


Figure D.1. Boyd Model solution of the kinetic data.

The slope of the line is -0.1611, which is equal to the $-\frac{3k_f}{KR_p}$. Here K is the linear equilibrium relationship constant between the q and C.

$$q_e = KC_e$$

The linear region of the *trans*-resveratrol- clinoptilolite adsorption isotherm plot was redrawn.

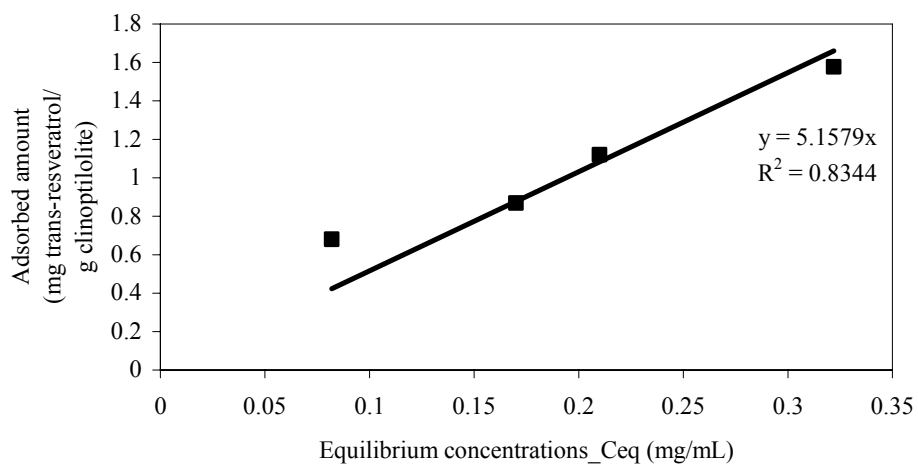


Figure D.2. Linear region of the adsorption isotherm graph.

From the slope of the curve, K is obtained as 5.16.

The average particle size of the clinoptilolite was 50 μm . So, external film mass transfer coefficient can be calculated as;

$$-\frac{3k_f}{KR_p} = -0.1611 = -\frac{3k_f}{5.16 * 50 * 10^{-6}} \times \frac{1 \text{ min}}{60 \text{ s}} \quad k_f = 0.83 \times 10^{-3} \text{ m/s}$$

D.2. Application of Adsorption Isotherms

Adsorption isotherms for *trans*-resveratrol adsorption on silk fibroin and clinoptilolite were investigated. To obtain isotherms' parameters, k_f and n for Freundlich isotherm, the linearization of the model equation can be written as;

$$\ln q_e = \ln k_F + n \ln C_e$$

The k_F and n values can be obtained from the intercept and slope, respectively, from the linear regression line from a plot of $\ln q_e$ versus $\ln C_e$.

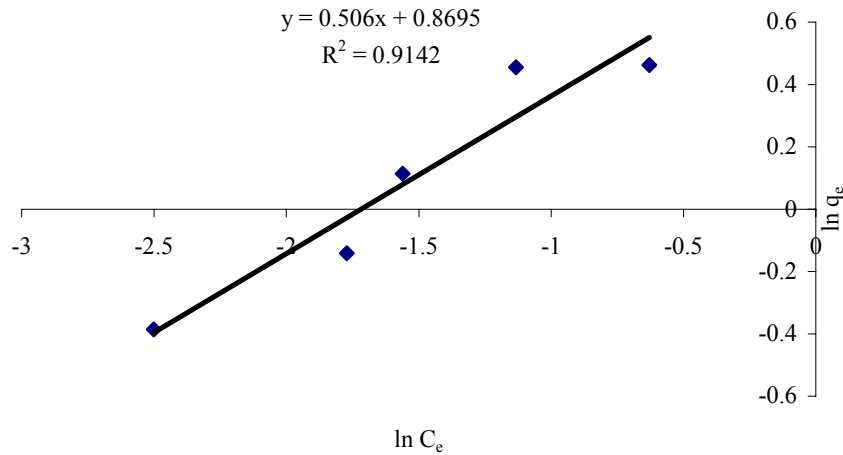


Figure D.3. Freundlich model curve of 51.5% pure *trans*-resveratrol adsorption on CL3 clinoptilolite.

The intercept of the curve is 0.8695, which is equal to $\ln k_F$, so k_F can be found as 3.385. The slope of the curve is 0.506, which is equal to n .

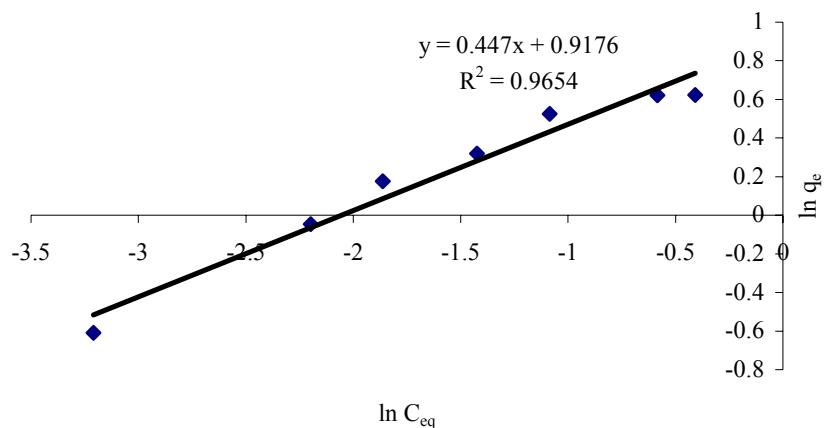


Figure D.4. Freundlich model curve of polyganum cuspaditum's *trans*-resveratrol (51.5%) adsorption on clinoptilolite rich CL5 sample.

The intercept of the curve is 0.917, which is equal to $\ln k_F$, so k_F can be found as 4.503. The slope of the curve is 0.447, which is equal to n .

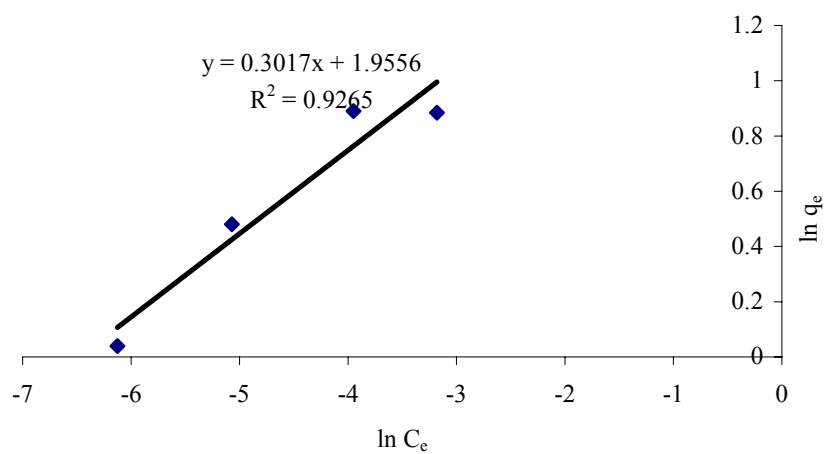


Figure D.5. Freundlich model curve of pure *trans*-resveratrol adsorption on clinoptilolite rich CL5 sample.

The intercept of the curve is 1.955, which is equal to $\ln k_F$, so k_F can be found as 7.04. The slope of the curve is 0.301, which is equal to n .

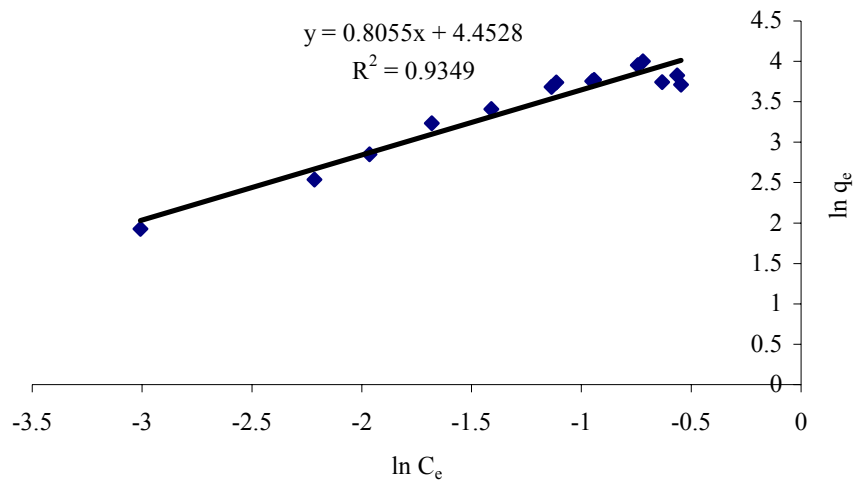


Figure D.6. Freundlich model curve of *trans*-resveratrol adsorption on silk fibroin.

The intercept of the curve is 4.4528, which is equal to $\ln k_F$, so k_F can be found as 85.86. The slope of the curve is 0.805, which is equal to n .

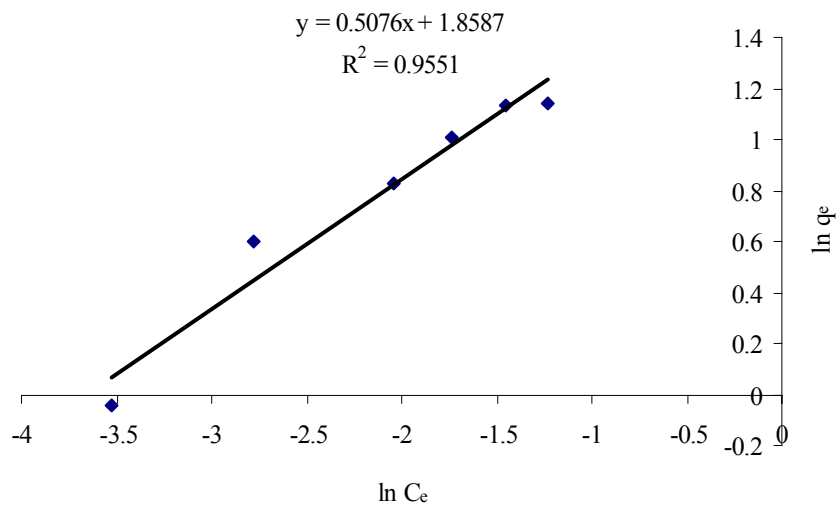


Figure D.7. Freundlich model curve of olive leaf crude extract adsorption on clinoptilolite.

The intercept of the curve is 1.8587, which is equal to $\ln k_F$, so k_F can be found as 6.41. The slope of the curve is 0.507, which is equal to n .

Langmuir isotherm has the following form:

$$q_e = \frac{q_{\max} k_L C_e}{1 + k_L C_e}$$

The Langmuir parameters were calculated by using the linearized equation of the Langmuir model. The linearized form of the equation is;

$$\frac{1}{q_e} = \frac{1}{q_{\max}} + \frac{1}{k_L q_{\max}} \frac{1}{C_e}$$

The plot between the $1/q_e$ versus $1/C_e$ is drawn and the intercept of the line gives $1/q_{\max}$ whereas the slope of it is equal to $1/k_L q_{\max}$.

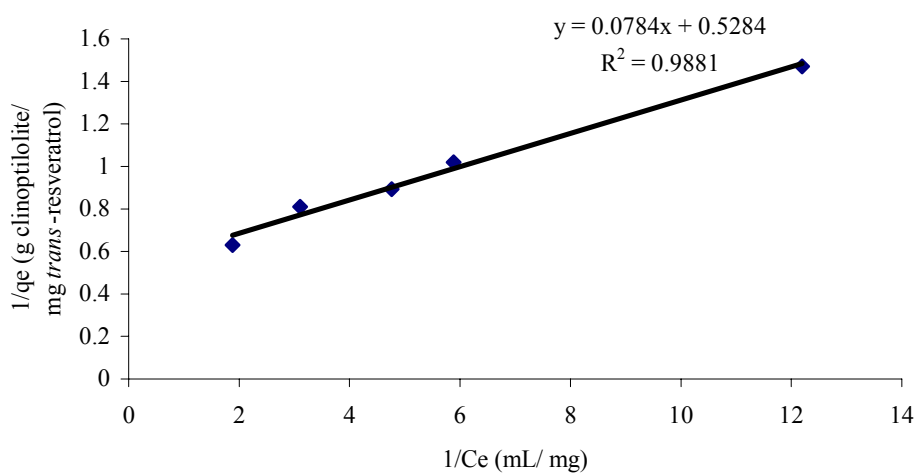


Figure D.8. Langmuir model curve of *trans*-resveratrol adsorption on clinoptilolite.

Intercept of the curve is 0.53 which is equal to $1/q_{\max}$. Then q_{\max} can be found as 1.89 mg *trans*-resveratrol/g clinoptilolite. The slope of the curve is 0.0784, which is equal to $1/k_L q_{\max}$. So, k_L can be calculated as 6.75 mg/mL.

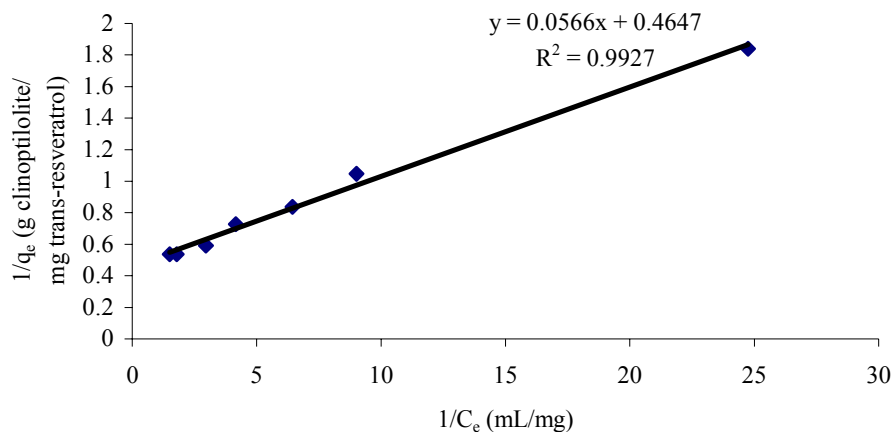


Figure D.9. Langmuir model curve of polyganum cuspaditum's *trans*-resveratrol (51.5%) adsorption on clinoptilolite rich CL5 sample.

Intercept of the curve is 0.46 which is equal to $1/q_{max}$. Then q_{max} can be found as 2.16 mg *trans*-resveratrol/g clinoptilolite. The slope of the curve is 0.0566, which is equal to $1/k_L q_{max}$. So, k_L can be calculated as 8.22 mg/mL.

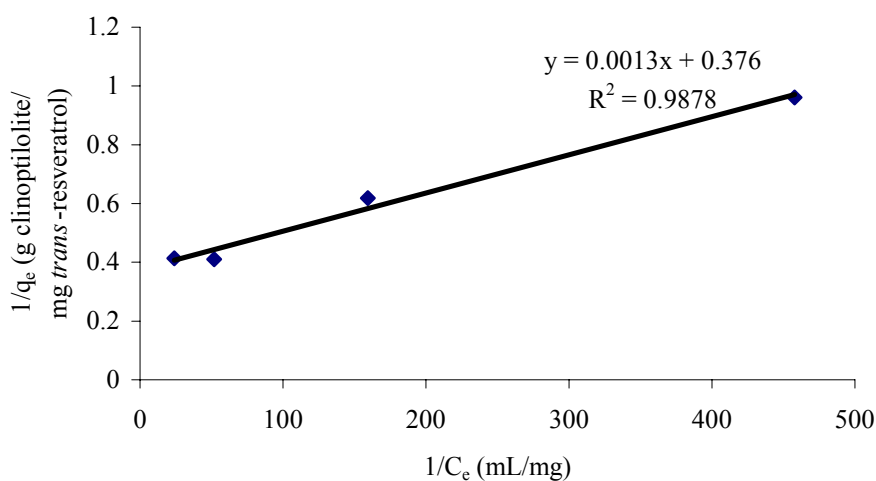


Figure D.10. Langmuir model curve of pure *trans*-resveratrol adsorption on clinoptilolite rich CL5 sample.

Intercept of the curve is 0.37 which is equal to $1/q_{max}$. Then q_{max} can be found as 2.66 mg *trans*-resveratrol/g clinoptilolite. The slope of the curve is 0.0013, which is equal to $1/k_L q_{max}$. So, k_L can be calculated as 28.92 mg/mL.

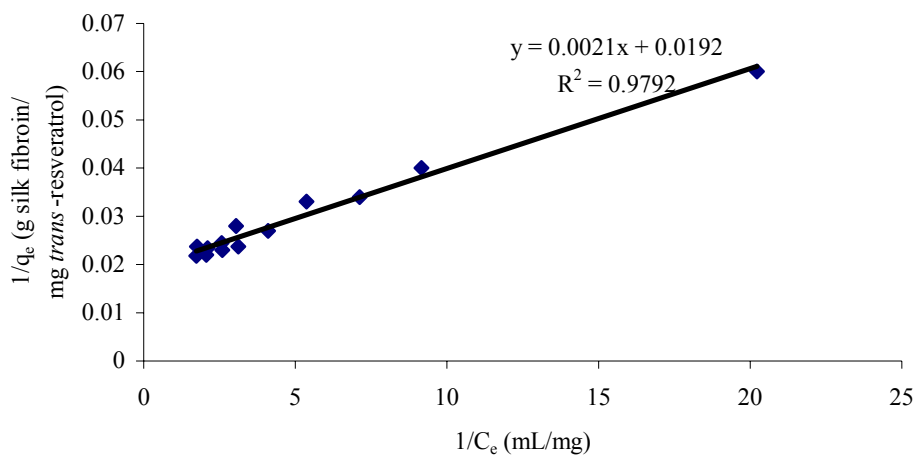


Figure D.11. Langmuir model curve of *trans*-resveratrol adsorption on silk fibroin.

Intercept of the curve is 0.0192 which is equal to $1/q_{max}$. Then q_{max} can be found as 52.08 mg *trans*-resveratrol/g clinoptilolite. The slope of the curve is 0.0021, which is equal to $1/k_L q_{max}$. So, k_L can be calculated as 9.14 mg/mL.

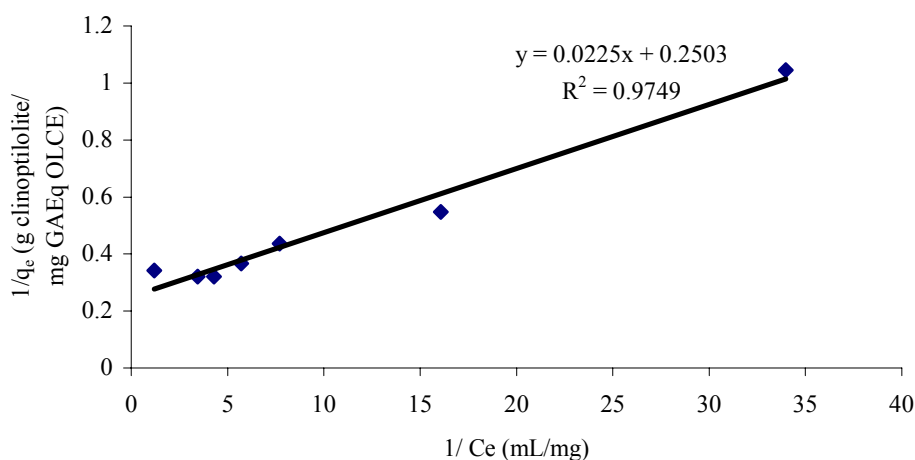


Figure D.12. Langmuir model curve of *olive leaf crude extract (OLCE)* adsorption on clinoptilolite.

Intercept of the curve is 0.2503 which is equal to $1/q_{max}$. Then q_{max} can be found as 3.99 mg OLCE/ g clinoptilolite. The slope of the curve is 0.0225, which is equal to $1/k_L q_{max}$. So, k_L can be calculated as 11.14 mg/mL.

D.3. Determination of Macropore Diffusivity

Equation 4.11 was used to calculate macropore diffusivity (D_p). For this purpose fractional uptakes (m_t/m_∞) versus time plot was plotted.

Table D.1. The plots used to calculate macropore diffusivity (D_p) for pure *trans*-resveratrol adsorption onto clinoptilolite rich CL5 sample at 40 °C

Ci	m_t/m_∞ versus time plot	$\ln(1 - m_t/m_\infty)$ versus t plot for $m_t/m_\infty > 0.7$
0.062		
0.039		
0.019		
0.01		

Equation 4.11 is;

$$\frac{m_t}{m_\infty} = 1 - \frac{6}{\Pi^2} \sum_{n=1}^{n=\infty} \frac{1}{n^2} \exp\left(-\frac{n^2 \Pi^2 \varepsilon_p D_p t}{R_p^2 (\varepsilon_p + (1 - \varepsilon_p)K)}\right) \quad (4.11)$$

For fractional uptakes greater than 70%, we may retain only the first term to obtain;

$$1 - \frac{m_t}{m_\infty} = \frac{6}{\Pi^2} \exp\left(-\frac{\Pi^2 \varepsilon_p D_p t}{R_p^2 (\varepsilon_p + (1 - \varepsilon_p)K)}\right) \quad (D.1)$$

By taking Ln of both sides;

$$\text{Ln}\left(1 - \frac{m_t}{m_\infty}\right) = \text{Ln}\left(\frac{6}{\Pi^2}\right) + \text{Ln}\left[\exp\left(-\frac{\Pi^2 \varepsilon_p D_p t}{R_p^2 (\varepsilon_p + (1 - \varepsilon_p)K)}\right)\right] \quad (D.2)$$

Rearranging the Equation D.2;

$$\text{Ln}\left(1 - \frac{m_t}{m_\infty}\right) = \left[\text{Ln}\left(\frac{6}{\Pi^2}\right) + \left(-\frac{\Pi^2 \varepsilon_p D_p}{R_p^2 (\varepsilon_p + (1 - \varepsilon_p)K)}\right)t \right] \quad (D.3)$$

The plot between the Ln $(1 - m_t/m_\infty)$ versus t is plotted and D_p is found from the slope of the plot. For an example solution;

The slope of the Ln $(1 - m_t/m_\infty)$ versus t plot of $C_i=0.062$ is -0.0292 .

$$-0.0292 = \left[\text{Ln}\left(\frac{6}{\Pi^2}\right) + \left(-\frac{\Pi^2 0.32 D_p}{(20 \times 10^{-6})^2 (0.32 + (1 - 0.32)63.209)}\right)t \right]$$

And D_p is found as; $0.0538 \times 10^{-10} \text{ m}^2/\text{s}$.

Table D.2. The plots used to calculate macropore diffusivity (D_p) for pure *trans*-resveratrol adsorption onto clinoptilolite rich CL5 sample at 40 °C; effect of particle size

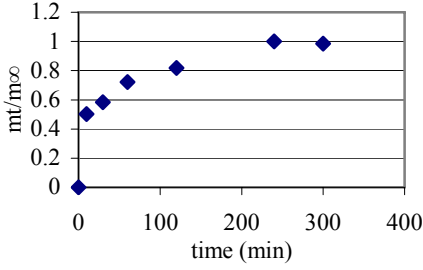
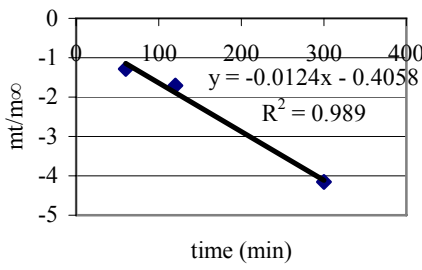
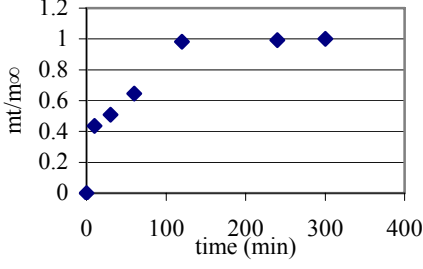
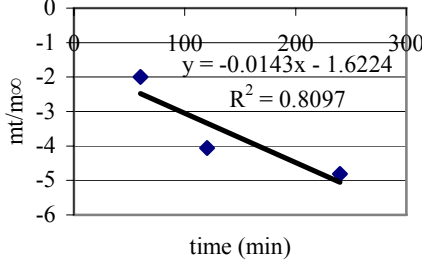
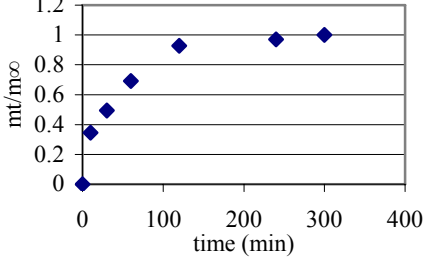
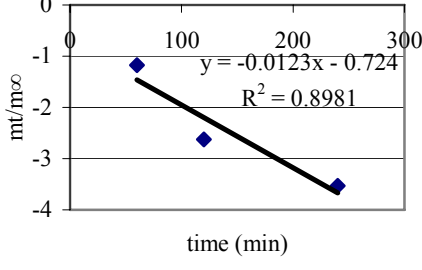
Particle size	m_t/m_∞ versus time plot	$\ln(1 - m_t/m_\infty)$ versus t plot for $m_t/m_\infty > 0.7$
Coarse		
Mid		
Fine		

Table D.3. The plots used to calculate macropore diffusivity (D_p) for pure *trans*-resveratrol adsorption onto clinoptilolite rich CL5 sample at 40 °C; effect of agitation speed

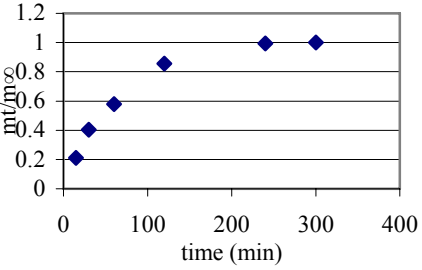
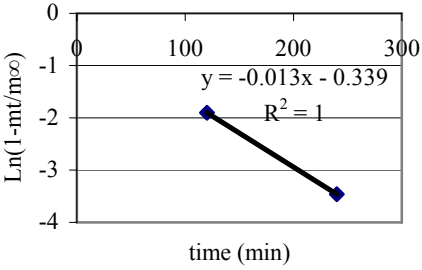
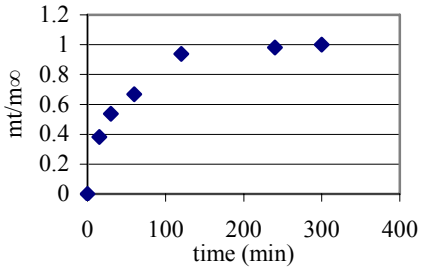
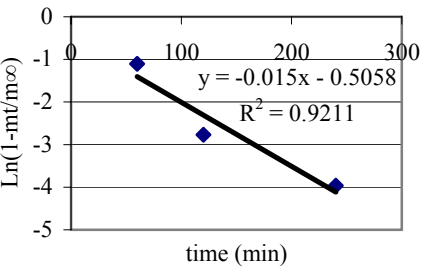
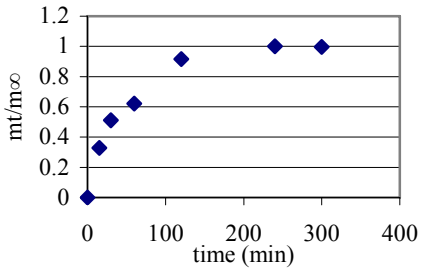
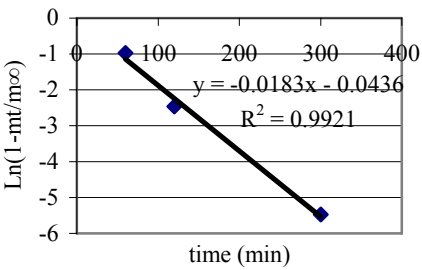
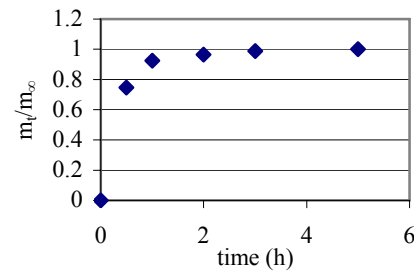
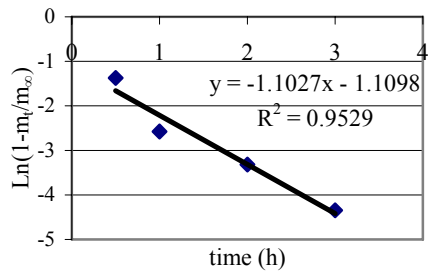
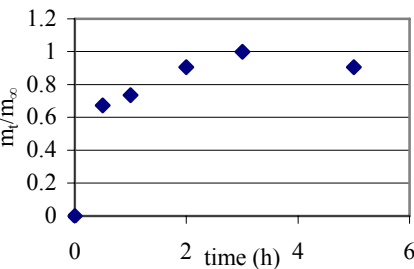
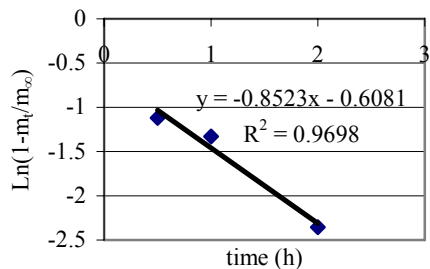
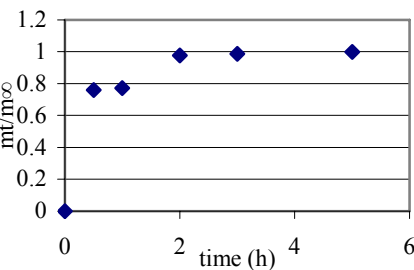
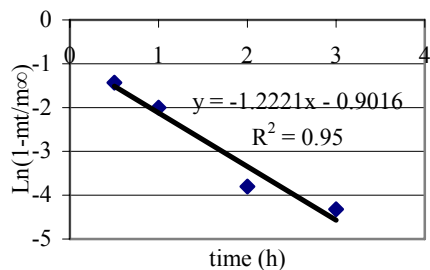
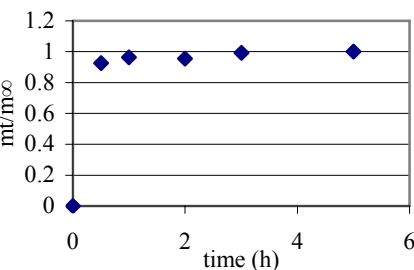
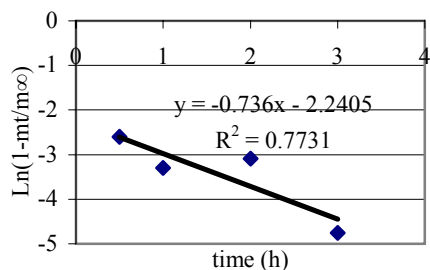
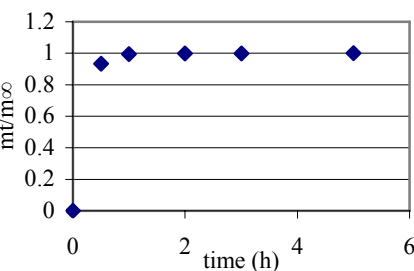
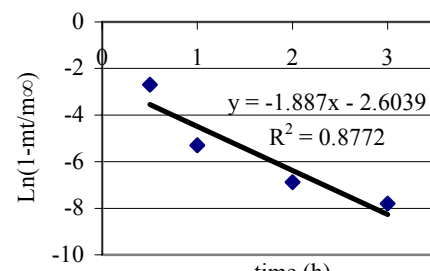
Agitation speed	m_t/m_∞ versus time plot	$\ln(1 - m_t/m_\infty)$ versus t plot for $m_t/m_\infty > 0.7$
50		
100		
150		

Table D.4. The plots used to calculate macropore diffusivity (D_p) for 51.5 % pure *trans*-resveratrol adsorption onto clinoptilolite rich CL5 sample at 40 °C

C_i	m_t/m_∞ versus time plot	$\ln(1 - m_t/m_\infty)$ versus t plot for $m_t/m_\infty > 0.7$
0.054		
0.072		
0.185		
0.38		
0.604		

D.4. Determination of Intraparticle Diffusion Rate Constant (k_d)

Equation 4.21 is used to calculate the intraparticle diffusion rate constant (k_d). Close to the equilibrium attainment portions of the uptake curves, k_d was calculated from the slope. The effect of agitation speeds, particle sizes and initial concentrations are given in the Figure D.13, D.14 and D.15-16, respectively.

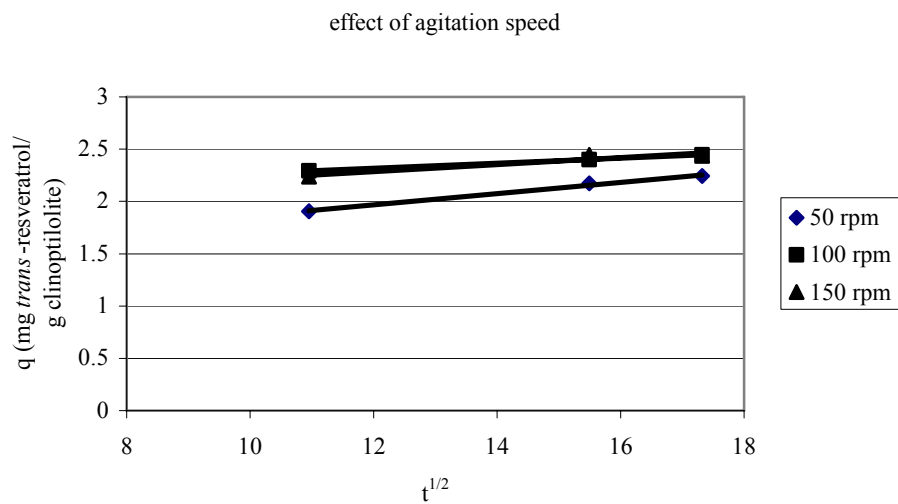


Figure D.13. The relationship between the k_d and q ; effect of agitation speed.

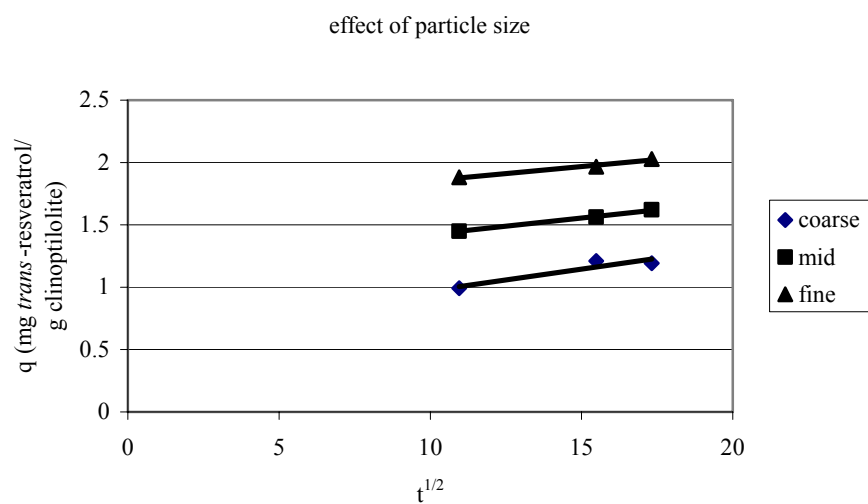


Figure D.14. The relationship between the k_d and q ; effect of particle size.

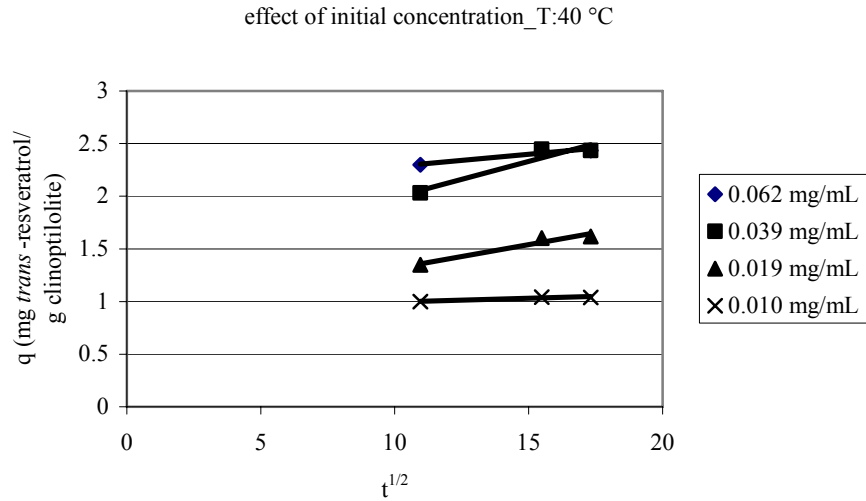


Figure D.15. The relationship between the k_d and q ; effect of initial concentration.

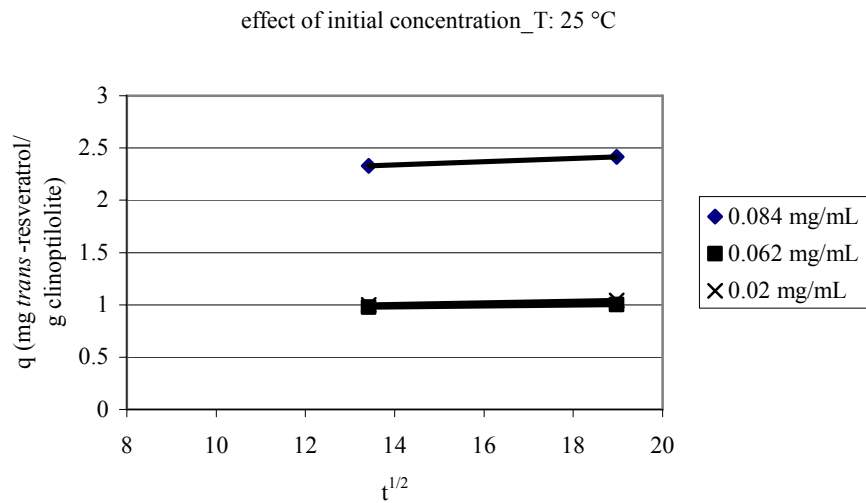


Figure D.16. The relationship between the k_d and q ; effect of initial concentration.

The relationship between the k_d and reciprocal square of the particle diameter is given in Figure D.17.

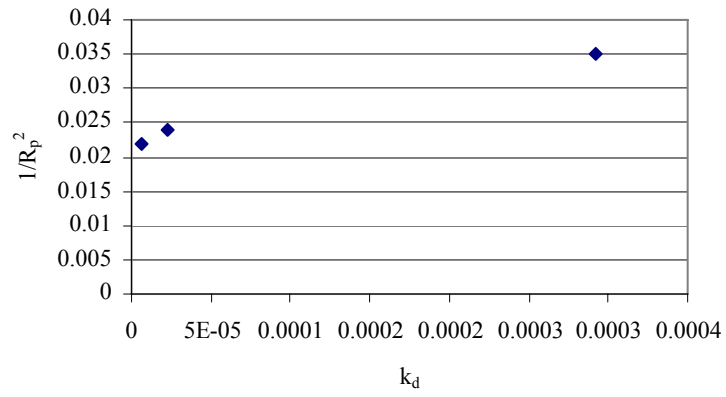


Figure D.17. The plot of the k_d and reciprocal square ($1/R_p^2$) of the particle diameter.

APPENDIX E

ANTIOXIDANT CAPACITY CURVES

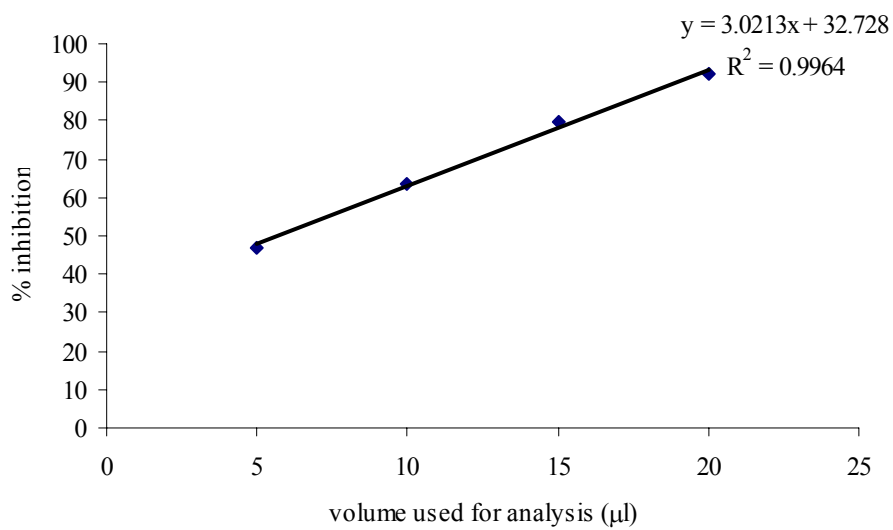
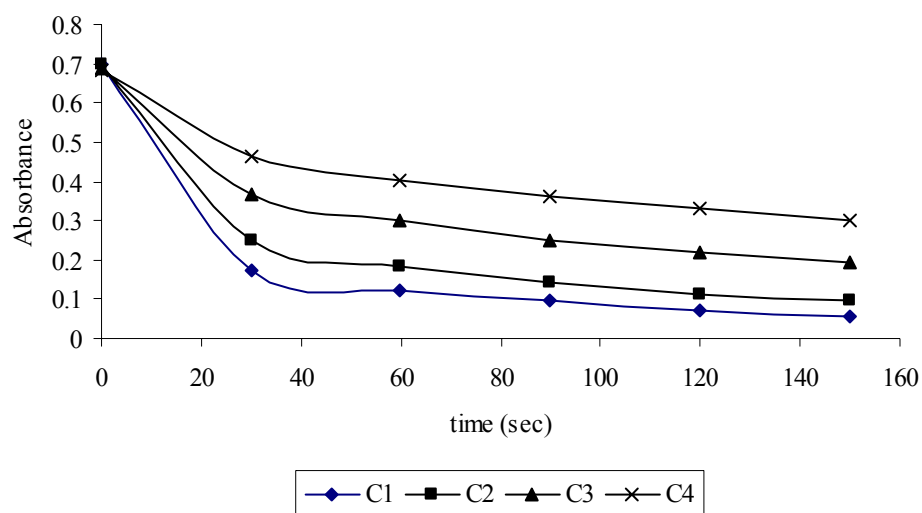


Figure E.1. Inhibition kinetics and inhibition percentage of *trans*-resveratrol.

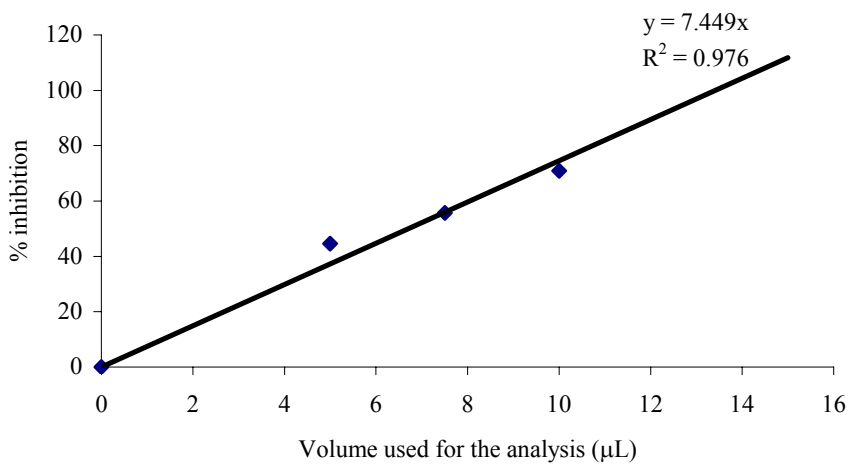
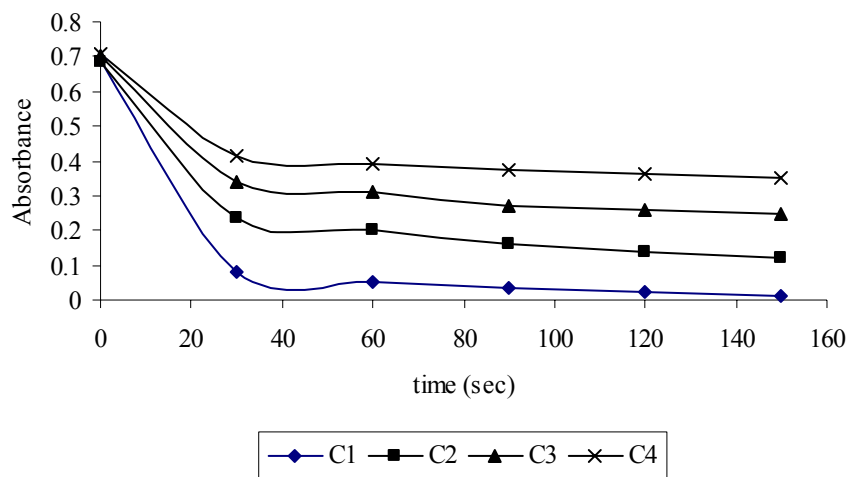


Figure E.2. Inhibition kinetics and inhibition percentage of freeze dried grape skin crude extract.

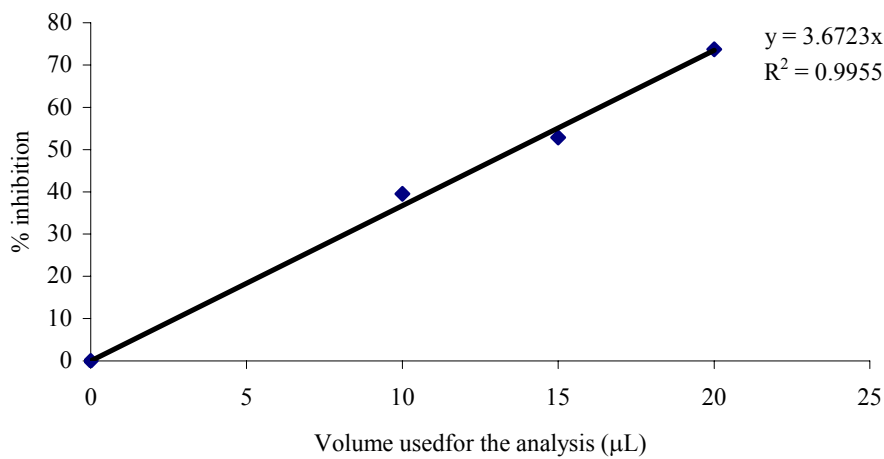
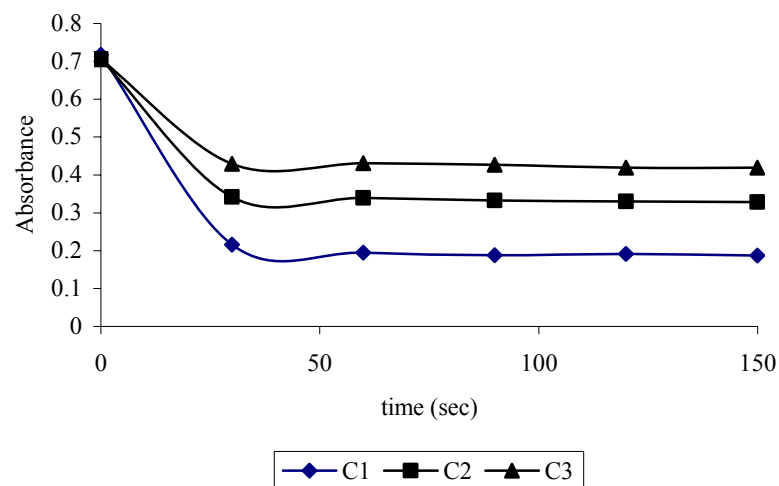


Figure E.3. Inhibition kinetics and inhibition percentage rutin.

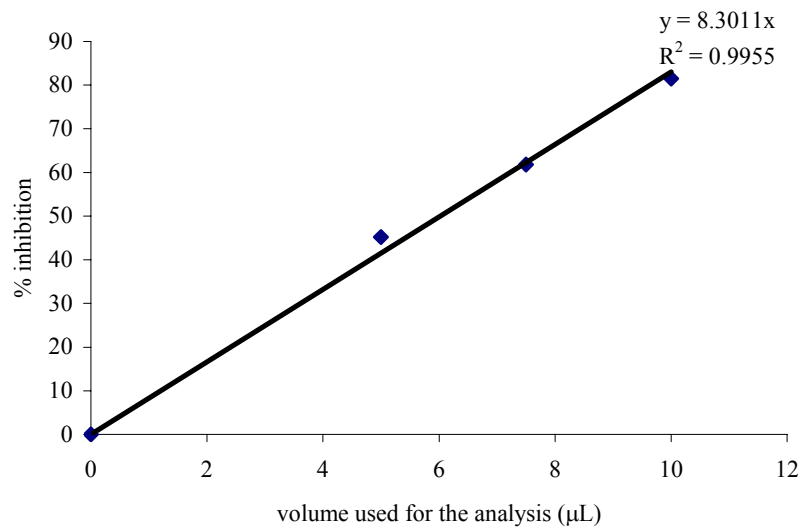
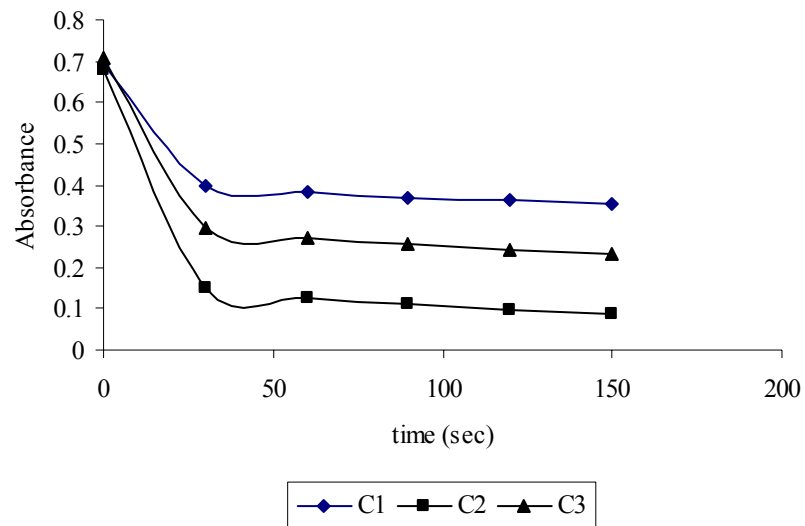


Figure E.4. Inhibition kinetics and inhibition percentage freeze dried olive leaf crude extract.

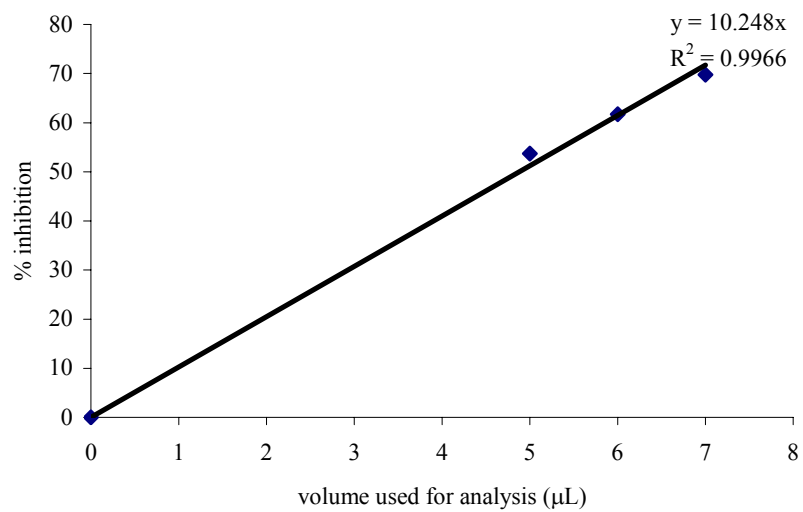
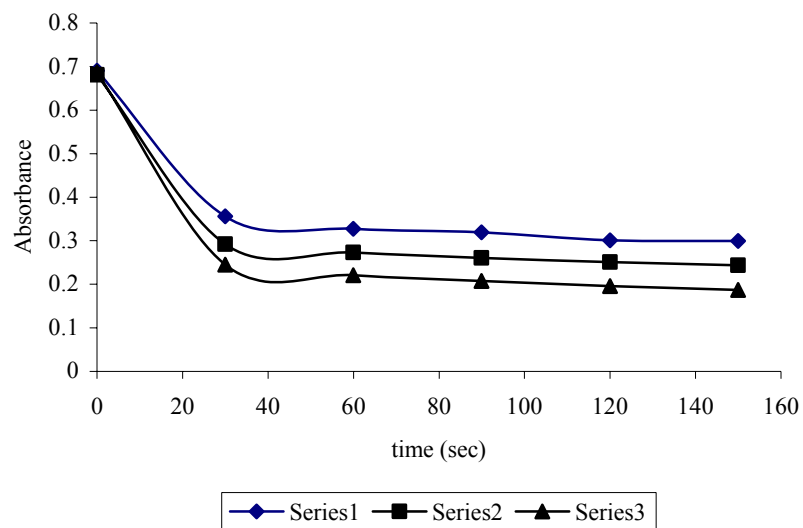


Figure E.5. Inhibition kinetics and inhibition percentage water fraction of olive leaf crude extract from silk fibroin filled column.

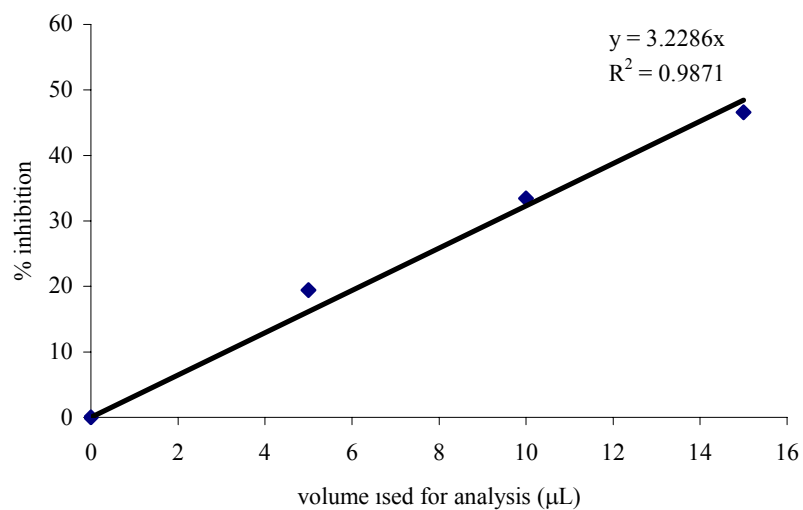
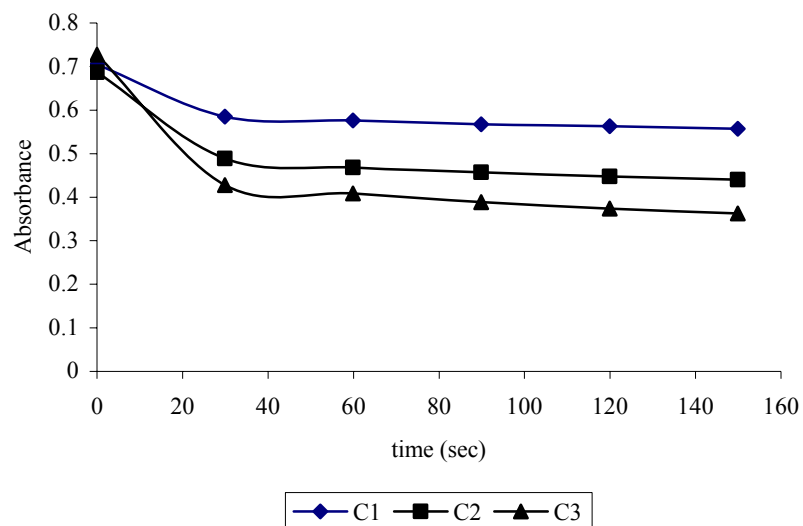


Figure E.6. Inhibition kinetics and inhibition percentage ethanol fraction of olive leaf crude extract from silk fibroin filled column.

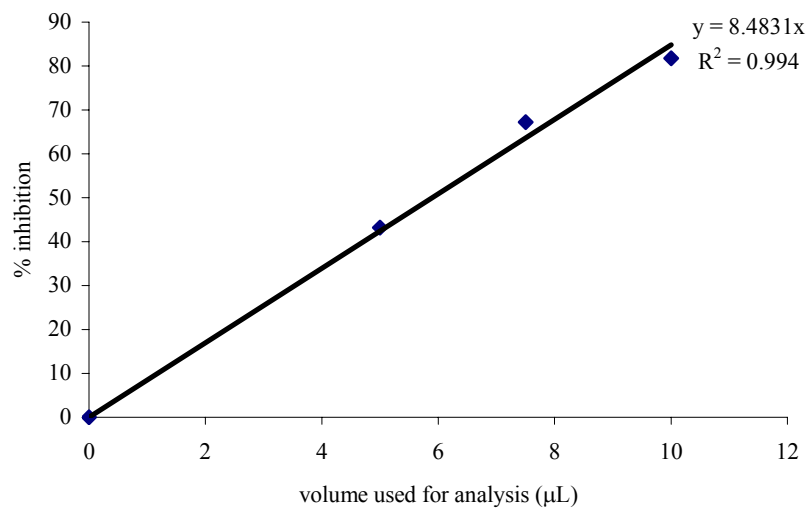
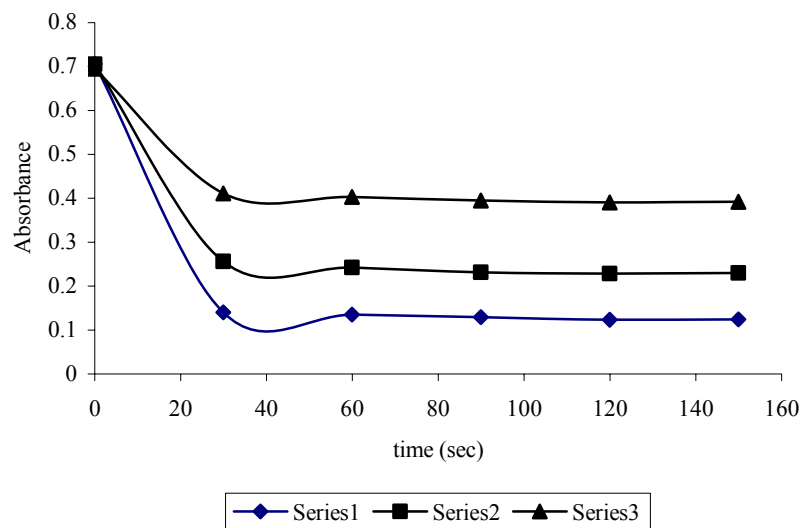


Figure E.7. Inhibition kinetics and inhibition percentage ethanol fraction of oleuropein standard from Extrasynthese.

APPENDIX F

ANTIMICROBIAL ACTIVITIES OF THE EXTRACTS AND ISOLATED FRACTIONS

F.1. Antimicrobial Activity and MIC Curves of Grape Skin Crude Extract.

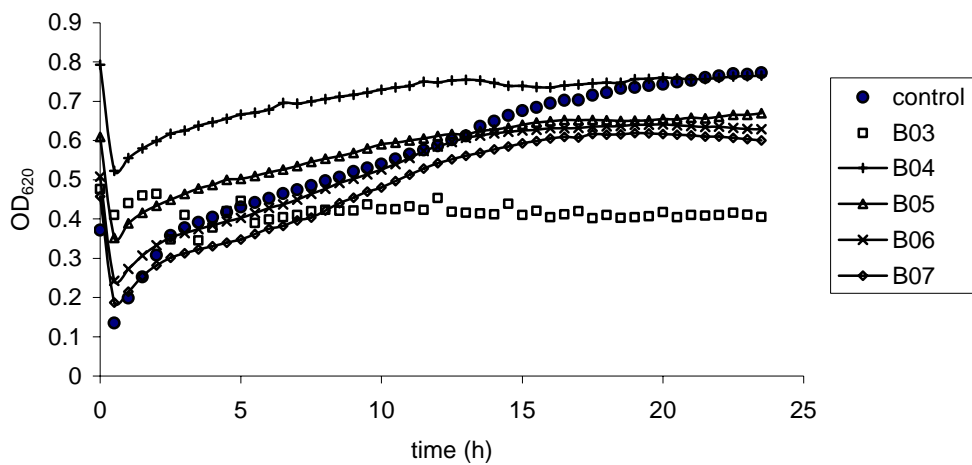


Figure F.1. MIC curves for *S. aureus*. ● negative control group (growth curve for *S. aureus*); observed growth profile in smoothed line; ◻ MIC value (6.25 mg/mL).

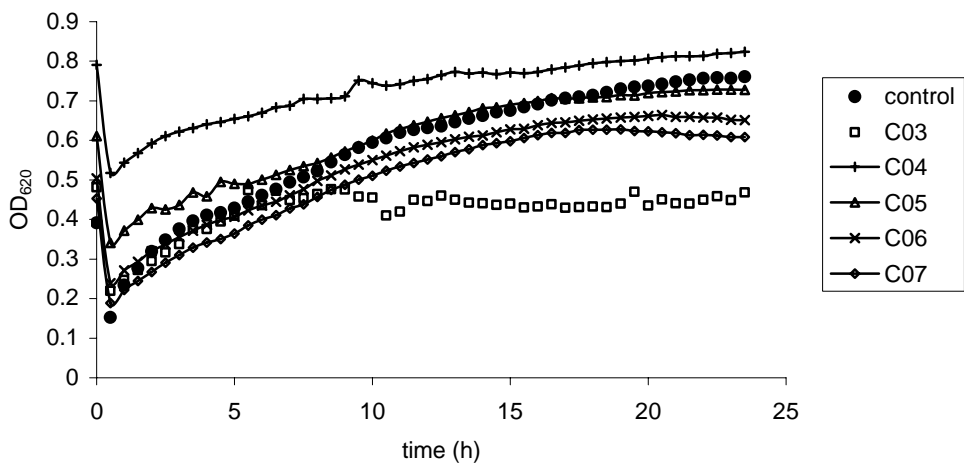


Figure F.2. MIC values for *S. Carnasus*. ● negative control group (growth curve for *S. carnosus*); observed growth profile in smoothed line. There is not any MIC value observed.

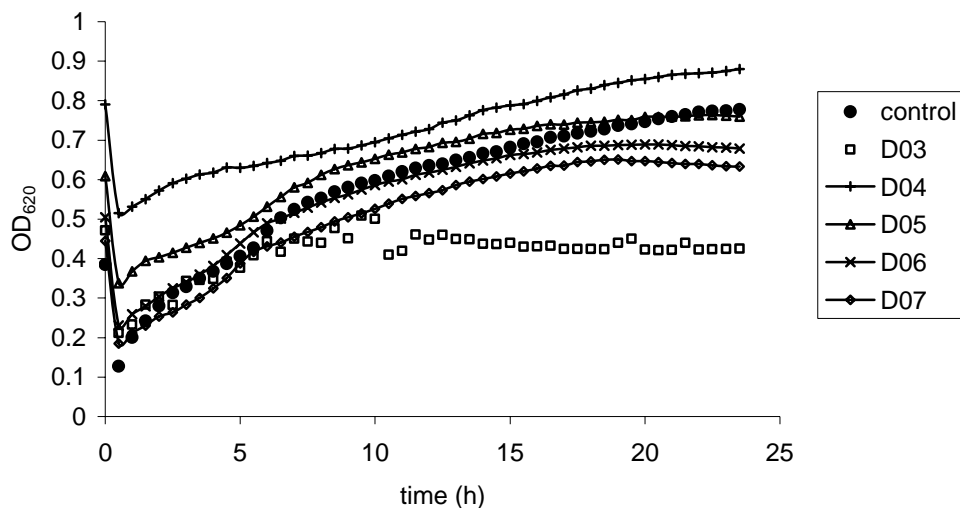


Figure F.3. MIC values for *E. Coli*. ● negative control group (growth curve for *E. Coli*); observed growth profile in smoothed line. There is not any MIC value observed.

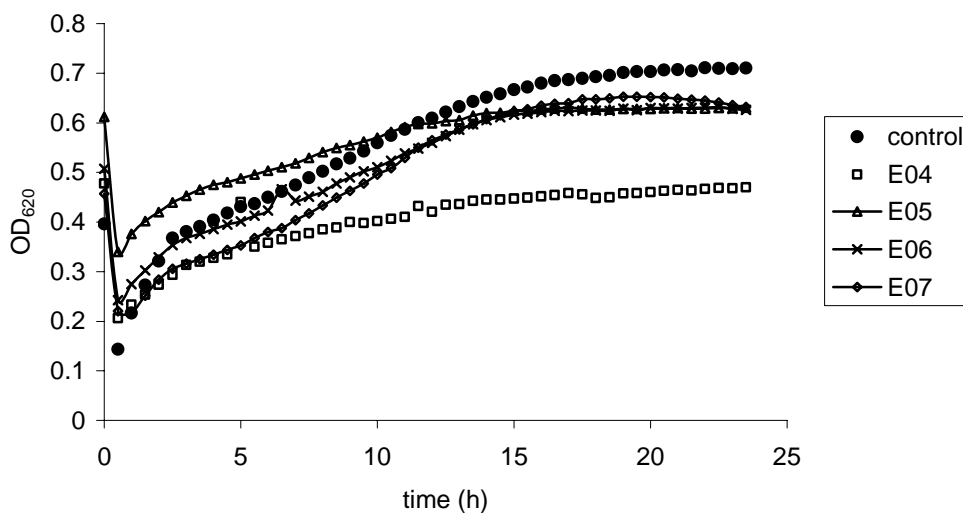


Figure F.4. MIC values for *Salmonella typhimurium* ● negative control group (growth curve for *Salmonella typhimurium*) □ MIC value (3.125 mg/mL).

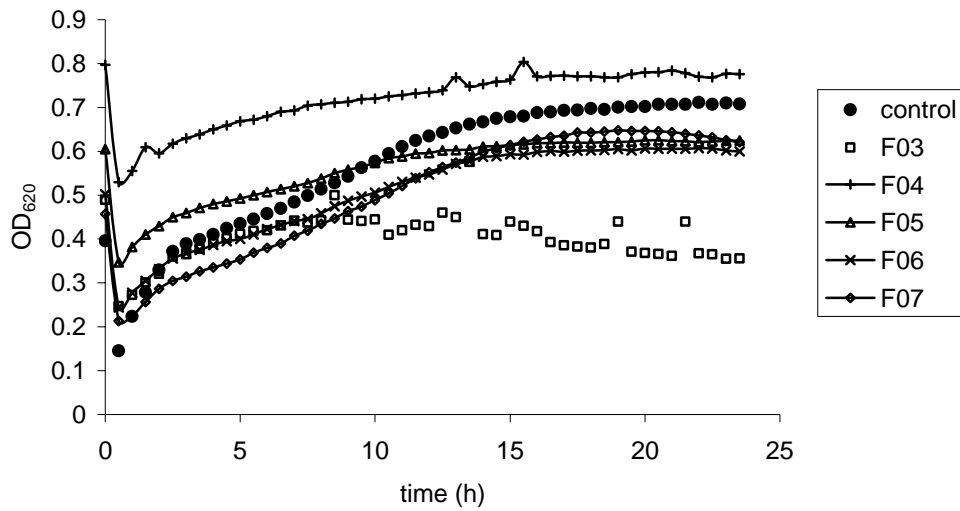


Figure F.5. MIC curves for *E. Coli* pathogen. ● negative control group (growth curve for *E. coli*); observed growth profile in smoothed line; ◻ MIC value (6.25 mg/mL).

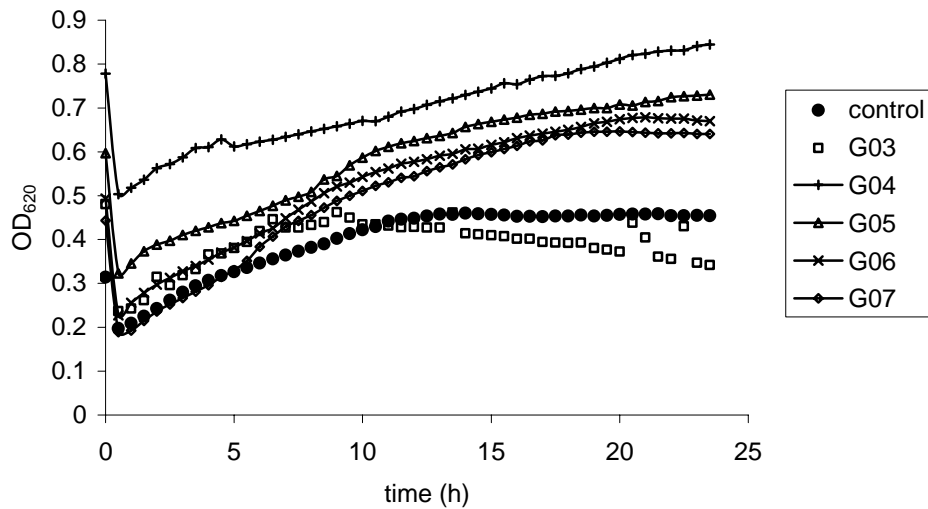


Figure F.6. MIC values for *L. innocua*. ● negative control group (growth curve for *L. innocua*); observed growth profile in smoothed line. There is not any MIC value observed.

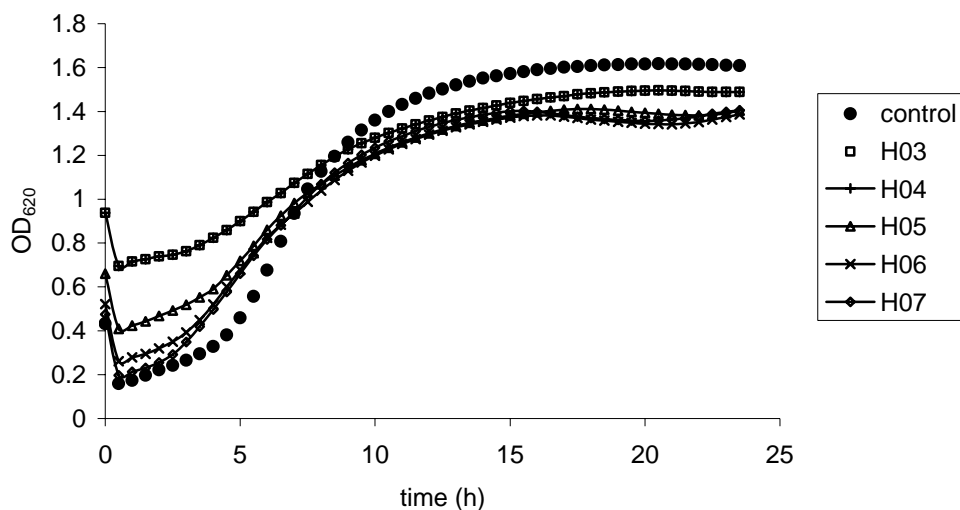


Figure F.7. MIC values for *L. plantarum*. ● negative control group (growth curve for *L. plantarum*); observed growth profile in smoothed line. There is not any MIC value observed.

F.2. Antimicrobial Activity and MIC Curves of Recovered *trans*-Resveratrol from Tianjin Extract.

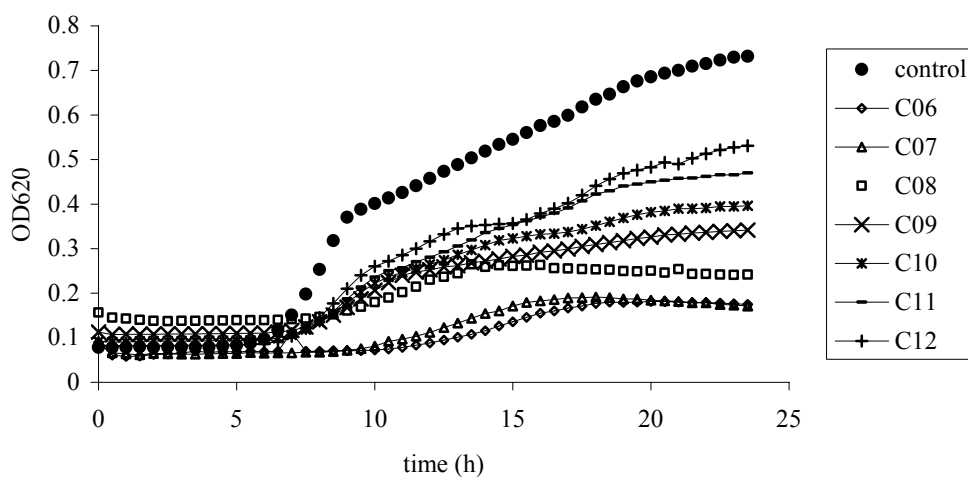


Figure F.8. MIC curves for *S. aureus*. ● negative control group (growth curve for *S. aureus*); observed growth profile in smoothed line; ◻ MIC value (0.39 mg/mL).

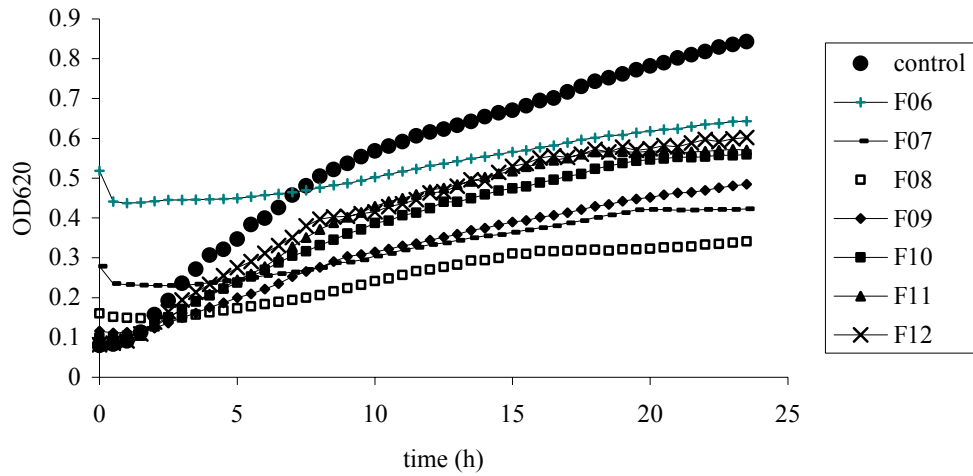


Figure F.9. MIC values for *S. Carnasus*. ● negative control group (growth curve for *S. carnosus*); observed growth profile in smoothed line; ◻ MIC value (0.39 mg/mL).

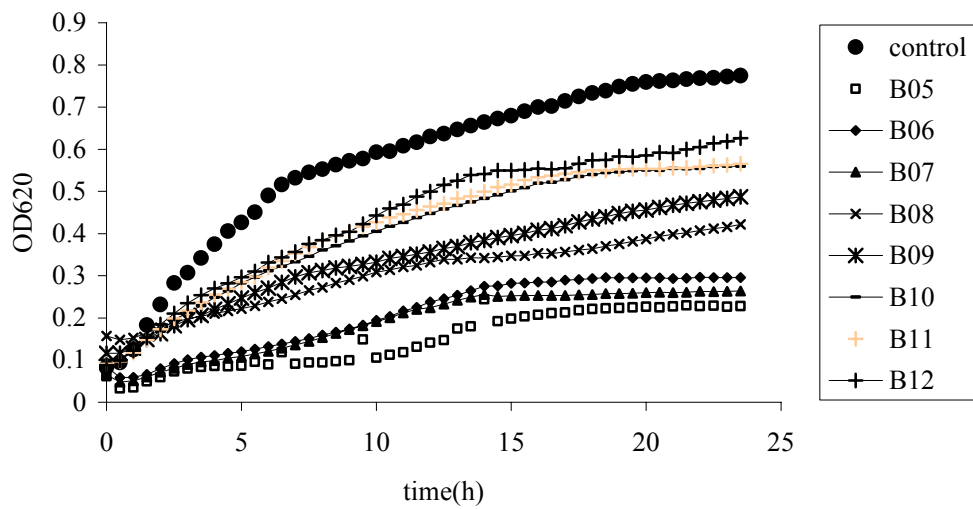


Figure F.10. MIC values for *E. Coli*. ● negative control group (growth curve for *E. Coli*); observed growth profile in smoothed line; ◻ MIC value (3.125 mg/mL).

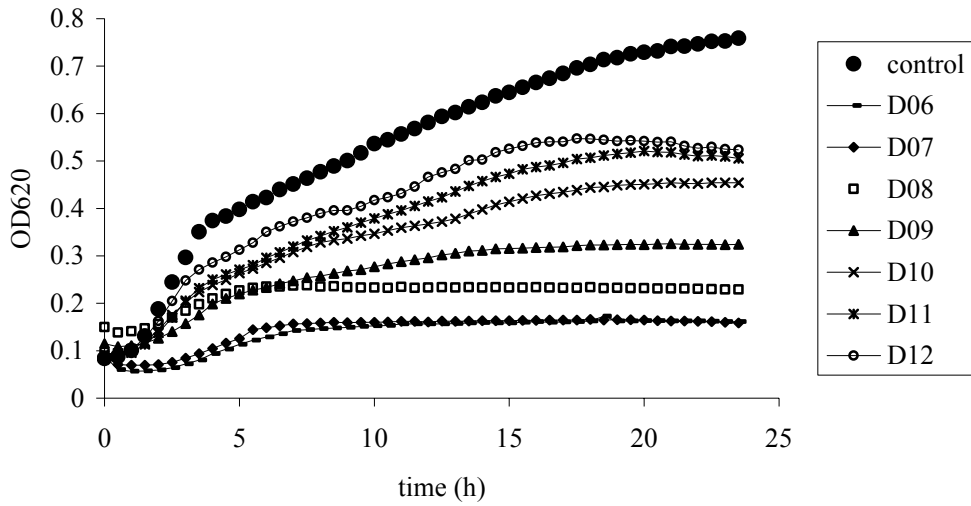


Figure F.11. MIC values for *Salmonella typhimurium* ● negative control group (growth curve for *Salmonella typhimurium*); observed growth profile in smoothed line; ◻ MIC value (0.39 mg/mL).

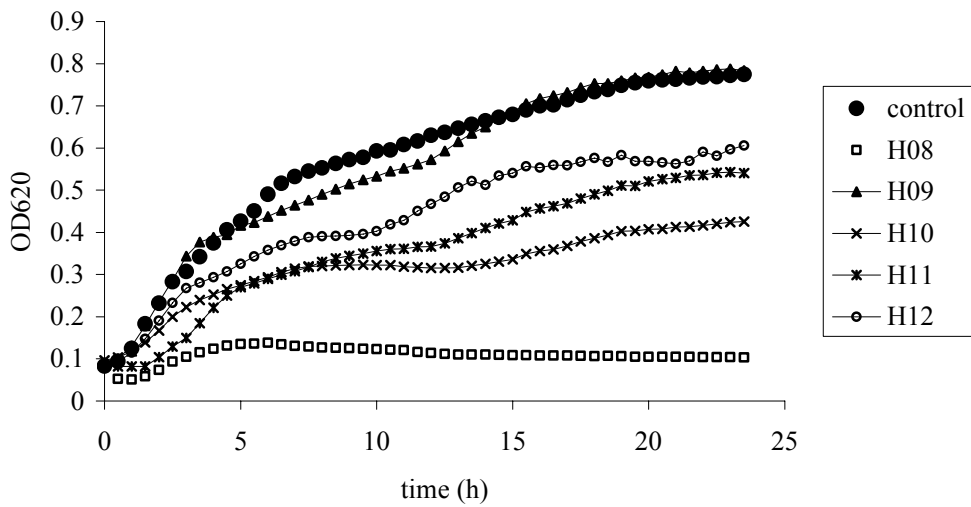


Figure F.12. MIC curves for *E. Coli* pathogen. ● negative control group (growth curve for *E. coli*); observed growth profile in smoothed line; ◻ MIC value (0.39 mg/mL).

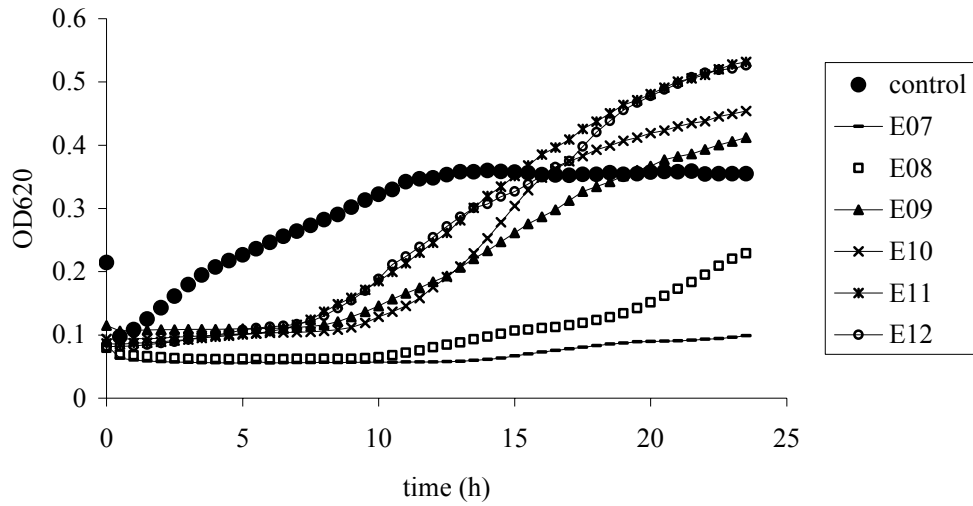


Figure F.13. MIC values for *Listeria innocua*. ● negative control group (growth curve for *L. innocuas*); observed growth profile in smoothed line; ◻ MIC value (0.39 mg/mL).

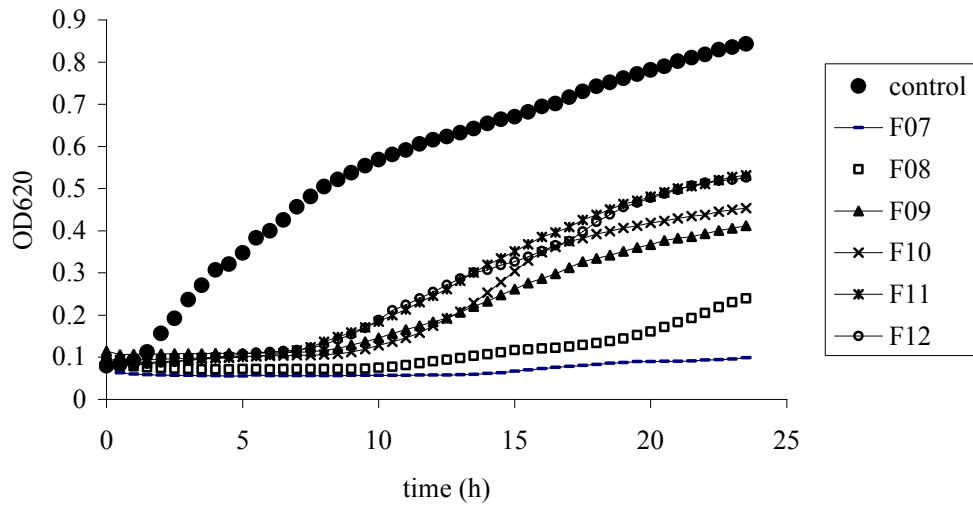


Figure F.14. MIC values for *L. plantarum*. ● negative control group (growth curve for *L. plantarum*); observed growth profile in smoothed line; ◻ MIC value (0.39 mg/mL).

EVREN ALTIOK

Date of Birth : 18.07.1977

Place of Birth : Turkey

Citizenship : Turkish

EDUCATION

[1995-1999] B.Sc. (Food Engineering)

Ege University

Department of food Engineering, Izmir, Turkey

[2000-2003] M.Sc. (Biotechnology Programme)

İzmir Institute of Technology

Biotechnology and Bioengineering Programme, İzmir, Turkey

Dissertation: Production of Grape Seed Extract

[2003-2010] Ph.D. (Chemical engineering)

İzmir Institute of Technology

Department of Chemical Engineering, İzmir, Turkey

Dissertation: Recovery of Phytochemicals Having Antimicrobial and Antioxidant Characteristics From Local Plants

PUBLICATIONS

Altıok, D.; ALTIOK, E.; Tıhminlioğlu, F. Physical, antibacterial and antioxidant properties of chitosan films incorporated with thyme oil for potential wound healing applications, **2010**, *Journal of Materials Science-Materials in Medicine*, 21, 2227-2236.

Kavak, D.D.; ALTIOK, E.; Bayraktar, O.; Ülkü, S. Pistacia terebinthus extract: As a potential antioxidant, antimicrobial and possible β -glucuronidase inhibitor, **2010**, *Journal of Molecular Catalysis B: Enzymatic*, 64, 167-171.

Yalcin, D.; Ozcalik, O.; ALTIOK, E.; Bayraktar, O. Characterization and Recovery of Tartaric Acid From Wastes of Wine and Grape Juice Industries, **2008**, *Journal of Thermal Analysis and Calorimetry*, 94, 767-771.

ALTIOK, E.; Bayçın, D.; Bayraktar, O.; Ülkü, S. Isolation of polyphenols from the extracts of olive leaves (*Olea euopeae* L.) by adsorption on silk fibroin, **2008**, *Separation and Purification Technology*, 62, 342-348.

ALTIOK, E.; Ülkü, S.; Bayraktar, O. Recovery of Proanthocyanidin From Waste of Turkish Traditional Product, Pekmez (Molasses), **2008**, *Food Science and Technology Research*, 13, 321-326.

Baycin, D.; ALTIOK, E.; Ulkü, S.; Bayraktar, O. Adsorption of Olive Leaf (*Olea Europaea* L.) Antioxidants on Silk Fibroin, **2007**, *Journal of Agriculture and Food Chemistry*, 55(4), 1227-1236.

ALTIOK, E.; Asbagh, L. A., Bulut, Ç.; Ülkü, S.; Bayraktar, O. Antioxidant, Antimicrobial and Cytotoxic Activities of Some Turkish Plant Extracts, **2006**, *Febs. Journal*, 273, 371-371.